The use of radio-nuclides (unsupported ^{210}Pb, ^{7}Be and ^{137}Cs) in air, rain and undisturbed soil as an environmental tools.

Thesis Submited by

Feraidoun Choubedar

for the degree of

Doctor of Philosophy

Department of Physics & Astronomy
University of Edinburgh
2000

IN THE NAME OF ALMIGHTY

Abstract

Soil inventories of atmospherically derived ^{210}Pb (radioactive half life 22.3 years) were used to determine deposition patterns of atmospherically derived aerosols averaged over decades at low altitude sites (51.6° N, 0.6° W) and quantify the enhancement in aerosol deposition by aerodynamically rough canopies (forest) relative to short vegetation (grass). ^{210}Pb and ^{7}Be (radioactive half life 53.4 days) in surface air and rain (55.6° N, 3.9° W) were measured to determine the concentrations of these radionuclide isotopes in the environment. Non-destructive gamma-spectrometry was used for all 3 parts using high purity germanium (HPGe) detectors. From the soil samples ^{137}Cs (radioactive half life 30.2 years) is measured and reported.

The annual average concentrations in surface air were found to be 0.19 ± 0.06 and 2.71 ± 0.66 mBq m^{-3} for ^{210}Pb and ^{7}Be, respectively. The annual fluxes of ^{210}Pb and ^{7}Be in rain were determined as 68 ± 10 and 787 ± 29 Bq m^{-2} y^{-1}, respectively. There was a seasonal variation for ^{7}Be concentrations in air and rain giving a spring high. The highest concentrations for ^{210}Pb were obtained when the air mass origin was from the continent. From the air and rain data for ^{210}Pb and ^{7}Be, similar washout scavenging ratios (W_s) were obtained, indicating they are scavenged from the atmosphere with a similar rate.

The average inventories to the canopies compared to the short vegetation for ^{210}Pb and ^{137}Cs for Geescroft forest (deciduous woodland) were about 23% and 49% larger than the open field inventories, respectively; the corresponding values for Broadbalk forest (deciduous shelter belt) were about 29% and 54%, respectively. Although these two forests are not far from each other and have the same altitude, the excess inventories for Broadbalk forest are larger than those for Geescroft forest and this could be due the fact that this forest is acting as an edge, because of its narrow width. The averaged flux for Rothamsted forest soils for ^{210}Pb was determined as 117 ± 4 Bq m^{-2} y^{-1}, for the soil and vegetation in the open grassland area, 144 ± 4 Bq m^{-2} y^{-1} for the deciduous woodland, and 151 ± 4 Bq m^{-2} y^{-1} for the deciduous shelter belt.

Analysis of the inventories of ^{210}Pb in Rothamsted soil gave long term average dry deposition fluxes of about 34 Bq m^{-2} y^{-1} for grassland, about 60 Bq m^{-2} y^{-1} for deciduous woodland and about 68 Bq m^{-2} y^{-1} for a deciduous shelter belt. These fluxes are equivalent to long term average deposition velocities respectively of 4.7 ± 0.6 mm s^{-1}, 8.4 ± 0.6 mm s^{-1} and 9.3 ± 0.5 mm s^{-1} for the aerosols in the size range 0.2- 0.5 μm. The deposition velocities for the woodlands are substantially larger than those obtained in the wind tunnel studies but are similar to field measurement by eddy co-variance methods.

Acknowledgements

This work was begun while the author was in receipt of 3 year scholarship from the University of Lorestan and the Iranian Ministry of Culture and Higher Education.

I would like to thank Professor Derek Branford, Professor David Fowler and Dr Keith Weston for their guidance and assistance during the course of this study.

I wish to thank Dr Masoud Vahabi-Moghadam who assisted with the field work and gave valuable advice during the course of this study.

I would like to thank all of the physics department workshop technicians who have been involved in making the sample holders, compressing devices and the corer. I also would like to thank Tom Davinson for computer support, Gordon Turnbull for helping to set up the equipment and Brain Cameron for helping to set up the rain gauge. My thanks also goes to Professor Allan Shotter for his support through the course of this study.

I would like to dedicate this document to my dear wife Parvaneh.

Declaration

No part of this thesis has been submitted for any other degree or professional qualification. In accordance with the University of Edinburgh regulation 3.8.7, I here state that:

- This thesis has been composed by myself.
- In the course of this study air and rain samples were collected in King's Buildings area and soil samples were collected at the Rothamsted experimental farm station in Harpenden. I have collected all the air and rain samples, and made a substantial contribution in the soil sampling expeditions. The work involved in the preparation, gamma assay, data analysis and interpretation reported here is my own.

Contents

Chapter one **1-23**
1: Introduction and background 1
1.1: Aerosols in the atmosphere 1
1.2: Radioactive tracer elements 2
1.3: Distribution of Uranium and Thorium in the soils 3
1.3.1: Emanation of radon and thoron from the soil 3
1.3.2: Natural radioactivity emitted from the earth surface (^{222}Rn to ^{210}Pb) 4
1.3.3: The spatial pattern of ^{222}Rn 5
1.3.4: Size distribution of ^{210}Pb 5
1.4: ^{210}Pb concentration and distribution in the atmosphere 7
1.5: Natural radioactivity produced by cosmic radiation: ^{7}Be 7
1.5.1: Size distribution of ^{7}Be particles 10
1.6: ^{210}Pb and ^{7}Be as environmental tools 11
1.6.1: Seasonal variability on deposition fluxes of ^{7}Be and ^{210}Pb 11
1.6.2: Atmospheric processes that cause seasonal variations in the deposition fluxes of ^{7}Be and ^{210}Pb 12
1.7: Mean residence time of the sub-micrometer aerosols in the global troposphere 13
1.8: ^{137}Cs in the atmosphere 14
1.9: Acid rain and acid deposition 15
1.10: Deposition processes 16
1.10.1: Sources of particles in the atmosphere 18
1.11: Deposition monitoring 20
1.11.1: Wet deposition 20
1.11.2: Cloud and fog deposition and dew 21
1.11.3: Dry deposition 21
1.12: Deposition in complex terrain 22
1.13: The application of ^{210}Pb inventories in soil and importance of this study . 22
Chapter two **24-63**
2: Sampling methods and measurements 24
2.1: Surface air measurements 24
2.1.1: Filter and site selection for surface air measurement 26
2.1.2: Background radiation measurements for surface air 27
2.1.3: Gamma-spectroscopy of the surface air samples 27
2.2: Rain measurements 30
2.2.1: Method and measuring procedures for rain samples 31
2.2.2: Site selection and background radiation measurements for rain samples 31
2.3: Soil measurements 33
2.3.1: Site selection 33

2.3.2: Self absorption in soil samples 34
2.3.3: Background radiation measurements for soil samples 35
2.3.4: Soil sample preparation and measuring procedures 36
2.3.5: Site details 36
2.4: Specifications of the detectors used 51
2.5: Electronics and data acquisition 51
2.6: Background reduction 55
2.7: Calibration techniques 56
2.7.1: Energy calibration 57
2.7.2: Efficiency calibration 58
2.7.3: Self absorption in the sample 63
Chapter three **64-111**
3: Analysis of the results 64
3.1: Surface air measurements of ^{210}Pb and ^{7}Be concentrations 64
3.1.1: Frequency distribution of ^{210}Pb and ^{7}Be 66
3.1.2: Effect of meteorological variables on concentrations of ^{210}Pb and ^{7}Be 69
3.1.3: Seasonal variables of ^{210}Pb and ^{7}Be concentrations 69
3.1.4: Effect of atmospheric pressure on ^{210}Pb and ^{7}Be concentrations . 70
3.1.5: Effect of air mass trajectory and source on ^{210}Pb and ^{7}Be concentrations 72
3.2: Rain measurements of ^{210}Pb and ^{7}Be 74
3.2.1: Total monthly concentrations of ^{210}Pb and ^{7}Be in precipitation . 75
3.2.2: Total monthly fluxes of ^{210}Pb and ^{7}Be in precipitation 76
3.2.3: Effect of meteorological variables on concentrations of ^{210}Pb and ^{7}Be 78
3.2.4: Seasonal variations of ^{210}Pb and ^{7}Be fluxes in precipitation 80
3.3: ^{210}Pb and ^{137}Cs inventories measured in Rothamsted soils 82
3.3.1: Absorption of the radiation by the soil samples 82
3.3.2: Correction procedures for self absorption 82
3.3.3: Atmospherically derived ^{210}Pb inventories 83
3.3.4: Specific activity profiles of ^{210}Pb and ^{137}Cs in soils 83
Chapter four **112-144**
4: Discussion of the results 112
4.1: Surface air measurements 114
4.1.1: Surface air pressure effects on ^{210}Pb and ^{7}Be concentrations .. 114
4.1.2: Continental, oceanic effects on ^{210}Pb and ^{7}Be concentrations . 115
4.1.3: Seasonal effects on ^{210}Pb and ^{7}Be concentrations and the effect of vertical transport on ^{7}Be concentrations 116
4.1.4: Possible relation of O_3 and ^{7}Be concentrations 119
4.1.5: Averaged annual concentrations of ^{210}Pb in surface air 120
4.1.6: Averaged annual concentrations of ^{7}Be in surface air 121
4.2: Rain measurements 124
4.2.1: Meteorological effects on ^{210}Pb and ^{7}Be concentrations

in precipitation 124
4.2.2: Seasonal effects on ^{210}Pb and ^{7}Be 125
4.2.3: Estimate of dry deposition for ^{210}Pb and ^{7}Be 125
4.2.4: Washout scavenging coefficient 128
4.2.5: Averaged annual concentration of ^{210}Pb and ^{7}Be in precipitation 129
4.3: Soil inventory measurements of atmospherically derived ^{210}Pb and ^{137}Cs. 132
4.3.1: Distributions of ^{210}Pb and ^{137}Cs in top soils 132
4.3.2: ^{210}Pb inventories in Rothamsted soils 133
4.3.3: ^{210}Pb inventories in Rothamsted soils 135
4.3.4: Deposition velocity of ^{210}Pb carrier aerosols 138
4.3.4.1: Deposition velocity calculated from rain data 138
4.3.4.2: Dry deposition velocity calculated from soil data 138
4.3.5: ^{210}Pb inventories into the canopies 142
4.3.6: ^{137}Cs inventories into the forests 142
4.3.7: The edge of the forest effects on deposition 142
Chapter five **145-153**
5: Conclusions 145
5.1: Surface air samples 146
5.2: Rainfall measurements 148
5.3: Atmospherically derived inventories of ^{210}Pb and ^{137}Cs in soil 150
Appendices **153-176**
Appendix A: 153
Table 3.1 154
Appendix B: 158
Table 3.2 159
Appendix C: 161
Table 3.3a 163
Table 3.3b 169
Table 3.4 173
Appendix D: Conversion factors 176
References **177-184**

Chapter 1

1. Introduction and background

The aim of this work is to use the soil inventory of atmospherically derived ^{210}Pb to quantify the enhancement in aerosol deposition by aerodynamically rough canopies of vegetation, especially trees, in low altitude regions relative to short vegetation. In particular a primary focus of the work is to quantify, the increased capture of aerosols by trees and to apply this information to understand and quantify the deposition of aerosol phase pollutants SO_4^{-2} and NO_3^-.

In this chapter, the general background, including the terminology used in this report, is explained. In chapter two, the sampling methods for collection of surface air, rain and soil are presented. Chapter three presents the results. Chapter four presents the discussion and interpretations of the results. Chapter five presents conclusions of the research.

1.1. Aerosols in the atmosphere.

A system of small particles or liquid droplets suspended in a gas phase is termed aerosol. Aerosols have to be small, not too much larger than a micrometre in radius, to remain suspended in the air for long periods. There are two main sources of fine particles in the atmosphere: primary materials that are directly derived from dispersal of solids from the earth's surface and secondary particulate material, which forms within the atmosphere through chemical reactions [Brimblecombe, 1996].

The pollutants maybe present as gases (e.g.; SO_2, NO, NO_2, HNO_3, NH_3, HCl, HF, O_3, CO, H_2O_2) or as particles. The particles suspended in air termed aerosols may contain a complex mixture of oxidised products of some of the primary and secondary gaseous pollutants listed above. However, the aerosols over Europe and N. America generally contain $(NH_4)SO_4$, NH_4NO_3 as well as aerosols of natural origin from sea spray [Fowler, 1986].

Atmospheric aerosols vary in size from about 1 nanometre diameter up to about 1 mm in diameter. Larger atmospheric particles are extremely rare as they are deposited rapidly by gravitational effects. In dry air, in the size range 10^{-3} to 10

micrometre the number concentration is commonly 10^3 to 10^4 cm^{-3} and at clean remote sites it can be 100's cm^{-3} [Twomey, 1979; Fowler et al., 1991].

1.2. Radioactive tracer elements.

Natural and artificial radioactive, aerosol-borne tracers are an ideal tool to study atmospheric transport processes. The source distribution of these elements is relatively well known. They are removed from the atmosphere by radioactive decay as well as by dry and wet-deposition [Rehfeld and Heimann, 1995].

The radioactive tracer isotopes become quickly attached to aerosols after their formation [Junge, 1963a]. The radii of the aerosol particles lie between 0.02 micrometre and 1 micrometre [Graustein and Turekian, 1986; Turekian et al., 1977; Feichter et al., 1991; Junge, 1963a; Brost et al., 1991; Feely et al., 1966; Rehfeld and Heimann, 1995].

These radionuclides trace the distribution and fate of their carrier aerosols. Radionuclides produced by cosmic rays and nuclear weapons originate in, or are delivered to, the stratosphere and upper troposphere, whereas radon is introduced from the land surface, and its daughters are produced primarily in the lower troposphere [Liu et al., 1984].

Three classes of radionuclides exist in the atmosphere, those produced by cosmic rays such as ^{7}Be and ^{10}Be, those produced by nuclear weapons testing or industrial activity such as transuranics and the fission products ^{90}Sr and ^{137}Cs, and those supplied from the earth's surface through the emination of the radon isotopes. Although this last group includes all the radioactive members of the uranium and thorium decay chains below ^{222}Rn and ^{220}Rn, we will be concerned primarily with ^{210}Pb in this research.

The earth's surface is the main source of the vast majority of atmospheric trace constituents, yet the processes that control the behaviour of trace constituents in the planetary boundary layer and that determine their flux into the free atmosphere and their deposition on the earth's surface remain poorly characterised. Characterising these processes is particularly important because of the critical roles that many of these trace species play in studying tropospheric chemistry, global climate and environmental degradation. Among the most reliable studies of the behaviour of trace species in the boundary layer are those based on ^{222}Rn (daughter of ^{226}Ra), daughters

of ^{222}Rn, including ^{210}Pb, and ^{137}Cs (product of nuclear fission, and nuclear weapons) [Monaghan, 1989].

1.3. Distribution of Uranium and Thorium in the soil.

Uranium and thorium are widely distributed in the earth's crust. Except in geologically recent sediments, there is equilibrium between parent and daughter nuclides in the decay chains from uranium and thorium to radium isotopes (^{226}Ra and ^{224}Ra) which are the precursors of ^{222}Rn and ^{220}Rn. Table 1.1 shows the mean specific activities of the uranium and thorium chains averaged over a world-wide selection of rock samples [Adams et al., 1959].

	Uranium chains		Thorium chain	
	(ppm U)	(Bq kg^{-1})	(ppm Th)	(Bq kg^{-1})
sedimentary rocks	2.5	33	26	6.5
Igneous rocks	3.5	48	13.5	59

Table 1.1. Abundance of radioactive elements by weight in rocks.

In 327 samples of surface soil from USA, Myrick et al. (1983) found mean activities of 41 and 35 Bq kg^{-1} for ^{226}Ra and ^{232}Th respectively. There are local variations according to the rock type, and in areas of mineralisation the activities may be up to 1000 times the average [Wilkening et al., 1972; Keller et al., 1982].

1.3.1. Emanation of radon and thoron from the soil.

The release of radon by radioactive minerals was known by the beginning of the 20th century. Although not identified as the radionuclide radon, the phenomenon was observed by Boltwood (1905, 1907, 1908) [cited in Barretto et al., 1972]. He introduce the term emanating power to describe the loss by emanation from radioactive minerals [Barretto et al., 1972].

The rates of ^{222}Rn emanation from different types of rocks and associated minerals were investigated by Barretto et al. 1972 who showed that, in general, rocks are poor emanators with the exception of the granite types which sometimes show a radon loss of more than 10% by mass. Weathering is an important factor in increasing the gaseous emanation.

^{222}Rn escape rates from various soils show a much broader range of emanation rates and percentage of radon loss, a fact which is believed to depend upon their physical state and mineralogy composition. However, their radon activity is more uniform, averaging 5.55-111 mBq h^{-1} kg^{-1}. Exceptions are found within the soils, particularly the residual types [Barretto et al., 1972].

The transport of ^{222}Rn and ^{220}Rn in the soil, and the factors affecting release to the atmosphere have been reviewed by Tannor (1964). The energy imparted by the alpha decay of their precursors causes radon atoms to recoil along a track of about 80 μm in air. Despite the very short range, it seems that release depends more on recoil than on diffusion within the mineral crystal. Emanation to the interstitial air may be primarily from ^{226}Ra or ^{224}Ra on the surface of the crystals [Chamberlain, 1991].

A small proportion of ^{222}Rn emanated from the earth's surface is redeposited as short-lived decay products, but most decay in the atmosphere to ^{210}Pb. The mean residence time of ^{210}Pb is short (a few days) compared with its radioactive half-life (22.3 years), so the downwards flux of ^{210}Pb, in atoms m^{-2} s^{-1}, should equal the upwards flux of ^{222}Rn.

Deposition of ^{210}Pb varies from about 0.83 to 365 Bq m^{-2} y^{-1} at glaciers and continental sites, respectively [Turekian et al., 1977]. At Milford Haven, Wales, the deposition was found to be 85 Bq m^{-2} y^{-1} [Peirson et al., 1966]. Calculations by Turekian et al. (1977) show a best fit to the measured fluxes if the average continental exhalation of ^{222}Rn is 372 Bq m^{-2} y^{-1} ($12x10^3$ atoms m^{-2} s^{-1}).

The emission rate of ^{222}Rn depends on the concentration of its precursor in the decay chain (^{226}Ra) in the earth's crust, the meteorological conditions and the properties of the soil like water content, porosity, snow cover, and forest [Martell, 1985; Mattsson, 1970; Dorr, 1984; Dorr et al., 1993]. The estimations of the global mean ^{222}Rn-emission vary between 7.2 $x10^3$ atoms m^{-2} s^{-1}[Lambert et al., 1982] and $12x10^3$ atoms m^{-2} s^{-1} [Turekian et al., 1977].

1.3.2. Natural radioactivity emitted from the earth surface (^{222}Rn to ^{210}Pb).

The earth's crust contains the radioactive element ^{238}U which decays through ^{226}Ra to ^{222}Rn. This element emanates out of the earth's crust into the atmosphere. ^{222}Rn (mean radioactive life-time of 5.52 days) is a water-insoluble inert gas which is lost from the atmosphere by radioactive decay to ^{210}Pb [Junge, 1963a]. The decay series of ^{238}U is shown in Figure 1.1. Lead-210 atoms (mean radioactive life-time of

32.3 years) become quickly attached to aerosol particles and are removed from the atmosphere primarily by dry and wet deposition.

Concentrations of ^{210}Pb have been found to increase with height in the atmosphere of the UK from 0.21 mBq kg^{-1} of air at ground level to 0.26 at 7.6 km and 0.36 mBq kg^{-1} in the stratosphere [Peirson et al., 1966]. In the mid-west USA, Moore et al. 1973 found a different profile, the concentration decreasing with height to 0.04 mBq kg^{-1} at the tropopause but increasing again to 0.28 mBq kg^{-1} in the stratosphere. The differences in the profiles reflect the geographical situations, the lower part of the profile over the UK being depleted by deposition during passage of air westwards over the Atlantic [Chamberlain, 1991].

Based on measurements made by Patterson and Lockhart (1964), the air column above 1 cm^2 area of soil to a height of 1.2 km contains 0.74 mBq of ^{210}Pb [cited in, Fisenne, 1968]. In terms of mass, ^{210}Pb is not abundant; there are about 10^4 to 10^5 aerosol particles for every atom of ^{210}Pb. It is, however, relatively easy to measure ^{210}Pb in aerosols since the anthropogenic mobilisation of ^{210}Pb is too small to cause contamination problems. ^{210}Pb thus acts as a natural radioactive tracer associated with the ambient sub-micrometre aerosol population [Graustein and Turekian, 1983].

1.3.3. The spatial pattern of the ^{222}Rn.

The oceanic ^{222}Rn emissions are about two orders of magnitude smaller than the continental emissions as a result of a smaller ^{226}Ra content of the ocean. Only approximately 2% of the atmospheric ^{222}Rn mass is of oceanic origin [Wilkening and Clements, 1975; Peng et al., 1979].

A quantitative interpretation of ^{226}Ra content of soil in terms of ^{222}Rn emission is difficult because only a fraction of the decaying ^{226}Ra atoms release ^{222}Rn to the soil gas. This fraction depends on the location of ^{226}Ra in the soil, in particular, the soil type, and varies over a wide range from 10 to 50% [Jacob and Prather, 1990].

1.3.4. Size distribution of ^{210}Pb.

Moore et al. (1980) found 83 ±13% of ^{210}Pb was associated with particles <0.6 μm in diameter. Sanak et al. (1981) found 70 to 90% of ^{210}Pb activity was attributed to particles <1.2 μm in diameter. Knuth et al. (1983) found on average 71% of ^{210}Pb was in particles below 0.58 μm and 2.8% was in particles above 3.45 μm.

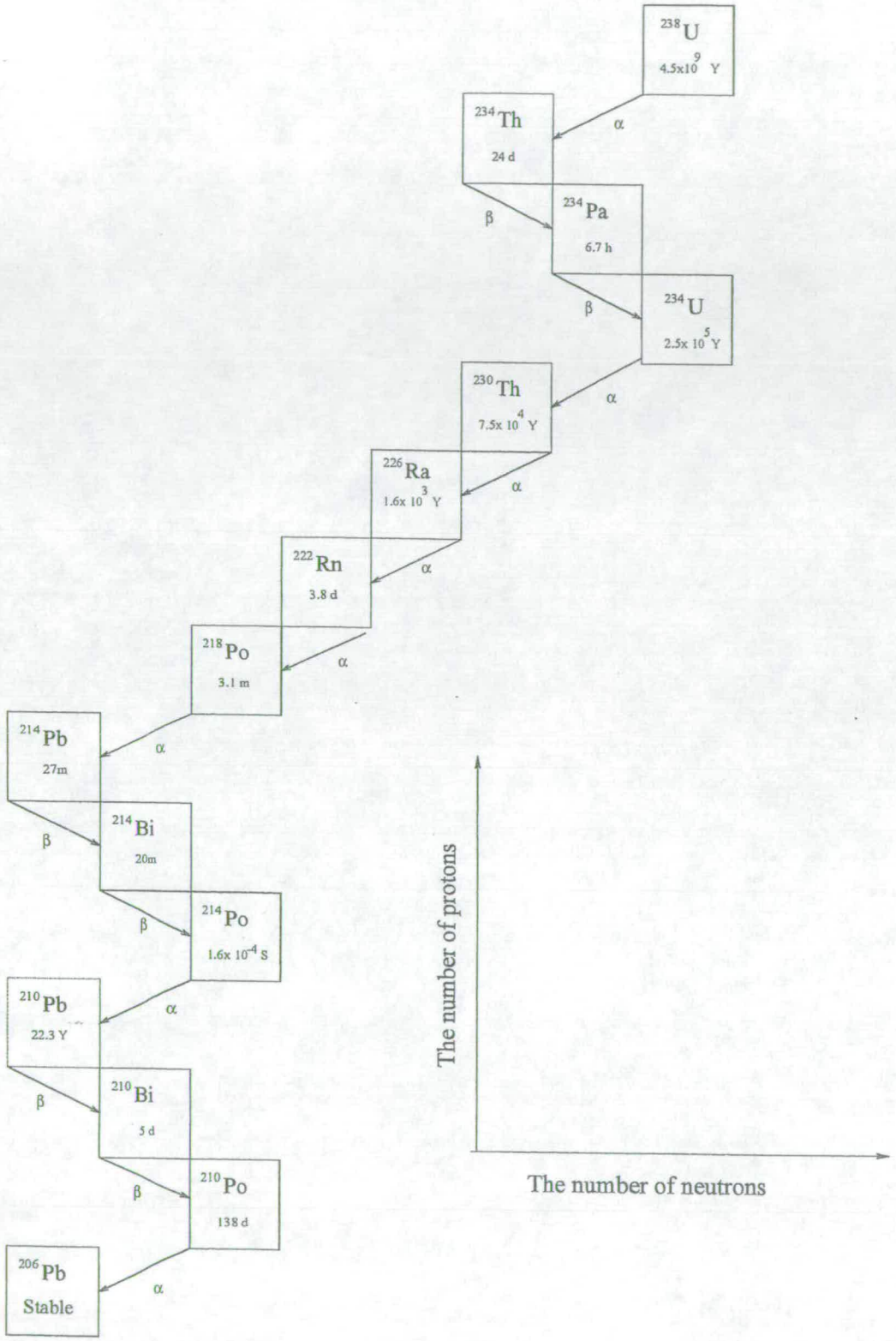

Figure 1.1. The ^{238}U series of naturally occurring radioactive decays.

Lockhart et al. (1965) found about 85% of ^{210}Pb is attached to particles of diameter <1.0 μm. Moore et al. (1973), Knuth and Knuston (1981) and Knuth et al. (1982), found that ^{210}Pb was associated with aerosols less than 1 μm both in continental and marine environments.

1.4. Lead-210 concentration and distribution in the atmosphere.

In recent years, a great deal of research has been done in the field of natural environmental radioactivity. In these studies the distribution of ^{210}Pb in the environment has been widely investigated and the data achieved have been used to produce a world-wide data base " http://glaciog.ujf-grenoble.fr/equipes/glacier " [Preiss et al., 1998].

This data base includes measurements performed with the different types of collectors that have been used for ^{210}Pb studies during the last four decades. Most of the data reported in the data base are annually averaged. The data base includes the ^{210}Pb concentration in surface air, the atmospheric deposition flux at the Earth's surface collected by different means (artificial collectors, soil, and snow), and finally the deposition flux at the water-sediment interface.

1.5. Natural radioactivity produced by cosmic radiation: ^{7}Be.

Primary cosmic rays (mainly protons) tend to travel along the Earth's magnetic field and enter the atmosphere predominantly over the magnetic poles. These protons strike atoms in the upper atmosphere and create a cascade of secondary and tertiary particles. Of interest to ^{7}Be production is the resulting flux of neutrons, which can continue downward in the atmosphere and collide with oxygen and nitrogen atoms to produce nuclear disintegrations, known as "stars", a small fraction of which produce ^{7}Be atoms. Beryllium-7 nuclei, generated by cosmic rays, travel along magnetic field lines, so the source is strongest near the poles (figure 1.2) [Koch et al., 1996].

The energy of the initial cosmic ray particle determines how deep into the atmosphere the subsequent cascade can penetrate before the secondary and tertiary particles are slowed by collisions and can no longer produce stars. The combinations of the rapid decrease with penetration depth of the flux of low energy neutrons and the increase with depth of atmospheric density (that is, the concentration of target nuclei) makes a peak ^{7}Be production in the middle of the atmosphere, [Junge, 1963b;

Brost et al., 1991]. About 67% of the ^{7}Be source is in the stratosphere [Lal, 1963; Koch et al., 1996].

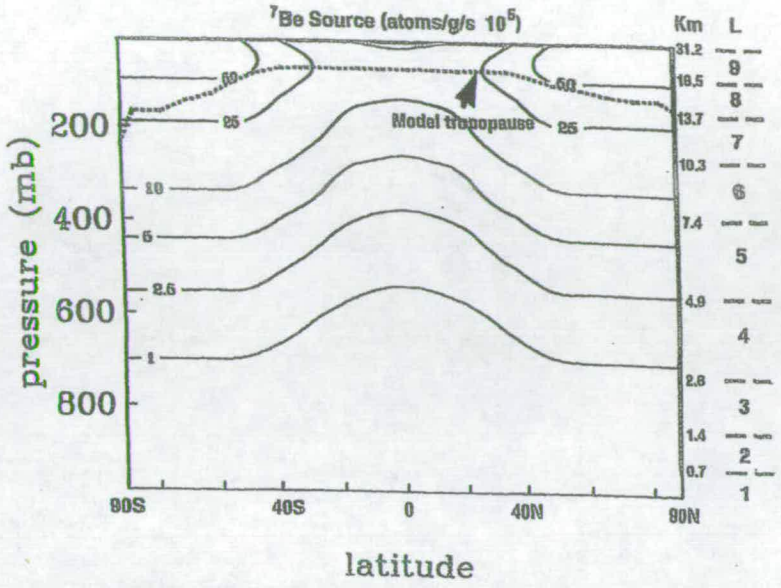

Figure 1.2. Beryllium-7 source [Lal and Peters, 1967]. Atmospheric pressure is shown in the left margin, and the altitudes of the general circulation model (GCM) layers are shown in the right-hand margin. Also shown is the annual average tropopause height in the GCM (dashed line). The units are ^{7}Be atoms s^{-1} (gram of air)$^{-1}$ x 10^{5} [cited in Koch et al., 1996].

A newly produced ^{7}Be atom diffuses until it encounters a particle, to which the atom becomes attached. Because most of the particulate surface area is found on particles with diameters between 0.03 and 1.0 micrometres, the ^{7}Be atoms usually attach to these sub-micron particles, and the future of the ^{7}Be atoms becomes that of the sub-micron atmospheric aerosol. Particles in this range do not grow in size or settle appreciably at heights greater than 20 km but instead just travel with the particle until the ^{7}Be radioactivity decays or until the particle leaves the troposphere, normally by being deposited on the surface [Brost et al., 1991].

^{7}Be production has negligible dependence on season or longitude, but varies with the 11-year solar cycle. When solar activity is high, cosmic rays are deflected away from the solar system, and ^{7}Be production decreases. Figure 1.3 shows annual average ^{7}Be concentrations at four sites with chronologically long data records, [Koch and Mann 1996]. Figure 1.3 also shows the annual average Wolf sunspot

series, an indicator of solar activity, which are anti-correlated with ^{7}Be [Koch and Mann 1996].

Lal and Peters (1967) show the cosmic ray intensity ratio between the solar maximum year 1958 and a minimum year 1954 as a function of atmospheric pressure and latitude (Figure 1.3). At 48° latitude and 200 metres this difference is about 40% [Koch et al. 1996].

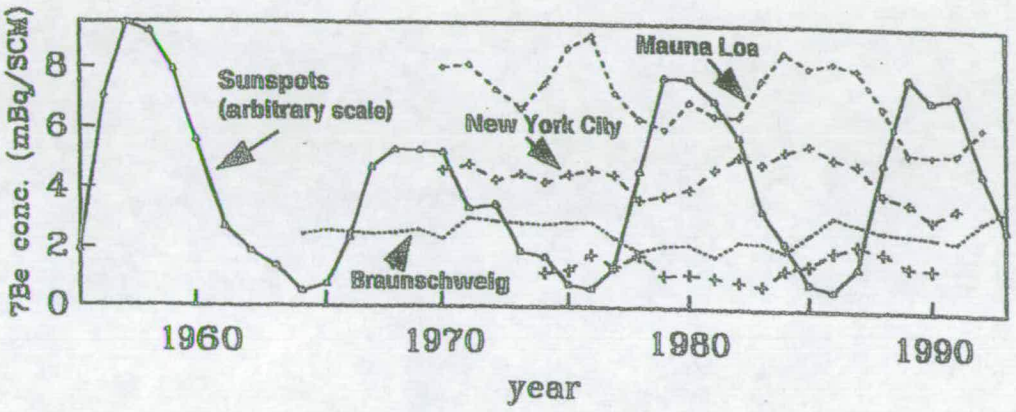

Figure 1.3. Observed annual average concentrations as a function of year from (top to bottom) Hawaii, New York City, Braaunschweig, Germany, and Skibotn, Norway. Solid line connects the annual average Wolf sunspot number as a function of year. The sunspot number is an index of solar activity [Taken from Koch et al., 1996].

A variety of atmospheric processes influence the surface air concentration of ^{7}Be. Although the timing and magnitude of their effects differ with location, the two processes that have the greatest short-term influences on ^{7}Be in surface air are precipitation, which scavenges the carrier aerosols, and downward transport.

Analysis of the spatial and temporal variation of ^{7}Be allows assessment of the influence of these processes on tropospheric aerosols [Koch et al., 1996]. The anti-correlation between ^{7}Be and solar activity has been noted in short records [O'Brien et al., 1991 ; Larsen, 1993] and in longer records from Germany [Hotzl et al., 1991; Koch et al. 1996]. ^{7}Be production is maximum in the stratosphere at about 20 km, and decreases approximately exponentially with decreasing altitude [Lal and Peters, 1967; Dutkiewitz and Husain, 1985].

The mean residence time is the survival time of the particles, with which the radionuclides are associated, in the air column relative to removal to the surface. The stratospheric mean residence time of 14 months [Reiter, 1975] exceeds the time required (six times the half-life) to establish steady state equilibrium between ^{7}Be

production and its removal by radioactive decay and atmospheric removal. Stratospheric ^{7}Be concentration is thus expected to remain unchanged from year to year, except for small variations (<10%) resulting from solar modulation of cosmic rays. In the troposphere, however, decreased production rates and rapid mixing [Beck and Kuroda, 1966; Gavini et al., 1974] result in ^{7}Be concentrations that are a hundred fold smaller than those in the stratosphere [Dutkiewicz and Husain, 1985].

Feely et al. (1988) stated that surface concentration of ^{7}Be depends on four processes: (1)wet scavenging, (2)stratosphere-to-troposphere exchange, (3)downward transfer in the troposphere, and (4)horizontal transfer from middle subtropical latitudes to higher and lower latitudes. Each of the four processes has its own seasonal cycle, so that the seasonal cycle of surface concentration of ^{7}Be is some complicated product of the four processes; at different locations different processes may be dominant, and the seasonal cycle in ^{7}Be can have one or more maxima in any season or maxima in many combinations of seasons. For example, stratosphere-to-troposphere exchange has a peak in spring and summer near the polar front and subtropical jet streams, so that the annual cycle in ^{7}Be may be dominated by this processes at certain middle-latitude stations, especially at high elevations. Similarly, the troposphere is less stable in summer than in winter; hence certain middle-latitude, continental stations might have concentration maxima in summer produced by this process (as long as the continental summertime maxima in precipitation do not suppress these concentration maxima). Arctic stations have late winter and early spring maxima owing to the horizontal transport patterns in winter and perhaps also to the lack of wet scavenging in winter. Concentrations at subtropical stations are dominated by wet scavenging, so that local precipitation and concentration are strongly negatively corrected [Feely et al. 1988; Brost et al. 1991].

1.5.1. Size distribution of ^{7}Be particles.

Air measurements at Richland, Washington (46° N, 119° W), indicate that 88% of the ^{7}Be was associated with <1.1 μm particles and 1% was attached to >7 μm particles [Young and Silker 1974]. Like atmospherically derived radionuclides, ^{7}Be rapidly becomes associated with aerosols, and its deposition on the earth's surface occurs by precipitation scavenging and by particle dry deposition. The contribution of dry deposition has been difficult to evaluate with direct measurements but is probably

minor in humid regions [Bondietti et al. 1984]. Brost et al. (1991) found ^{7}Be atoms attached to aerosol particles in the size range between 0.025 to 1 μm.

1.6. Lead-210 and beryllium-7 as environmental tools.

^{210}Pb and ^{7}Be are two radionuclides which have been widely used as useful tracers for studying cloud scavenging and precipitation processes, aerosol transit and residence times in the troposphere, aerosol deposition velocities, air water exchange rates, aerosol trapping by above ground vegetation, and deposition patterns of airborne contaminants. Even though the sources of these two nuclides to the atmosphere are distinctly different, both are highly particle reactive and thus get attached to aerosols in the atmosphere soon after production.

1.6.1. Seasonal variability on depositional fluxes of ^{7}Be and ^{210}Pb.

It has been shown that there are seasonal variations on the depositional fluxes of ^{7}Be and ^{210}Pb. The seasonal increases in the depositional fluxes of these nuclides are commonly attributed to the injection of ^{7}Be-enriched stratospheric air to the troposphere [Olsen et al., 1985a and 1985b; Todd et al., 1989]. However, Feely et al. (1981 & 1989) have addressed the seasonal variability of ^{7}Be at several locations around the globe from ^{7}Be measurements of air samples and have observed that several additional meteorological variables, such as seasonal variability of the amount of precipitation and vertical mixing of lower and upper troposphere, could explain the seasonal variability of ^{7}Be concentrations in surface air at many locations [Baskaran, 1995].

Even though a general linear relationship between the amount of precipitation and depositional fluxes of ^{7}Be and ^{210}Pb has been observed [Olsen et al., 1985a; Dibb, 1989; Todd et al., 1989; Schuler et al., 1991; Baskaran et al., 1993] in many places, a quantitative evaluation on the precipitation-normalised seasonal variations of the depositional fluxes of ^{7}Be and ^{210}Pb is lacking [Baskaran, 1995].

The amount of precipitation from location to location varies from season to season and from year to year. Since >90% of the depositional fluxes of atmospherically derived nuclides are derived through wet precipitation, the amount of precipitation has a major influence on the depositional fluxes of ^{7}Be and ^{210}Pb [Olsen et al., 1985a and 1985b; Dibb, 1989; Todd et al., 1989; Baskran et al., 1993]. Even though the production rate and transport are important, they do not vary in time as

much as the precipitation does. Recently, it has been found that pulsed rain events, with greater or equal to 5 cm of precipitation in a single day, brought down significant amounts of ^{7}Be and ^{210}Pb. For example, a recent study on depositional fluxes of ^{7}Be and ^{210}Pb at Galveston, Texas, indicated that 4-6% of the total number of rainy days, in the form of 4-6 heavy rain events, bring about 20-30% of the annual total amount of deposition of ^{7}Be and ^{210}Pb [Baskaran et al., 1993]. It has also been observed that the annual depositional fluxes of ^{7}Be and ^{210}Pb increases with the increase in the amount of precipitation [Nevissi, 1985; Baskaran et al., 1993].

For a constant annual flux of ^{210}Pb or ^{7}Be, any increase in the deposition fluxes of ^{7}Be and ^{210}Pb during one season in a year should theoretically lead to a minimum depositional flux during another season in the same year. However, the season(s) where the depositional fluxes of these nuclides are consistently minima at different geographical location is not known [Baskaran, 1995].

1.6.2. Atmospheric processes that cause seasonal variations in the depositional fluxes of ^{7}Be and ^{210}Pb.

Since ^{7}Be is of cosmogenic origin and its production rate is high in the upper troposphere, its concentration in the air increases with increasing altitude from the surface of the earth. ^{210}Pb, on the other hand, has a higher production rate in the lower troposphere and relatively lower production rates in the upper troposphere. Hence, its concentration in air is expected to decrease with elevation from ground due to a decrease of ^{222}Rn [Moore and Poet, 1976].

However, recent model prediction by Balkanski et al. (1993) suggests that there is a weak gradient of ^{210}Pb between the continental mixed layer and the troposphere. The longer residence times of ^{210}Pb aerosols in the tropics are attributed to the frequent convective updraft of ^{222}Rn to higher altitudes where precipitation is infrequent. There seems to be no published data to confirm this model of precipitation. Owing to the distinctly different sources of ^{210}Pb and ^{7}Be, steep concentrations gradients between the upper and lower troposphere are commonly maintained. Seasonal variations in the surface air concentrations of ^{7}Be as well as in the depositional fluxes of ^{7}Be and ^{210}Pb have been observed in many places. It has been shown that the surface air concentration of ^{7}Be depends on wet scavenging, stratosphere-troposphere exchange of air masses, downward transfer of aerosols in

the troposphere, and horizontal movements of aerosols from subtropical and lower and higher latitudes.

The seasonal variation in the depositional fluxes of ^{7}Be as well as in the surface air is a complicated function of all four processes since each of these processes can have its own seasonal cycle [Brost et al., 1991]. Feely et al. [(1981) and (1989)] have carried out the most detailed study on the seasonal variations in surface air concentrations of ^{7}Be using data sets from 28 sites in different regions around the world.

1.7. Mean residence time of the sub-micrometre aerosols in the global troposphere.

For a wide range of sub-micrometer particles, it is generally believed that the aerosol removal from the atmosphere is a first order process. This could therefore be characterised by a scavenging coefficient λ_s, defined in the same way as a radioactive constant λ, i.e. by the ratio of the flux removed per unit of time to the reservoir content. However, contrary to radioactivity, the scavenging varies considerably in space and time, more particularly with altitude and meteorological conditions, since the in-cloud scavenging is dominant. True local and instantaneous values of λ_s are unknown. However, some authors have measured what could be called an average value of λ_s in a given air mass and for a span of a few days. In that case λ_s is generally expressed by its reciprocal, the aerosol residence time $\tau = 1/\lambda_s$ [Lambert et al., 1983].

A first difficulty in determining this average residence time is that an air mass is not a well closed reservoir, so that it is necessary to know, in addition to its initial content, all possible kinds of inflow, and outflow. On the other hand, it is well known that radon is a gas emitted into the atmosphere from the surface of the continents.

The atmospheric ^{222}Rn disappears only by radioactive decay with a half-life of 3.825 days. Contrary to this, its decay products are metal atoms, which are rapidly trapped by the atmospheric aerosols and subsequently removed from the atmosphere (figure 1.1). Therefore in each reservoir (troposphere and stratosphere), the production of a nuclide by radioactive decay of its precursor is balanced simultaneously by its own radioactivity and by the fluxes of atoms transferred to-or-from other reservoirs, and in the case of the troposphere, by aerosol scavenging [Lambert et al., 1983].

Balkanski et al. (1993) have reported the residence times of ^{210}Pb at southern mid-latitudes are about 5 days and at northern mid-latitude varies from about 5 days in winter to 10 days in summer. In the tropospheric column, this time is 20 days over Antarctica and 10-15 days in the tropics.

The longer residence times in the tropics and at northern mid-latitudes in summer are due to frequent convective pumping of ^{222}Rn to high altitudes. For ^{7}Be the mean residence time is estimated to be 21 days [Koch et al., 1996]. Figure 1.4 shows the zonally averaged annual mean tropospheric residence time of ^{7}Be and ^{210}Pb aerosols [Moore et al., 1973].

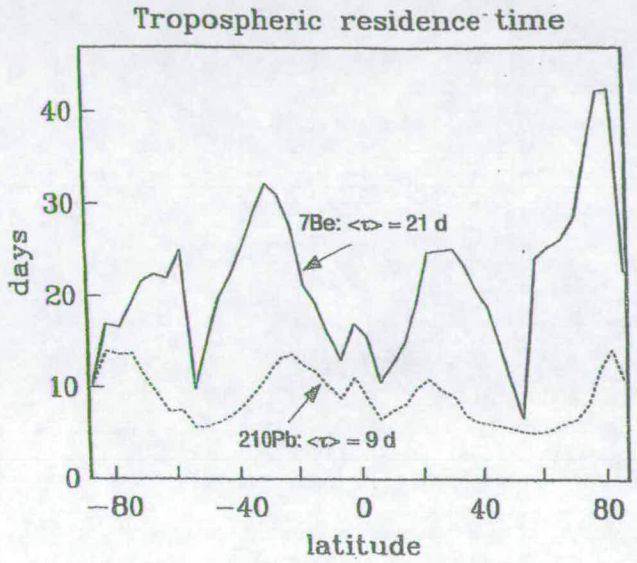

Figure 1.4 . Zonally averaged, annual mean tropospheric residence times of ^{7}Be (solid) and ^{210}Pb (dashed) as a function of latitude [cited in Koch et al., 1996].

1.8. Caesium-137 in the atmosphere.

Caesium-137 was injected into the stratosphere by atmospheric testing of nuclear weapons and nuclear reactor accidents. The injection of ^{137}Cs from weapon test programmes into the atmosphere are roughly 50% between 1962 and 1964, 25% before 1962 and 25% after 1964. Major nuclear accidents have released significant quantities of ^{137}Cs and other radionuclides into the atmosphere. The important ones are the Windscale reactor fire in the UK in 1957, a chemical explosion in a Soviet plant treating active wastes, and in 1986 a massive release from Chernobyl in the Ukraine, due to reactor melt-down.

^{137}Cs, along with other stratospheric aerosols, is transferred to the mid-latitude troposphere by tropopause folds, which results in episodic injections of stratospheric air [Danielson, 1968]. Crick and Linsley (1983) have estimated the release of ^{210}Po in the accident to Windscale reactor to the atmosphere as 8.8 TBq (240 Ci), (Bismuth was irradiated in the reactor to make ^{210}Po for use in nuclear weapons). Like ^{210}Pb and ^{7}Be, ^{137}Cs is carried by sub-micrometer aerosols, delivered to the earth's surface by the scavenging of those aerosols and immobilised in most soils [Volchok, 1980]. The physical half-life of ^{137}Cs, 30.2 years, is similar to that of ^{210}Pb .

The different sources of these isotopes lead to differing vertical distributions of ^{137}Cs and ^{210}Pb . Over the USA the ^{210}Pb concentration typically decreases by a factor of 10 between ground level and the tropopause, where as the concentration of fission products, such as ^{90}Sr and ^{137}Cs, does not change systematically with altitude [Moore and Poet, 1976; Rehfeld and Heimann, 1995].

Pulford et al. (1995) found that Cs is held as a simple metal-humate salt by ionic bonding, where as Pb is held by more complex bonding, possibly involving the formation of conjugated ketonic structures. Cs forms weaker complexes with humic acid than Pb (Table 1.2); in both cases, however, the stability constant decreases with increasing pH. This evidence suggests that Cs is much more mobile than Pb in organic soils [Pulford et al., 1995].

	pH	logk
Cs	5.3	1.43
Cs	6.4	0.72
Pb	5.2	6.53
Pb	6.3	3.82

Table 1.2. Stability constant (as logk) for Cs or Pb-humic acid complexes at different pH values [Pulford et al., 1995].

1.9. Acid rain and acid deposition.

Acid rain is known to arise as a consequence of pollutants emitted into the atmosphere. However, some important details of the transport and deposition mechanisms are poorly understood. Acid rain became an environmental issue in the 1960's. The precipitation monitoring network set up in Europe in the mid-1960's convinced many scientists that the pH of rainfall in Europe was declining.

In theoretical terms, the dissolution of carbon dioxide in rainwater should yield a solution with a pH of about 5.6. However, measurements made even in remote and unpolluted areas suggest that rain can exhibit widely ranging pH values. Naturally occurring acidic precipitation can form through the presence of organic acids or the oxidation products of naturally emitted sulphur and nitrogen compounds. However, natural rainfall acidity does not have pH values of less than 4.0 that are observed today [Brimblecombe, 1996].

Initially the term "acid rain" was used to describe precipitation with anomalously low pH values. However, over the years writers also used it to described the dry deposition of gases and particulate pollutants. This is often called "acid deposition", whereby sulphuric acid formation can make acidification important more than a thousand kilometres from the source of the precursor gases. Popular usage has sometimes broadened the term "acid rain" to describe air pollution in general [Brimblecombe, 1996].

The mean pH of rainfall in the British Isles, Germany and the low countries currently lies close to 4.4. This suggests a marked decrease from the natural pH of rainfall. Changes in the type of fuel used, economic shifts and desulphurisation have led to reductions in sulphur emissions, but have often increased the relative importance of NO_x emissions, particularly those from vehicles. Atmospheric acidity is increasingly derived from nitrogen rather than sulphur compounds, which has led to rising nitric acid deposition [Brimblecombe, 1996].

1.10. Deposition processes.

Aerosols and gases may be transferred from the atmosphere to the earth's surface by a variety of processes which may be conveniently divided into wet deposition and dry deposition (Figure 1.5). Wet deposition is a group of indirect processes in which the pollutants are incorporated into cloud, rain, snow, or hail, and transferred to the ground by precipitation. Dry deposition is the term used for processes by which gases or particles are deposited directly on to terrestrial surfaces; this includes the absorption of reactive gases at the ground and the gravitational and turbulent deposition of particles [Fowler, 1986].

The mechanisms by which air pollutants are transferred to forests is by dry and wet deposition and in wind-driven cloud water, the later being referred to as occult deposition. Occult deposition rates to forests in identical weather conditions

may vary by an order of magnitude depending on forest structure. Estimates of wet, occult and dry deposition on Keilder Forest, England, and Whitetop Mountain, USA, show substantial differences in occult deposition which are only partly explained by differences in cloud frequency [Unsworth and Wilshaw, 1989].

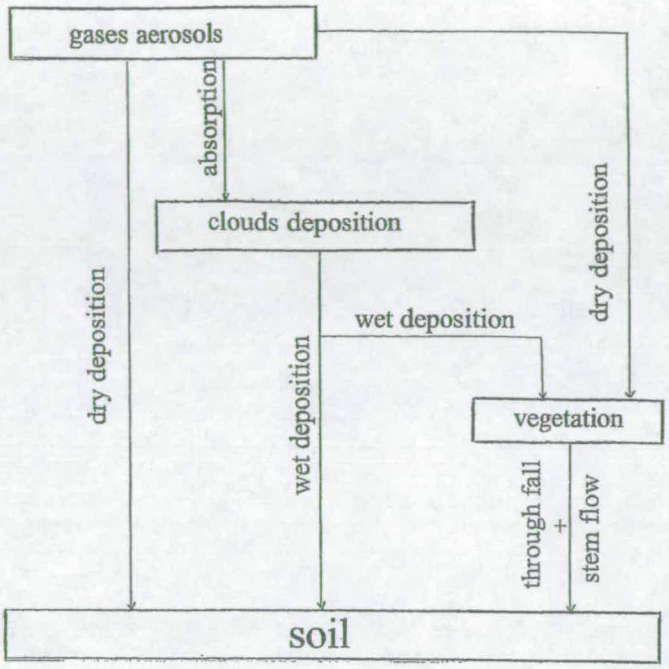

Figure 1.5. Schematic representation of deposition processes.

The measurements of Lovett (1988) were made at a forest site and he found that the efficiency of capture of cloud droplets by forest is much higher than by short vegetation. The rate of deposition expressed as a deposition velocity varies from between 10 to 40 mm s^{-1} over moorland to >100 mm s^{-1} over aerodynamically rougher surfaces, for example, forests [Twomey, 1979].

Dry deposition of particles has received less attention then the deposition of acidic gases. This is partly because the results of wind tunnel studies suggest that the deposition velocity may be very small for sub-micron particles. Also, the complexity of deposition processes of particles implies that it is difficult to perform field measurements appropriately. However, there is a need for a proper quantification of fluxes to evaluate critical loads of acidic deposition and abatement strategies of atmospheric pollution [Ruijgrok et al., 1995].

Many studies have suggested that dry deposition can contribute up to 60% of total inputs of sulphur to forest and lake ecosystems [e.g. Likens et al., 1977; Eaton et al, 1978, 1980; Grennfelt et al., 1985; Hultberg, 1985; Lindberg et al., 1986; Brachet, 1987; Norton et al., 1988; Shepard et al., 1990]. This fraction probably changes with distance from major emission source areas [Gibson, 1986] and with different time periods [Likens et al., 1990].

1.10.1. Sources of particles in the atmosphere.

The contribution of anthropogenic sources to particulate $SO_4^{=}$, NO_3^{-} and NH_4^{+} in the atmosphere is mainly the results of emissions of the precursor gases SO_2, NO_x and NH_3 (Table 1.3). In the atmosphere both SO_2 and NO_x are subject to chemical transformation processes by oxidants such as H_2O_2, O_3 and OH radicals, which lead to the formation of H_2SO_4 -containing aerosols and gaseous HNO_3.

Source	Amount	Reference
Total Northern Hemisphere Sulphur	79.0 [Tg(S) y^{-1}]	Graf et al., (1997)
Total Southern Hemisphere Sulphur	22.8 [Tg(S) y^{-1}]	Graf et al., (1997)
Total Global NO_x Emissions	52.6 [Tg (N) y^{-1}]	Seinfeld & Pandis, (1998)
Total Global Ammonia Emissions	53.6 [Tg (N) y^{-1}]	Adames et al., (1999)

Table 1.3. Global Sulphur, NO_x, and Ammonia Emissions into the Atmosphere. For more details see figures 1.6- 9.

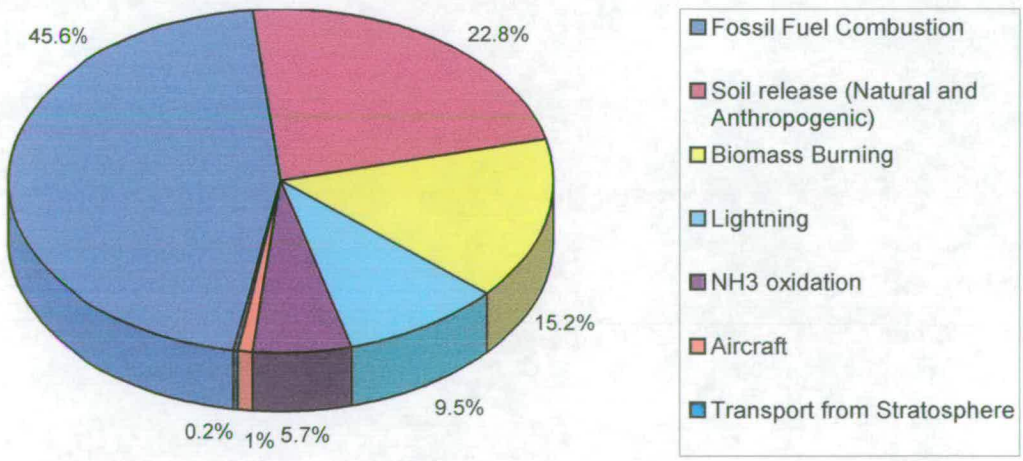

Figure 1.6. Global Emissions of NO_x by source, typical of the last decade. Total Emission 52.6 Tg N y^{-1}[Seinfeld & Pandis, 1998].

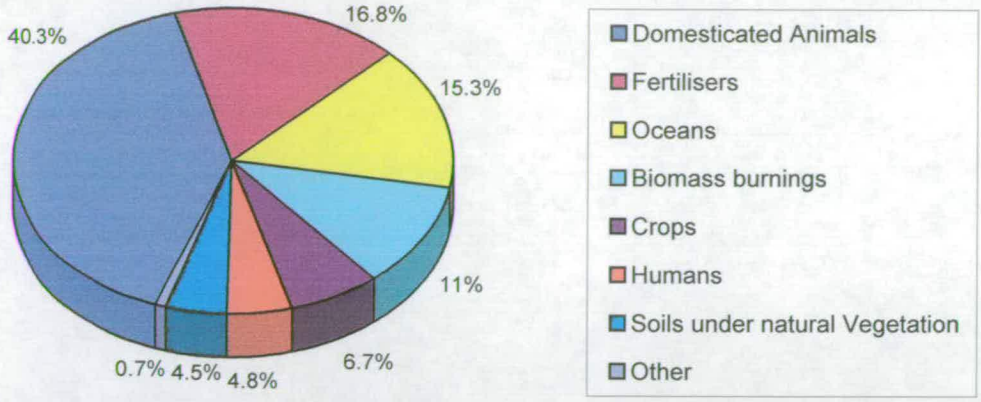

Figure 1.7. Global Ammonia Emissions by source, Total amount 53.6 Tg N y^{-1}, [Adames et al., 1999].

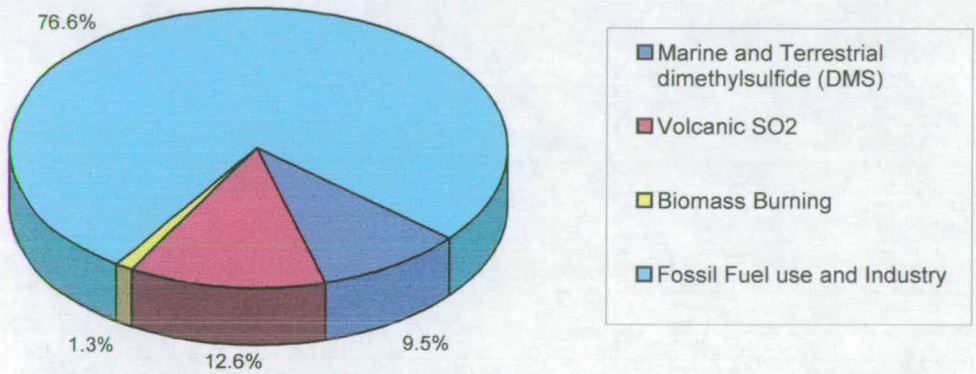

Figure 1.8. Northern Hemisphere Sulphur emissions by source, Total emissions 79.0 Tg S y^{-1}, [Graf et al., 1997].

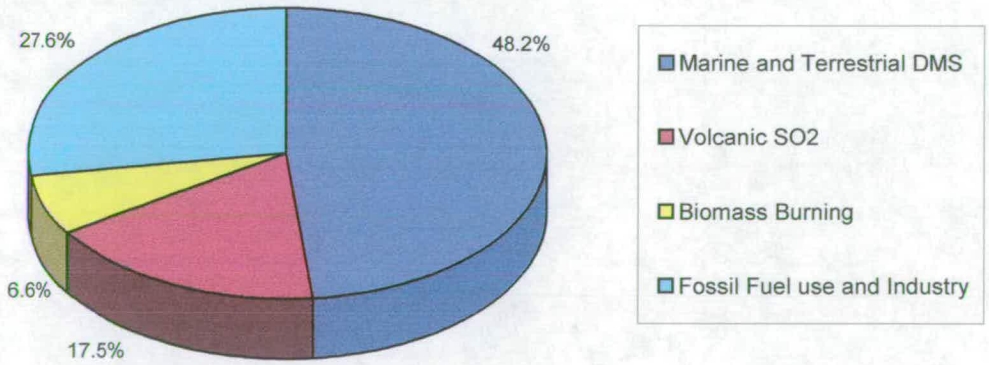

Figure 1.9. Southern Hemisphere Sulphur emissions by source, Total emissions 22.8 Tg S y^{-1}, [Graf et al., 1997].

These two products then may react further under typical European conditions with NH_3, so that both $SO_4^=$ and NO_3^- are in the aerosol phase. This chemical transformation process is generally referred to as "gas-to-particle" conversion giving "secondary aerosols". Gas-to-particle conversion rates are low for SO_2 (of the order of 1-2% per hour). Natural sources can emit aerosols as well as gaseous precursors. For example, sulphur compounds are emitted in both phases from volcanoes and the oceans. Wind erosion of soil is a well known source of large particles, which can be neutralising agents for acidic compounds. The peak of aerosol mass of anthropogenic origin is normally in the 0.1-1 μm range, due to the underlying transformation processes of gaseous precursors [Ruijgrok et al., 1995].

The mass distribution function of anthropogenic $SO_4^=$ aerosol exhibits a log-normal distribution characterised by a mass median diameter (MMD) of 0.48 ± 0.1 μm and geometric standard deviation σ_g of 2.00 ± 0.29 [Whitby, 1978].

Milford and Davidson (1987) reviewed 42 observations of $SO_4^=$ size distributions from continental locations (urban and non-urban). As an average MMD they report 0.52 ±0.23 μm. The same paper shows that 7 distributions from marine areas have an MMD of 2.3 ±1.8 μm. For NH_4^+, Whitby gives an MMD of 0.38±0.08 μm and σ_g=1.95 ±0.38.

1.11. Deposition monitoring.

Deposition monitoring may generally serve at least one of the following purposes, (a) determining ecosystems at risk, (b) evaluating temporal and spatial trends, (c) developing numerical models, or (d) estimating deposition effects.

1.11.1. Wet deposition.

Wet deposition is defined as the processes by which atmospheric pollutants become associated with cloud and precipitation droplets (or particles) and are subsequently delivered to the earth's surface in precipitation. The amount of compounds thus received per unit of area of the surface is defined as the wet deposition. Wet deposition is measured by collecting precipitation in samplers placed in the open field. Precipitation is collected in bottles for time period typically ranging from a day to a months and the sample is analysed for its chemical composition.

Wet deposition is equal to the amount of precipitation per unit area of the funnel of the sampler multiplied by the measured concentration of the pollutant in the

sample. The use of wet-only samplers, in which the funnel is open to the atmosphere only during precipitation events, is widely recommended.

1.11.2. Cloud and fog deposition and dew.

Vegetation may intercept cloud and fog droplets or directly collect water vapour that forms dew. Cloud droplets typically are in the diameter range 10-50 μm and can be efficiently captured by vegetation [Fowler & Cape, 1984; Fowler et al., 1989; Hicks et al., 1989]. Impaction to, and interception by foliage and other obstacles in their path may be very effective. Low-cloud droplets usually contain higher concentrations of pollutants than are found in rain, and cloud water deposition may exceed annual precipitation , especially at high elevation sites [Lovett, 1988]. In Europe at altitudes of 400 m above sea level and above, low clouds are present between 500 and 2000 hours per year [Fowler et al., 1991]. Cloud water deposition might be a significant input mechanism for such regions in Europe. Dew is water vapour condensed on relatively cool bodies (vegetation). Therefore, fresh dew usually contains very low concentrations of pollutants [van Aalst and Erisman, 1991; Romer et al., 1990]. Dew may play an important role in the processes which effect dry deposition estimates.

1.11.3. Dry deposition.

Dry deposition is the processes whereby gases and aerosols are deposited directly from the atmosphere to terrestrial and aquatic surfaces. Dry deposition is governed by the concentration in air, turbulent transport processes in the atmospheric boundary layer, gravitational settling (for sufficiently large particles), molecular diffusion or other transport processes near the surface, the chemical and physical nature of the depositing species, and the capability of the surface to capture or absorb gases and particles [Erisman and Baldocch, 1994].

As an alternative to direct measurement, knowledge of dry deposition process can be used to infer dry deposition fluxes from basic information on routinely measured air concentrations and meteorological parameters. The flux is inferred as a product of ambient concentration of the chemical of interest and its dry deposition velocity. The dry deposition velocity is derived using a multiple-resistance transfer model [Hicks et al., 1987]. The resistance model provides a framework for coupling individual processes, some being surface dependent or pollutant dependent.

The three major resistances are the aerodynamics resistance R_a, a near surface boundary resistance R_b, and the surface resistance R_c. R_c is estimated from dry deposition measurements, from published data, or from use of a more detailed canopy model [Erisman and Baldocch, 1994].

1.12. Deposition in complex terrain.

Results from throughfall measurements and deposition modelling have shown that dry deposition to forest edges is considerably enhanced compared to deposition inside the stand. Dry deposition is found to decrease with distance from the forest edge. The width of the zone with enhanced dry deposition never exceeds five edge heights. The deposition enhancements in forest edges are found to be influenced by stand density, edge aspect and pollution climate [Wiman, 1988; Draaijers and Erisman, 1993]. Until recently, edge effects have not been incorporated in present-day regional scale and receptor oriented deposition models: deposition is treated as a one-dimensional transfer to a homogeneous surface with infinite length. For the Netherlands, approximately 30% higher dry deposition amounts for forest are computed when taking into account edge effects [Pul et al., 1992].

1.13. The application of ^{210}Pb inventories in soil and importance of this study.

In this research, we use the inventories of ^{210}Pb in soil to quantify the enhancement in aerosol deposition by aerodynamically rough canopies relative to short vegetation in low level regions and complete the previous studies carried out by Mourne (1993) and Moghadam (1998). Similar sampling procedures and techniques were used for all of the studies with different goals. The wet deposition in the areas of complex topography was investigated by Mourne and the fluxes of ^{210}Pb at high elevation (~800 m asl). The increased inventories of ^{210}Pb due to seeder-feeder scavenging of orographic cloud were also investigated. Moghadam's investigation was carried out at medium and high elevation sites (>400 m asl). In all of these studies, ^{137}Cs fluxes for soils were measured at the same time as ^{210}Pb flux measurements. Comparisons of the data, together with discussions, are presented in section 4.3 in chapter 4 of this thesis. None of the fluxes at all of these locations had previously been reported and therefore the information obtained here in this study and previous studies (Mourne and Moghadam) are of great value to complete the

^{210}Pb database. Hence the results from this study provide a chance to further interpret the earlier data onto capture of hill cloud by forest using ^{210}Pb.

The specific goals of the current study are as follow:

To obtain the concentrations and fluxes of ^{210}Pb and ^{7}Be in air and rain measured in Edinburgh (Latitude 55° 56′ N, Longitude 3° 9′ W).

Use the obtained concentrations and fluxes of ^{210}Pb and ^{7}Be to estimate the dry deposition of these isotopes at this region.

Investigate the meteorological effects on the air and rain concentrations of ^{210}Pb and ^{7}Be.

Measure the inventories of atmospheric derived ^{210}Pb and ^{137}Cs to the Rothamsted soil.

Finally, to estimate the long term (>10 years) average deposition rate of aerosol onto vegetation using ^{210}Pb inventory methods.

This method is fully discussed in chapter four of this thesis and conclusions are drawn in chapter five. All errors in this study are root mean square (rms) $\pm\sigma$ counting errors unless stated otherwise.

Chapter 2

2. Sampling methods and measurements.

In this chapter, the experimental methods and measuring procedures are reported. The sampling program is described in three different sections, surface air, rainfall and soil. Although the sampling method for each section is different, the radioactivity measuring techniques (gamma-ray spectrometry) are similar. The determination of the detector relative efficiencies and calibrations, electronic set up, sample collection methods, sample preparation, etc., are explained in the following sections of this chapter.

2.1. Surface air measurements.

In order to measure ^{210}Pb and ^{7}Be concentrations in surface air, analyses were carried out on Gelman type A/E Glass Fibre filters ($8''x10''$) that had been used in a high volume (HV) air sampler (model GMWL-2000 H) installed on the roof of James Clark Maxwell Building (JCMB) in the King's Buildings (KB) area at Edinburgh University, (Latitude 55^{o} 56′ N, Longitude 3^{o} 9′ W), about 30 meters above the ground (Fig. 2.1).

Different experiments were carried out to determine the best arrangements for the collection time of samples and the best counting procedures. The High Volume air sampler was used for different time intervals of 24, 48, 72, 98, 148, 212, and 240 hours. Each of the filters were counted separately and then groups of filters were compressed to determine the effect of the different geometries and attenuation of gamma-rays in the filters. The reason for compressing the filters was that at the time we were concerned that collecting one filter a week would cause it to block with aerosols and thus change the flow rate. At first, two filters were compressed, (in specially designed holder), then three, etc. until six filters were compressed together. The compressed filters were placed in a 70.6 mm holder.

The filter compression was carried out to have more aerosols in the holder at any one time to improve the statistical accuracy. However, the use of more compressed filters, (e.g. 6 filters, thickness 6 mm), resulted in about 18 % of the

Figure 2.1. The high volume air sampler is located on the roof of JCMB.

gamma rays not reaching the detector, of which about 6 % was due to attenuation in the filter and about 12 % to the extra 6 mm distance of the outer aerosols from the detector. Based on these results, it was decided to reduce the distance of the aerosols from the detector. Furthermore, when we were able to measure the flow rate at the beginning of sample collection and after a week of collection, it was found that the flow rate did not change significantly in this period. Therefore, it was decided to sample at about weekly intervals, press the filter to a pellet, 48 mm in diameter and 3.7 mm thick, place it into the sample holder (48 mm in diameter), and measure its gamma radiation. This gives good statistical accuracy, less attenuation and less geometry loss.

The flow rate of the high volume air sampler was measured by using an air velocity meter (model 1650) to measure the face velocity of air passing through the filter. The measurements were carried out at many different points across the area of

the filter and the averaged value was taken to be the speed of air flow over the whole filter. Knowing the area of each filter, the rate of air volume through each filter was calculated by multiplying the area by the speed of the flow. The air speed measurements were made for each filter separately and found to be between 0.89 and 2.79 m^3 min^{-1} over the total 100 measured surface air samples.

2.1.1. Filter and site selection for surface air measurements.

Investigations for the site selection and equipment set up were carried out during November 1996. From the literature and the past sampling programs, it was decided to choose the roof of JCMB for the sampler's location. Although Whatman-41 glass-fibre filter have been mostly used previously, Gelman glass-fibre filters, type A/E, were chosen for this work. The Gelman filters were easily broken up into particles by crushing them inside a specially made holder for this purpose (the holder was made in the physics workshop). On the other hand, the Whatman filters could not be easily broken up so they had to be folded or cut up to fit the holder. In some cases maybe only a part could be used for gamma-spectrometry. Where Whatman filters were used (e.g. Turekian et al. 1989), the sampler's running time was more than a week to collect enough ^{210}Pb aerosols for reasonable statistical errors. This was because only part of the filter could be used. For our measurements, we used all the exposed area of the filter and in a week of running time we had enough aerosol on the filters to have a good counting statistical error (about 5% for ^{210}Pb and 1% for ^{7}Be), even for oceanic air masses. Another advantage of using Gelman filters is the reproducible geometry for each filter (48 mm in diameter and 3.7 mm thickness), which reduces the systematic errors. Furthermore, Turekian et al. (1989) have reported the capture efficiency of Whatman and Gelman filters for sub-micron aerosols in the marine boundary layer to be 80 % and 90+ %, respectively.

A pellet from a filter was made, placed in a holder and its gamma-radiation determined by the NGC detector (see section 2.5). The concentration of ^{210}Pb and ^{7}Be was then determined for each filter. The collection time was mostly about one week for each sample.

It was attempted to measure the air flow speed at the beginning and the end of each sampling period, for all of the filters. This was found to be very difficult for a few of them. The main difficulty was due to high winds. Only when weather permitted has this been done. Because of the very low fluctuations observed, about

1% of the flow rate (flow rate was measured during the sampling period, i.e. if the sampling period was 1 week at the start and the end of that 1 week), the flow rate was assumed to be constant through the sampling period for the other samples. The speed was always measured when new brushes were fitted (about every two weeks), and when a new motor blower was fitted (in total, 5 motor blowers were used).

The sampling programme was started on 4th of December 1996 and ended on 31st of January 1999. In total 100 samples were collected and measured. The results of these measurements are reported in chapter three. Mean working life time for each motor blower was found to be about 5 months and the mean life time of each pair of brushes was about two weeks.

2.1.2. Background radiation measurements for surface air.

The background radiation to the detector has been reduced but it can not be completely eliminated. The measured background radiation was mostly due to the shielding materials and x-rays, mainly at low energies about 29, 46.5, 64, 93, and 186 keV.

It is important to carefully determine the background in the 46.5 keV energy region since ^{210}Pb gamma emission is at this energy. The measurement of the background radiation was carried out with an empty holder and a blank filter compressed as a pellet in the holder. No contribution was observed from the pellet within statistical errors. These measurements were done at least four times and the averaged values were used for the background radiation of a holder and a blank filter. This value has to be subtracted from the measured active filter value to get the absolute aerosol contribution to each sample.

2.1.3. Gamma-spectroscopy of the surface air samples.

Figure 2.2 shows plot of gamma-spectrometry for a typical filter measured immediately after the sampling period and five days later. We concluded that most peaks are from some short lived isotopes which decay almost completely after about four days. The peak with the highest intensity was at 238.6 keV. By measuring the count rate at this energy and plotting the values against time on a semi-log paper, the half-life of the associated isotope was found to be about 10.6 hours. From this half-life and the other energies [i.e. 115, 300, and 415 keV], it was established that the isotope involved can only be ^{212}Pb, a grand-daughter of ^{220}Rn from the thorium series

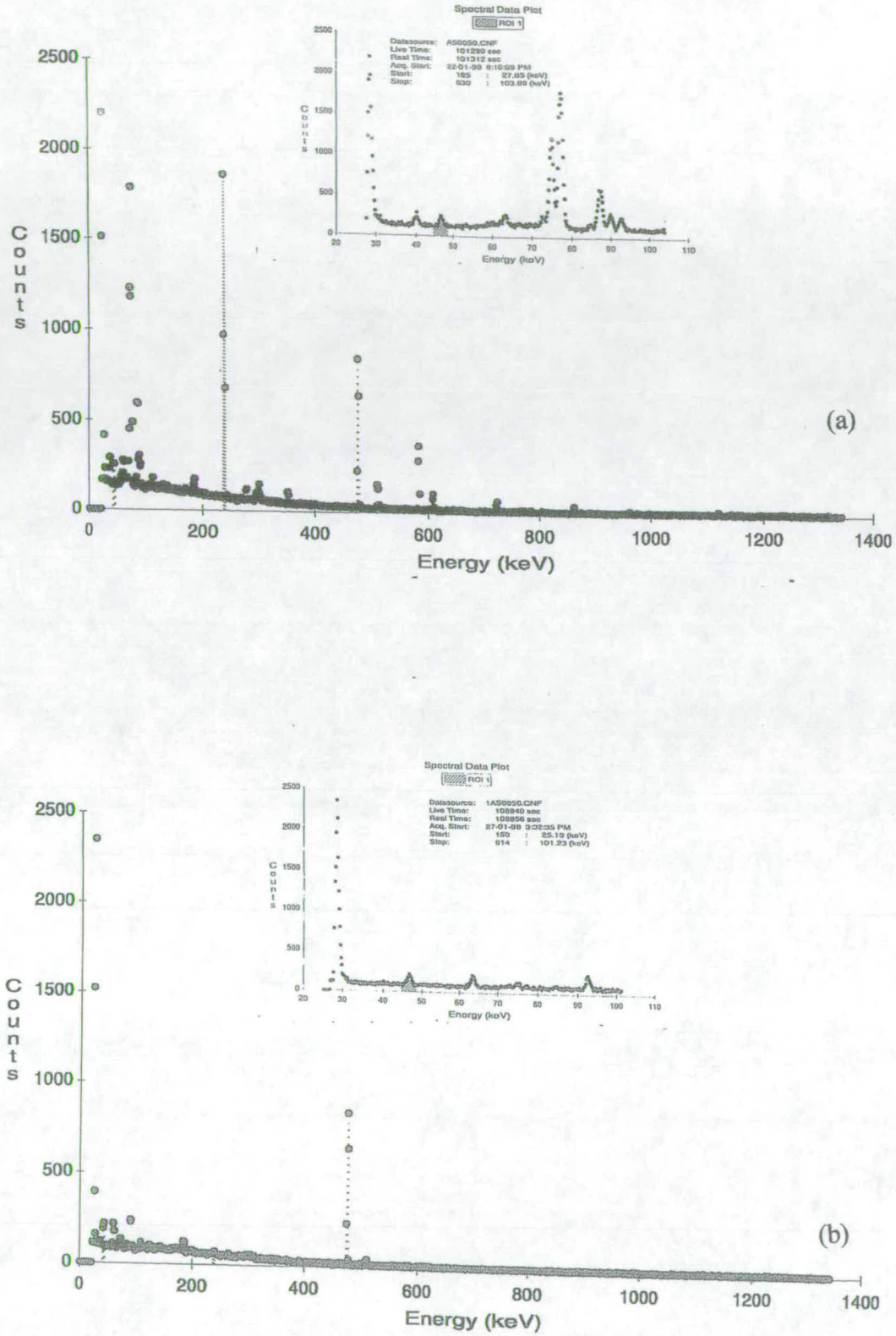

Figure 2.2. Plot of a gamma ray spectrum for the same filter measured (a)immediately after the sampling period and (b)five days later.

of naturally occurring radioactive decay (figure 2.3).

Hence, to reduce the effect of these decays, it was decided to measure the activity of the filters about five days after the sampling period was completed and for ^{7}Be (477.5 keV), correcting to the last date of collection. This reduced the error in the ^{210}Pb measurements by 50 %.

Because of the short half-life of ^{220}Rn, it could be assumed ^{212}Pb is produced from local soils and it has a remote chance of being transported from far distance.

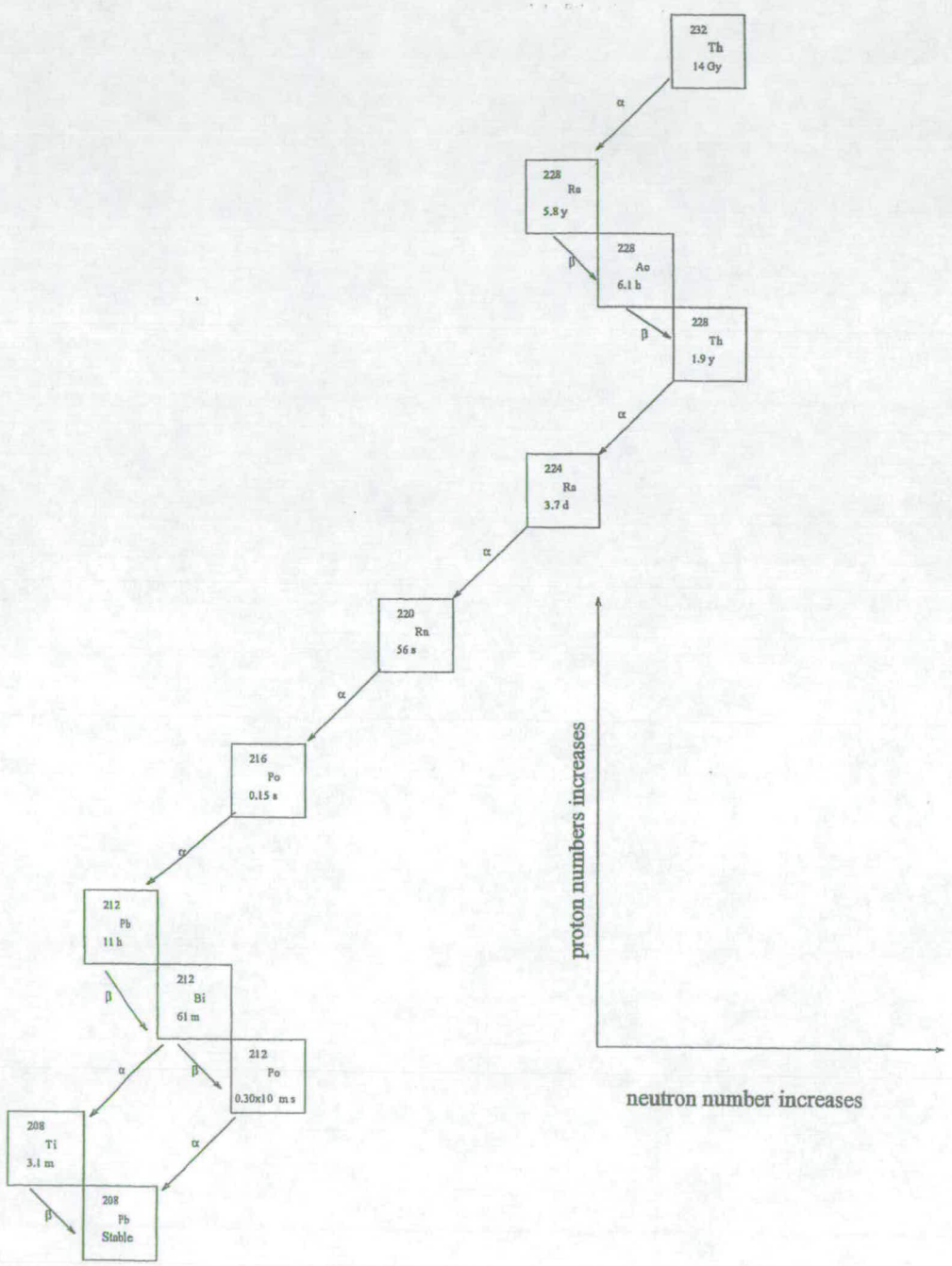

Figure 2.3. The thorium series of naturally occurring radioactive decays.

2.2. Rain measurements.

Since most atmospheric aerosols are ultimately scavenged by rain, a set of collection trays, total area of 0.55 m^2 were prepared and set, to investigate the concentrations of ^{210}Pb and ^{7}Be in rain (figure 2.4). The collected rain was transferred into large beakers, some ammonia solution (min 28%, Analytical Reagent), was added to raise the solution's pH to about 11. The pH was measured by a pH meter 7010, Amphel gel-fitted pH electrode. The pH meter was calibrated before each measurement using three buffers at pH 4.00 ± 0.02, 7.00 ± 0.02 and 9.20 ± 0.02.

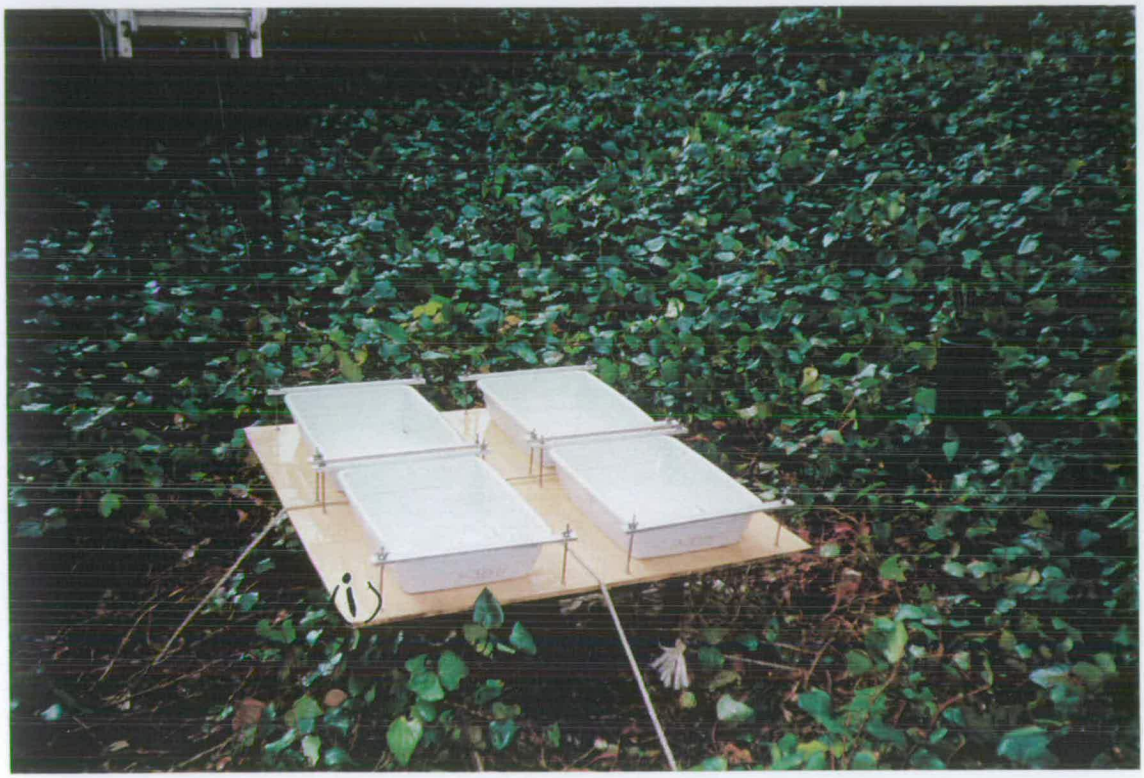

Figure 2.4: The rain collection site, (i) four collection trays at fixed position, (ii) rain gauge.

Some lead- and aluminium-nitrate, 20-40 cm^3, depending on the volume of the rain, was added to the total solution and left for at least seven days. ^{210}Pb and ^{7}Be aerosols precipitate in the solution within this period. Lead-nitrate standard solution (concentration 1000±2 mg l^{-1}) and Aluminium-nitrate[$Al(NO_3)_3$ $9H_2O$] concentration equal to 1001 ± 2 mg l^{-1} were used.

The total volume of the solution was passed through a 15 cm diameter, Whatman Fibre Glass filter type GF/C. Then the filter was left to dry at the room temperature before it is pressed to a pellet (48 mm in diameter and about 1 mm

thick). Finally the pellet was placed into a holder for gamma-spectrometry. The sampling procedures have been taken from Clifton (1991).

2.2.1. Method and measuring procedures for rain samples.

First, the method used by Clifton (1991) was adopted and then some changes were made to it, due to the following reasons. In the Clifton method, at the start of the rain collection, (about 1 cm in depth), 1 molar nitric acid is added to the collection trays. The reason for this was explained, by Clifton, to be for preventing the precipitated aerosols from being blown away, if the precipitation evaporates and the collection trays get dry. To raise the pH level to the required value, (about 11), we had to use a large amount of ammonia solution. Following consultation with researchers at the chemistry department it was discovered that nitric acid is not needed for any reaction to take place. Discussion with Mr Clifton at the same time revealed that nitric acid was used for evaporation reasons only, and in his present research he is using detergents instead of nitric acid. The weather in the Edinburgh area never gets dry enough to evaporate the total solution in the collection trays. As a check on the need to use nitric acid two of the collection trays were set without nitric acid while the other two contained nitric acid. After the same time of collection, their activities were the same. For the above reasons, the Clifton method was revised and the collection was carried out without nitric acid.

The first objective was to collect a sample for each precipitation event and determine the activity associated with that sampling period. However, in practice this was not possible for many, reasons such as the frequency of the rain, small volume of rain, small collection trays area. Hence, this procedure was soon changed and the total precipitation was collected for each month and considered as one single sample.

In total 32 samples were collected during the period of October 24th, 1997 to January 31st, 1999. To measure the precipitation volume for each sample, a 15 cm standard rain gauge was prepared and set beside the collection trays.

2.2.2. Site selection and background radiation measurements for rain samples.

An open area in the KB on the court yard adjacent to JCMB was chosen and prepared for the rain collection. A board of 1 m^2 in area was fixed on a stall 0.5 meter high above the ground. Four collection trays of total collection area 0.55 m^2 were mounted on the board and held firmly by 8 aluminium rods over their edges and

tightened with screws. The board was held to a fixed position on the ground by two ropes passing over it and pinned into the ground. The trays were washed and rinsed always before each precipitation collection.

The collected precipitation was transferred to large beakers. After chemical treatments and filtering the total volume of the collected rain, the filter was dried over night the room temperature and the following day the filter was crushed in the same device and with the same procedures described in section 2.1.2 for air samples and the pellet was transferred to a 48 mm holder for gamma-spectroscopy. The background radiation for a blank filter with a holder was determined. Most of the peak energies are at about 29, 46.5, 64, 93.5, and 186 keV, which are mostly from the shielding materials. In our gamma-spectroscopy the peak at 46.5 keV is the most important one to measure accurately. This measured value is then calculated as disintegrations per second (dps), subtracted from the measured value for each filter at this energy band to find out the absolute value of ^{210}Pb in the filter.

The measured value for the ^{7}Be activity in the filter was decay corrected to the last date of collection for each filter using the radioactive decay formula in section 2.7.2. The rain results are reported in chapter three of this thesis.

2.3. Soil measurements.

Because organic matter in soils retains ^{210}Pb quantitatively, many soils act as efficient integrating collectors of the atmospheric deposition of ^{210}Pb [Turekian et al., 1977; Nozaki et al., 1978]. If the soil is in steady state with respect to ^{210}Pb, the rate of loss of ^{210}Pb by radioactive decay is exactly equal to the rate of atmospheric input. Measuring the activity of atmospherically derived ^{210}Pb in a soil core is therefore equivalent to measuring the time-averaged aerosol deposition rate [Graustein and Turekian, 1983]. When scavenged from the atmosphere along with carrier aerosols, ^{210}Pb is retained by the organic-rich surface horizontal soil which acts as an efficient integrating collector [Lewis 1977].

Forest soils are generally well suited for ^{210}Pb deposition rate measurements [Graustein and Turekian, 1983]. We measured the excess ^{210}Pb (^{210}Pb-^{226}Ra) in each section of the core. We assumed that all of the atmospherically deposited ^{210}Pb has been measured when we reach a depth at which there is no excess ^{210}Pb.

Gamma spectroscopy allows us to measure ^{226}Ra and ^{137}Cs at the same time as ^{210}Pb. It is simple non-destructive and a relatively inexpensive technique. Chemical processing used before is destructive, time consuming and relatively complex [Joshi 1987]. Procedure used here has a great advantage in that it does not require the leaching and radiochemical separation of ^{210}Pb or ^{210}Po.

2.3.1. Site selection.

In order to assay the ^{210}Pb standing crop in a soil profile, two criteria for site selection must be satisfied. First, the site should be relatively flat to diminish down-slope losses of the soil by erosion. Second, the site should be free of any natural or man-made disturbances during the last 100 years (roughly 5 half-lives of ^{210}Pb) [Nozaki et al., 1978]. ^{210}Pb total inventory in undisturbed soils may be used as a measure of total aerosol deposition averaged over about 30 years, approximately the mean nuclear life time (30.2 years). Recently the technique has been applied to quantify the total deposition of pollutants in areas of complex topography [Mourne, 1993; Fowler et al., 1995; Branford et al., 1998; Moghaddam, 1998].

On the bases of the above criteria, soil samples were collected from locations at Rothamsted experimental station in Harpenden, Hertfordshire, England during Feb. 1998. By driving a 10 cm-diameter, 25 cm thick, corer in to the soil, five sets of soil samples were obtained at each site (in total 10 sites were sampled), from 2

woodlands, (Geescroft and Broadbalk), and 3 adjacent open areas. At least one core at each site was driven to a depth of 20 cm. In total 50 samples were collected and were divided to 150 sub-samples. The details of these sub-samples are in section 2.3.5.

2.3.2. Self absorption in soil samples.

Analysis of ^{210}Pb in sediment samples can involve leaching or dissolution of the samples, followed by chemical purification and counting of either the β–particles emitted by the daughter, ^{210}Bi, or the α–particles emitted by the grand daughter, ^{210}Po. Direct analysis of ^{210}Pb is also possible [Gaggeler et al., 1976], by measuring 46.5 keV gamma-rays emitted in approximately 4% of the decays of the nuclide [Kocher, 1981]. The principal difficulty in applying gamma-ray analysis to ^{210}Pb measurements in whole sediment samples, is that self-absorption of the radiation by the sample is relatively difficult to correct because the attenuation coefficient for the 46.5 keV gamma-rays is highly depended on sample composition. As a result, the relative gamma ray emission from sediment samples varies widely depending on mineralogy. This requires either that the composition be accurately known or that some method to correct for self-absorption be used. We used a direct measurement of ^{210}Pb gamma-ray transmission to determine the absorption characteristics for each sample and to correct for self attenuation [Cutshall et al., 1983].

For a transmitted beam of gamma-rays the attenuation follows the familiar equation,

$$T = I\, e^{-\mu\rho x} \qquad \text{.... (2.1)}$$

in which T and I are the attenuated and unattenueted beam intensities, μ is the total attenuation coefficient ($cm^2\ g^{-1}$), ρ is the material density ($g\ cm^{-3}$) and x is the path length (cm). The self absorption equation is also well known,

$$O = A\,[(1-e^{-\mu\rho x})/\mu\rho x] \qquad \text{.... (2.2),}$$

where O is the attenuated sample output and A is the sample photon emission rate. To obtain a correction factor for self-absorption, we measure T and I and compute A/O from,

$$(A/O) = [\ln(T/I) / (T/I - 1)] \quad \text{.... (2.3).}$$

The result is multiplied by the measured sample output to estimate the unattenuated output [Cutshall et al. 1983].

The Cutshall technique was performed for all of the individual soil samples, using ^{210}Pb, ^{133}Ba and ^{137}Cs radioactive standard point sources, for emitted energies of 46.5 keV, 356 keV and 661.6 keV, respectively, to measure the attenuation at ^{210}Pb, ^{214}Pb and ^{137}Cs γ-energies.

The values obtained were about, 17 - 89 %, 8 - 40 %, and 3 - 12 % for ^{210}Pb, ^{214}Pb and ^{137}Cs, respectively. The density of the soils varied from 402 to 1382 kg m^{-3}. The lowest and highest values were for R5Ea and R3Ec, respectively.

2.3.3. Background radiation measurements for soil samples.

The soil sample gamma-spectroscopic studies were all carried out using a REGe detector, (see section 2.5). As described in the previous sections, similar procedures as for surface air and rain samples were carried out to measure the background radiation due to the detector surroundings.

The holders used for this part were made from perspex. They were 70.6 mm in diameter by 26.5 mm deep and had a thin wall (0.4 mm). After calibration and set up of the detector, the background radiation was measured by placing an empty holder into the detector and recording the background radiation. This was done for five different holders and their results were averaged. The values at the energies of 46.5 and 351.9 keV were accurately measured and recorded as the detector's background for this geometry. Actual background radiation contributing to the total background value measured for each sample was calculated knowing the percentages due to attenuation and the percentage due to surrounding background. These values were subtracted from the total values to find out the actual contribution from the soil.

2.3.4. Soil sample preparation and measuring procedure.

The sample preparation was carried out at the Scottish Agricultural College (SAC). They were weighed, air dried at 30° C, reweighed, ground and sieved with a 2 mm mesh screen. Stones above 2 mm were discarded on the assumption that such close systems are in radioactive equilibrium with respect to ^{226}Ra and ^{210}Pb, and do not contain any atmospherically derived ^{137}Cs. The samples of remaining material were re-weighed and stored in plastic bags, ready for subsequent radioanalysis by gamma-ray spectrometry systems at the Nuclear Physics Laboratory of Edinburgh University.

Portions of each sub-sample were placed in sample holders and left to come into equilibrium in readiness for the gamma-spectroscopy measurements. The sub-sample was sealed and left for at least 15 days before its gamma-radiation was measured. The measuring time for these samples was varied between 19 and 63 hours in order to reach a reasonable statistical error for ^{210}Pb. The variation of the time depended on the activity of the sample. The low time was normally for the top 5 cm horizon of each sample (i.e. section "a"), and the longer time corresponded to the lowest section of the core (i.e. section "c"). At the end of each gamma-spectroscopic the attenuation correction for each sample was carried out (procedure for which is described in section 2.7.2). The values were corrected for the sample's total weight and for the time decay are corrected to the date of collection. The total activity of each sample was calculated, summed over the total core, and averaged over the site, to find the total inventory for each site.

2.3.5. Site details.

In total from 10 sites, 50 samples were collected and divided to 150 sub-samples from 3 open areas and two woodlands. All of the samples were taken using a 10 cm diameter and 25 cm long corer, as shown in Figure 2.5. The details of each site and sample are given in the following pages. Figures 2.6 to 2.16 are photographs of the sites and overhead trees.

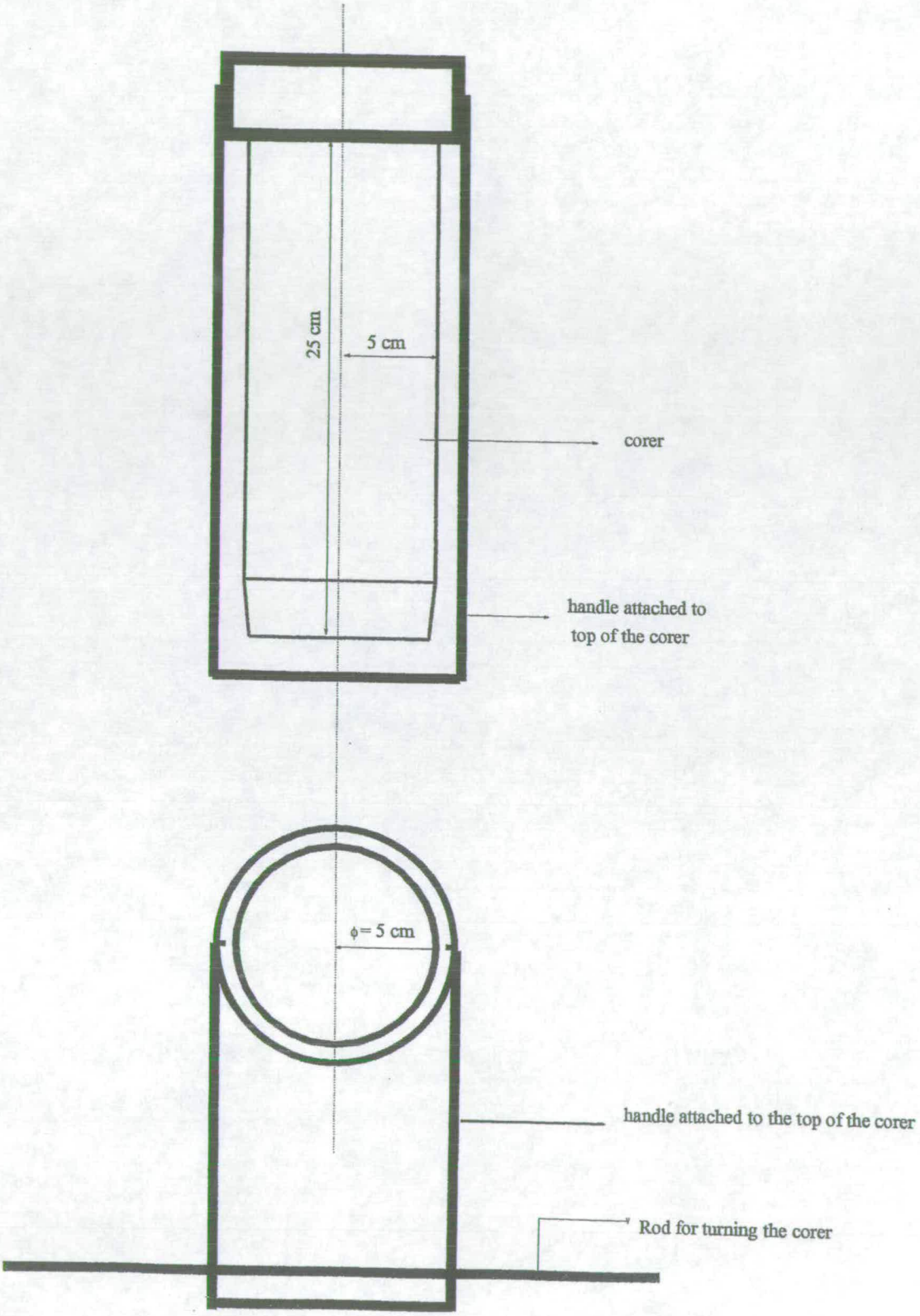

Figure 2.5. Schematic diagram of the corer. Top: Side view, handle down. Bottom: Top view, handle out to the side.

Figure 2.6 . In the middle of the photo is site R1 and near the far left is site R2.

Figure 2.7. A view of the edge of the Geescroft forest (R3 to R6).

	sub-samples	depth of each section (cm)	density of each sub-sample (g cm^{-3})
Site one (R1) Open field covered with grass undisturbed for about 50 years about 300 meters north from the edge of the Geescroft forest.	R1Aa	0 - 5	0.630
	R1Ab	5 - 10	0.928
	R1Ac	10 - 20	1.151
	R1Ba	0 - 5	0.768
	R1Bb	5 - 10	1.112
	R1Bc	10 - 15	1.233
	R1Ca	0 - 5	0.768
	R1Cb	5 - 10	1.063
	R1Cc	10 - 20	1.221
	R1Da	0 - 5	0.981
	R1Db	5 - 10	1.138
	R1Dc	10 - 16	1.125
	R1Ea	0 - 5	0.747
	R1Eb	5 - 10	1.068
	R1Ec	10 - 15	1.154
	sub-samples	depth of each section (cm)	density of each sub-sample (g cm^{-3})
Site two (R2) Open field covered with uncut grass undisturbed for about 50 years about 320 meters north from the edge of the Geescroft forest.	R2Aa	0 - 5	0.677
	R2Ab	5 - 10	1.011
	R2Ac	10 - 16	1.157
	R2Ba	0 - 5	0.657
	R2Bb	5 - 10	1.036
	R2Bc	10 - 16	1.117
	R2Ca	0 - 5	0.704
	R2Cb	5 - 10	1.105
	R2Cc	10 - 20	1.250
	R2Da	0 - 5	0.783
	R2Db	5 - 10	1.031
	R2Dc	10 - 16	1.134
	R2Ea	0 - 5	0.803
	R2Eb	5 - 10	0.988
	R2Ec	10 - 14	1.062
	sub-samples	depth of each section (cm)	density of each sub-sample (g cm^{-3})
Site three (R3) Geescroft forest 2 m from the edge of the forest 50° NE in the forest and normal to the edge.	R3Aa	0 - 5	0.713
	R3Ab	5 - 10	1.121
	R3Ac	10 - 15	1.070
	R3Ba	0 - 5	0.981
	R3Bb	5 - 10	1.217
	R3Bc	10 - 15	1.212
	R3Ca	0 - 5	0.937
	R3Cb	5 - 10	1.184
	R3Cc	10 - 15	1.275
	R3Da	0 - 5	1.130
	R3Db	5 - 10	1.224
	R3Dc	10 - 17	1.367
	R3Ea	0 - 5	1.039
	R3Eb	5 - 10	1.262
	R3Ec	10 - 20	1.382

Figure 2.8. The edge of the Geescroft forest (site R3) and the tops of the trees for this site.

	sub-samples	depth of each section (cm)	density of each sub-sample (g cm^{-3})
Site four (R4) Geescroft forest about 5 m from the edge at position 80° NE in the forest and normal to the edge.	R4Aa	0 - 5	0.698
	R4Ab	5 - 10	1.000
	R4Ac	10 - 15	1.113
	R4Ba	0 - 5	0.677
	R4Bb	5 - 10	1.137
	R4Bc	10 - 14	1.193
	R4Ca	0 - 5	0.933
	R4Cb	5 - 10	1.185
	R4Cc	10 - 15	1.241
	R4Da	0 - 5	0.782
	R4Db	5 - 10	1.166
	R4Dc	10 - 20	1.256
	R4Ea	0 - 5	0.722
	R4Eb	5 - 10	1.102
	R4Ec	10 - 18	1.173
	sub-samples	depth of each section (cm)	density of each sub-sample (g cm^{-3})
Site five (R5) Geescroft forest about 10 meters from the edge of the forest facing 80° NE in the forest and normal to the edge.	R5Aa	0 - 5	0.693
	R5Ab	5 - 10	1.269
	R5Ac	10 - 20	1.008
	R5Ba	0 - 5	0.724
	R5Bb	5 - 10	1.230
	R5Bc	10 - 15	1.303
	R5Ca	0 - 5	0.635
	R5Cb	5 - 10	1.063
	R5Cc	10 - 19	1.303
	R5Da	0 - 5	0.651
	R5Db	5 - 10	1.125
	R5Dc	10 - 16	1.271
	R5Ea	0 - 5	0.402
	R5Eb	5 - 10	0.731
	R5Ec	10 - 17	1.133
	sub-samples	depth of each section (cm)	density of each sub-sample (g cm^{-3})
Site six (R6) Geescroft forest about 20 meters from the edge of the forest facing 85° NE in the forest and normal to the edge.	R6Aa	0 - 5	0.802
	R6Ab	5 - 10	1.155
	R6Ac	10 - 16	1.217
	R6Ba	0 - 5	0.759
	R6Bb	5 - 10	1.209
	R6Bc	10 - 17	1.223
	R6Ca	0 - 5	0.817
	R6Cb	5 - 10	1.023
	R6Cc	10 - 17	1.255
	R6Da	0 - 5	0.827
	R6Db	5 - 10	1.057
	R6Dc	10 - 20	1.167
	R6Ea	0 - 5	0.824
	R6Eb	5 - 10	1.145
	R6Ec	10 - 18	1.235

Figure 2.9. Five metres from the edge of the Geescroft forest (site R4), and the tops of the trees for this site.

Figure 2.10. Ten meters from the edge of the Geescroft forest (site R5), and the tops of the trees for this site.

Figure 2.11. Twenty meters from the edge of the Geescroft forest (site R6), and the tops of the trees for this site.

	sub-samples	depth of each section (cm)	density of each sub-sample (g cm^{-3})
Site (R7). Open field undisturbed for more than 100 years. Only the grass has been cut and left on the land. It is situated about 50 meters north of the Broadbalk woodland and about 15 meters south from 3 trees.	R7Aa	0 - 5	1.001
	R7Ab	5 - 10	1.177
	R7Ac	10 - 15	1.195
	R7Ba	0 - 5	1.023
	R7Bb	5 - 10	1.185
	R7Bc	10 - 20	1.268
	R7Ca	0 - 5	1.097
	R7Cb	5 - 10	1.187
	R7Cc	10 - 16	1.303
	R7Da	0 - 5	0.972
	R7Db	5 - 10	1.069
	R7Dc	10 - 17	1.265
	R7Ea	0 - 5	1.014
	R7Eb	5 - 10	1.173
	R7Ec	10 - 18	1.182
	sub-samples	depth of each section (cm)	density of each sub-sample (g cm^{-3})
Site eight (R8). Broadbalk woodland about 30 meters wide, in the middle of the canopy. Almost all ash trees.	R8Aa	0 - 5	1.086
	R8Ab	5 - 10	1.166
	R8Ac	10 - 20	1.242
	R8Ba	0 - 5	1.019
	R8Bb	5 - 10	1.173
	R8Bc	10 - 17	1.200
	R8Ca	0 - 5	1.098
	R8Cb	5 - 10	1.111
	R8Cc	10 - 17	1.193
	R8Da	0 - 5	1.025
	R8Db	5 - 10	1.127
	R8Dc	10 - 16	1.187
	R8Ea	0 - 5	1.106
	R8Eb	5 - 10	1.211
	R8Ec	10 - 15	1.258
	sub-samples	depth of each section (cm)	density of each sub-sample (g cm^{-3})
Site nine (R9). Broadbalk woodland about 30 meters wide, at the edge of the forest on the west side. Almost all ash trees.	R9Aa	0 - 5	0.907
	R9Ab	5 - 10	1.090
	R9Ac	10 - 20	1.187
	R9Ba	0 - 5	0.803
	R9Bb	5 - 10	1.073
	R9Bc	10 - 19	1.175
	R9Ca	0 - 5	0.992
	R9Cb	5 - 10	1.157
	R9Cc	10 - 17	1.177
	R9Da	0 - 5	0.950
	R9Db	5 - 10	1.129
	R9Dc	10 - 15	1.141
	R9Ea	0 - 5	0.907
	R9Eb	5 - 10	1.041
	R9Ec	10 - 15	1.129

Figure 2.12. The open field near the Broadbalk forest (site R7).

Figure 2.13. Side view of the Broadbalk forest from site R7.

Figure 2.14. In the middle of the Broadbalk forest (site R8), and the view of the tops of the trees for this site.

Figure 2.15. On the west side of the Broadbalk forest at the edge (site R9), and the tops of the trees for this site.

	sub-samples	depth of each section (cm)	density of each sub-sample (g cm^{-3})
Site ten (R10). Broadbalk woodland about 30 meters wide, on the east side of the canopy close to the edge. Almost all the trees are ash.	R10Aa	0 - 5	0.983
	R10Ab	5 - 10	1.100
	R10Ac	10 - 19	1.210
	R10Ba	0 - 5	1.027
	R10Bb	5 - 10	1.170
	R10Bc	10 - 20	1.199
	R10Ca	0 - 5	1.104
	R10Cb	5 - 10	1.192
	R10Cc	10 - 15	1.133
	R10Da	0 - 5	1.032
	R10Db	5 - 10	1.093
	R10Dc	10 - 16	1.117
	R10Ea	0 - 5	1.071
	R10Eb	5 - 10	1.163
	R10Ec	10 - 17	1.194

Figure 2.16. The east side of the Broadbalk forest at the edge (site R10), and a view of the tops of the trees for this site.

2.4. Specifications of the detectors used.

Direct quantitative measurement of many radionuclides in bulk environmental matrices is now possible by gamma-spectrometry using a modern computer assisted spectral interpretation. The detector resolution becomes extremely valuable for the identification and precise measurement of radionuclides in these samples. Semiconductor germanium (Ge) detector systems are especially well suited in this respect because of their ability to resolve close lying peaks and to detect weak sources of discrete energies when superimposed on a broad continuum [Knoll, 1989].

The usefulness of semiconductors for radiation measurements stems from the special properties created at a junction where *n*- and *p*-type semiconductors are brought into contact to form a single system with its own characteristics. The reverse-biased *n-p* junction constitutes an attractive radiation detector. The depletion region is the active volume of the detector. Electron-hole pairs produced there by radiation can be collected swiftly and efficiently [Tsoulfanidis, 1989; Knoll, 1989].

Two high purity germanium (HPGe) detectors were used for gamma spectrometry in this study. For soil samples, a Reversed-Electrode Coaxial Germanium (REGe) manufactured by Canberra, 4.4 cm in diameter by 4.3 cm length, with a thin Be window (0.5 mm) is used. The detector relative efficiency is 12.9% at 1.33 MeV [relative to a 7.62 x 7.62 cm NaI (Tl) scintillation detector, at a source-detector spacing of 25 cm], and its FWHM resolution is 865 eV at 122 keV. The second detector (NCG), manufactured by Detector Systems GmbH (DSG), also has a coaxial configuration. It is 4.4 cm in diameter, has a length of 3.8 cm and has a relative efficiency of 11.1%. The resolution is 810 eV at 122 keV. The second detector was used primarily for surface air and rain samples.

2.5. Electronics and data acquisition.

Both Ge detectors included a cryostat and pre-amplifier, detector bias supply,

linear amplifier, analog-to-digital converter (ADC), multi-channel storage of the spectrum and a micro-processor with display screen, printer and data storage facilities and finally a background-radiation shield, which surrounds the detector.

Figure 2.17 shows a schematic diagram of the gamma spectrometer systems; this scheme is typical of most gamma ray spectrometer.

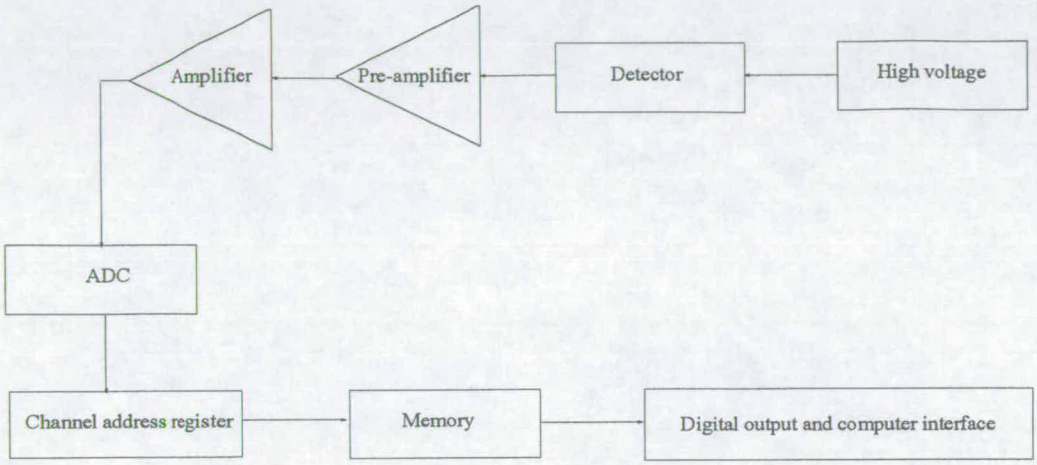

Figure 2.17. Schematic diagram of a typical gamma-spectrometer.

Figure 2.18 shows the set up of the gamma-detectors, including the shielding, computers, electronics and the printer. The cryostat consists of a reservoir or Dewar containing the cooling medium and a vacuum-chamber housing the detector. Liquid nitrogen (LN_2) is the most common medium for detector cooling, and was used for the measurements reported here. The cryostat used with the REGe detector is a dipstick type. The detector is mounted at the end of a copper cooling-finger, which conducts the liquid nitrogen temperature from the reservoir to the detector. An integral type cryostat has been used in conjunction with the second Ge detector. In this case, the detector chamber is permanently attached to the Dewar.

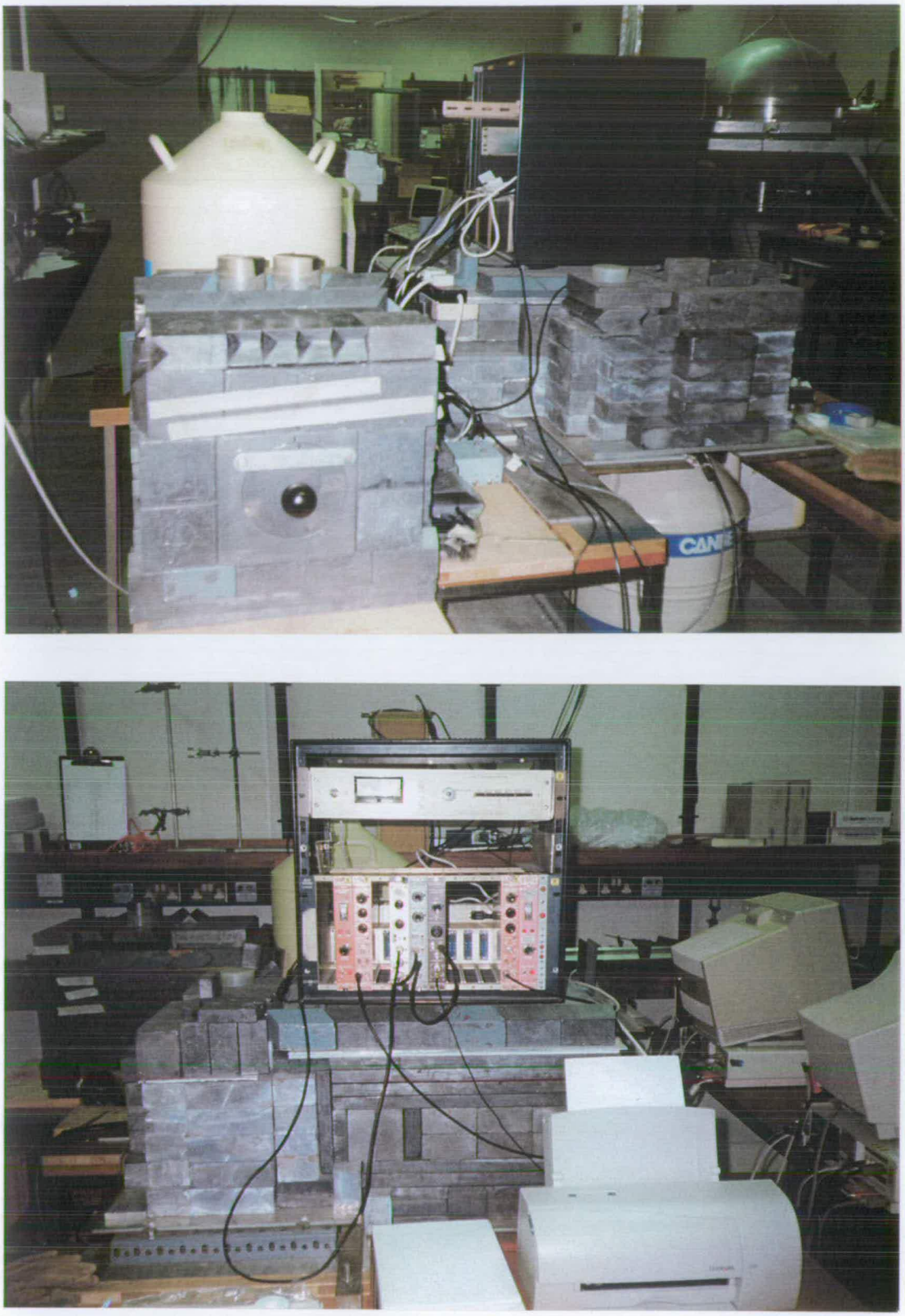

Figure 2.18. The set up for Ge-detectors. (a) Shows the detectors inside the lead shields. NGC is on the left hand side and REGe together with NaI (Tl) are on the right side of the photo. (b) On the top of the shield the electronics for the detectors and on the right of the photo the PCs and on the front bench the printer is located.

The systems used were typical in that the pre-amplifier was supplied as standard components. The pre-amplifier plays the roles of collecting and integrating the charge deposited in the detector, converting it into an output voltage pulse, and providing an optimised coupling between the output of the detector and the rest of the main amplifier. The pre-amplifiers were located as close as possible to the detectors to minimise the effect of stray capacitance, and in order to take advantage of the cooling which aids the preamplifier to operate with low noise [Tsoulfanidis, 1989].

Two 0-5 kV Ortec high-voltage power supply units were used to provide 3 and 2 kV bias supplies required by the first (REGe) and second (NGC) detectors, respectively. The function of the main amplifier (Ortec 572) is to amplify the signal from the preamplifier and shape it to a convenient form for optimum analog to digital conversion. In this process, a strict proportionality between input and output amplitudes (i.e. linear amplification) must be preserved. Linear amplifiers manufactured by Ortec, were used for both spectrometers. The Gaussian type of shaping was selected with time constants of 6 μs for both systems. Amplified and shaped pulses from the two detectors were analysed by a Canberra AccuSpec PC-based multi-channel analyser (MCA), which contains a computer-controlled, 100 MHz, Wilkinson type ADC with 8 K channels of spectral memory. The ADC is the backbone of an MCA which converts the amplitude of a voltage pulse from analog to digital format. In a Wilkinson type ADC, the input signal is used to charge a capacitor, which is then discharged at a constant rate. This run down is timed by counted pulses from a constant frequency oscillator to give a number proportional to the charge on the capacitor. These numbers which correspond to the analog amplitudes at the ADC input, are fed to a dedicated memory and sorted into a histogram to record the number of events counted in each pulse-height interval. The contents of each memory channel can then be displayed on a screen or printed out to give a pulse height spectrum, which is actually a representation of the gamma energy

spectrum observed by the detector [Knoll, 1989]. The spectra were accumulated in 8192 channels for each detector and covered an energy interval of 0.8-1343.2 keV and 5.1-1385.9 keV for NGC and REGe, respectively. Data acquisition were performed on Dell 486 PCs, using Canberra Genie-PC (Version 2.1) software, together with operating system (OS/2), windows 3.11.

2.6. Background reduction.

In all low level activity measurements (environmental radiation), there are advantages in reducing the contribution of background radiation under peaks, which is mainly from the Compton backgrounds of higher energy gamma-rays. Reduction of the gamma background helps in identifying the low intensity peaks, which is difficult in the presence of the Compton continuum and gamma rays not from the sample. The main radiation background is from natural radioactive isotopes of uranium and thorium as well as cosmic rays. Natural radionuclides may be present in the system components, the surrounding environment, within the sample matrix itself, and for surface air samples, other radionuclides collected on the filters.

Both the detector and sample being counted are usually enclosed in a *castle* of high-Z material (normally lead) to reduce the background contribution of the surrounding environment, (fig. 2.18). The cosmic-ray component, however, can be removed only through massive amounts of shielding. An alternative arrangement is the elimination of the highly penetrating cosmic radiation through the use of an *anticoincidance shield* (also called *Compton suppression system*) [Knoll 1989]. This arrangement not only provides a greatly reduced natural background but also removes much of the Compton interference from radionuclides within the sample matrix.

In this technique, a central Ge detector is surrounded by a second large detector which is usually made of NaI (Tl), plastic scintillator, or BGO. A popular anti-Compton system is the commercialised NaI (Tl) crystal which has cylindrical

geometry with a 3 inch hole in the centre [Kiang et al., 1993]. Gamma-rays which undergo Compton scattering and thereby deposit only a portion of their energy in the Ge detector, may be detected in the NaI crystal. Suitable anti-coincidence circuitry cancels the signal from the Ge detector and only those pulses not accompanied by pulses from the NaI crystal are stored in the spectrum.

An anti-coincidence unit is an electronic device that accepts pulses (events) in two input channels and provides an output signal *only* if the two events *do not* arrive with a set time period τ. The REGe detector was operated in conjunction with an annular NaI(Tl) scintillation guard detector to reduce the Compton continuum. This detector was used only for soil samples measurements.

For the purpose of achieving adequate background levels, both Ge detectors were surrounded by 10 cm thick lead shields constructed from low-activity lead bricks. This is the optimum thickness of lead shielding for such an application. A greater thickness would result in an increased background due to the build-up of tertiary cosmic-ray particles [Lindstrom et al., 1990].

The lead shield for the NGC detector was constructed using brass plate as the support for the ceiling. A copper inner sleeve of approximately 1 cm thickness was also mounted to shield the detector from background-^{210}Pb gamma rays and lead-fluorescence K X-rays [ANSI, 1991].

2.7. Calibration Techniques.

The main objectives of gamma-ray spectrometry are, first, to determine the energy spectrum of gamma radiation emitted from a sample in order to identify the corresponding radionuclides, and secondly to determine the number of gamma rays emitted. These objectives are achieved by energy calibration and efficiency calibration, respectively.

2.7.1. Energy calibration.

A good energy calibration is an essential requirement for the operation of a gamma-spectrometer system. This is most conveniently achieved using standard radioactive point sources of ^{210}Pb, ^{241}Am, ^{133}Ba, ^{22}Na, ^{137}Cs, and ^{60}Co, which cover the energy range of interest for environmental radioactivity measurements. The calibration was established by measuring the positions of selected full-energy gamma-ray peaks whose energies are known precisely. A typical result of such an energy calibration is shown in Figure 2.19.

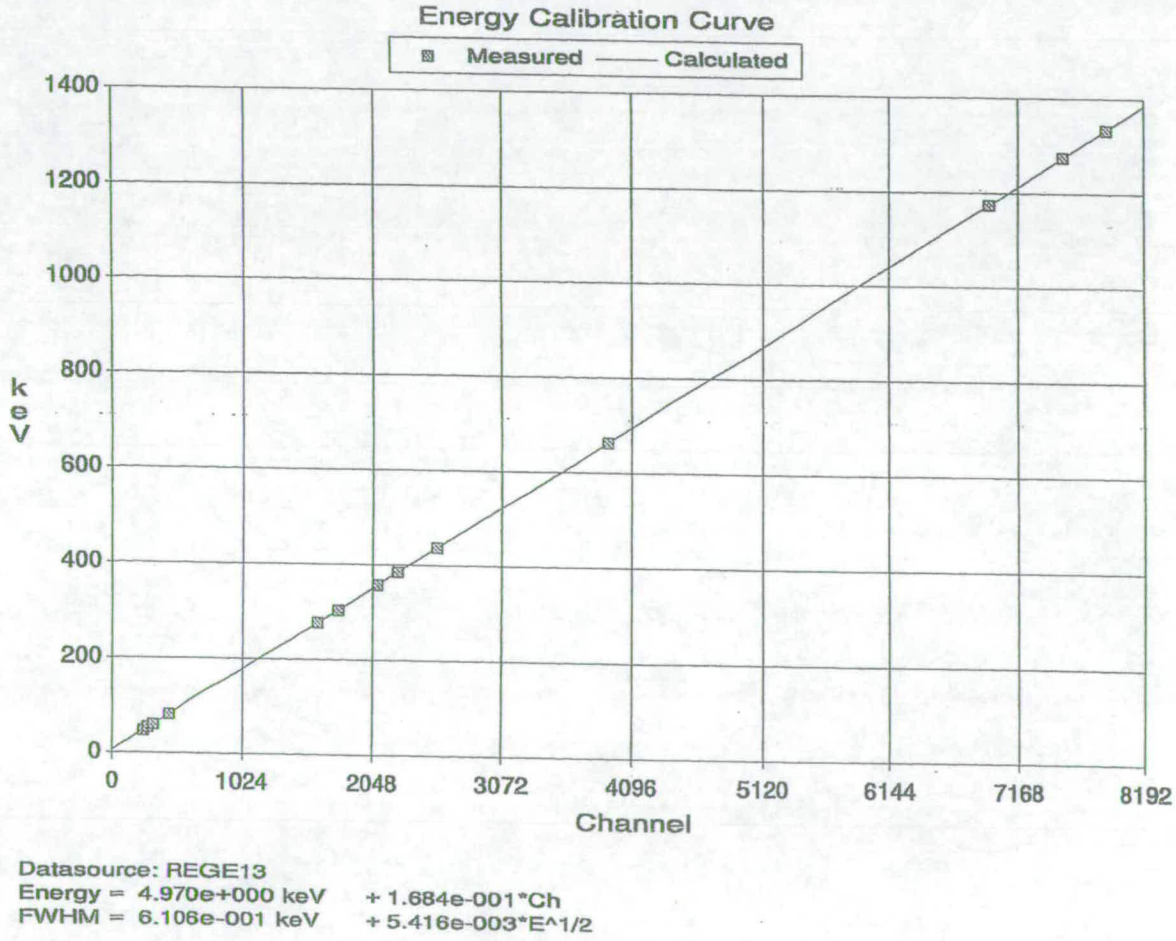

Figure 2.19. Energy calibration for the REGe spectrometer using standard point sources

2.7.2. Efficiency calibration.

The basis of all quantitative radioactivity measurements is the direct proportionality between the amount of radioactive substance in the sample and the intensity of the measured radiation. Not all the gamma rays emitted by a specific source will strike the detector. Moreover, only a fraction of the incident photons will undergo an interaction which will be actually registered by the system. Therefore, an accurate efficiency calibration of the system is necessary to quantify radionuclides present in a sample.

It is a general practice in gamma-ray spectrometry to establish a calibration curve as a function of energy for a defined geometry and energy range. In most cases, it is the full-energy peak efficiency (εFEP), i.e., the efficiency for photoelectric conversion, which is desired. This is given by the total count rate in the photopeak for each gamma-ray divided by the total output of the source . It is a function of both detector geometry and intrinsic efficiency. This is usually accomplished by preparing practical calibration standards in an appropriate matrix to the sample under consideration, from appropriate certified radionuclides.

However, for the measurements reported here a different procedure based on standard radioactive point sources was adopted as this gives more information. Two holders were specially designed and made for this part of measurements. One 48 mm in diameter (used for air and rain samples) and the other 70.6 mm (used for soil samples). They were made in the physics workshop in perspex with 0.4 mm thickness. Twenty-one fixed positions were marked clearly on each of them , shown in figure 2.20. Each point source was positioned at all 21 locations for a limited time, depending on the source's activity, (between 15 minutes to one hour), for each measurement. For each geometry arrangement, these measurements were carried out and the efficiency for each energy was calculated. The efficiencies at the face of both detectors, for both holders were measured. For the 48 mm holder the measurements

were carried out at a distance 3.7 and 1 mm away from the face of the detector (NCG), for air and rain samples, respectively (see sections 2.1.3 and 2.2.1 for more details). Measurements at 3.7 mm and 1 mm away from the face of the detectors were carried out with a blank filter (pressed to a pellet), between the point source and the detector's window (face of the detector).

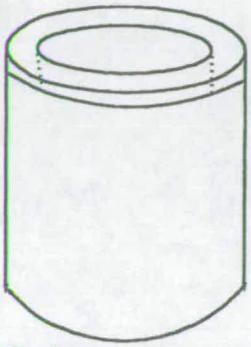

Side view of 48 mm holder.

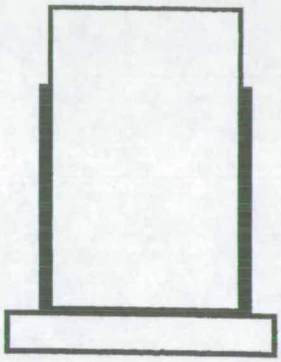

Side view of holder for compressing the filters.

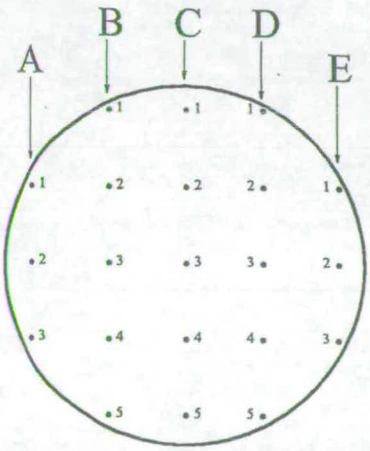

Top view: Arrangements of 21 points to measure, the detectors efficiency. The numbers show the position of each point i.e. A1 means position 1 under column A etc.

Figure 2.20 . Schematic diagram of the special holder used for energy and efficiency calibration.

For the 70.6 mm holder, (which was used for soil samples), the measurements were carried out in the same way as above except that the distance from the detector was 26.5 mm and nothing was placed between the source and the detector. The total number of counts for each of the 21 measurements was determined, averaged to find a single value. This value was divided by the measurement time to determine counts recived per second. Using the following information and formula these values were converted to efficiencies at known energies. Dividing each disintegration per second by the source activity (Bq), and the branching ratio of the source at the known energy, the efficiency at that energy and the geometry was calculated. When all the points are measured, they were plotted to establish a full energy efficiency curve for each known geometry. A typical result of such an efficiency calibration is shown in Figure 2.21.

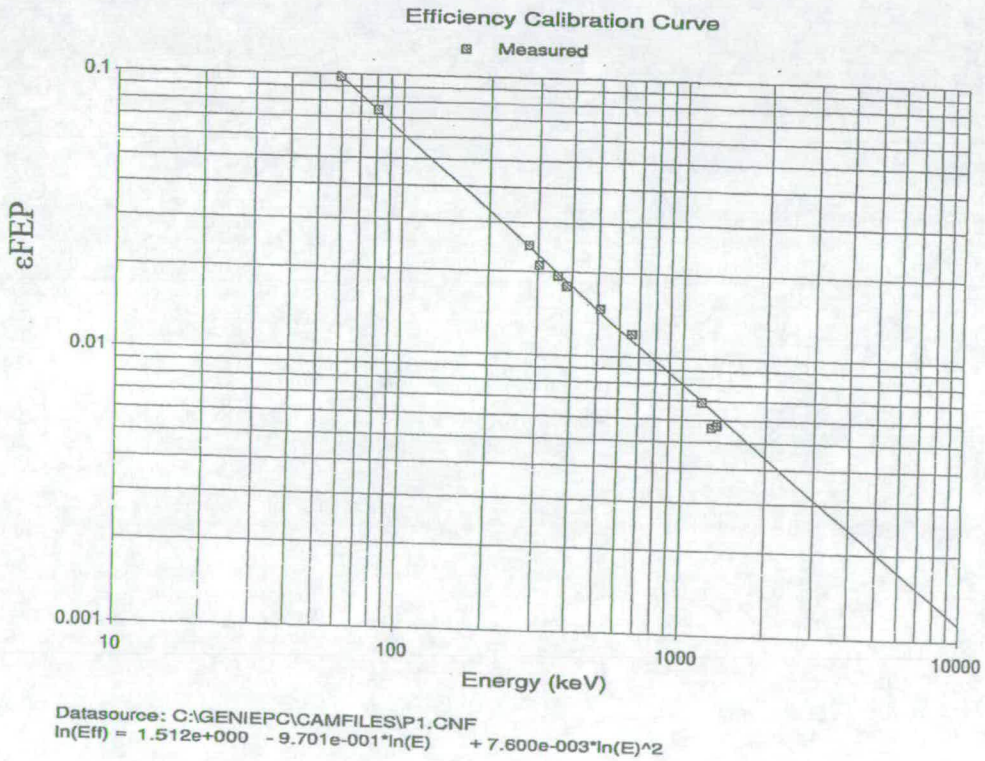

Figure 2.21. Typical full-energy peak efficiencies for gamma-rays of different energy of the REGe spectrometer.

The efficiency values used for the results in this thesis are the averaged values for each set of measurements. For decay correction of the activity of each point source the following formulas were used,

$$A(t) = A(0)\, e^{-\lambda t} \qquad \text{.... (2.4), and}$$

$$\tau_{1/2} = \ln 2/\lambda \qquad \text{.... (2.5)},$$

where, A(t) is activity of radioactive nuclei at time t,

A(0) is activity of radioactive nuclei at time zero, and

λ is the decay constant.

Table 2.3 shows the certificate of the radioactive point sources used and figure 2.22 shows the decay diagrams of the radioisotopes used for this section and other sections of the thesis.

Certificate of measurement of gamma reference sources R 0894

Nuclide	^{241}Am	^{133}Ba	^{137}Cs	^{60}Co	^{88}Y	^{22}Na	^{54}Mn	^{203}Hg	^{57}Co
Colour Code	Red	White	Yellow	Light Green	Black	Cream	Blue	Pink	Dark Green
Source No.	7Q059	7R051	7S055	7U044	7Y092	7X042	7V070	7W095	7T065
Activity, µCi	1.057	1.145	1.078	1.158	1.200	1.090	1.162	2.205	1.008
Accuracy %	5.0	7.0	6.0	3.9	6.7	5.4	7.0	6.0	6.0
ESD %	1.7	2.4	2.0	1.3	2.3	1.8	2.4	2.0	2.0

Activity reference time 1200 GMT on 1 March 1978
Wipe test: each source has passed a wipe test with an acceptance limit of 0.005 µCi.
Accuracy is defined as the OVERALL UNCERTAINTY of the result.
Definitions of the terms used in this certificate and further details of the sources are given in the data sheet provided with each set or replacement source.

Set No 960 Checked by D Parker. Approved by for Managing Director A. Mathias

The Radiochemical Centre Amersham England

Table 2.3. Certificate of radioactive point sources, used for calibration and efficiency measurement.

When the activity or gamma-ray emission rates of a limited number of radionuclides are to be measured, and if there is a calibration source available which contains the same nuclides as the actual source, there is no need to make use of any efficiency calibration curve. Instead, the "radio-nuclide related" efficiency method would be the choice which is the most accurate and straightforward. This method measures a standardisation coefficient for a selected gamma ray emitted from each specific radio-nuclide. The coefficient then converts the net peak-area counting rate to the activity of the radio-nuclide being measured .

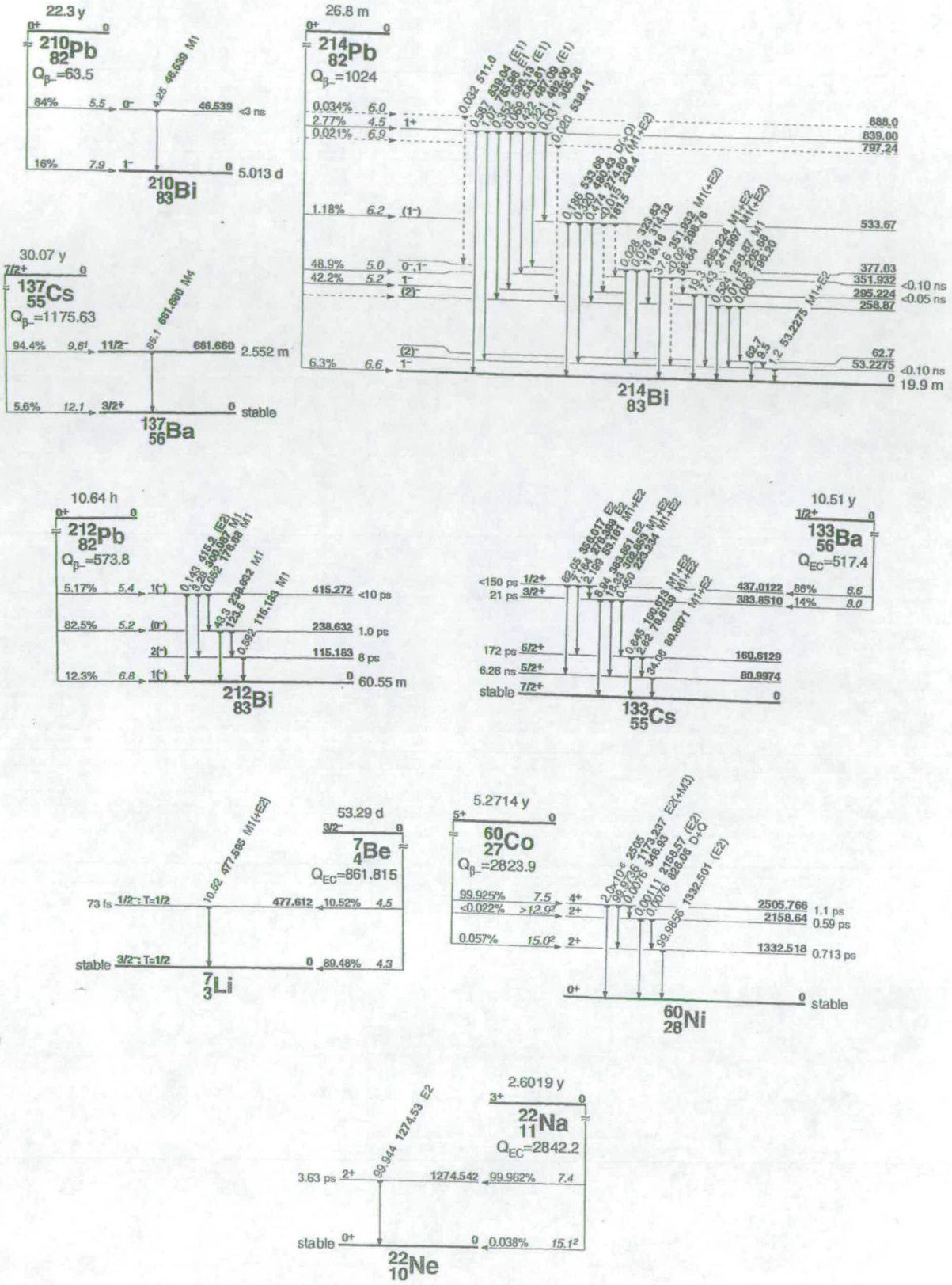

Figure 2.22. Decay diagrams of the radio isotopes used for different parts of this research.

In the present study, efficiencies for ^{210}Pb and ^{137}Cs gamma were determined by radionuclide-related method, and the efficiency for ^{214}Pb, ^{7}Be gamma was derived from appropriate efficiency curves. The details of the ^{210}Pb point source used for calibration and efficiency extracted from Amersham certificate of calibration was as follow:

source activity	code number	source number	accuracy
200 kBq	RBR8121	FM400	±4%

Calibrations of the detectors were accomplished by preparing a specially designed holder with fixed points, (i.e. figure 2.20.) matrices in geometry identical to those used for the samples. To achieve a reproducible source-to-detector distance, thin-walled (0.4 mm), perspex sample holders 70.6 mm in diameter by 26.5 mm deep for soil samples, and 48 mm in diameter by 8.5 mm deep, for air and rain samples, were precisely machined which mount onto the detectors.

2.7.3. Self absorption in the samples.

A further important aspect in the measurement of environmental samples is that of self-attenuating effects within the sample. The attenuation coefficient for gamma rays in the energy range of interest varies significantly from the low to the high end of the region and with sample density. In this study, the Cutshall method [Cutshall et al., 1983] was applied for sample self-attenuation correction of the γ-rays from ^{210}Pb, ^{214}Pb, and ^{137}Cs in soil samples. For surface air and rain samples, this effect was not significant, because the sample holder was specially designed in a way to minimise this effect and the fibre glass density is very low.

A device was designed and made to press the air and rain filters to a very thin pellet (3.7 and 1 mm, respectively) and the pellets then transferred to a 48 mm in diameter and 8.5 mm deep sample holders for gamma-spectroscopy (outer diameter of NCG detector is 69 mm).

Chapter 3

3. Analysis of the results.

In this chapter, the results of measured ^{210}Pb and ^{7}Be in surface air and rain, and ^{210}Pb and ^{137}Cs in soil samples are reported together with an analysis. The collection and measurement methods were explained in chapter two. The detailed data for each of the sections are separately reported in appendices A, B, and C at the end of this thesis.

3.1. Surface air measurements of ^{210}Pb and ^{7}Be concentrations.

A total of 100 air samples, mostly taken over about a 1 week sampling period but ranging from 1 day to 18 days, were collected and analysed for radioisotopes ^{210}Pb and ^{7}Be in surface air. The sampling period was from December 4th 1996 to January 31st 1999. The sampling procedures used were as explained in section 2.5. Concentrations of ^{210}Pb and ^{7}Be (mBq m^{-3}) were calculated from the air volume which passed through the filter. To calculate the concentration of each radioisotope the activity of each isotope is divided by the volume of air filtered during the sampling period. The flow rate of the air was determined by multiplying the area of the exposed filter (m^2) and the speed of the air through the filter (m s^{-1}). The flow rate for these 100 samples varied between 0.013 and 0.042 m^3 s^{-1} although most values were close to 0.025 m^3 s^{-1}. Multiplication of the flow rates with the measurement times gave the calculated air volumes.

Figures 3.1 and 3.2 show the measured ^{210}Pb and ^{7}Be concentrations (mBq m^{-3}) in surface air, respectively, and the temporal variations of these two isotopes, for each filter, measured from December 1996 to January 1999. The errors shown on the graphs were counting statistical errors ($\pm\sigma$). The complete table of data for these measurements is shown in Appendix A, Table 3.1. The ^{210}Pb concentrations varied from 0.028 ± 0.008 to 0.619 ± 0.016 mBq m^{-3} for all 100 measured samples
These variations were due to a number of effects, including the type of air mass, precipitation events, deposition mechanisms and transportation of air masses.

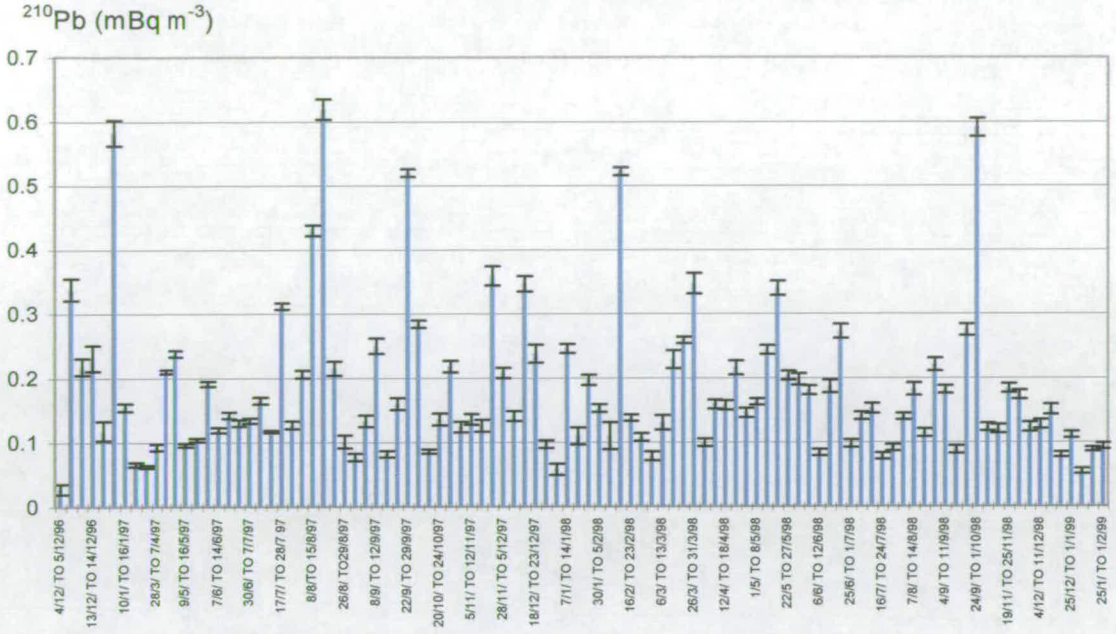

Figure 3.1. The concentrations of ^{210}Pb (mBq m^{-3}) in air, for each filter during December 1996 to January 1999. The errors on the graphs are the $\pm\sigma$ statistical counting errors.

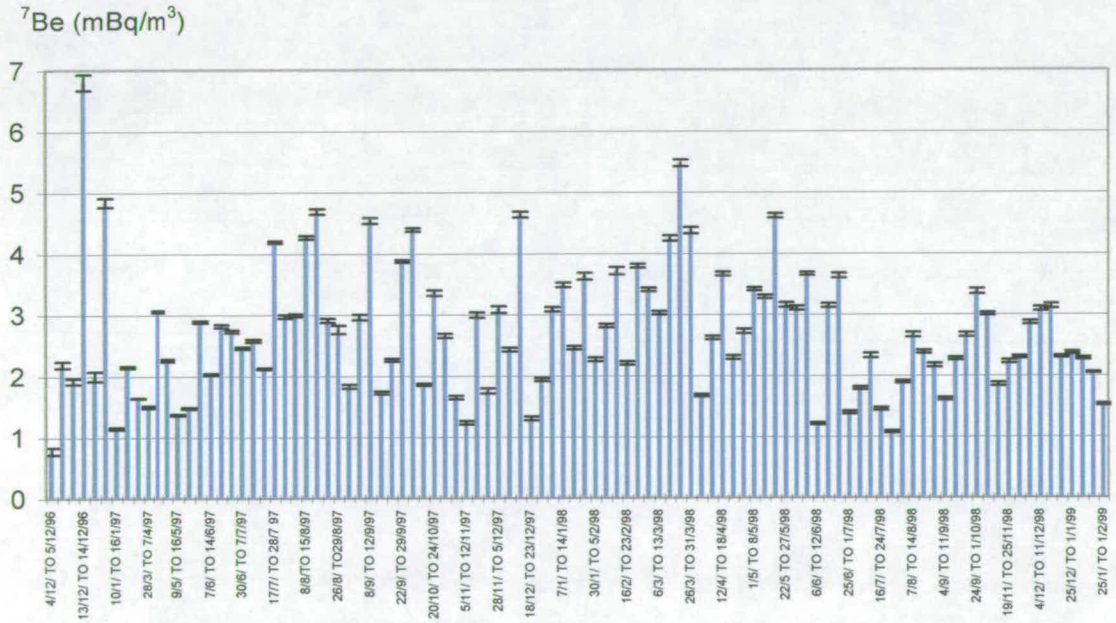

Figure 3.2. The concentrations of ^{7}Be (mBq m^{-3}) in air, for each filter during December 1996 to January 1999. The errors on the graphs are the $\pm\sigma$ statistical counting errors.

For ^{210}Pb, the important parameter is the origin of the air masses, i.e. whether it is from continental or oceanic regions. In general, the concentrations of ^{210}Pb in

continental air masses are much larger than those from the oceanic regions, as ^{210}Pb is derived from ^{222}Rn emitted from soil.

The concentrations of ^{7}Be in surface air varied from 0.782 ± 0.058 to 6.81 ± 0.128 mBq m^{-3} in 100 measured samples. These variations could be due to different effects, including precipitation and vertical and horizontal transport of the air masses. The most important effects reported are the vertical transport processes within the atmosphere. The variations of ^{210}Pb are larger than the variation of ^{7}Be concentrations. This is clearly shown in the graphs.

3.1.1. Frequency distribution of ^{210}Pb and ^{7}Be.

The frequency distributions of ^{210}Pb and ^{7}Be in surface air are plotted in figures 3.3 and 3.4, respectively. These frequency distributions are compared with widely known distributions. For ^{210}Pb the frequency distribution was compared with a Lognormal Distribution using equation 3.1, [Evans et al., 1993]. These are shown with a line on the graphs and the frequency distribution of ^{210}Pb and ^{7}Be from the surface air measurements are shown as bar diagrams.

$$P = \{ 8 / [x\ \sigma (2\pi)^{1/2}] \} \exp\{ [- \mathrm{Log}(x / m)]^2 / [2\sigma^2] \} \qquad \text{.....(3.1)}$$

Here, P is the probability density function,

x is the range $0 \leq x \leq \infty$,

m is the median (0.7), and

σ is the shape parameter (0.3).

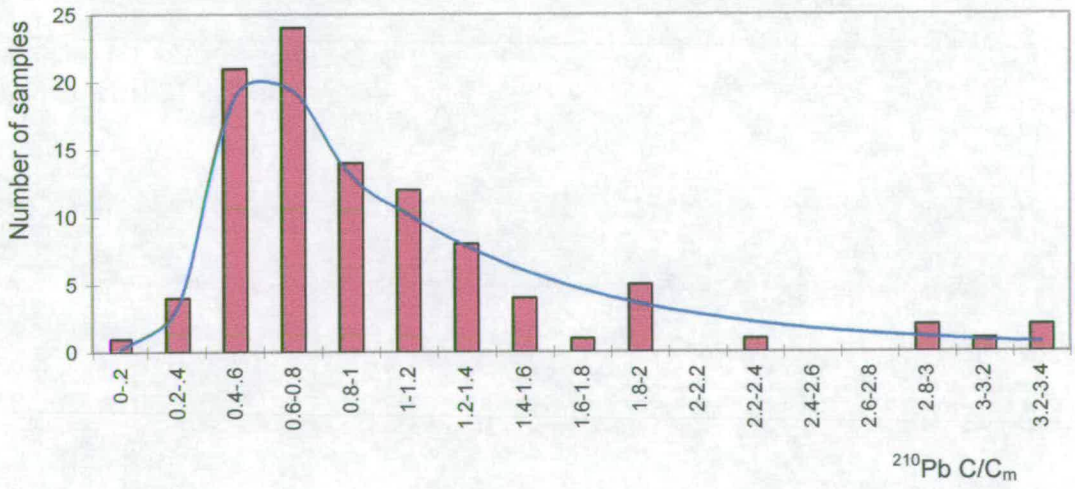

Figure 3.3. Bar diagram shows the distribution of ^{210}Pb in surface air measured from December 1996 to January 1999. The line fitted to the diagram is calculated from a Lognormal distribution formula as described by equation 3.1 and explained in the text. C is the concentration in each sample and C_m is the mean concentration for the 100 filters.

For ^{7}Be the distribution was compared with a Normal (Gaussian) Distribution using equation 3.2 [Evans et al., 1993].

$$P = \{ 17 / [\sigma (2\pi)^{1/2}] \} \exp\{ [-(x-\mu)^2] / [2\sigma^2] \} \quad \text{..... (3.2)}$$

Here, P is the probability density function,

x is the range $0 \leq x \leq \infty$,

μ is the median (1.1), and σ is the shape parameter (0.3).

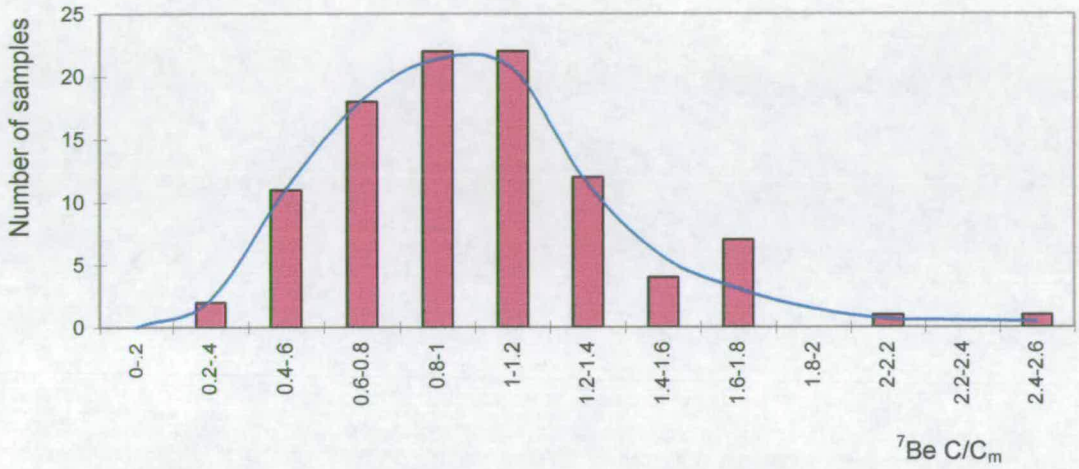

Figure 3.4. Bar diagram shows the distribution of ^{7}Be in surface air measured from December 1996 to January 1999. The line fitted to the diagram is calculated from a normal distribution formula as described by equation 3.2 and explained in the text. C is the concentration in each sample and C_m is the mean concentration for the 100 filters.

Volume weighted averaged monthly concentrations of ^{210}Pb and ^{7}Be were plotted against each other and rainfall at the same period of measurement in figures 3.5, 3.6, and 3.7, respectively. The rain data used were from the nearest meteorological weather station (Turnhouse, Edinburgh Airport).

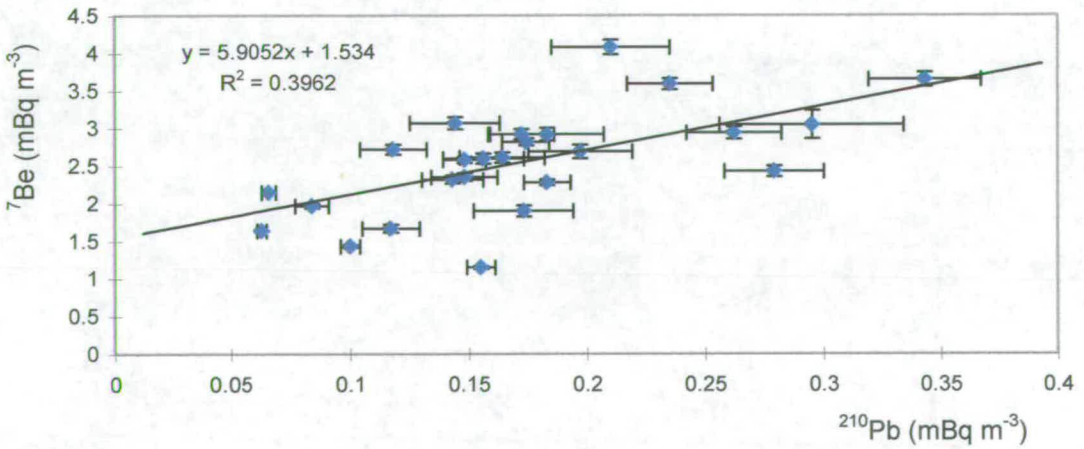

Figure 3.5. Monthly concentrations of ^{7}Be and ^{210}Pb (mBq m^{-3}) in air samples.

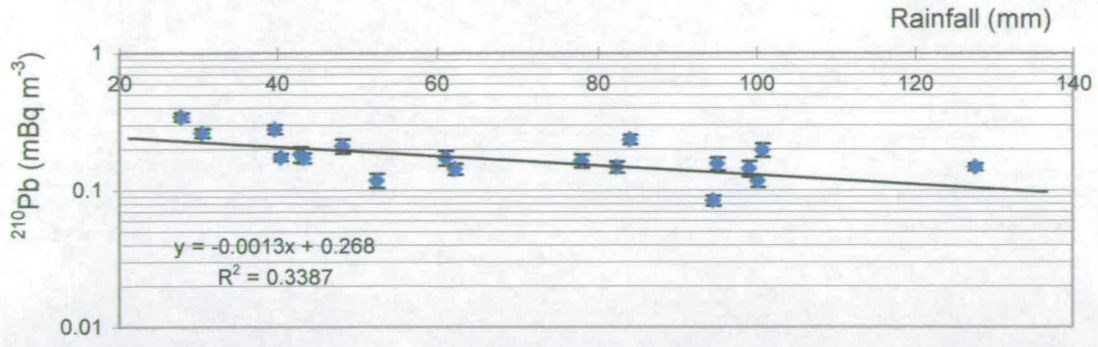

Figure 3.6. Monthly concentrations of ^{210}Pb (mBq m^{-3}) in air samples against the amount of rainfall in the same period. The rain data were from Turnhouse (Edinburgh Airport) meteorological station.

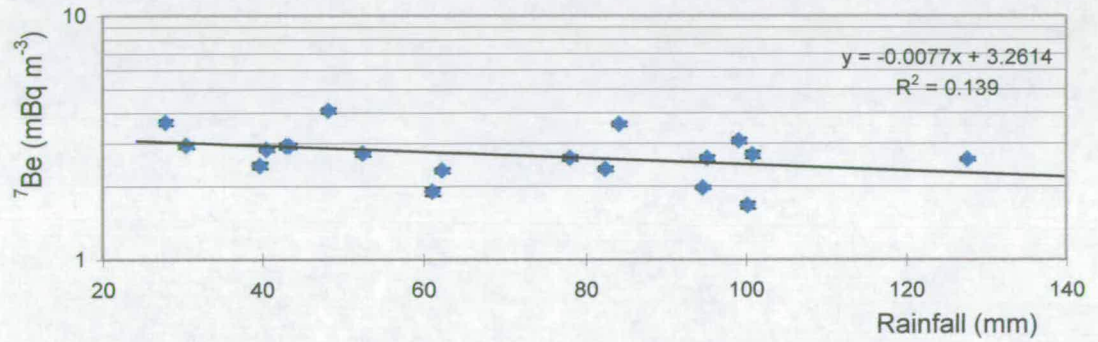

Figure 3.7. Monthly concentrations of ^{7}Be (mBq m^{-3}) in air samples against the amount of rainfall in the same period. The rain data were from Turnhouse (Edinburgh Airport) meteorological station.

To calculate these monthly concentrations equation 3.3 was used,

$$C \times V = A \qquad \text{..... (3.3)},$$

where, C is the concentration of ^{210}Pb or ^{7}Be for each filter (mBq m^{-3}),

V is the volume of air passed through each filter (m^{-3}), and

A is the activity of ^{210}Pb or ^{7}Be in each filter (mBq).

The following equation was used to calculate the average monthly volume-weighted concentrations of ^{210}Pb and ^{7}Be.

$$\bar{A} = (\Sigma A_i) / (\Sigma V_i) \qquad \text{.....(3.4)},$$

where, $\bar{A}$ is the average monthly values for ^{210}Pb or ^{7}Be,

ΣA_i is the sum of the activities at i = 1,2,3,.... n, and

ΣV_i is the sum of the volume at i = 1,2,3,.... n.

The errors were calculated using equation 3.5,

$$E_m = [\text{sqrt}(\Sigma E_i)/n] \qquad \text{.....(3.5)},$$

where, E_m is error calculated for each month,

ΣE_i is the counting statistical errors for i samples, i = 1,2,3,....n, and

n is the number of samples.

In figure 3.5, all of the measurements taken for 25 months are plotted, whereas figures 3.6 and 3.7 show 18 months of the results. The reason for plotting the reduced (18 month) data set is that, for the last 18 months (from June 1997 to January 1999), all of the possible days in each month were measured, whereas in the early months of measurements (from Dec. 1996 to June 1997), due to unforeseen problems including failure of the sampler's motor, some of the samples were lost and they were not therefore included in monthly measurements. In each measuring month, the variations could be considerable depending on the type of air mass, as can be noted from figures 3.1 and 3.2, and Table 3.1 in Appendix A. The detailed analysis of data was therefore restricted the shorter 18 month data set.

Figure 3.5 shows an approximately linear relationship between the monthly concentrations of ^{210}Pb and ^{7}Be in the air samples which could be described with the equation,

$$Y = 5.91\,X + 1.53 \qquad \text{.....(3.6),}$$

where, Y and X are the concentrations of ^{7}Be and ^{210}Pb (mBq m^{-3}) in surface air, respectively.

3.1.2. Effect of meteorological variables on concentrations of ^{210}Pb and ^{7}Be.

Precipitation data at the air sampling site were not available for the whole sampling period. Therefore the data from Turnhouse meteorological station were used to plot figures 3.6 and 3.7, which show a clear decline in concentrations of both ^{210}Pb and ^{7}Be in air as the volume of precipitation during the sampling period increased.

3.1.3. Seasonal variables of ^{210}Pb and ^{7}Be concentrations.

The seasonal concentrations of ^{210}Pb and ^{7}Be in air are plotted in figures 3.8 and 3.9. To find the seasonal concentrations, the data for June 1997 to January 1999 were considered using the same arguments stated for the averaged monthly concentrations. These plots are based on 18 months of data, from 1997 and 1998. The concentrations were extracted from the original values listed in table 3.1, appendix A.

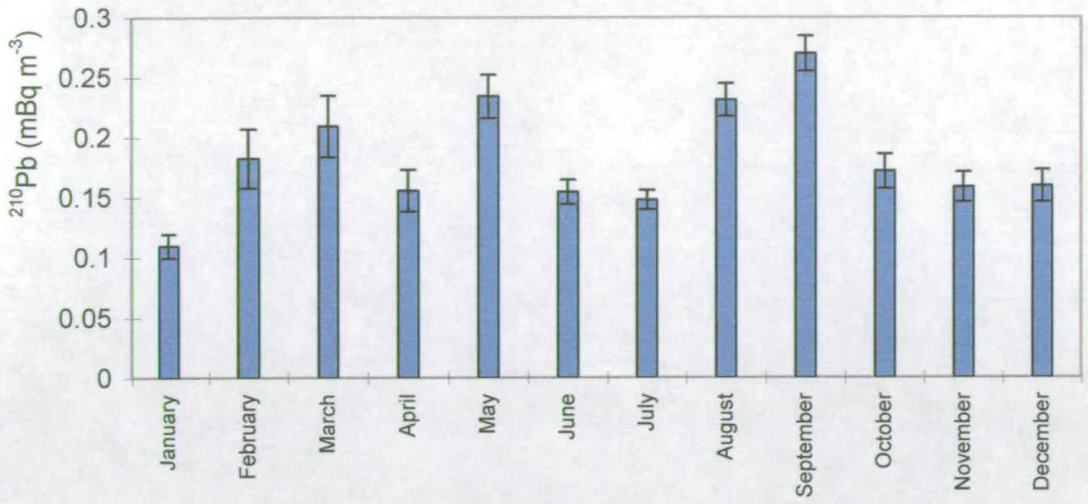

Figure 3.8. Seasonal concentrations of ^{210}Pb (mBq m^{-3}) in air from June 1997 to January 1999.

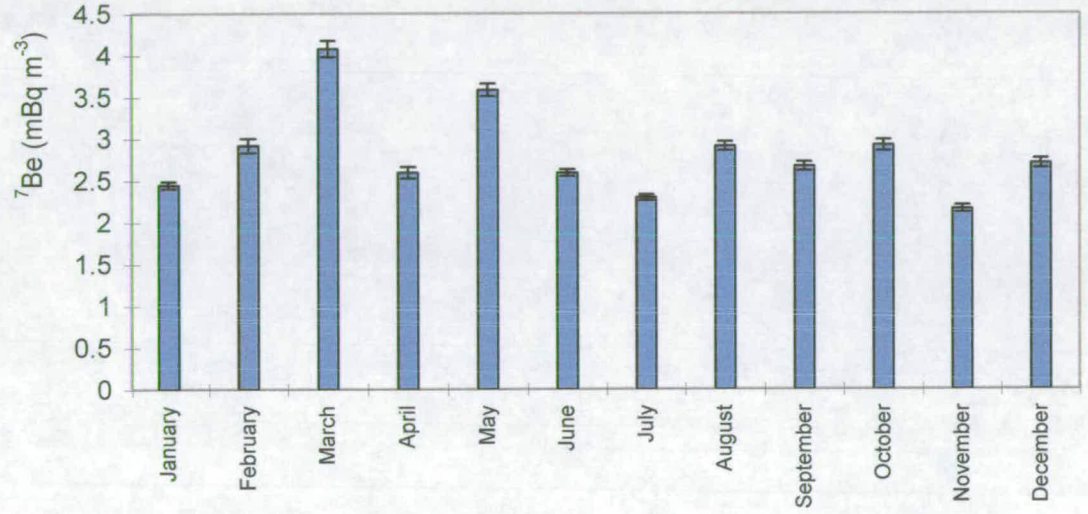

Figure 3.9. Seasonal concentrations of ^{7}Be (mBq m^{-3}) in air from June 1997 to January 1999. The error bars were the root mean square of the samples errors for each month.

3.1.4. Effect of atmospheric pressure on ^{210}Pb and ^{7}Be concentrations.

Meteorological surface pressure maps were used to determine the atmospheric pressure, wind direction and the origin of air masses. The air mass back trajectories for 4 days were used to identify the source and air mass type. Precipitation events during this time or other meteorological changes to the air parcel were not considered.

To examine the effect of atmosphere pressure on the ^{210}Pb and ^{7}Be concentrations for each samples figures 3.10 and 3.11 were plotted, respectively. A scheme was adopted using the isobar charts where high pressure (HP) were ascribed an index +1, low pressure (LP) -1 and mixed HP and LP zero. The x-axis of the graphs are the % contributions of the HP and the LP determined for each filter first and then combined in to clusters to provide a binned value, i.e. for a 5 days sampling period, if we had 3 days of HP and 2 days of LP we have [(+3-2)/ 5] which is reported as 20% HP on the graph, etc.. The errors are the standard deviations at each bin. The trend line on the graphs are linear fit to the data.

The concentrations of ^{210}Pb and ^{7}Be at a type range of air masses were averaged and binned in 20% rays to determine the concentration at that point. The errors on the graphs are the deviation of the concentrations at each bin, and were calculated using equation 3.7.

$$E = \text{sqrt} \{ [\Sigma (C_i - C_m)^2] / (n-1) \} \quad \text{....(3.7),}$$

where, E is the error at each point,

C_i is the concentration at each point i, where i = 1,2,3,....,

C_m is the mean concentration for each point.

n is the number of points in each bin.

These results show for high pressure the concentrations of both isotopes are larger.

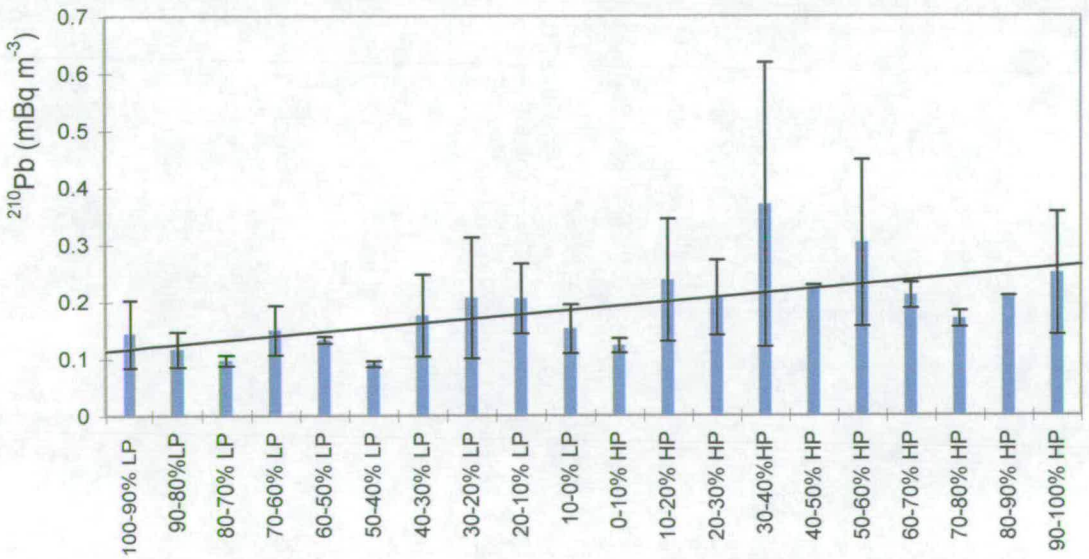

Figure 3.10. Low-High air masses pressure and ^{210}Pb (mBq m^{-3}) concentrations in air during Dec. 96 to Jan. 99. The error bars are the standard deviations of ^{210}Pb at each bin. The units shown on the x-axis are explained in section 3.1.4. $R^2 = 0.41$.

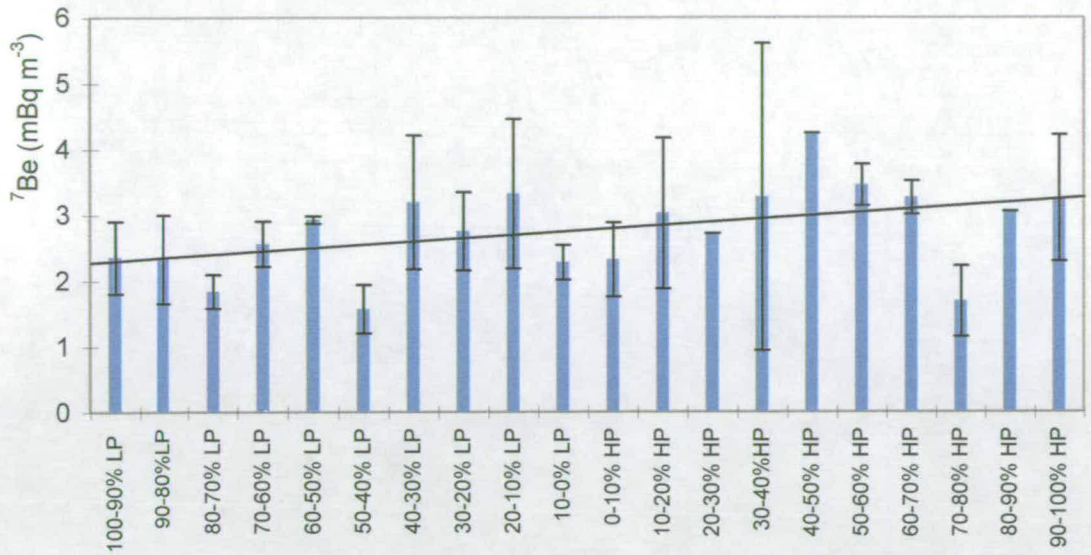

Figure 3.11. Low-High air masses pressure and ^{7}Be (mBq m^{-3}) concentrations in air during Dec. 96 to Jan. 99. The error bars are the standard deviations of ^{7}Be at each point. The units shown on the x-axis are explained in section 3.1.4. $R^2 = 0.20$.

3.1.5. Effect of air mass trajectory and source on ^{210}Pb and ^{7}Be concentrations.

To investigate the effect of the origin of air masses (i.e. continental or oceanic) figures 3.12 and 3.13 were plotted for ^{210}Pb and ^{7}Be, respectively. A scheme was adopted using the isobar charts where continental air mass (C) were ascribed an index +1, oceanic air mass (O) -1 and mixed continental and oceanic zero. The x-axis of the graphs are the % contributions of "C" and "O" determined for each filter first and then combined in to clusters to provide a binned value, i.e. for a 6 days sampling period if we had 1 day of C and 4 days of O and 1 day mixed we have [(+1-4+0) / 6], reported as 50% O on the graph, etc..

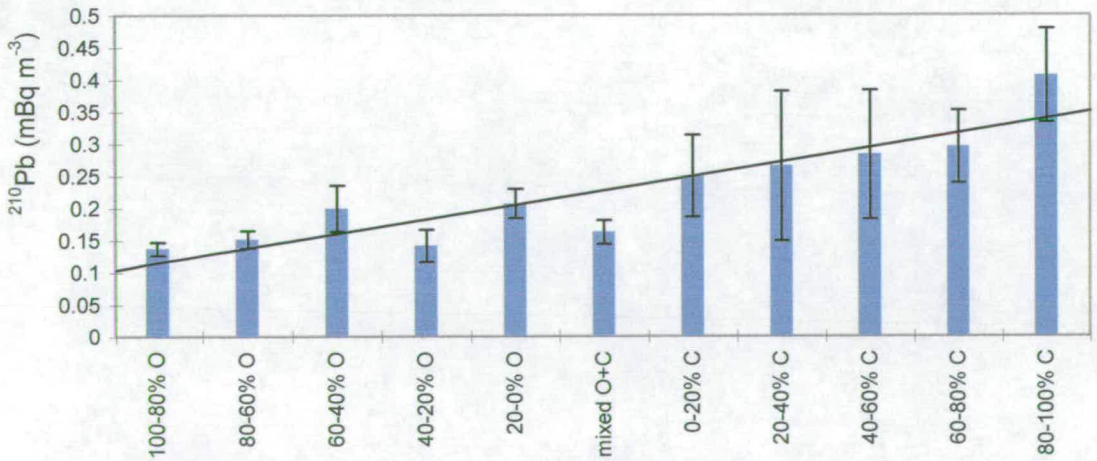

Figure 3.12. Concentrations of ^{210}Pb (mBq m^{-3}) and percentages of Continental-Oceanic air masses for 100 air filters in air samples. The error bars are the standard deviation of ^{210}Pb concentration at each bin. The units shown on the x-axis are explained in section 3.1.5. $R^2 = 0.81$.

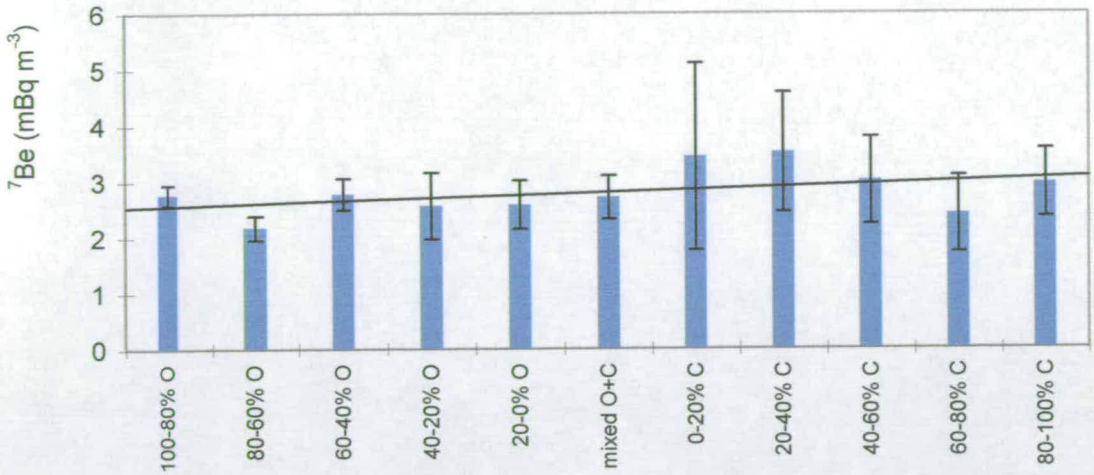

Figure 3.13. Concentrations of ^{7}Be (mBq m^{-3}) and percentages of Continental-Oceanic air masses for 100 air filters in air samples. The error bars are the standard deviation of ^{7}Be concentration at each bin. The units shown on the x-axis are explained in section 3.1.5. $R^2 = 0.16$.

Wind direction at the sampling station for each day was deduced from the surface pressure charts, during December 1996 to January 1999. A breakdown of the wind directions into 8 octants for the 12 highest and 12 lowest concentrations of ^{210}Pb in air samples are plotted in figure 3.14. The percentages shown are the fraction of time the wind fell in each of the octants.

The annual average concentrations of ^{210}Pb and ^{7}Be were found to be 0.19 ±0.06 mBq m^{-3} and 2.71 ±0.66 mBq m^{-3} respectively. These annual concentrations were determined using the data from June 1997 to January 1999. The uncertainties quoted (standard deviations) were calculated using equation 3.11.

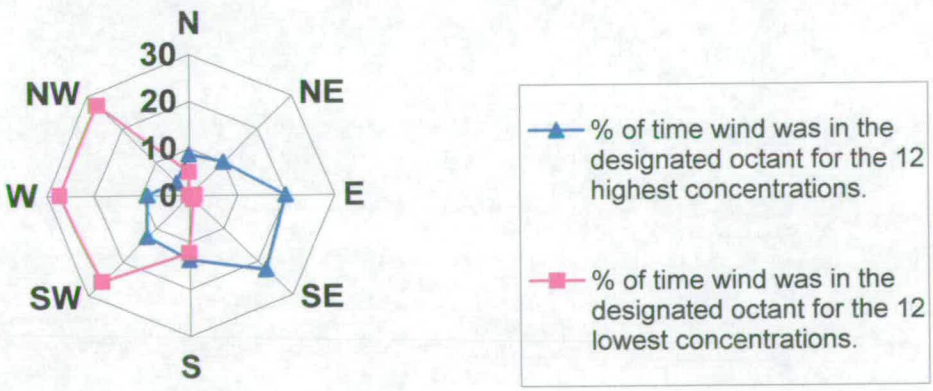

Figure 3.14. Wind direction diagram for 12 highest and 12 lowest concentrations of ^{210}Pb in 100 air samples collected from December 1996 to January 1999. The wind direction at each segment was divided according to the total wind directions for the highest or lowest concentrations, i.e. for highest concentrations, the number of days of wind arriving to Edinburgh from the North was 7 and the total days were 80, therefore the wind from the North is 8.75% of the total, etc.

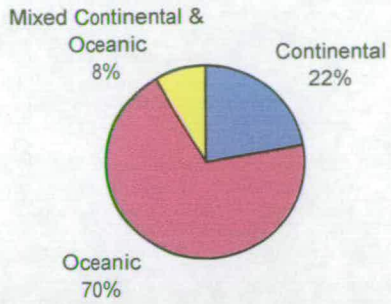

Figure 3.15. The percentages of Continental and Oceanic air masses filtered During the period of Dec. 96 to Jan. 99. Determined from the meteorological weather maps.

3.2. Rain measurements of ^{210}Pb and ^{7}Be.

In this part of the study, the total atmospheric deposition (dry + wet) of ^{210}Pb and ^{7}Be were collected using a continuously open collector to provide both the flux and concentrations in rain. In total, 31 rain samples, mostly taken over one month sampling periods but ranging from 2 to 31 days, were collected and measured from October 24th 1997 to January 31st 1999. The deposition fluxes of ^{210}Pb and ^{7}Be isotopes were determined using the procedures as explained in section 2.6, chapter 2. The complete set of results for concentrations and fluxes of ^{210}Pb and ^{7}Be are shown in table 3.2, as reported in Appendix B.

The total monthly fluxes of ^{210}Pb and ^{7}Be in rain are plotted in figures 3.16 and 3.17, respectively. To calculate these fluxes the total activity for each sample was divided by the total area of the collection trays (5500 cm^2). The variations of fluxes are shown on the graphs. These fluxes varied by a factor of about 11 (from 0.09 ± 0.01 to 1.02 ± 0.03 mBq cm^{-2}), and about 9 (from 1.62 ± 0.03 to 14.02 ± 0.13 mBq cm^{-2}) for ^{210}Pb and ^{7}Be, respectively.

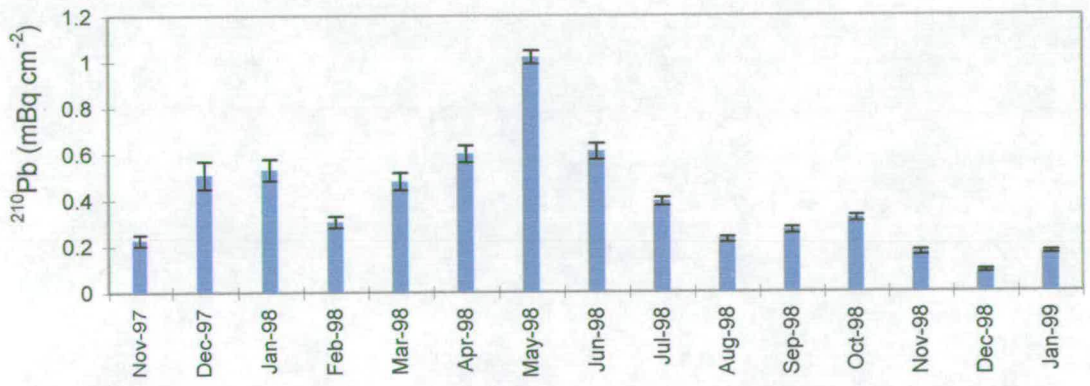

Figure 3.16. The total monthly ^{210}Pb flux in rain (mBq cm^{-2}), collected and measured from November 1997 to January 1999. The errors were the counting statistical errors ±σ.

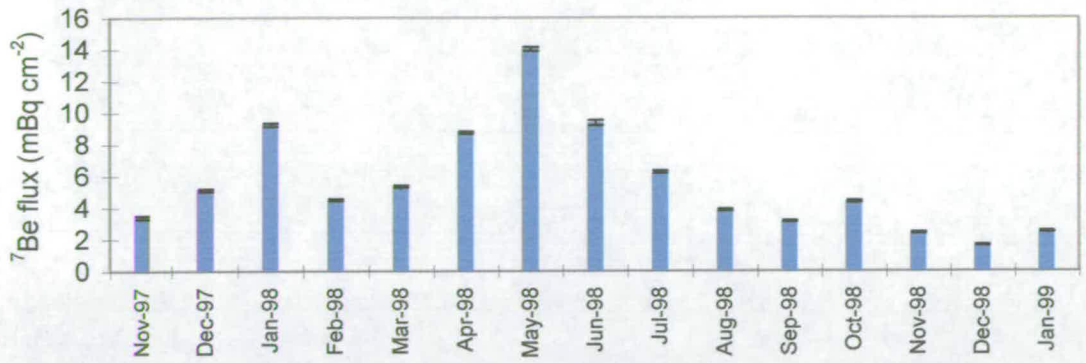

Figure 3.17. The total monthly ^{7}Be flux in rain (mBq cm^{-2}), collected and measured from November 1997 to January 1999. The errors were the counting statistical errors $\pm\sigma$.

Most of the samples were exposed for a month and therefore produce a monthly flux. The concentrations of ^{210}Pb and ^{7}Be were plotted against each other as shown in figure 3.18. Their concentrations were increased or decreased with a similar rate which means that these two isotopes have a linear relationship with each other, as indicated with equation 3.8.

$$Y = 13.52\ X \qquad \text{....(3.8)}$$

Here, Y and X are the concentrations of ^{7}Be and ^{210}Pb (mBq l^{-1}), respectively.

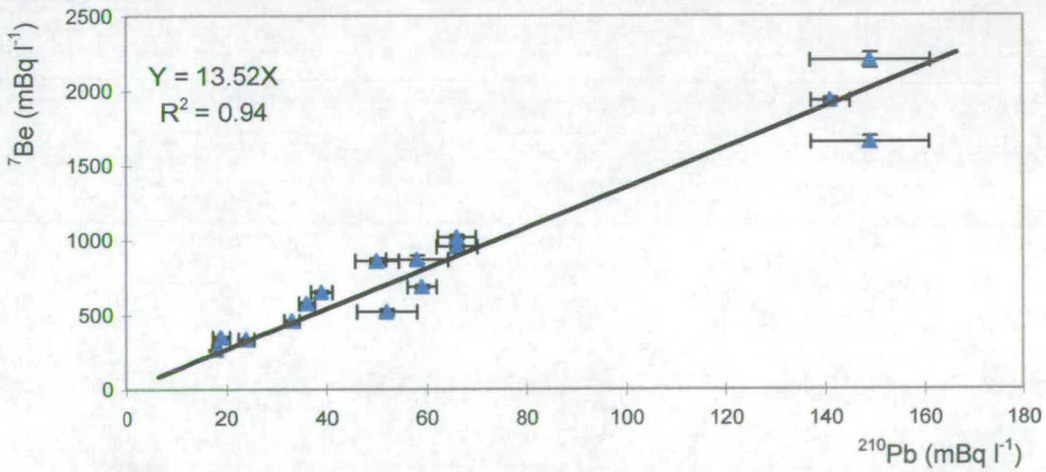

Figure 3.18. Monthly concentrations of ^{7}Be in rain samples (mBq l^{-1}) versus ^{210}Pb monthly concentrations (mBq l^{-1}). The error bars are the counting statistical errors $\pm\ \sigma$.

3.2.1. Total monthly concentrations of ^{210}Pb and ^{7}Be in precipitation.

The total monthly concentrations of ^{210}Pb and ^{7}Be were plotted against the monthly rainfall in figures 3.19 and 3.20, respectively. The errors shown on the

graphs are the ± σ counting errors from the measurements for the single monthly values and for the others determined using equation 3.5. The rainfall data were measured close to the sampling site for ^{210}Pb and ^{7}Be.

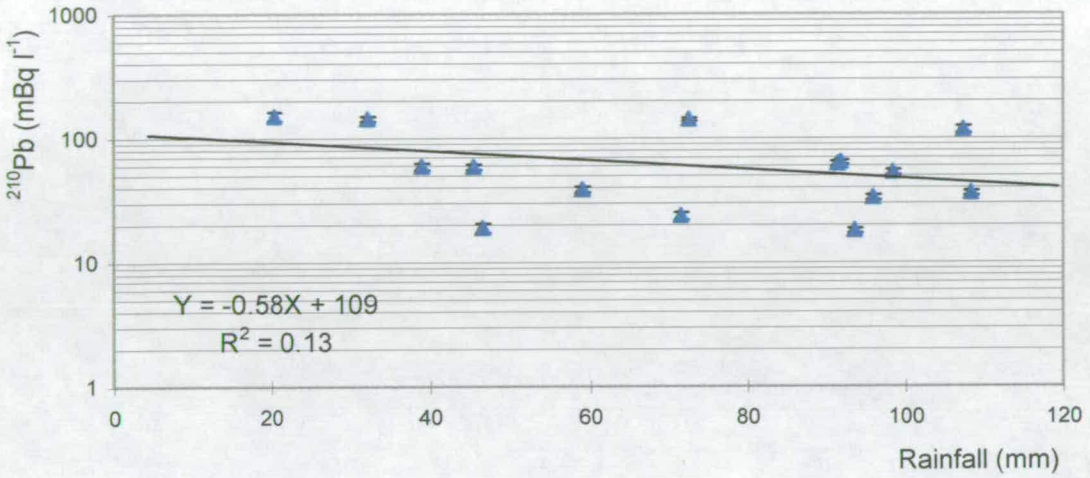

Figure 3.19. Monthly concentration of ^{210}Pb (mBq l^{-1}) in rain versus the amount of rain at the same period. The rain data was measured at the sampling site.

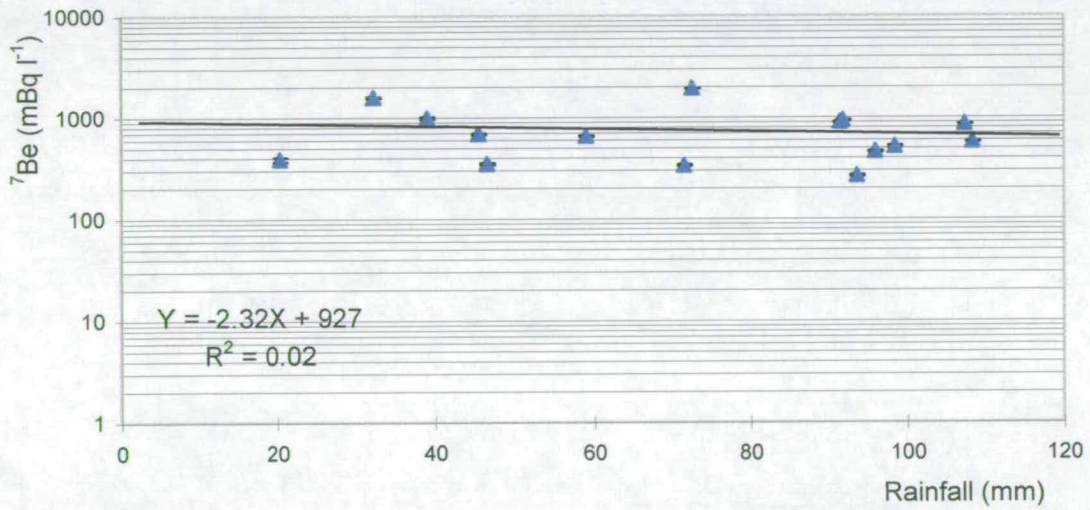

Figure 3.20. Monthly concentration of ^{7}Be (mBq l^{-1}) in rain versus the amount of rain at the same period. The rain data was measured at the sampling site.

3.2.2. Total monthly fluxes of ^{210}Pb and ^{7}Be in precipitation.

The total monthly fluxes of ^{210}Pb and ^{7}Be are plotted against monthly rainfall amount from November 1997 to January 1999 in figures 3.21 and 3.22, respectively.

The errors shown on the graphs are the ± σ counting statistical errors from the measurements for the single monthly values and for the others determined using equation 3.5. The trend line equations showing the relation between the ^{210}Pb and ^{7}Be fluxes (mBq cm^{-2}) and the monthly amount of rainfall (mm) are equations 3.9 and 3.10, respectively. These graphs are used to estimate the dry deposition on to the collector of these radioisotopes over this period as explained in chapter four.

$$Y\ [^{210}Pb\ (mBq\ cm^{-2})] = (2.5*10^{-3})\ X\ [precipitation\ (mm)] + 0.21 \quad ....(3.9)$$

$$Y\ [^{7}Be\ (mBq\ cm^{-2})] = (43*10^{-3})\ X\ [precipitation\ (mm)] + 2.5 \quad ....(3.10)$$

Here, Y is the flux of ^{210}Pb or ^{7}Be (mBq cm^{-2}), and X is the total monthly rainfall (mm).

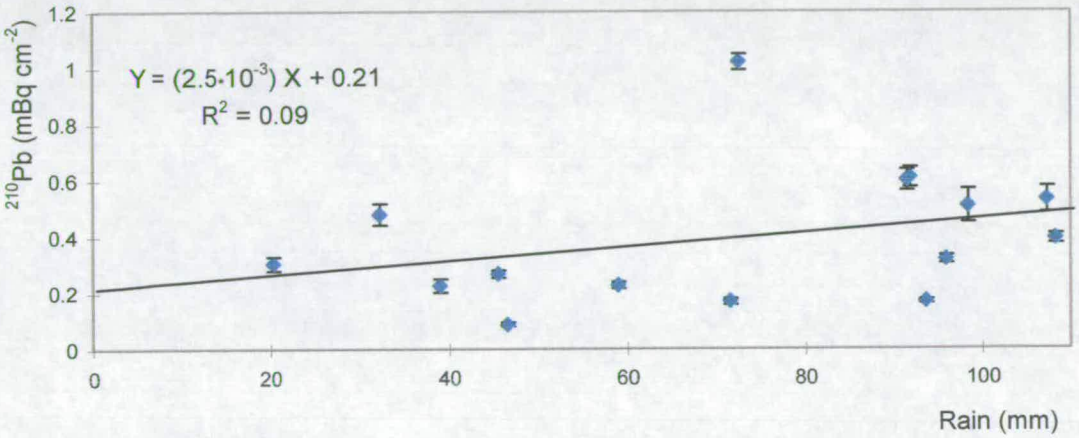

Figure 3.21. The monthly flux of ^{210}Pb (mBq cm^{-2}) in rain verses the rainfall amount. The rain data is measured at the sampling site.

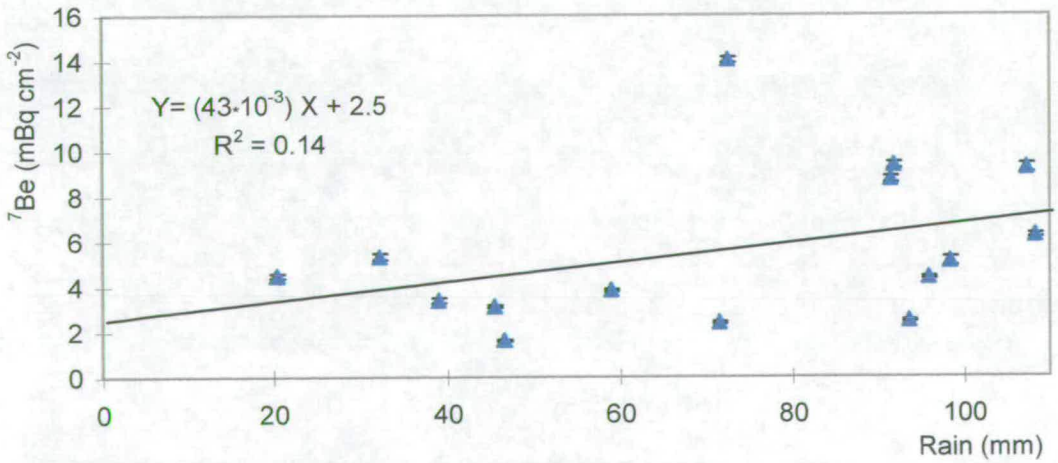

Figure 3.22. The monthly flux of ^{7}Be (mBq cm^{-2}) in rain verses the rainfall amount. The rain data is measured at the sampling site.

3.2.3. Effect of meteorological variables on concentrations of ^{210}Pb and ^{7}Be.

To determine the atmospheric pressure and the origin of air masses associated with the measured concentrations of ^{210}Pb and ^{7}Be, meteorological surface pressure charts were used. The air mass back trajectories for 4 days prior to the rain event were traced from the origin. Precipitation events and other meteorological changes to the air parcel during the trajectory were not considered. To examine the effect of atmosphere pressure on ^{210}Pb and ^{7}Be concentrations (mBq l^{-1}) figures 3.23 and 3.24 were plotted, respectively. The error bars on the graphs, calculated using equation 3.7, are the standard deviations of the concentrations in each bin. These graphs show that for high pressure the concentrations of both isotopes are larger.

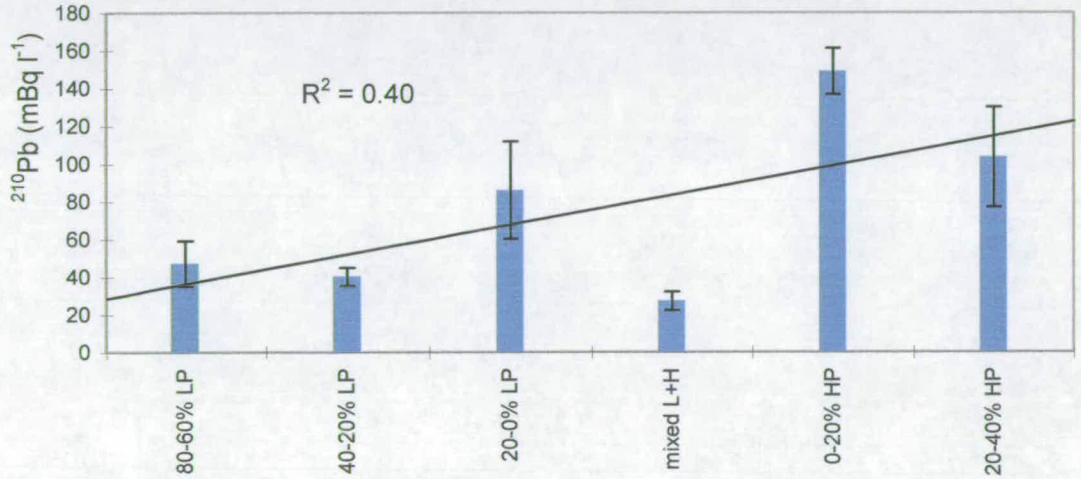

Figure 3.23. The concentrations of ^{210}Pb (mBq l^{-1}) in rain samples plotted against the surface atmospheric pressure. These concentrations were binned to average value for each bin. The units shown on the x-axis are explained in section 3.1.4.

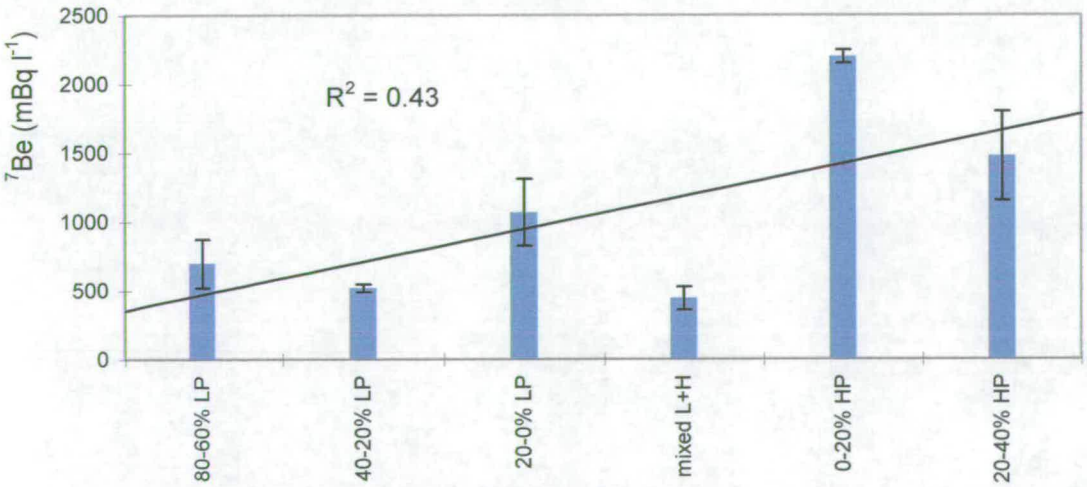

Figure 3.24. The concentrations of ^{7}Be (mBq l^{-1}) in rain samples plotted verses the surface atmospheric pressure. These concentrations were binned to average value at each bin. The units shown on the x-axis are explained in section 3.1.4.

To investigate the effect of the origin of air masses (i.e. continental or oceanic) figures 3.25 and 3.26 were plotted for ^{210}Pb and ^{7}Be, respectively. The total measured 31 samples were used then to get the percentages of continental and oceanic air masses.

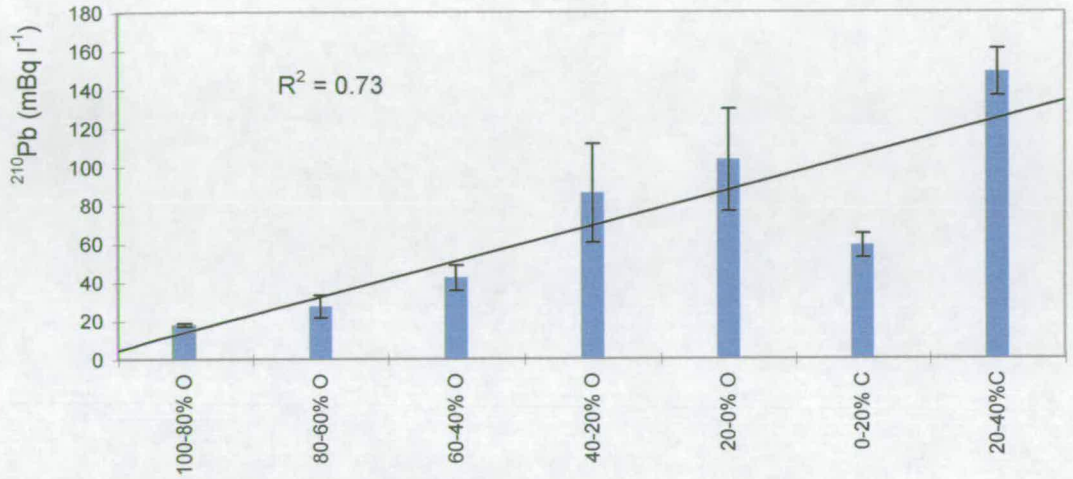

Figure 3.25. The concentrations of ^{210}Pb (mBq l^{-1}) in rain samples plotted against the continental and oceanic air masses. These concentrations were binned to provide average value. The units shown on the x-axis are explained in section 3.1.5.

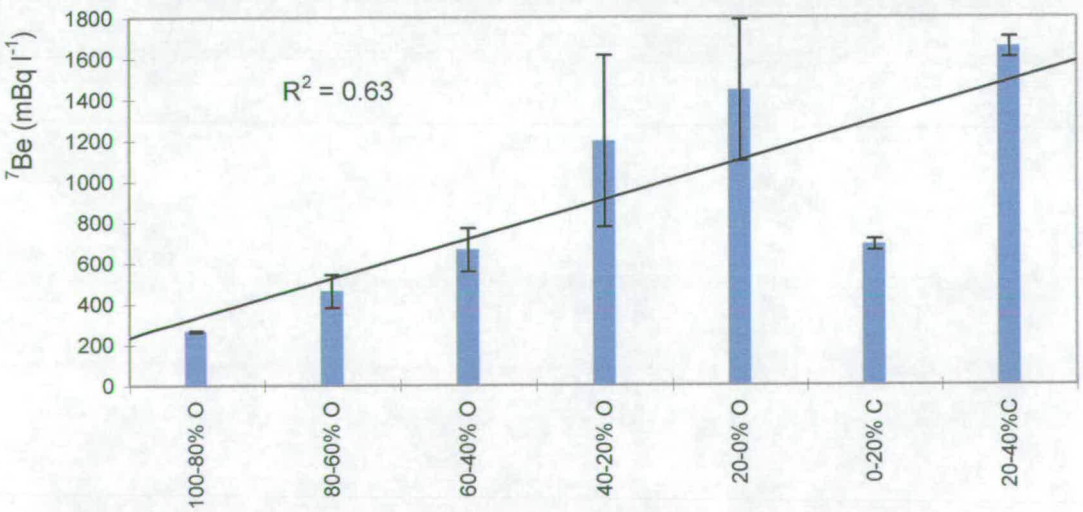

Figure 3.26. The concentrations of ^{7}Be (mBq l^{-1}) in rain samples plotted against the continental and oceanic air masses. These concentrations were binned to get the average value at each bin. The units shown on the x-axis are explained in section 3.1.5.

3.2.4. Seasonal variations of ^{210}Pb and ^{7}Be fluxes in precipitation.

The seasonal fluxes of ^{210}Pb and ^{7}Be were plotted in figures 3.27 and 3.28, respectively. To calculate the fluxes for each season, equation 3.4 and the data in table 3.2 were used.

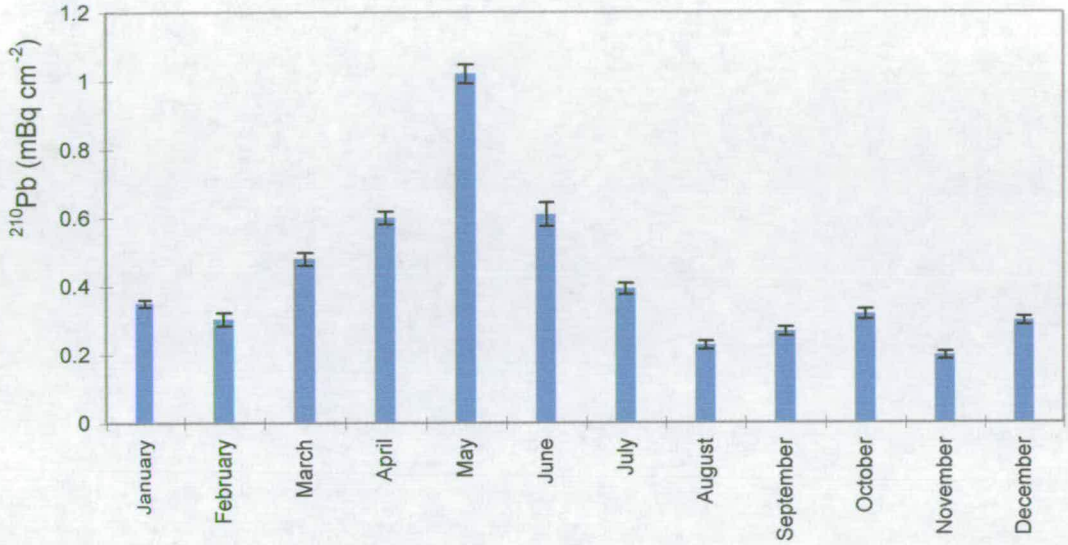

Figure 3.27. The seasonal variations of ^{210}Pb total deposition flux (mBq cm^{-2}) in rain samples.

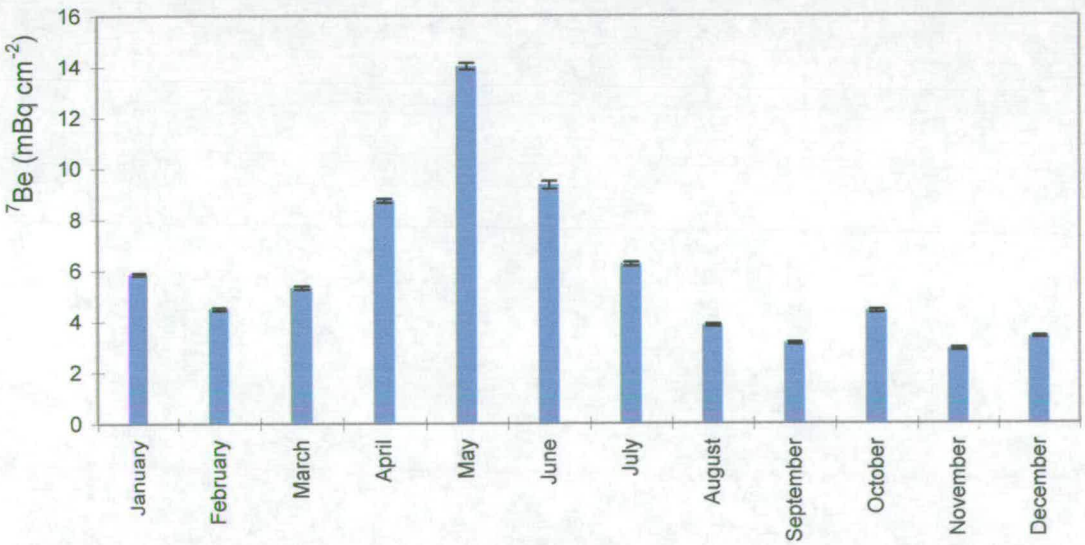

Figure 3.28. The seasonal variations of ^{7}Be total deposition flux (mBq cm^{-2}) in rain samples.

Due to the fact that these plots are based on 15 months of data, some concentrations, (i.e. 3 months of November, December and January), for ^{210}Pb and ^{7}Be are based on combined results from 1997 and 1998. The concentration of these isotopes, during

the 15 month of measurement, varied by a factor of 5.16 (from 0.198 ± 0.011 to 1.02 ± 0.028 mBq cm^{-2}) and 4.63 (from 2.90 ± 0.056 to 14.02 ± 0.128 mBq cm^{-2}) for ^{210}Pb and ^{7}Be, respectively.

The measured annual fluxes of ^{210}Pb in rain was 0.400 ± 0.005 (mBq cm^{-2}) and for ^{7}Be was 5.69 ± 0.02 mBq cm^{-2}. Their annual concentrations in rain were 62.6 ± 9.3 and 732 ± 27 mBq l^{-1}, for ^{210}Pb and ^{7}Be, respectively. The concentrations were obtained by dividing the total activity (mBq) by the total rainfall (litre of rain), using the data reported in table 3.2 appendix B, from November 1997 to January 1999.

3.3. ^{210}Pb and ^{137}Cs inventories measured in Rothamsted soils.

In this section, the deposition rates of atmospherically derived ^{210}Pb and ^{137}Cs for the forests and open areas of Rothamsted experimental farm are reported. The measurements were obtained from the profiles of inventories from core samples of undisturbed soils. In total, 150 sub-samples obtained from 10 sites, were analysed. The complete data set is presented in tables 3.3_a, 3.3_b, and 3.4 reported in Appendix C. The errors reported in tables 3.3_a, 3.3_b and 3.4 were the counting statistical errors ($\pm\sigma$).

3.3.1. Absorption of the radiation by the soil sample.

The gamma spectroscopy of each sub-sample provided a direct measurement of the activity of radioisotopes ^{210}Pb, ^{214}Pb, and ^{137}Cs in the soil. The procedures were explained in section 2.3. Self-absorption of the radiation by the sample is important and must be corrected for. To provide the correction and quantify the capture and attenuation of the gamma rays in the soil, standard point sources of ^{210}Pb, ^{133}Ba, and ^{137}Cs were used. Procedures of Cutshall et al. (1983) were used to analyse the data as explained in chapter 2. For each sub-sample the capture and attenuation varied with the density of the soil, i.e. as the soil density increased the capture and attenuation increased. The variations of self absorption in the soil were most important for the low energy ^{210}Pb peak (46.5 keV) and less important for ^{214}Pb (351.9 keV) and ^{137}Cs (661.9 keV). Measurements were made for all of the 150 sub-samples of the soil. The measured self absorption value for the 150 sub-samples of the soil ranged from 17 to 89 %, 8 to 40%, and 3 to 12 % for ^{210}Pb, ^{214}Pb and ^{137}Cs, respectively.

3.3.2. Correction procedures for self absorption.

Knowing the self absorption of the soil, corrections were made for the background radiation at 46.5 keV and 351.9 keV before the activity was calculated. These corrections were very important for ^{210}Pb isotopes. Having corrected for the above, the true contributions of each isotope to the activity of the soil could be determined. The activity of each sub-sample was calculated knowing the branching ratio (b_γ) and the full-energy peak efficiency (ε_{FEP}) of detection at each isotope energy and using equation 3.11.

$$A = \{ (\gamma s^{-1}) / [(\varepsilon_{FEP}) (b_\gamma)] \} \qquad \text{....(3.11),}$$

where A is the activity of each radioisotope in the holder,

$\gamma\ s^{-1}$ is the gamma counts per second of each isotope detected by the detector,

ε_{FEP} is the full-energy peak efficiency of the detector for each isotope, and

b_γ is the branching ratio of the gamma rays.

3.3.3. Atmospherically derived ^{210}Pb inventories.

The atmospherically derived component of ^{210}Pb in soil must be distinguished from that produced in situ by the decay of ^{214}Pb. If no ^{222}Rn were lost to the atmosphere from the soils, then the atmospherically derived ^{210}Pb would be equal to the excess of ^{210}Pb over ^{214}Pb.

$$(^{210}Pb)_{atm} = (^{210}Pb)_m - (^{214}Pb)_m \quad \text{....(3.12),}$$

where, $(^{210}Pb)_{atm}$ is the specific activity of the atmospherically derived ^{210}Pb,

$(^{210}Pb)_m$ is the specific activity of measured ^{210}Pb, and

$(^{214}Pb)_m$ is the specific activity of measured ^{214}Pb.

This procedure assumes equilibrium between the activity of ^{214}Pb and the activity of the supported ^{210}Pb in the sample and is reasonable since the two isotopes, ^{214}Bi ($\tau_{1/2}$= 20 m) and ^{214}Po ($\tau_{1/2}$= 1.6×10^{-4} s), are also short-lived. The activity of the atmospherically derived ^{210}Pb rapidly decreases with depth in a soil. Deeper than 20 cm, the quantity is usually too small to be detected. The inventory of ^{210}Pb and ^{137}Cs in the soil for each holder were calculated and corrected for each sub-sample's weight. The results of each sub-sample activity were decay corrected to obtain the ^{210}Pb and ^{137}Cs inventories on 2nd February 1998, so that the data from different cores may be directly compared.

The total inventory of ^{210}Pb and ^{137}Cs in each core was determined by summing the contribution of each section of the core. The complete data set is reported in table 3.5. Details of these measurements were reported in chapter two. Each site is identified by a letter "R" and a number, for example R1 represents site 1. For each site, we removed 5 cores which were identified by capital letters A, B, C, D, and E.

3.3.4. Specific activity profiles of ^{210}Pb and ^{137}Cs in soil.

Figures 3.29 to 3.48 show the specific activity profiles of ^{210}Pb and ^{137}Cs (Bq kg^{-1}) with depth in the soil. The error bars shown on the graphs are the one-sigma ($\pm\sigma$) percentage counting errors. The one-sigma percentage counting error for ^{210}Pb

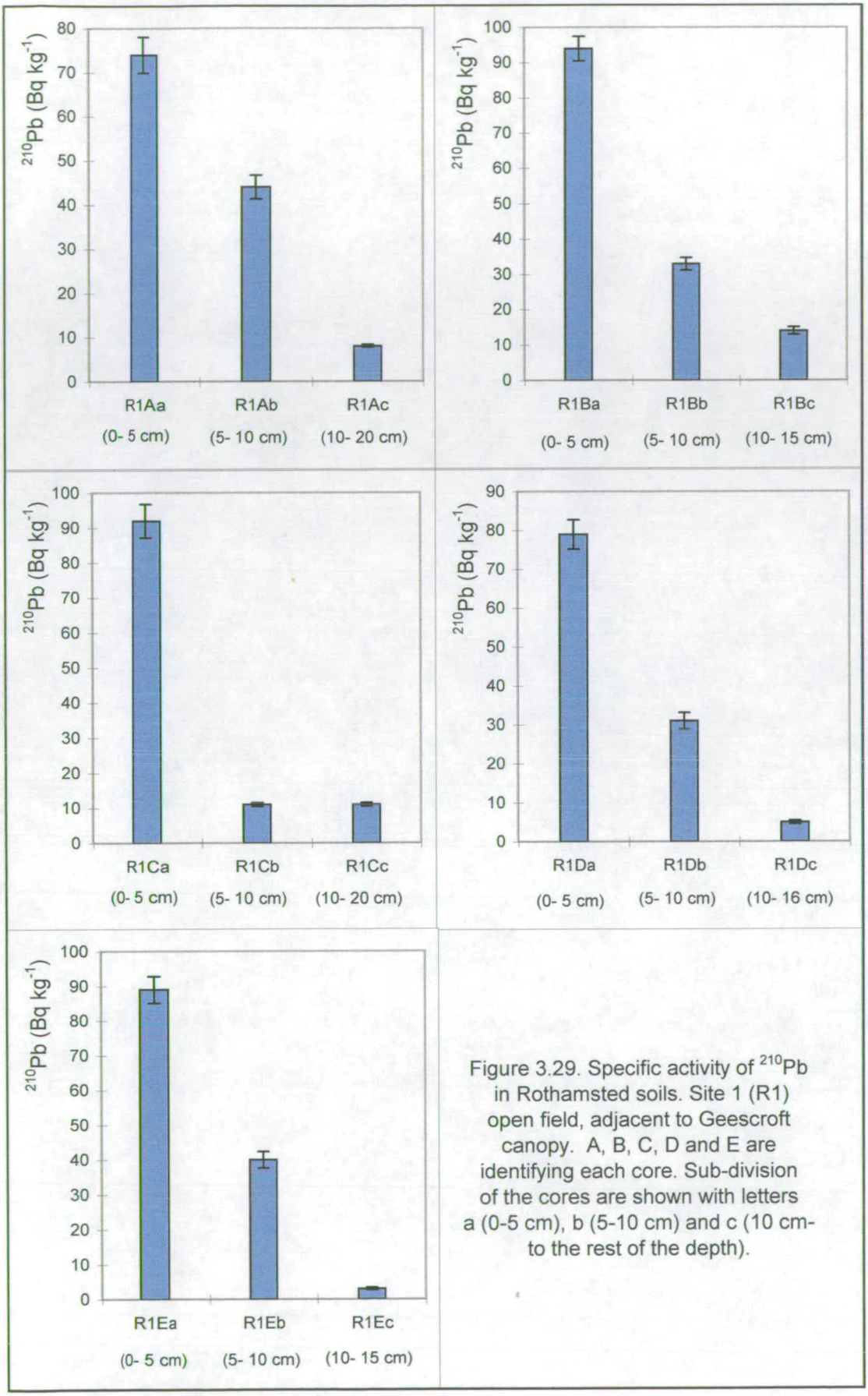

Figure 3.29. Specific activity of ^{210}Pb in Rothamsted soils. Site 1 (R1) open field, adjacent to Geescroft canopy. A, B, C, D and E are identifying each core. Sub-division of the cores are shown with letters a (0-5 cm), b (5-10 cm) and c (10 cm- to the rest of the depth).

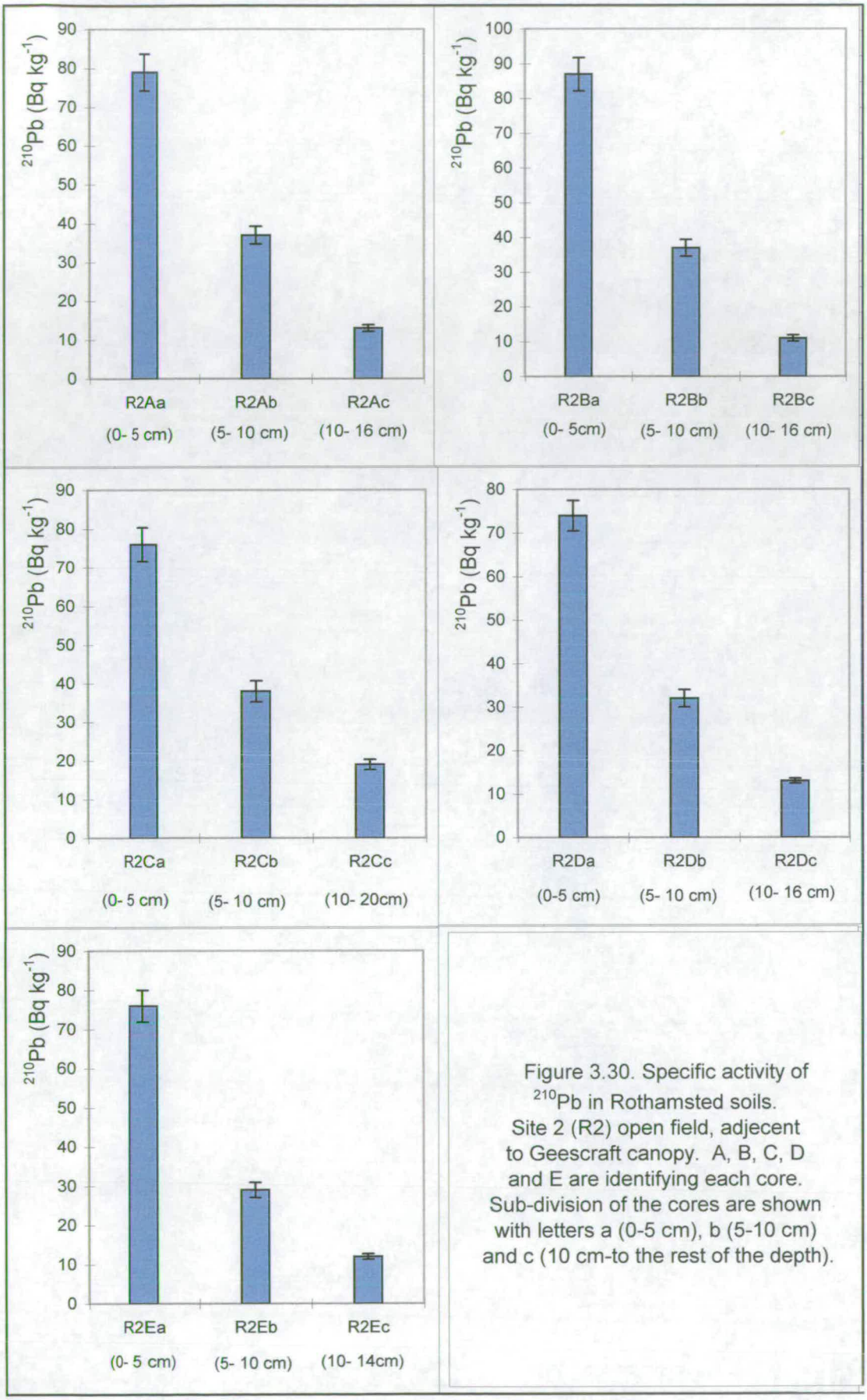

Figure 3.30. Specific activity of ^{210}Pb in Rothamsted soils. Site 2 (R2) open field, adjecent to Geescraft canopy. A, B, C, D and E are identifying each core. Sub-division of the cores are shown with letters a (0-5 cm), b (5-10 cm) and c (10 cm-to the rest of the depth).

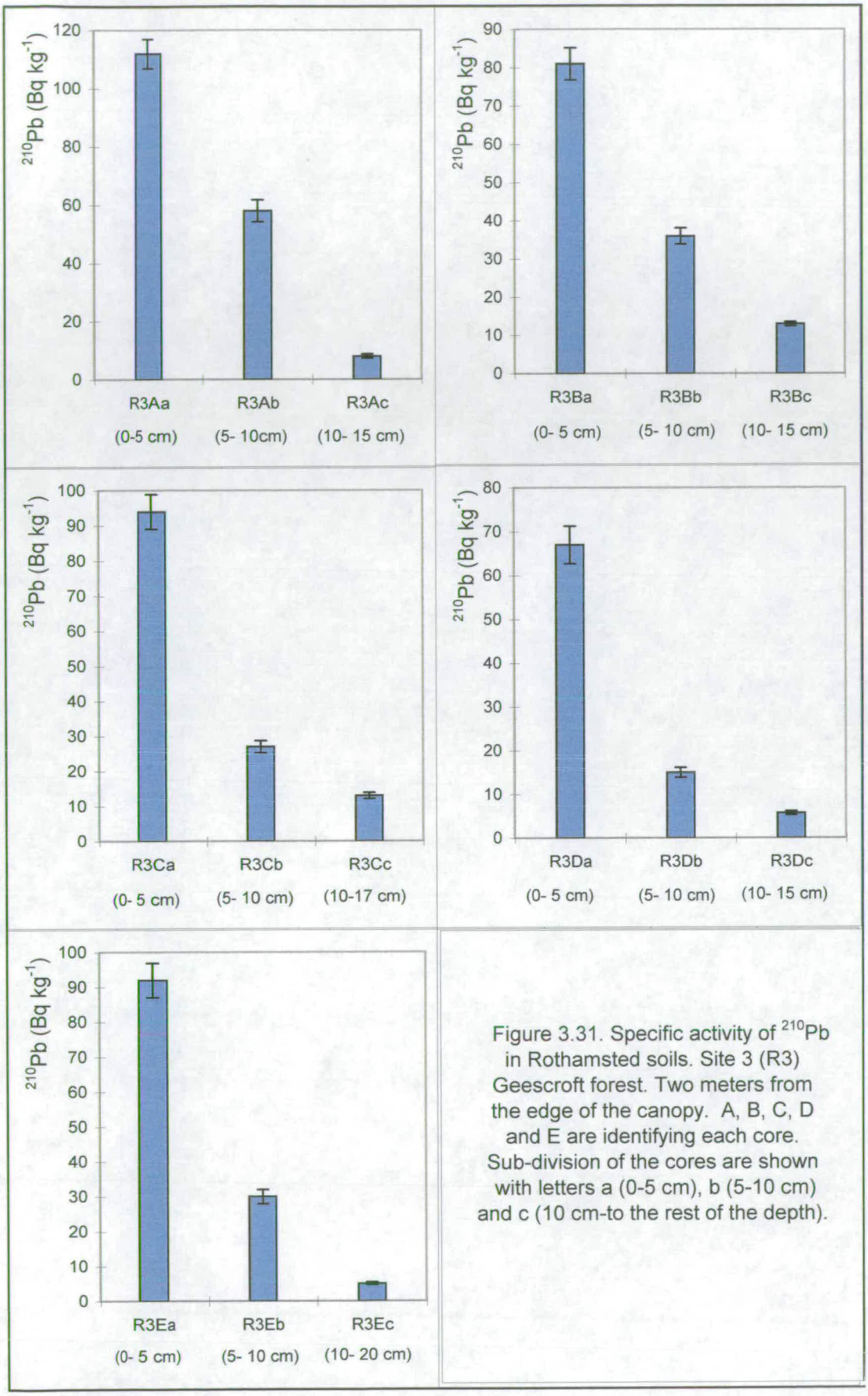

Figure 3.31. Specific activity of ^{210}Pb in Rothamsted soils. Site 3 (R3) Geescroft forest. Two meters from the edge of the canopy. A, B, C, D and E are identifying each core. Sub-division of the cores are shown with letters a (0-5 cm), b (5-10 cm) and c (10 cm-to the rest of the depth).

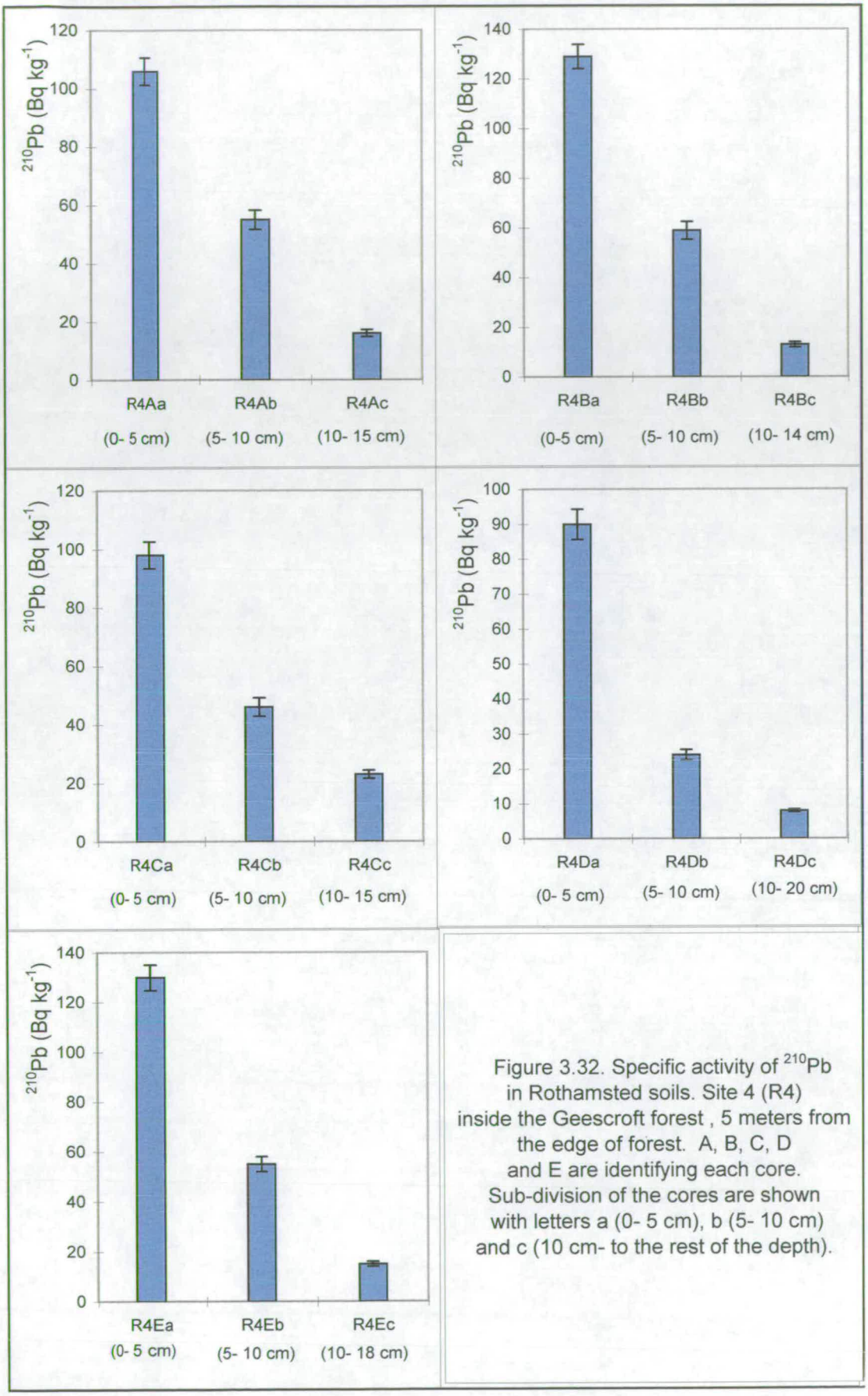

Figure 3.32. Specific activity of ^{210}Pb in Rothamsted soils. Site 4 (R4) inside the Geescroft forest , 5 meters from the edge of forest. A, B, C, D and E are identifying each core. Sub-division of the cores are shown with letters a (0- 5 cm), b (5- 10 cm) and c (10 cm- to the rest of the depth).

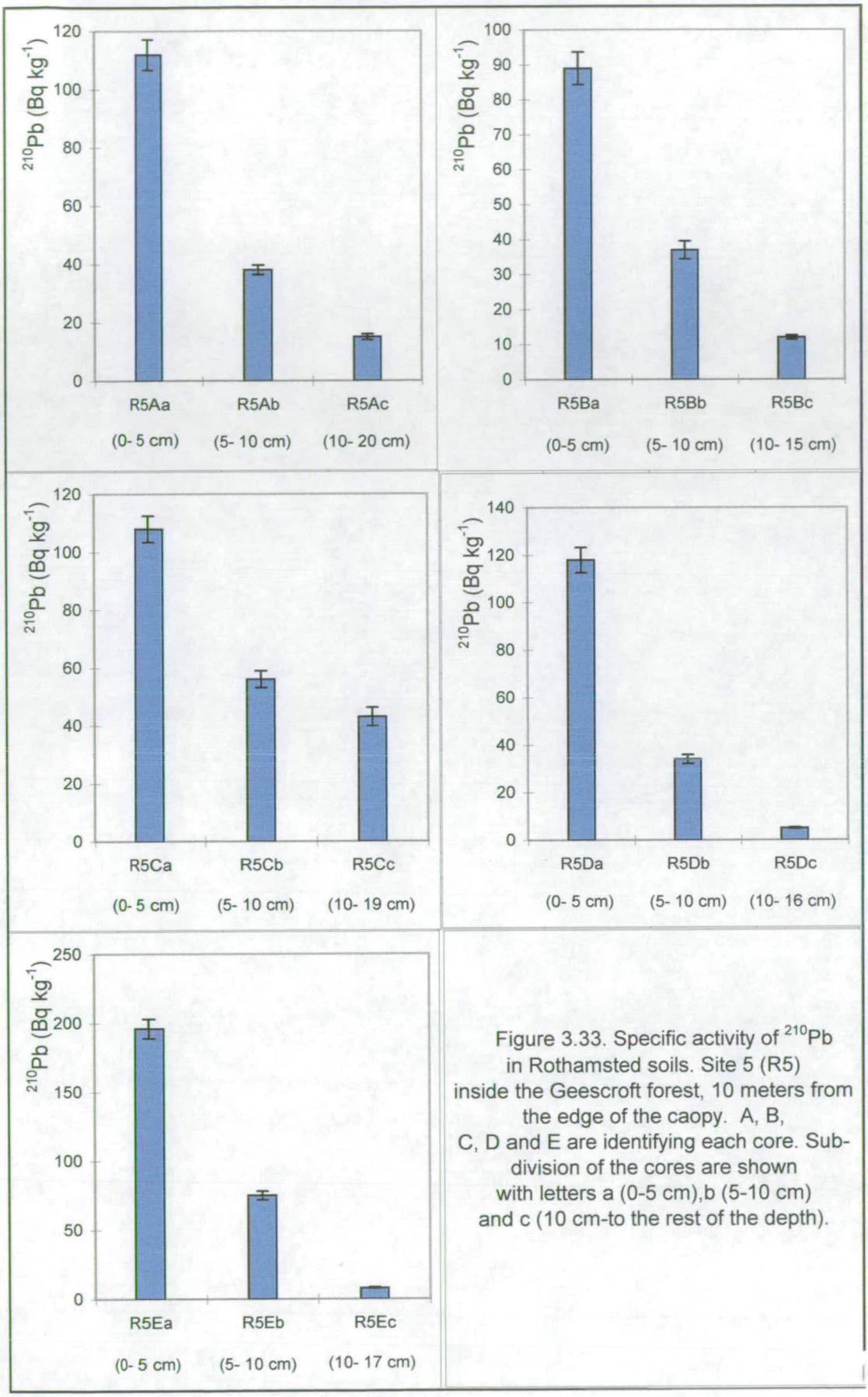

Figure 3.33. Specific activity of ^{210}Pb in Rothamsted soils. Site 5 (R5) inside the Geescroft forest, 10 meters from the edge of the caopy. A, B, C, D and E are identifying each core. Sub-division of the cores are shown with letters a (0-5 cm),b (5-10 cm) and c (10 cm-to the rest of the depth).

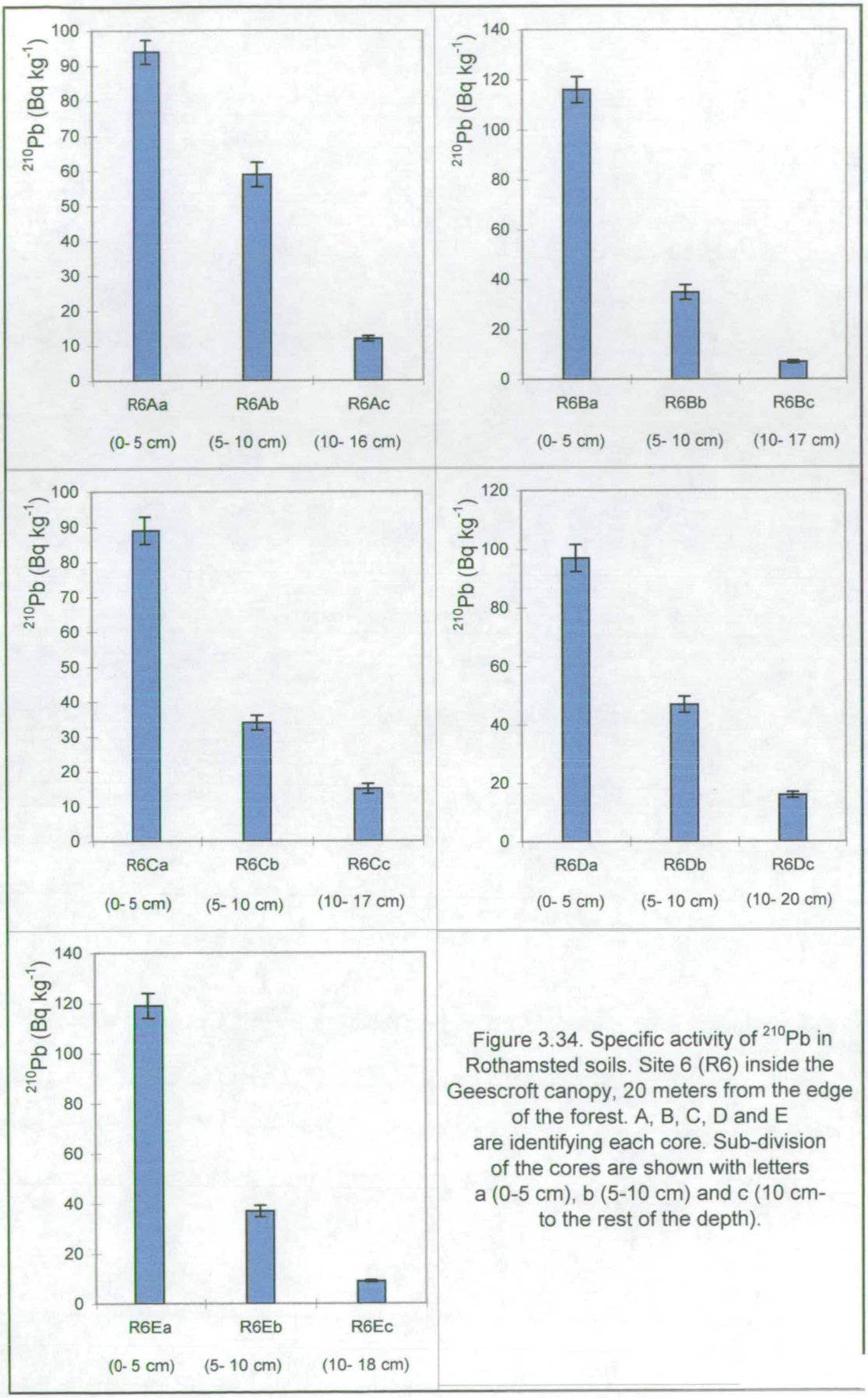

Figure 3.34. Specific activity of ^{210}Pb in Rothamsted soils. Site 6 (R6) inside the Geescroft canopy, 20 meters from the edge of the forest. A, B, C, D and E are identifying each core. Sub-division of the cores are shown with letters a (0-5 cm), b (5-10 cm) and c (10 cm- to the rest of the depth).

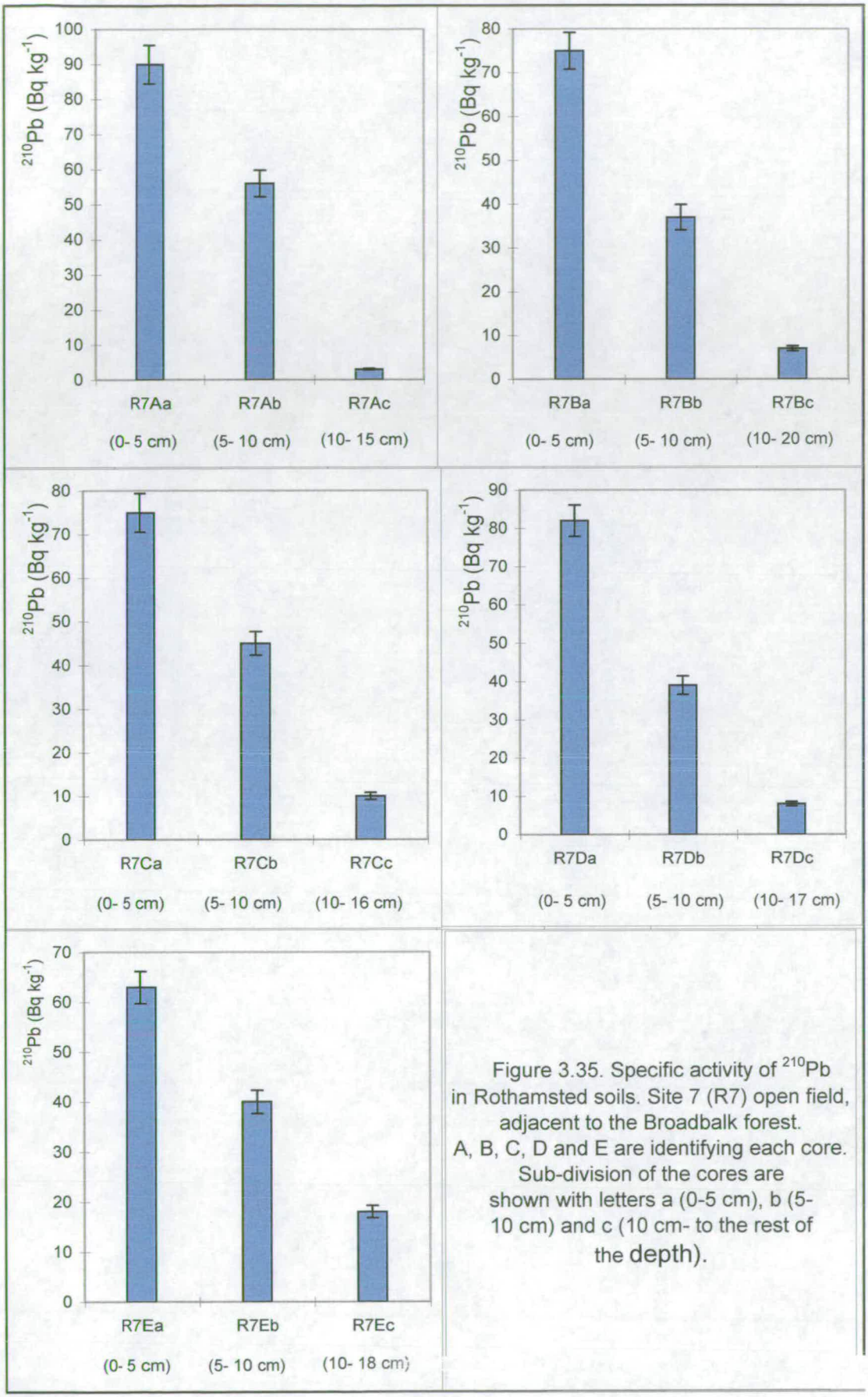

Figure 3.35. Specific activity of ^{210}Pb in Rothamsted soils. Site 7 (R7) open field, adjacent to the Broadbalk forest. A, B, C, D and E are identifying each core. Sub-division of the cores are shown with letters a (0-5 cm), b (5-10 cm) and c (10 cm- to the rest of the depth).

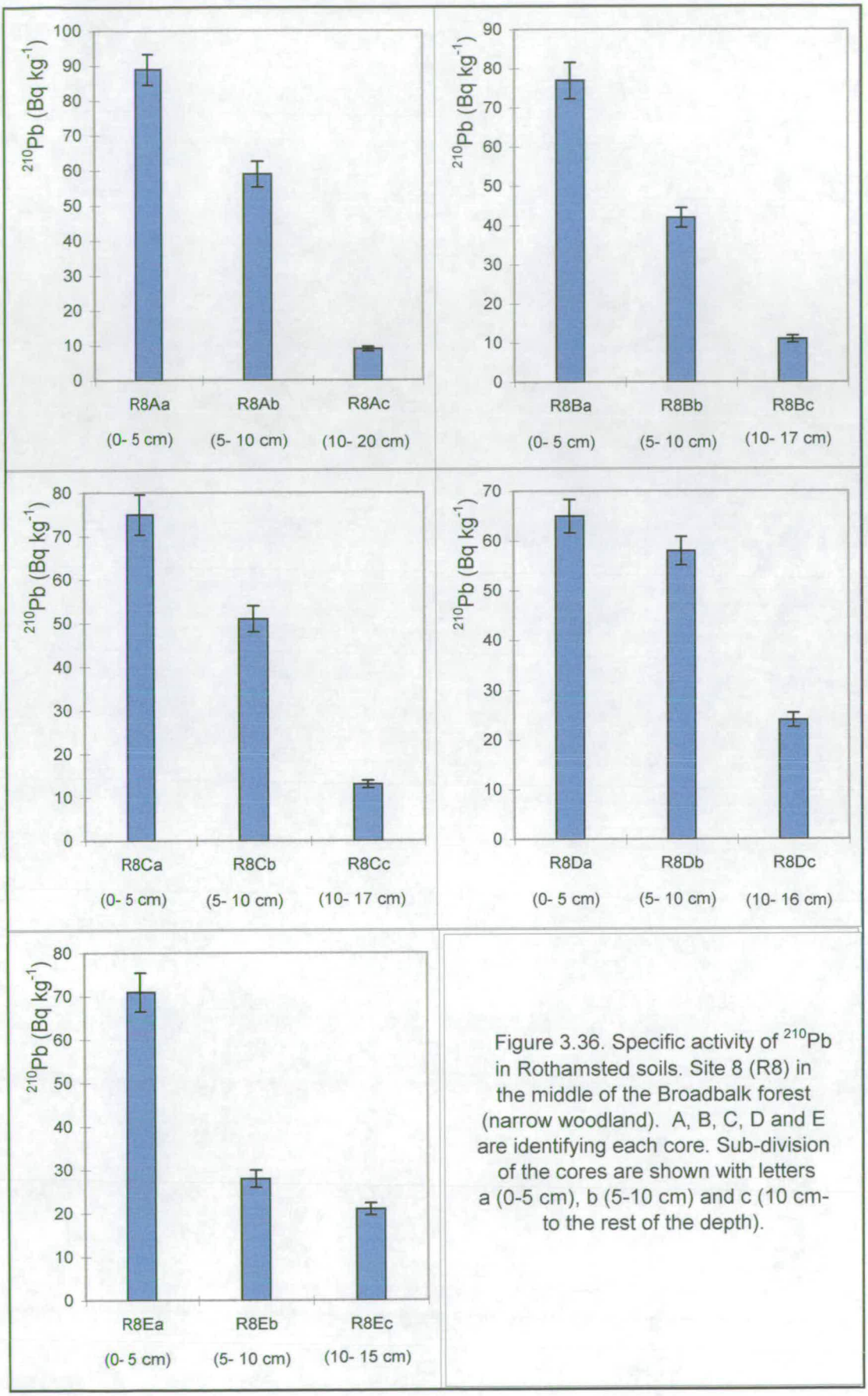

Figure 3.36. Specific activity of ^{210}Pb in Rothamsted soils. Site 8 (R8) in the middle of the Broadbalk forest (narrow woodland). A, B, C, D and E are identifying each core. Sub-division of the cores are shown with letters a (0-5 cm), b (5-10 cm) and c (10 cm- to the rest of the depth).

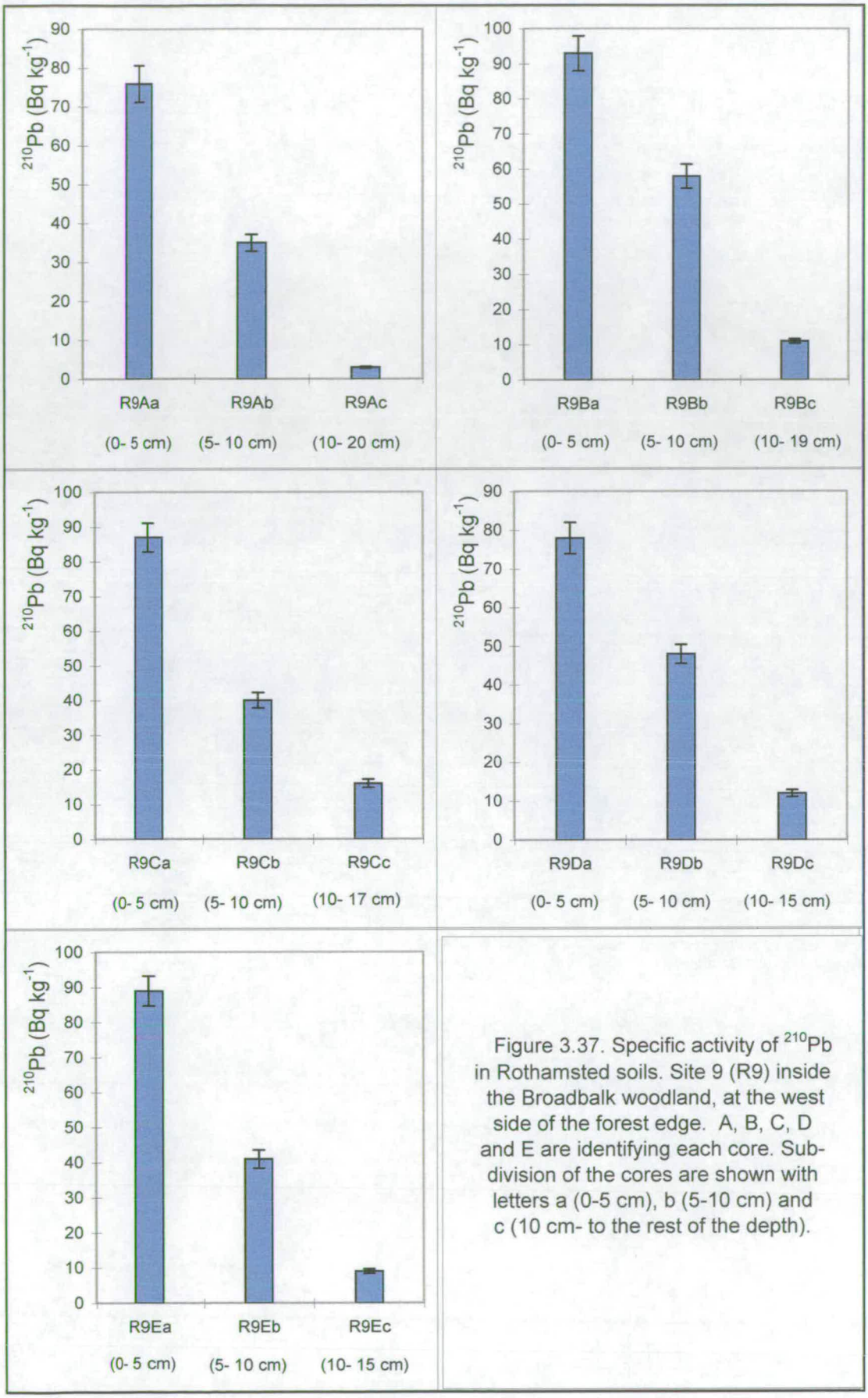

Figure 3.37. Specific activity of ^{210}Pb in Rothamsted soils. Site 9 (R9) inside the Broadbalk woodland, at the west side of the forest edge. A, B, C, D and E are identifying each core. Sub-division of the cores are shown with letters a (0-5 cm), b (5-10 cm) and c (10 cm- to the rest of the depth).

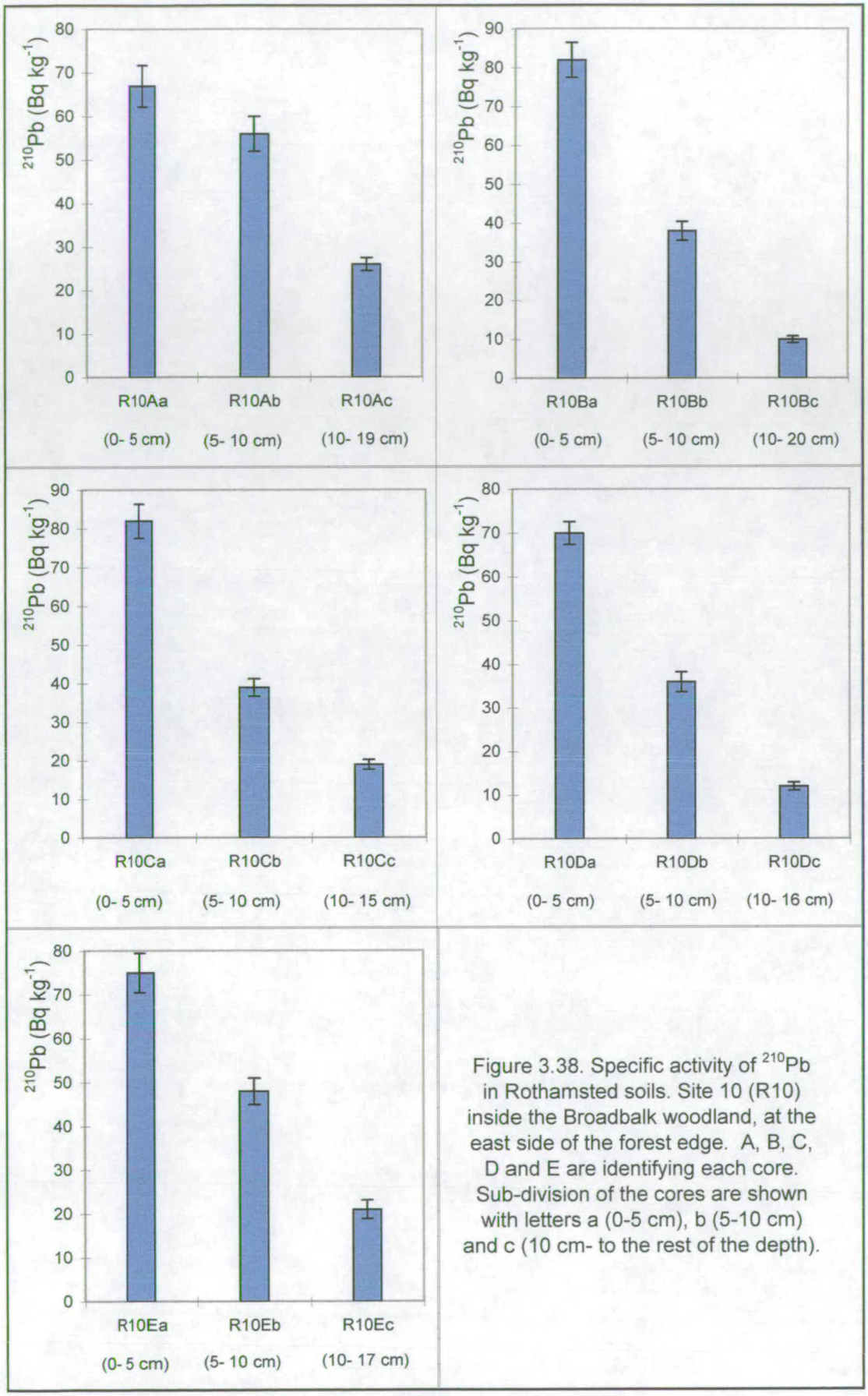

Figure 3.38. Specific activity of ^{210}Pb in Rothamsted soils. Site 10 (R10) inside the Broadbalk woodland, at the east side of the forest edge. A, B, C, D and E are identifying each core. Sub-division of the cores are shown with letters a (0-5 cm), b (5-10 cm) and c (10 cm- to the rest of the depth).

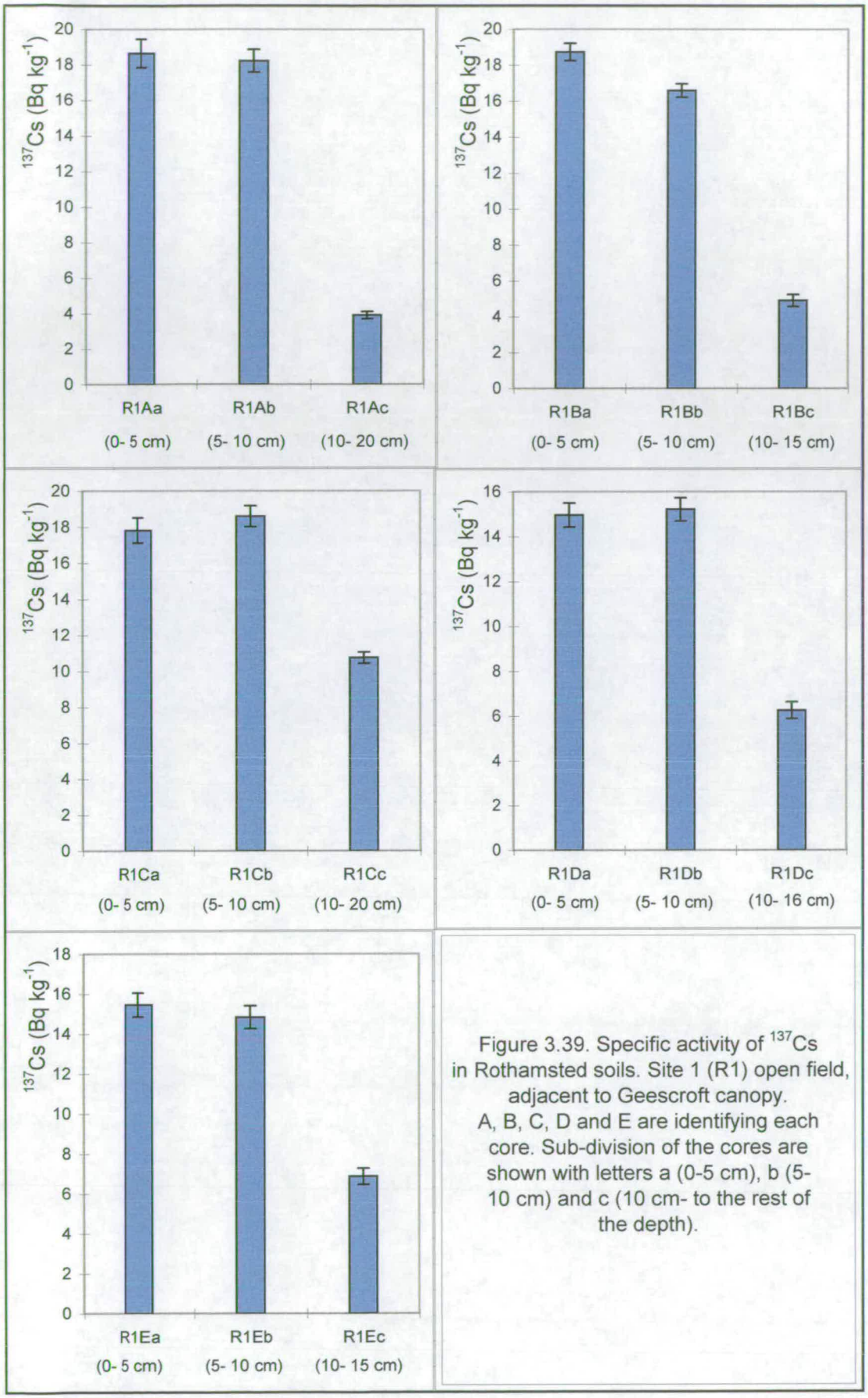

Figure 3.39. Specific activity of ^{137}Cs in Rothamsted soils. Site 1 (R1) open field, adjacent to Geescroft canopy. A, B, C, D and E are identifying each core. Sub-division of the cores are shown with letters a (0-5 cm), b (5-10 cm) and c (10 cm- to the rest of the depth).

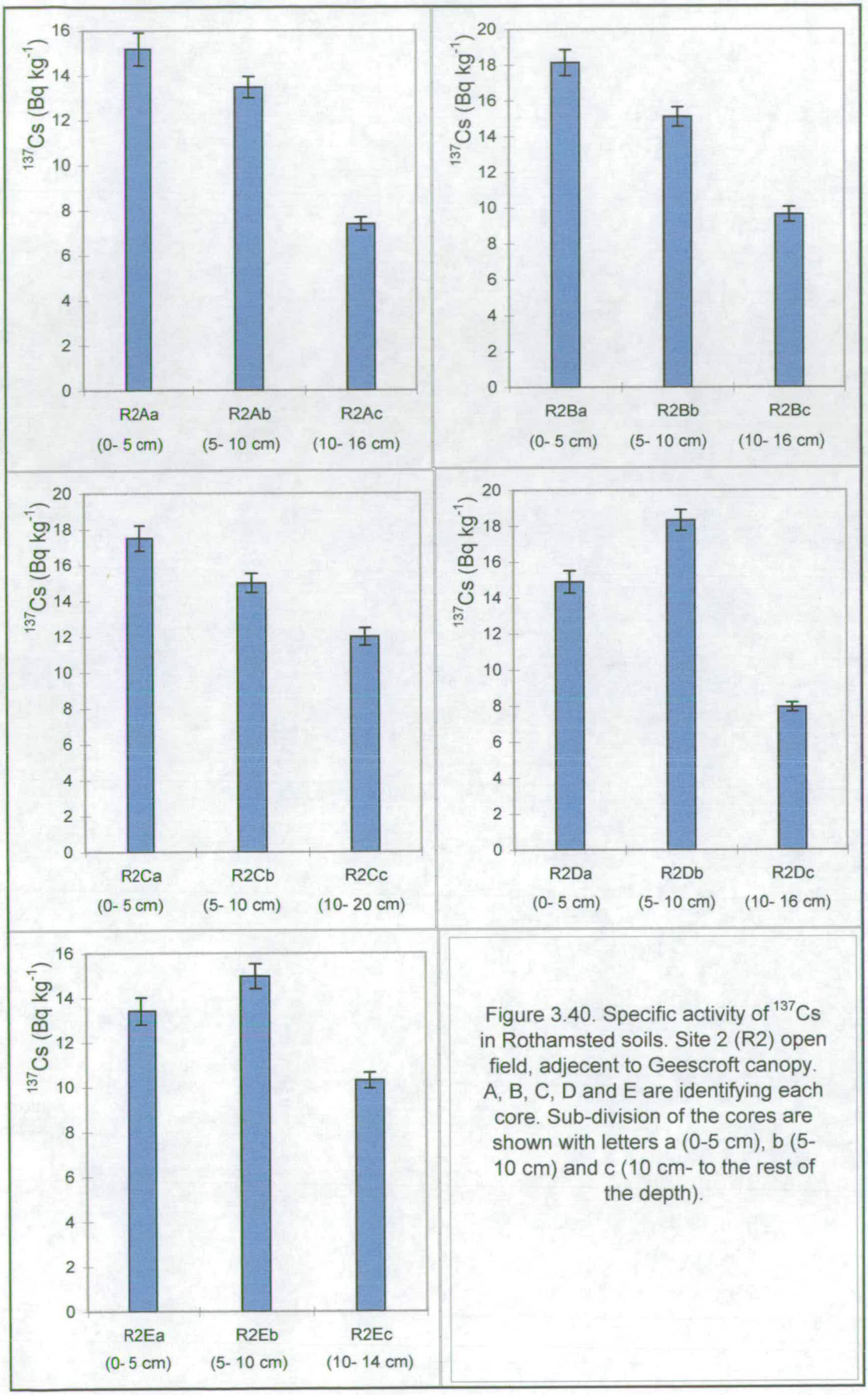

Figure 3.40. Specific activity of ^{137}Cs in Rothamsted soils. Site 2 (R2) open field, adjecent to Geescroft canopy. A, B, C, D and E are identifying each core. Sub-division of the cores are shown with letters a (0-5 cm), b (5-10 cm) and c (10 cm- to the rest of the depth).

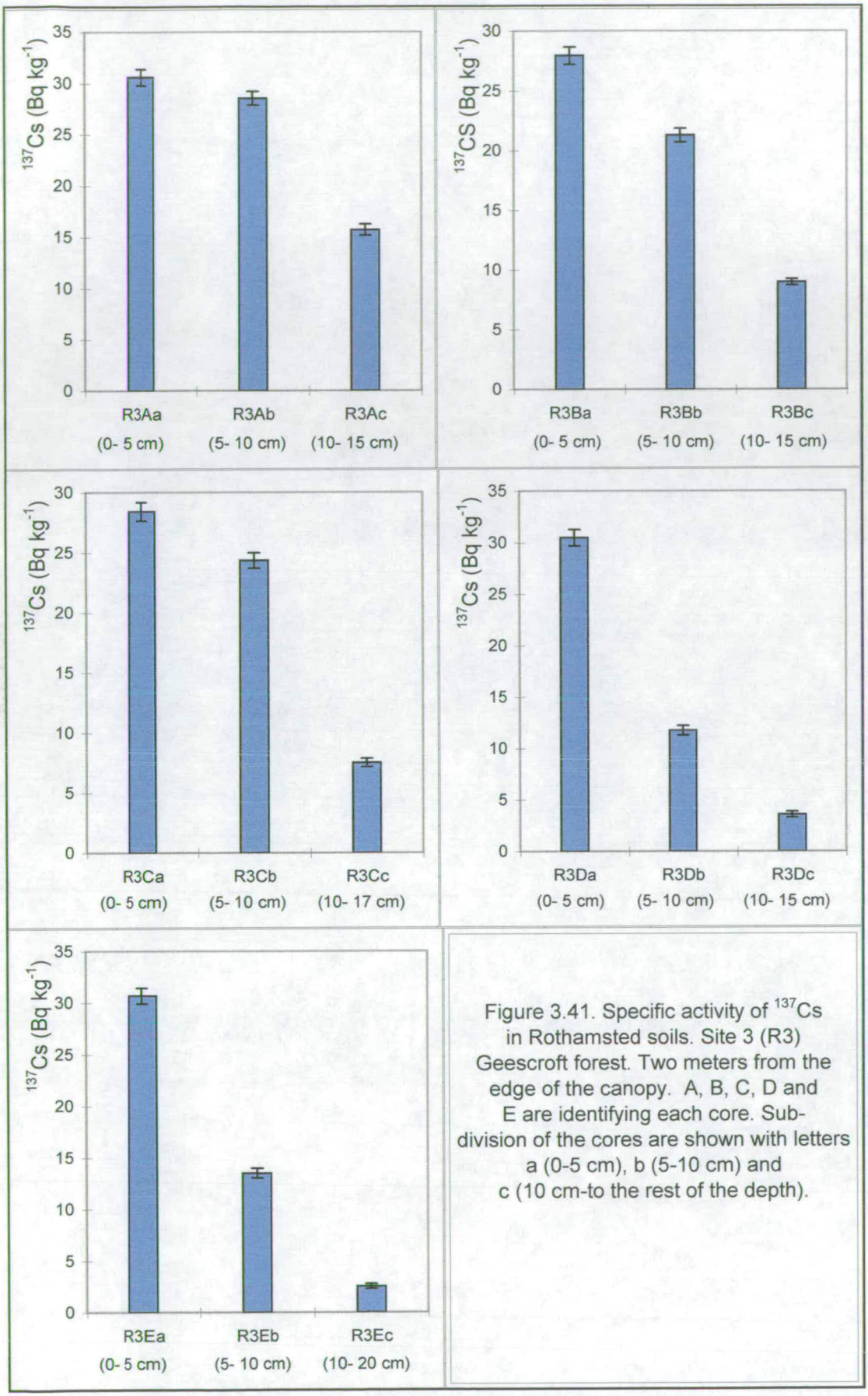

Figure 3.41. Specific activity of ^{137}Cs in Rothamsted soils. Site 3 (R3) Geescroft forest. Two meters from the edge of the canopy. A, B, C, D and E are identifying each core. Sub-division of the cores are shown with letters a (0-5 cm), b (5-10 cm) and c (10 cm-to the rest of the depth).

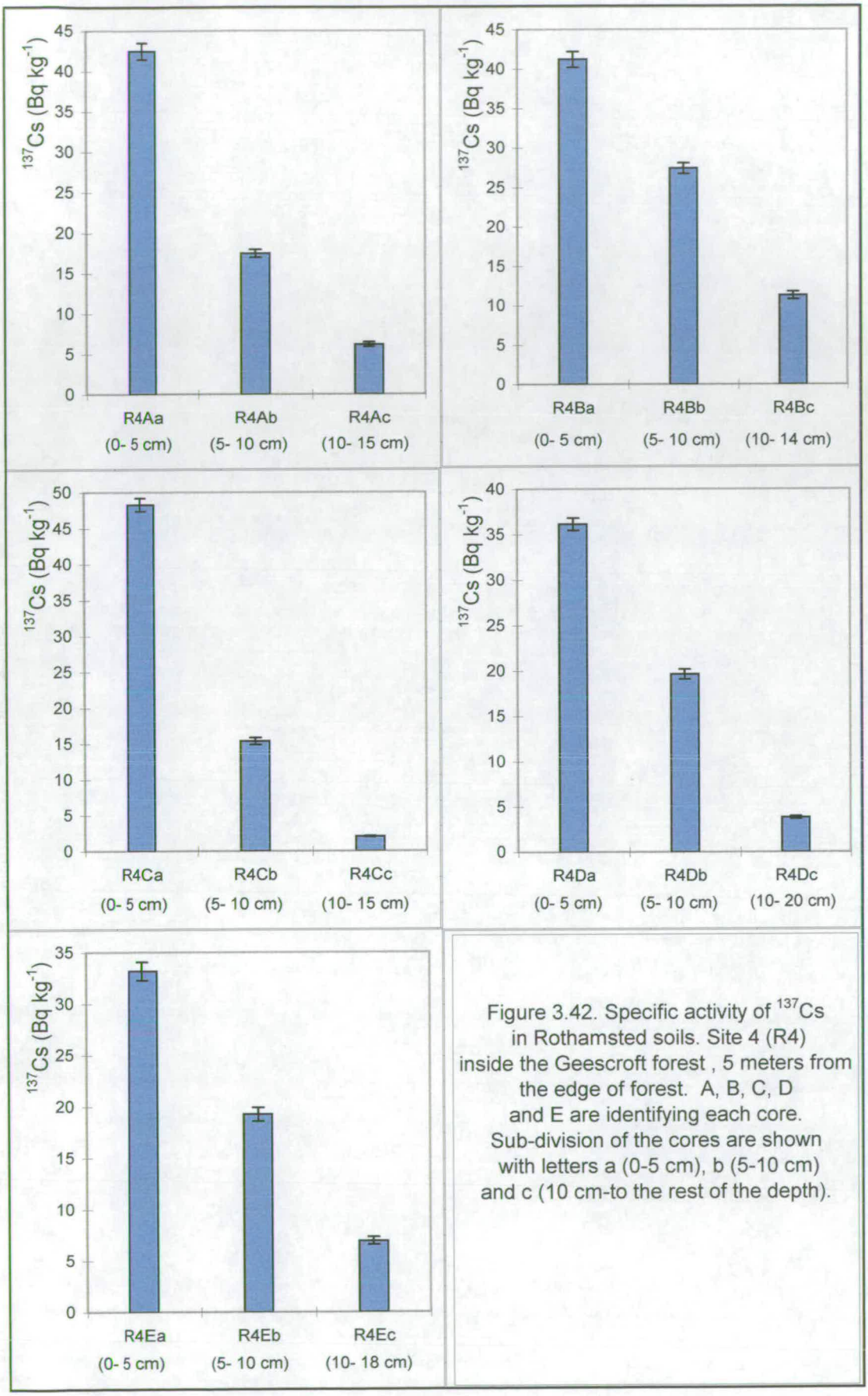

Figure 3.42. Specific activity of ^{137}Cs in Rothamsted soils. Site 4 (R4) inside the Geescroft forest , 5 meters from the edge of forest. A, B, C, D and E are identifying each core. Sub-division of the cores are shown with letters a (0-5 cm), b (5-10 cm) and c (10 cm-to the rest of the depth).

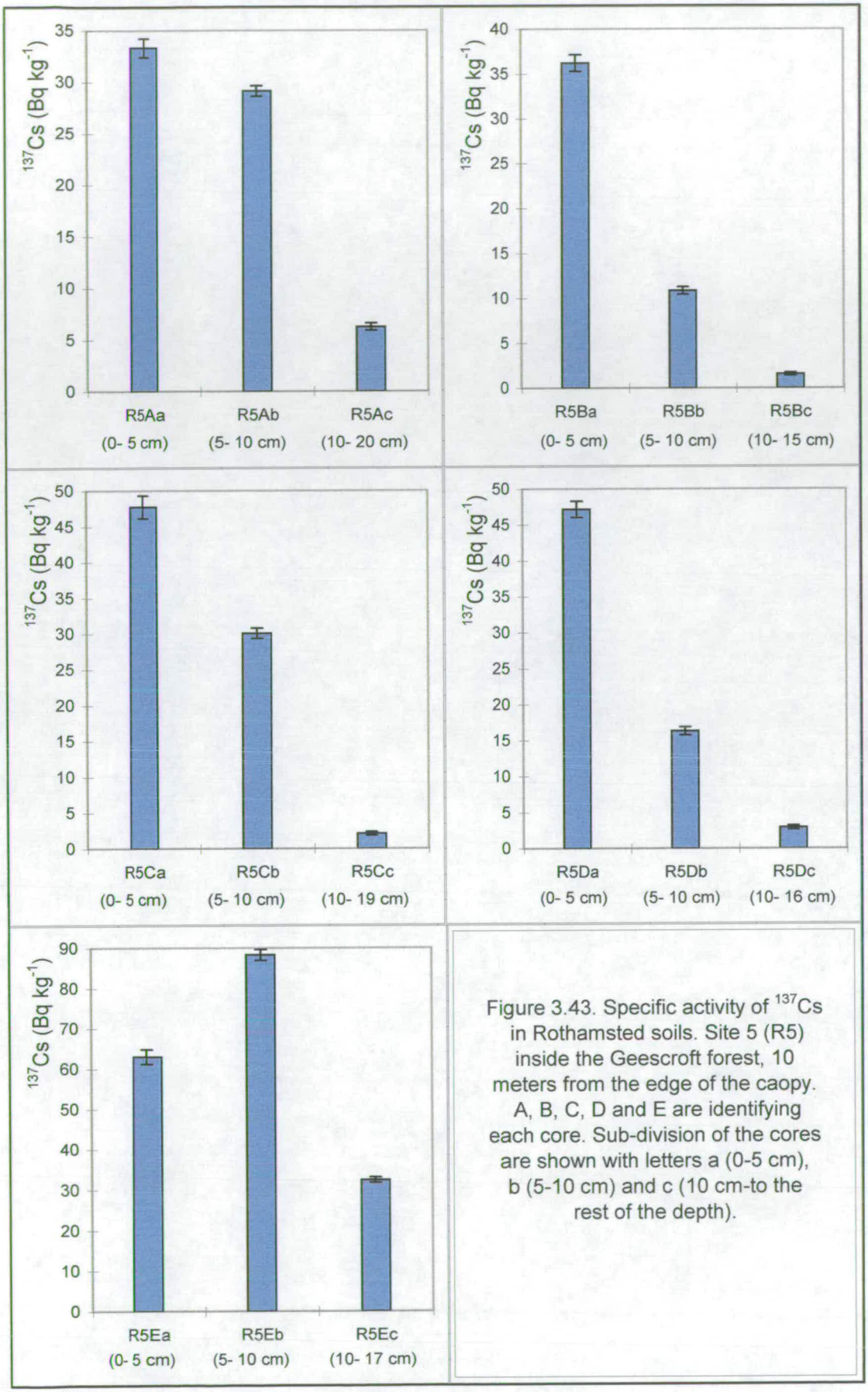

Figure 3.43. Specific activity of ^{137}Cs in Rothamsted soils. Site 5 (R5) inside the Geescroft forest, 10 meters from the edge of the caopy. A, B, C, D and E are identifying each core. Sub-division of the cores are shown with letters a (0-5 cm), b (5-10 cm) and c (10 cm-to the rest of the depth).

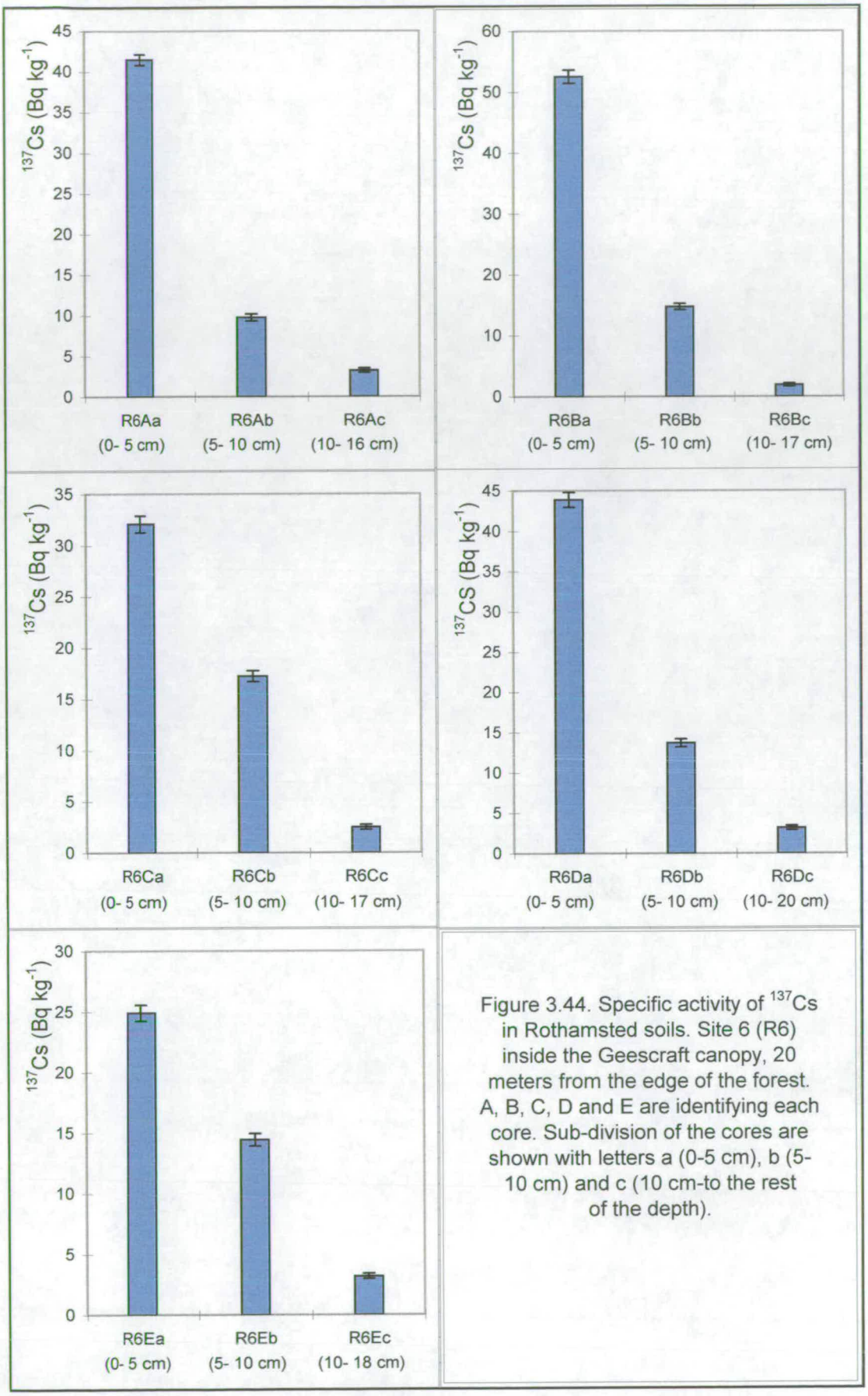

Figure 3.44. Specific activity of ^{137}Cs in Rothamsted soils. Site 6 (R6) inside the Geescraft canopy, 20 meters from the edge of the forest. A, B, C, D and E are identifying each core. Sub-division of the cores are shown with letters a (0-5 cm), b (5-10 cm) and c (10 cm-to the rest of the depth).

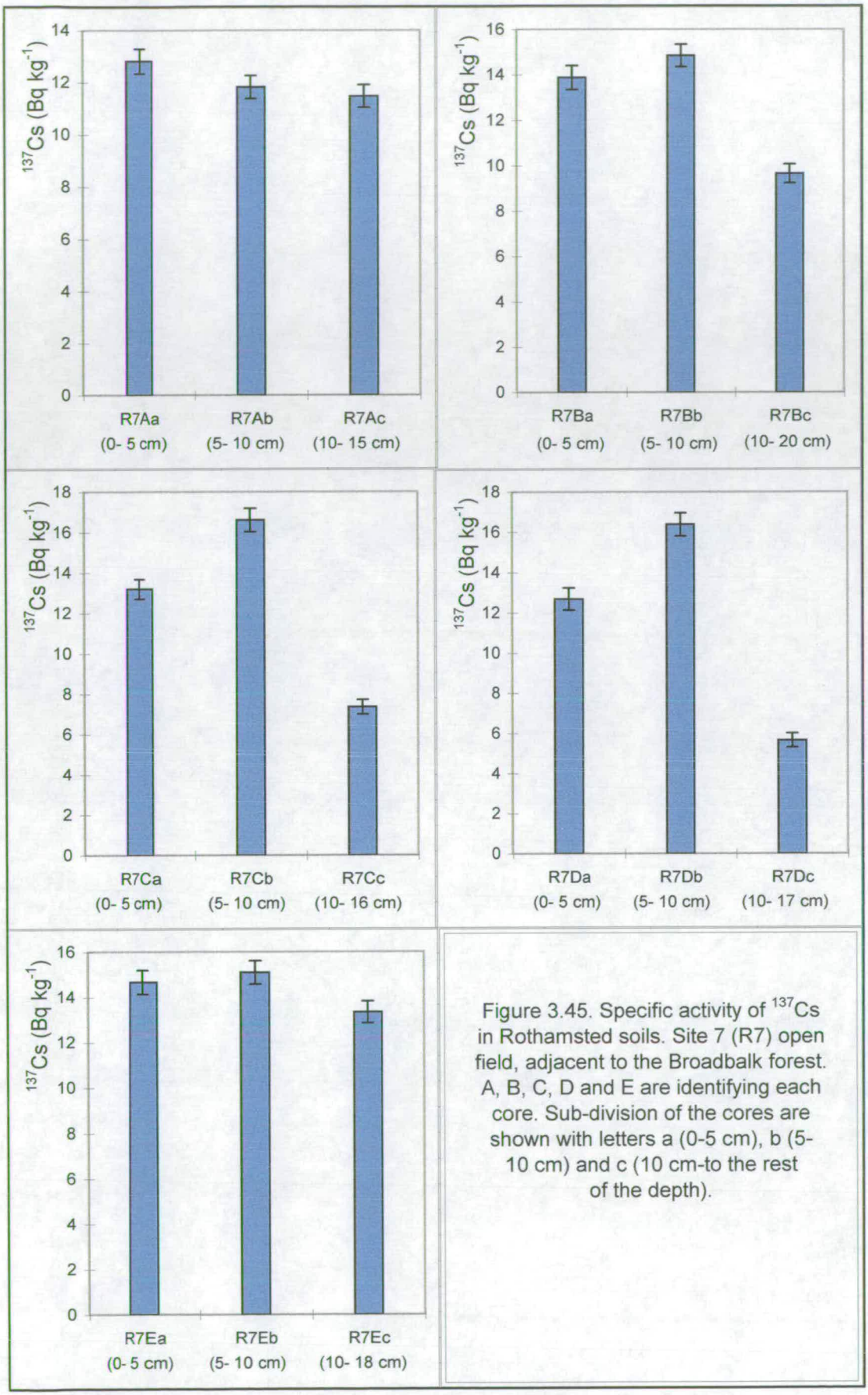

Figure 3.45. Specific activity of ^{137}Cs in Rothamsted soils. Site 7 (R7) open field, adjacent to the Broadbalk forest. A, B, C, D and E are identifying each core. Sub-division of the cores are shown with letters a (0-5 cm), b (5-10 cm) and c (10 cm-to the rest of the depth).

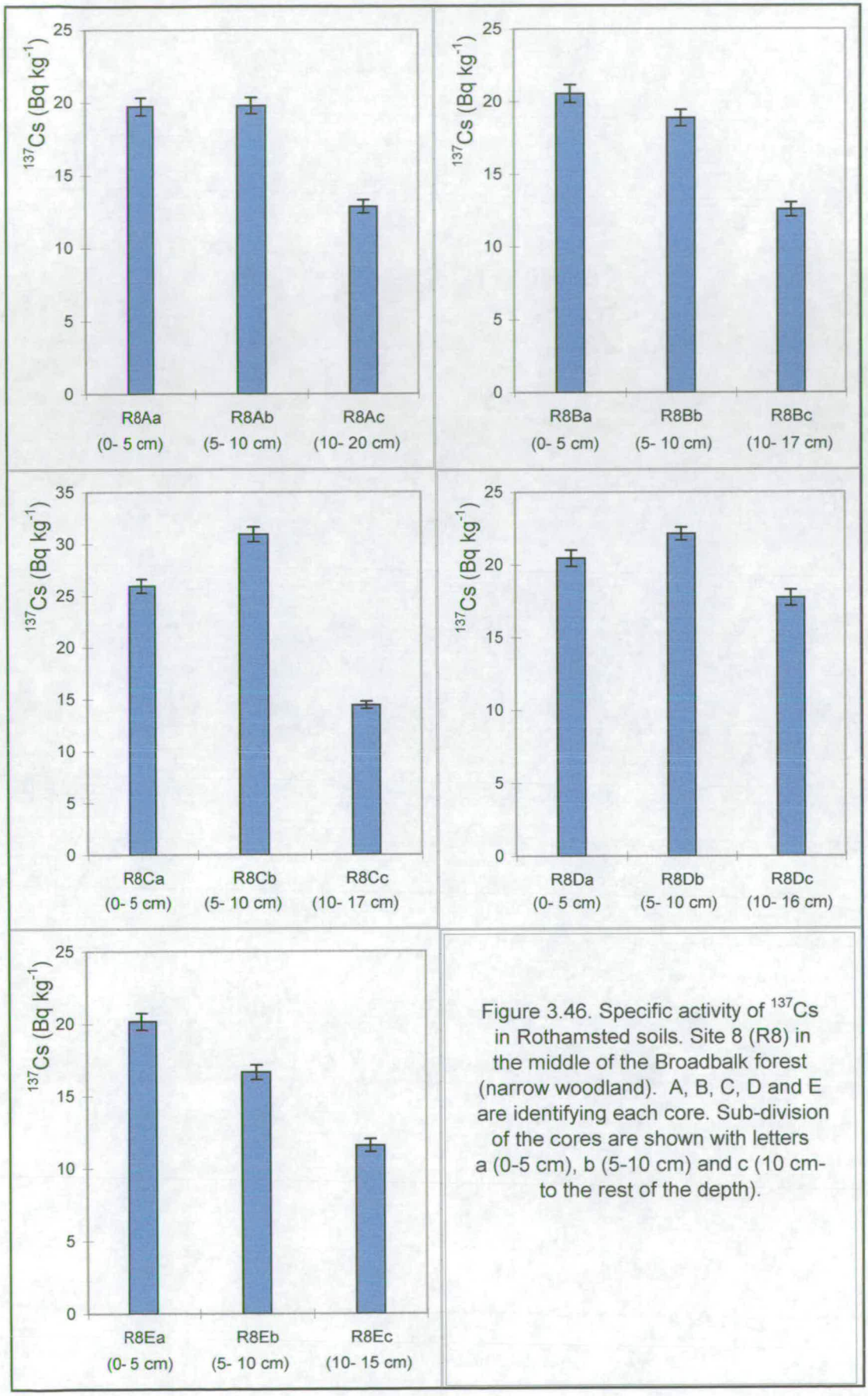

Figure 3.46. Specific activity of ^{137}Cs in Rothamsted soils. Site 8 (R8) in the middle of the Broadbalk forest (narrow woodland). A, B, C, D and E are identifying each core. Sub-division of the cores are shown with letters a (0-5 cm), b (5-10 cm) and c (10 cm- to the rest of the depth).

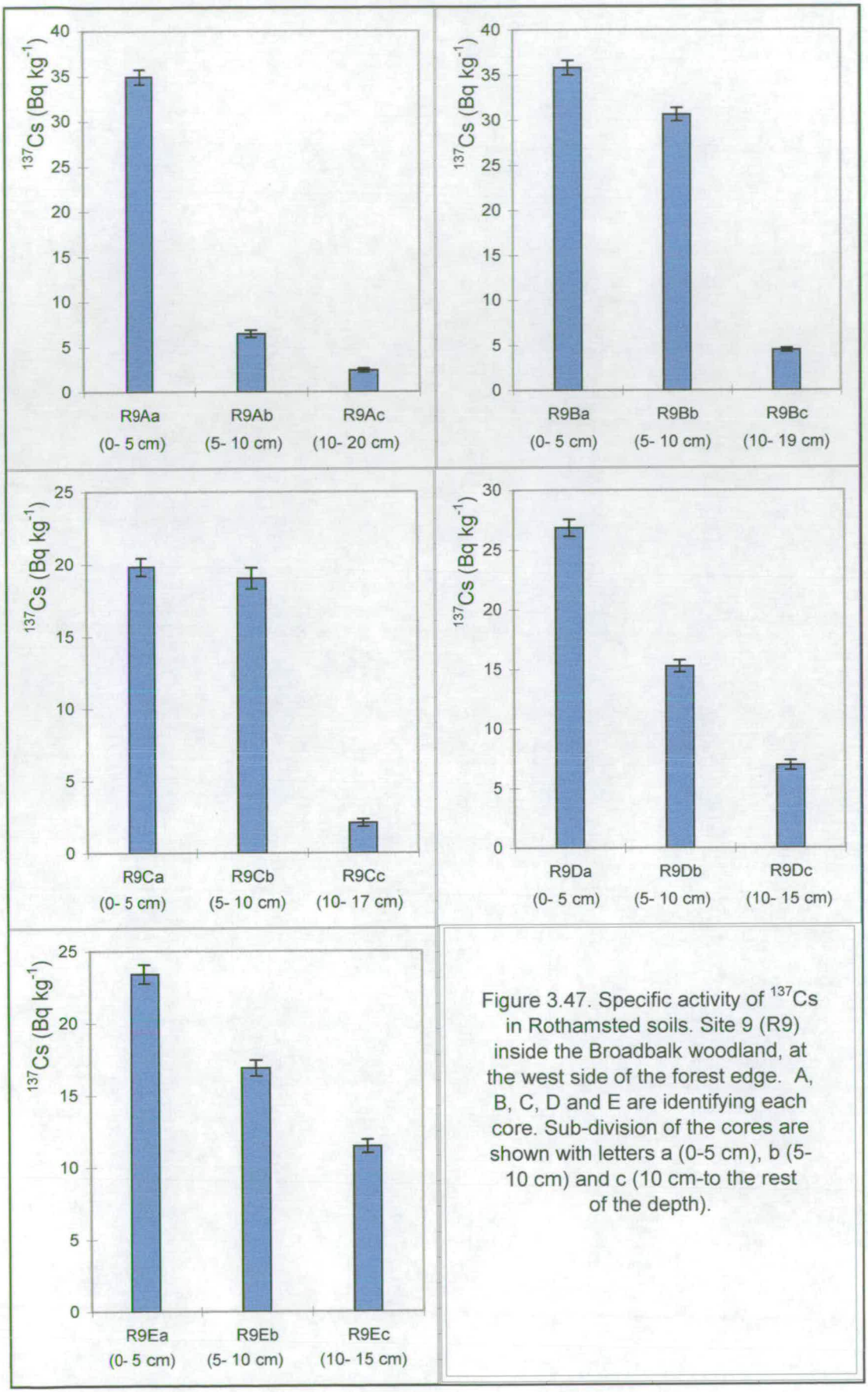

Figure 3.47. Specific activity of ^{137}Cs in Rothamsted soils. Site 9 (R9) inside the Broadbalk woodland, at the west side of the forest edge. A, B, C, D and E are identifying each core. Sub-division of the cores are shown with letters a (0-5 cm), b (5-10 cm) and c (10 cm-to the rest of the depth).

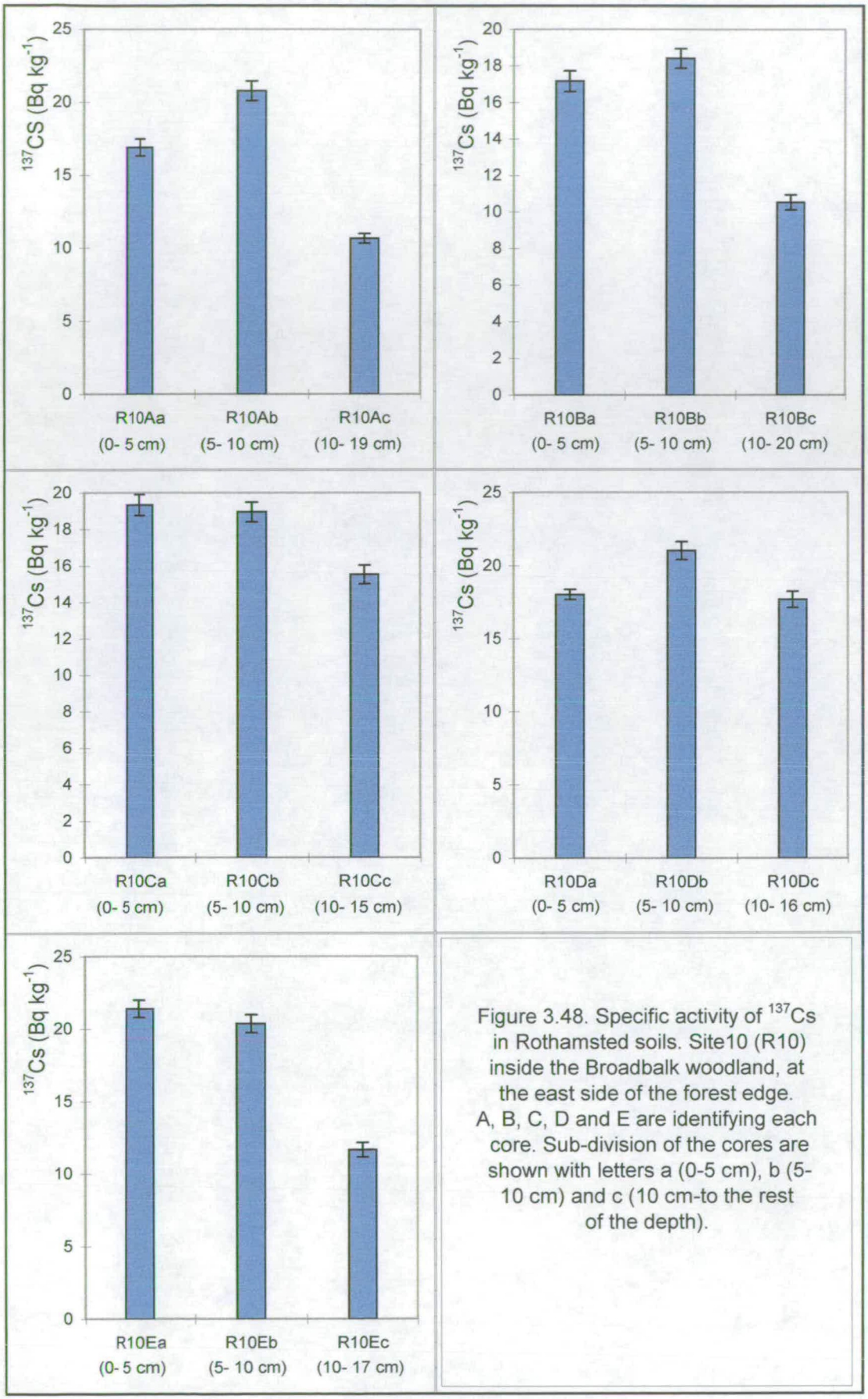

Figure 3.48. Specific activity of ^{137}Cs in Rothamsted soils. Site10 (R10) inside the Broadbalk woodland, at the east side of the forest edge. A, B, C, D and E are identifying each core. Sub-division of the cores are shown with letters a (0-5 cm), b (5-10 cm) and c (10 cm-to the rest of the depth).

and ^{137}Cs activity measurements depends on the activity concentration of each isotope in the soil sample. These errors for ^{210}Pb ranged from 3.6 to 7.1% for most active (i.e. top section 0-5 cm) and 4.1 to 11.7% for lower activity (i.e. bottom section beyond 10 cm depth) of the soil, respectively. For ^{137}Cs these errors were 1.6 to 4.8% for most active and 2.1 to 12.8% for less active soils, respectively.

Most of the total ^{210}Pb inventories were detected in the 0-10 cm depth of the soils. These were between 78 to 96% of the total ^{210}Pb inventories integrated over the core depth, with a mean value of 88%. This implies that only about 12% of the total measured ^{210}Pb inventories reside at depths deeper than 10 cm. For ^{137}Cs the mean inventories below 10 cm are about 19% of the total measured inventories. The ^{137}Cs activity in the soil deeper than 10 cm is higher than the ^{210}Pb activity for the same soil due to the higher mobility of ^{137}Cs in soil (see chapter 1, table 1.2).

The total mean inventories of atmospherically derived ^{210}Pb and ^{137}Cs at each core and each sampling site are presented in tables 3.5 and 3.6, respectively. The errors given in table 3.5 for the ^{210}Pb and ^{137}Cs inventories represent the root mean square of one-sigma counting statistical error obtained from each core. The errors given in table 3.6 for the ^{210}Pb and ^{137}Cs inventories are the standard deviation.

Table 3.5. The total inventories of ^{210}Pb and ^{137}Cs (Bq m^{-2}) in each core.

Core	Total inventory of ^{210}Pb in each core section Bq m^{-2}	Total inventory of ^{137}Cs in each core section Bq m^{-2}	^{210}Pb error Bq m^{-2}	^{137}Cs error Bq m^{-2}
R1A	4119	1528	47	12.5
R1B	4179	1412	41	9.5
R1C	4078	1996	41	12.8
R1D	4005	1444	49	11.3
R1E	3707	1340	44	11.9
R2A	4204	1398	53	10.8
R2B	4042	1490	52	11.4
R2D	3670	1568	26	6.2
R2E	3490	1378	43	10.5
R3A	4787	2016	58	10.4
R3B	4384	2000	52	10.7
R3C	4535	2051	60	12.1
R3D	4506	2157	77	15.3
R3E	4837	1785	67	12.5

Table 3.5 continued from page 104

R4A	4556	1812	50	10.5
R4B	4795	1937	50	10.4
R4C	4664	2000	54	10
R4D	4611	2279	55	11.2
R4E	4952	1553	49	10.3
R5A	4355	1878	46	10
R5B	4542	1588	58	11.2
R5C	4741	1938	50	13.5
R5D	4177	1788	48	11.3
R5E	4398	1861	38	9.6
R6A	4707	1403	52	7.7
R6B	4318	1861	56	11.2
R6C	4416	1633	50	10.8
R6D	4998	1867	56	11.2
R6E	4856	1714	51	11.6
R7A	3978	1180	56	8.7
R7B	3785	1407	54	10.3
R7C	3623	1117	47	8.1
R7D	3709	1211	44	10.5
R7E	3671	1313	43	9.2
R8A	4829	1970	57	12.4
R8B	4998	2142	65	13.3
R8C	4856	2546	64	12.1
R8D	4817	1872	51	9.6
R8E	4431	1554	68	9.6
R9A	4847	1814	69	13.6
R9B	4827	2135	55	11.3
R9C	5009	1493	55	12.4
R9D	4913	1749	59	11.4
R9E	4958	1750	60	11
R10A	4697	1687	66	10
R10B	4978	2000	63	13.1
R10C	4760	1841	57	10.7
R10D	4668	2092	48	11.4
R10E	5075	1936	67	12.2

Table 3.6. The atmospherically derived ^{210}Pb and ^{137}Cs inventories (Bq m^{-2}) averaged over each site. The error the standard deviations in each site calculated using equation 3.7.

Location of each site	Mean ^{210}Pb inventories (Bq m^{-2})	Mean ^{137}Cs inventories (Bq m^{-2})
Open field near Geescroft forest (R1)	4018 ± 185	1544 ± 262
Open field near Geescroft forest (R2)	3852 ± 334	1459 ± 89
Edge of the Geescroft forest (R3)	4610 ± 194	2002 ± 136
Geescroft forest 5 m from the edge (R4)	4716 ± 159	1916 ± 266
Geescroft forest 10 m from the edge (R5)	4443 ± 212	1811 ± 135
Geescroft forest 20 m from the edge (R6)	4659 ± 288	1696 ± 191
Open field near Broadbalk forest (R7)	3753 ± 139	1246 ± 115
In the middle of Broadbalk forest (R8)	4786 ± 211	2017 ± 365
At the east side of Broadbalk forest (R9)	4911 ± 76	1788 ± 230
At the west side of Broadbalk forest (R10)	4836 ± 181	1863 ± 251

Figures 3.49 to 3.56 show the atmospheric derived ^{210}Pb and ^{137}Cs inventories (Bq m^{-2}) in Geescroft and Broadbalk woodland compared with an open field for each core and their mean inventories over each site. The errors in figures 3.50, 3.52, 3.54 and 3.56 are the standard deviations of inventories in each site calculated using equation 3.7.

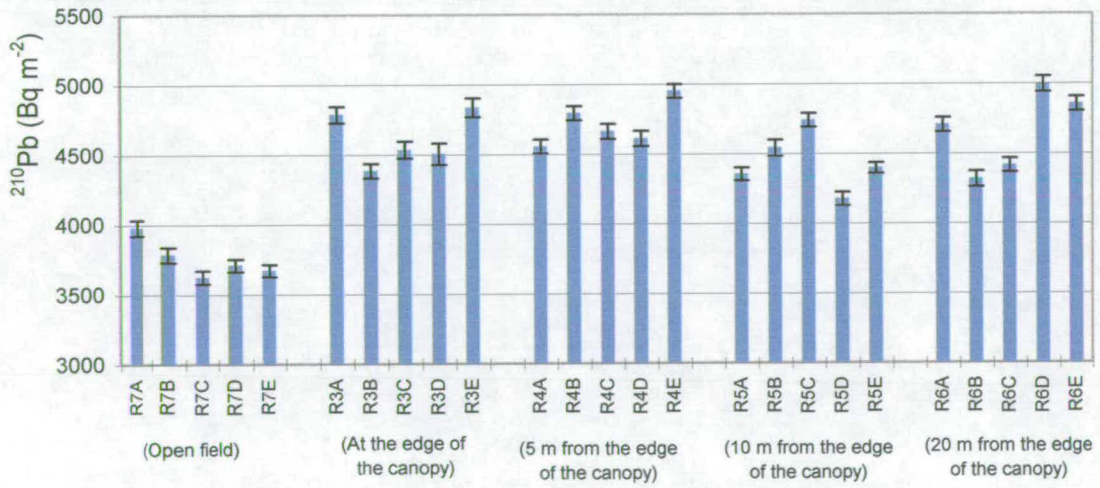

Figure 3.49. Atmospheric ^{210}Pb (Bq m^{-2}) inventories measured in soil samples from each sampling in the open field (R7A-E), edge of the canopy (R3A-E), 5 m from the edge (R4A-E), 10 m from the edge (R5A-E), and 20 m from the edge (R6A-E) at Geescroft canopy.

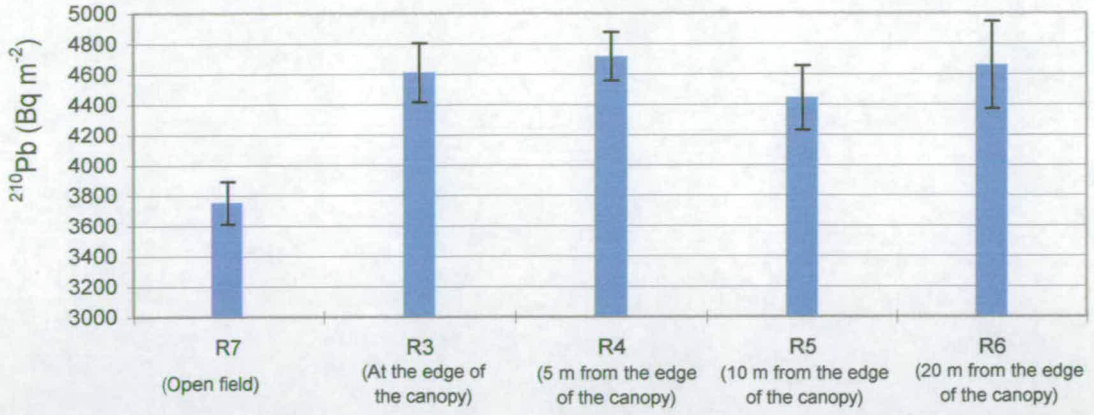

Figure 3.50. Mean atmospheric ^{210}Pb (Bq m^{-2}) soil inventories in the open field (R7), edge of the canopy (R3), 5 m from the edge (R4), 10 m from the edge (R5), and 20 m from the edge (R6) at Geescroft canopy.

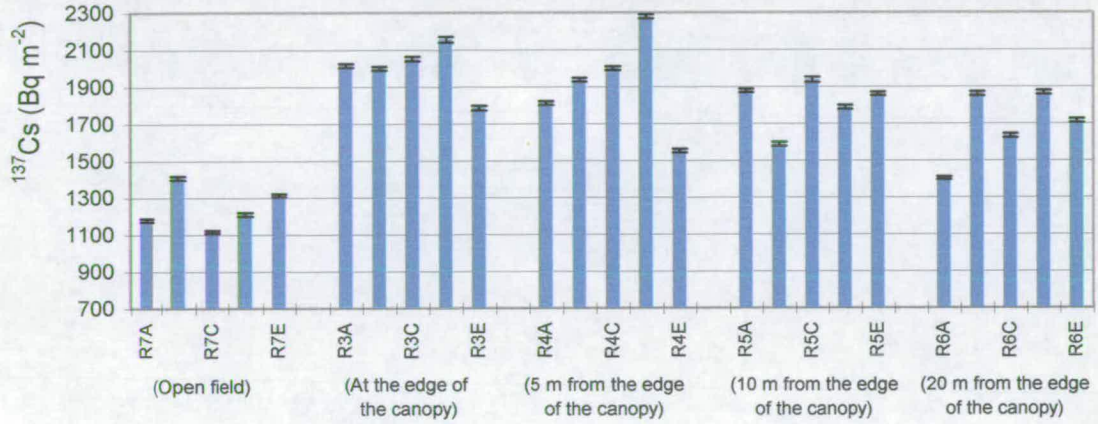

Figure 3.51. Atmospheric ^{137}Cs (Bq m^{-2}) inventories measured in soil samples from each sampling point in the open field (R7A-E), edge of the canopy (R3A-E), 5 m from the edge (R4A-E), 10 m from the edge (R5A-E), and 20 m from the edge (R6A-E) at Geescroft canopy.

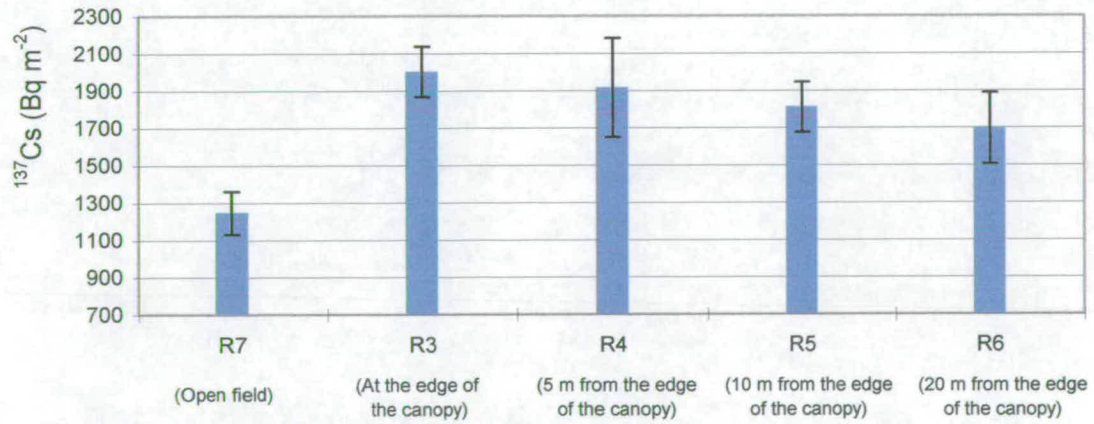

Figure 3.52. Mean atmospheric ^{137}Cs (Bq m^{-2}) soil inventories in the open field (R7), edge of the canopy (R3), 5 m from the edge (R4), 10 m from the edge (R5), and 20 m from the edge (R6) at Geescroft canopy.

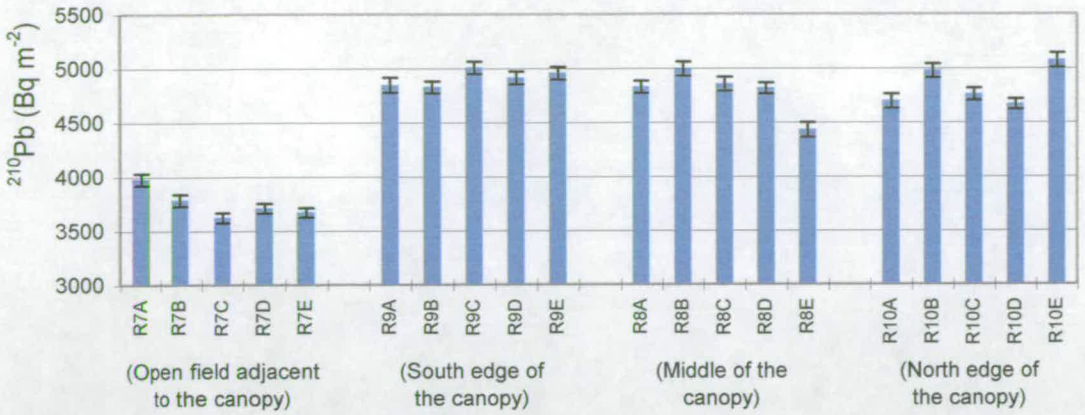

Figure 3.53. Atmospheric ^{210}Pb (Bq m^{-2}) inventories measured in soil samples from each sampling point in the open field (R7A-E), south edge of the canopy (R9A-E), middle of the canopy (R8A-E), and north edge of the canopy (R10A-E) at Broadbalk canopy.

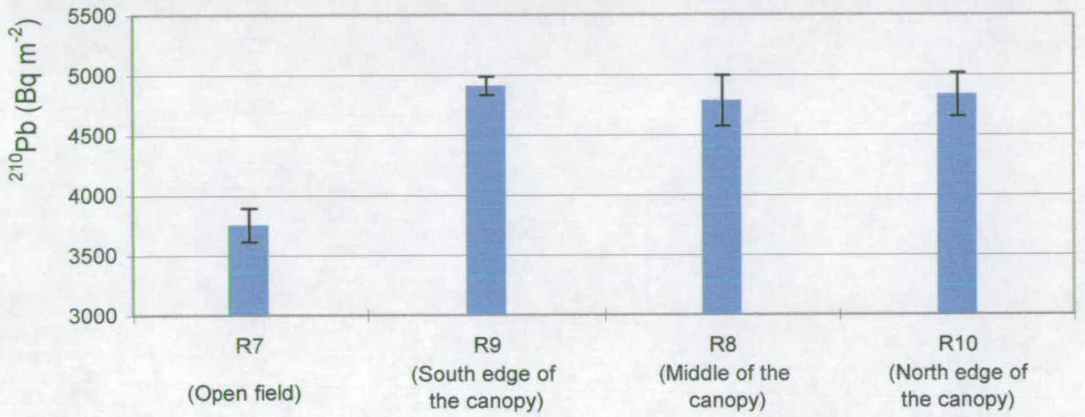

Figure 3.54. Mean atmospheric ^{210}Pb (mBq m^{-2}) soil inventories in the open field (R7), south edge of the canopy (R9), middle of the canopy (R8), and north edge of the canopy at Broadbalk canopy.

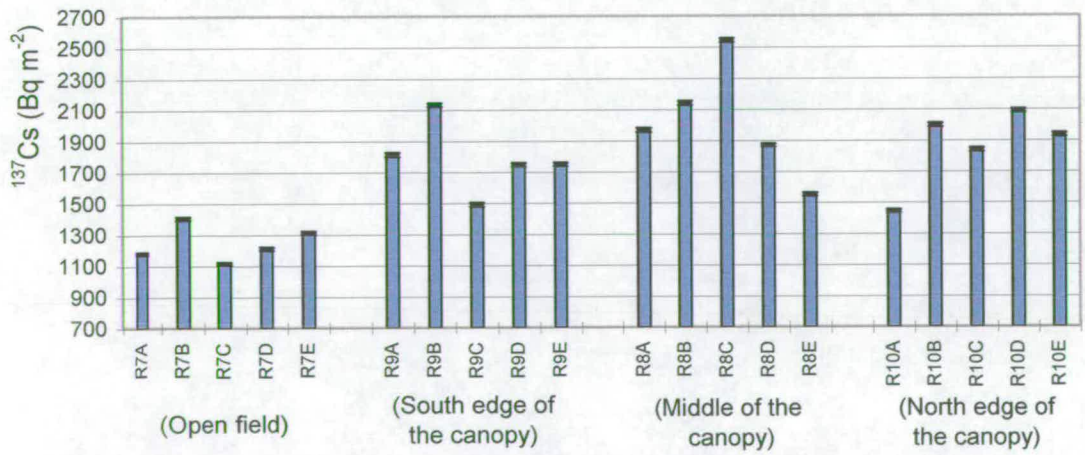

Figure 3.55. Atmospheric ^{137}Cs (Bq m^{-2}) inventories measured in soil samples from each sampling point in the open field (R7A-E), south edge of the canopy (R9A-E), middle of the canopy (R8A-E), and north edge of the canopy (R10A-E) at Broadbalk canopy.

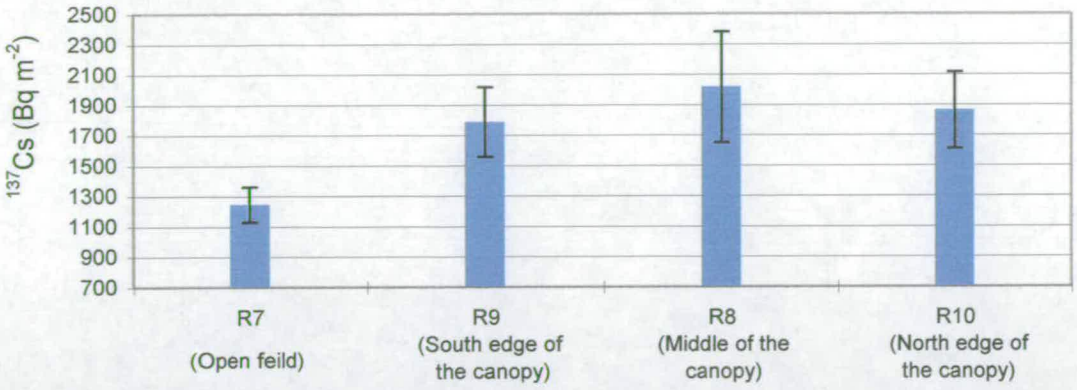

Figure 3.56. Mean atmospheric ^{137}Cs (mBq m^{-2}) soil inventories in the open field (R7), south edge of the canopy (R9), middle of the canopy (R8), and north edge of the canopy at Broadbalk canopy.

To compare the inventories for the forest to those of an adjacent grass field in order to determine whether trees in the forest capture more aerosols than the open field, we measured soils from inside the canopies and from nearby open fields, as described in chapter 2. Two open fields near to the Geescroft forest site 1 and site 2, and one for Broadbalk woodland site 7, were measured. The history of sites 1 and 2 showed that they were undisturbed for about 50 years, the grass had been cut and removed. In the case of site 7, the grass had been cut and left on the site. A barrier protects it from disturbance. When the analysis were completed, sites 1 and 2 showed the inventories were uncertain of disturbances. A further investigation about the history of these sites revealed that they might have been disturbed. For that reason and the fact the forests were not far away from each other, site 7 was therefore chosen as reference for both of the woodlands.

The atmospherically derived ^{210}Pb and ^{137}Cs inventories into the forests exceed those in adjacent open areas, indicating that forest sites receive larger atmospheric inputs. The value of these inventories are shown in table 3.7. The errors are the standard deviation of the mean inventories within each of the canopies and the open area as determined using equation 3.7.

The excess inventories for ^{210}Pb were about 25.7% and 30.9% for Geescroft and Broadbalk canopies, respectively. The excess inventories for ^{137}Cs were about 60.7% and 68.9% for Geescroft and Broadbalk forests, respectively. Figures 3.57 and 3.58 show the excess inventories of atmospherically derived ^{210}Pb and ^{137}Cs (Bq m^{-2}) to each canopies compared with the open field, respectively.

Table 3.7. The average atmospherically derived ^{210}Pb and ^{137}Cs (Bq m^{-2}) to each location. The errors are the deviations of the mean inventories calculated using equation 3.7.

Locations of the sites	Average ^{210}Pb (Bq m^{-2}) atmospherically derived inventory	Average ^{137}Cs (Bq m^{-2}) atmospherically derived inventory
Open field grassland	3753 ± 139	1246 ± 115
Geescroft canopy	4607 ± 135	1856 ± 119
Broadbalk canopy	4844 ± 124	1920 ± 164

The ^{210}Pb inventories in different cores from the same sampling location were relatively uniform; the standard deviation of measurements were approximately 20, 22, and 14% for open grassland, Geescroft canopy and Broadbalk canopy, respectively.

Under the steady-state condition, the inventory of unsupported (atmospherically derived) ^{210}Pb in an undisturbed soil core is given by the formula (Benninger et al., 1975),

$$F\ (Bq\ m^{-2}\ y^{-1}) = I\ (Bq\ m^{-2}) \times \lambda\ (y^{-1}) \qquad ....(3.13),$$

where, F is the flux, I is the inventory measured from the undisturbed soil core, and λ is the radioactive decay constant (0.03114 y^{-1} for ^{210}Pb).

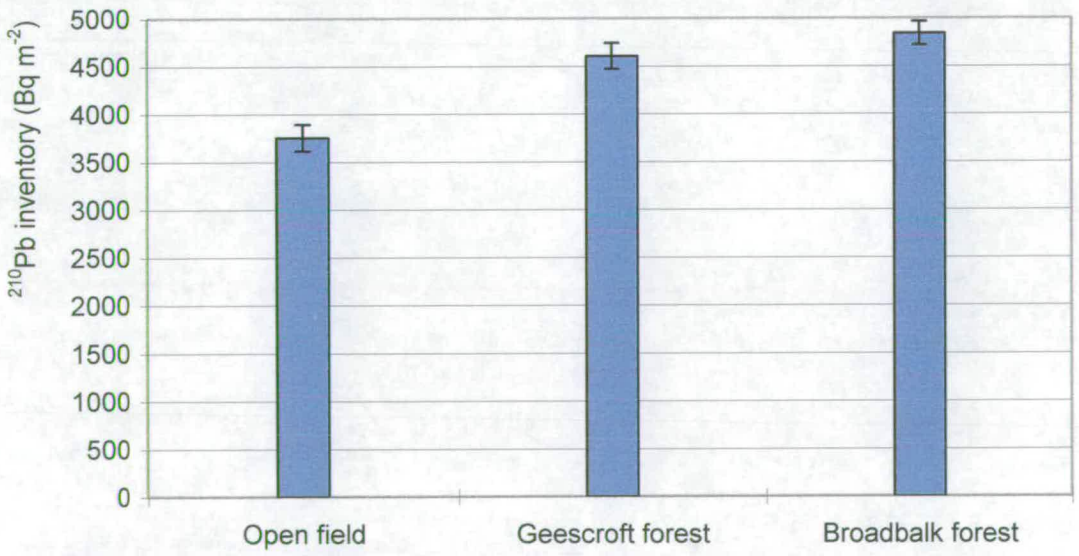

Figure 3.57. Mean atmospheric ^{210}Pb inventories (Bq m^{-2}) in open field and canopies compared to show the excess inventories due to the effect of trees.

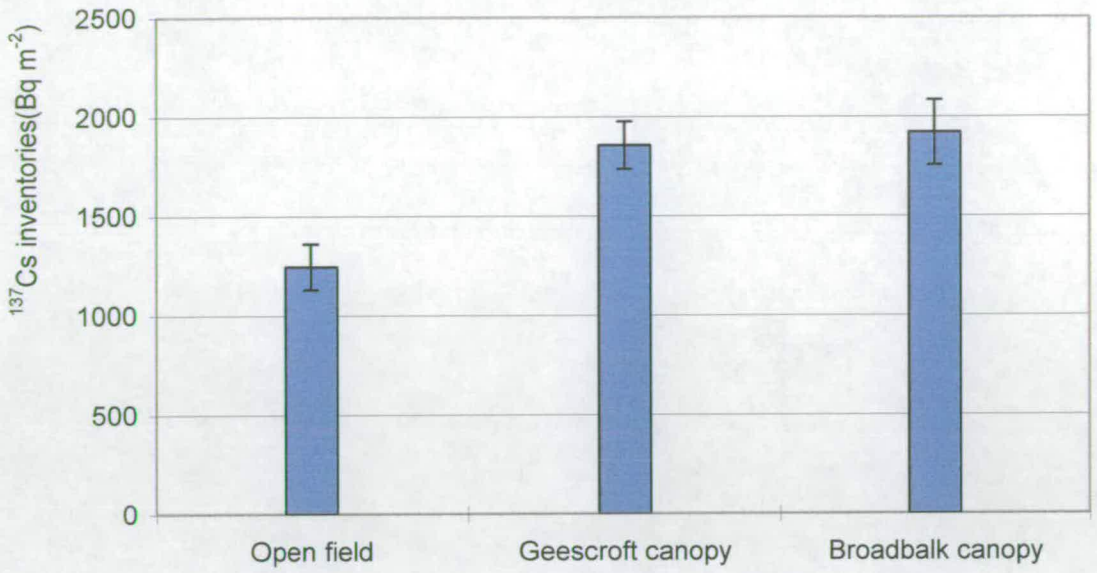

Figure 3.58. Mean atmospheric ^{137}Cs inventories (Bq m^{-2}) in open field and canopies compared to show the excess inventories due to the effect of trees.

The average flux for atmospherically derived ^{210}Pb was measured to be about 117, 143, and 151 Bq m^{-2} y^{-1}, for open grassland, Geescroft canopy and Broadbalk canopy, respectively.

Chapter 4

4. Discussion of the results.

Air and precipitation samples: Air and precipitation samples were collected continuously for 25 and 16 months, respectively, to quantify atmospheric concentrations and deposition of the radioisotopes ^{210}Pb (half-life 22.3 years) and ^{7}Be (half-life 53.4 days). The concentrations and fluxes of these isotopes, reported in chapter 3, are discussed, interpreted and compared with the published literature in sections 4.1 for air and 4.2 for rain in this chapter.

The air and rain data have been used to investigate the questions relating to atmospheric behaviour of ^{210}Pb and ^{7}Be and aerosols such as:

- What are the concentrations of ^{210}Pb and ^{7}Be in this particular region?
- How do the concentrations and fluxes of ^{210}Pb and ^{7}Be isotopes vary with the type of air mass?
- What are the relationships between the ^{210}Pb and ^{7}Be concentrations and predicted fluxes of these nuclides?
- What is the relationship of the ^{210}Pb and ^{7}Be radionuclide fluxes to precipitation?
- How are the fluxes of the two radionuclides related to their atmospheric concentrations?
- Is there any relationship between concentrations of O_3 and ^{7}Be in the atmospheric boundary layer?
- How could we use the concentration and flux data to estimate dry deposition, and calculate the precipitation scavenging coefficient.
- What porportion of the total deposition is contributed by dry deposition?

Soil inventories: The soil inventory of atmospherically-derived ^{210}Pb is used to quantify the enhancement in aerosol deposition by aerodynamically rough canopies. A total of 150 samples from 10 sites were analysed and the results of the atmospherically-derived inventories of ^{210}Pb and ^{137}Cs (half-life 30 years) were reported in section 3.3.

The measured atmospheric ^{210}Pb and ^{137}Cs inventories in Rothamsted soils are discussed, interpreted and compared with the published literature in section 4.3. The soil data were used to explain some of the questions set here, such as;

- What effect the trees could have on aerosol deposition relative to short vegetation?
- Why do the fluxes of ^{210}Pb and ^{137}Cs behave differently? and why is the excess atmospheric deposition of ^{137}Cs larger than ^{210}Pb in the same core?
- What is the woodland edge effect and how could it be explained for our results?
- What is the deposition velocity of the carrier aerosols of ^{210}Pb and how does it compare with the wind tunnel results?
- What are the depositions of ^{210}Pb and ^{137}Cs for the Rothamsted soils?

The conclusions of the results are drawn together and reported in chapter five.

4.1. Surface air measurements.

Surface air measurements were performed by pumping and filtering the air at an elevation of 30 metres above the ground (~ 85 m asl.) on the roof of James Clark Maxwell Building (JCMB) in Kings Building's area of Edinburgh University.

^{210}Pb concentration in surface air results mainly from two factors; (1) the ^{210}Pb sources and (2) the transport and deposition mechanisms, which are driven by atmospheric circulation, dry deposition and precipitation. When the air mass is stable, ^{222}Rn and its daughters accumulate in the boundary layer leading to high surface concentration of ^{210}Pb. A consequence is that, when seasonal anticyclones (high pressure) occur over a continental area, air masses become enriched in ^{210}Pb relative to oceanic air. Thus continental regions with frequent anti-cyclonic conditions experience higher annual ^{210}Pb concentrations, and vice versa for the cyclonic (low pressure) zones.

The source of ^{7}Be is the cosmic ray induced spallation of atmospheric nitrogen and oxygen. The production rate of ^{7}Be increases nearly exponentially with altitude so that it is about 2 orders of magnitude higher at the tropopause than it is at the surface [Lal and Peters, 1967].

Four processes affect the surface air concentration of ^{7}Be [Feely et al., 1988]: wet deposition, mass exchange between the stratosphere and the troposphere, vertical transport in the troposphere and horizontal transport. The two processes that have the greatest short-term influences on ^{7}Be in surface air are precipitation, which scavenges the carrier aerosols, and downward transport.

4.1.1. Surface air pressure effects on ^{210}Pb and ^{7}Be concentrations.

To illustrate the effect of air mass type on ^{210}Pb and ^{7}Be concentrations figures 3.10-14 have been plotted. To determine the origin of these air masses, the meteorological surface pressure charts from European Meteorological Bulletin were used and the parcel of air tracked back in time for 4 days to define the trajectories of the different air masses at different period of time for each sample. Precipitation events during the transport time or other meteorological changes to the air parcel were not considered.

The high pressure (anti-cyclonic) and low pressure (cyclonic) surface air pressure were extracted from the weather pressure charts and plotted for ^{210}Pb and ^{7}Be, in figures 3.10 and 3.11, respectively, to investigate the relationship between the

concentration of these radionuclides and the weather system's pressure. For high pressure system a plus one, for low pressure system a minus one, and for the mixed low and high pressures zero is adopted. The filtering time for each sample was different and varied. During this time interval many different weather systems were passed through the sampling site, the x-axis of the graphs was explained in section 3.1.4.

Figure 3.10 shows the relationship of ^{210}Pb concentration and the surface pressure. It is clear that when high pressure is over the sampling station, the ^{210}Pb concentration is larger and at low pressure the ^{210}Pb concentration is smaller. Figures 3.12 and 3.14 also show that high concentrations of ^{210}Pb were associated with continental air masses and low concentrations of ^{210}Pb were associated with oceanic air masses.

4.1.2. Continental, oceanic effects on ^{210}Pb and ^{7}Be concentrations.

For each parcel of air arriving at our sampling station, a plus one and minus one is adopted for continental and oceanic air masses, respectively. Zero is adopted for mixed continental and oceanic air masses. From this arrangement a continental-oceanic index has been established. Figures 3.12 and 3.13 are plotted for ^{210}Pb and ^{7}Be, respectively. The x-axis of the graphs was explained in section 3.1.4.

The plots for ^{210}Pb (fig. 3.12 and 3.14) show the relationship between ^{210}Pb and the type of air mass; i.e. for higher concentrations of ^{210}Pb a larger fraction of continental air mass is present.

Figure 3.14 has been plotted for the 12 highest and 12 lowest concentrations of ^{210}Pb, chosen from 100 measured air samples as a wind direction diagram, to illustrate the effect of wind direction and continental-oceanic air masses on ^{210}Pb. The diagram shows the frequency of wind direction for the 12 highest and 12 lowest concentrations. To find the percentage contributions from each direction the wind direction within each segment (direction) was divided to the total wind directions for the highest or lowest concentrations, i.e. for highest concentrations the number of days wind arriving to Edinburgh from the North was 7 and the total days for 12 highest concentrations were 80 therefore the wind from the North is considered as 8.75% of the total etc.

This diagram clearly shows the effect of different air masses. For high concentrations of ^{210}Pb, the air masses are from the east and south (i.e. continent),

and for low concentrations of ^{210}Pb, the air masses are from the west and north (i.e. ocean) of our sampling station. This finding agrees with the prediction of Wilkening and Clements (1975), that the ^{222}Rn exhalation rate from the ocean is only about 2% of that from the land surface. Figure 3.15 shows the contribution of air masses during the air sampling period.

Overall, for the 100 air samples, the air masses were 22.2% from continental regions, 69.4% from oceanic regions and 8.4% from mixed continental and oceanic regions, which is shown in figure 3.15.

A relationship between ^{7}Be and continental or oceanic air masses is not expected because ^{7}Be is of stratospheric origin. However, there is a weak relationship between air masses and ^{7}Be concentrations (fig. 3.13). This could be due to the fact that the air masses tracked during these four days are transported horizontally and some vertical transport is also taking place. Therefore, this could bring more ^{7}Be isotopes to the surface, and most of the time continental air masses are associated with high pressure, which is associated with subsidence bringing more ^{7}Be isotopes into the surface air. An alternative interpretation is that air of continental and oceanic origin have different precipitation scavenging on their pathway to Edinburgh.

4.1.3. Seasonal effects on ^{210}Pb and ^{7}Be concentrations and the effect of vertical transport on ^{7}Be concentrations.

The origins of ^{210}Pb and ^{7}Be are different (as explained in chapter one), and this causes concentrations in air to depend on different processes, some of which vary with season. To examine the seasonal effects of ^{210}Pb and ^{7}Be concentrations in the surface air figures 3.8 and 3.9 were plotted. The procedure to plot these graphs was fully explained in chapter 3 section 3.1.3. Figure 3.8 shows the highest and lowest seasonal concentrations of ^{210}Pb are in September and January, respectively. Investigating the origin of the air masses during these two periods, the air masses were from continental sources on 52 and 24% of the total days, respectively. Since ^{210}Pb concentration in the air is mainly dominated by continental air masses (see section 4.1.2 for more details), this further demonstrate the importance of the origin of the air masses for ^{210}Pb concentrations in air.

However, it is believed that at least four factors are important in causing the seasonal variations in ^{7}Be concentrations. (1) wet scavenging, (2) stratosphere-to-troposphere exchange, (3) downward transfer in the troposphere, and (4) horizontal

transfer from middle subtropical latitudes to higher and lower latitudes. Each of the four processes has its own seasonal cycle, so that the seasonal cycle of surface concentrations of ^{7}Be is some complicated product of the four processes. At different locations, different processes may be dominant, and the seasonal cycle in ^{7}Be can have one or more maxima in any season or maxima in many combinations of seasons [Feely et al., 1989].

To show the seasonal variation of ^{7}Be concentration in air, figure 3.9 has been plotted. Many different authors have predicted that the concentration of ^{7}Be in surface air is maximum during spring time in the northern hemisphere, [e.g., Baskaran, 1995; Koch and Mann, 1996]. The main reason for that is reported to be enhanced spring time transport of air masses enriched with ^{7}Be from the top of the troposphere and stratosphere and normally high pressure is present at this period. The seasonal high for ^{7}Be was determined in March, which agrees with the prediction of other researchers.

For many sites both in the northern and southern hemisphere, ^{7}Be concentrations were at their highest during the warmer seasons and at their lowest during the cooler seasons. In figure 4.1 the mean monthly concentrations of 4 sites in North America and our measuring data are plotted. The ^{7}Be concentrations are highest at each of these sites during the warmer mid-year months. In figure 4.2, similar data are plotted for three South American sites. Again the highest ^{7}Be concentrations occur during the warmer months, here at the beginning and the end of the calendar year. The data in figures 4.1 and 4.2 show various differences in detail between sites, as expected if a variety of factors may influence the concentration of ^{7}Be to be found at any specific site during a given month. The concentrations of ^{7}Be for each site were different and many reasons could have affected these variations e.g. precipitation and altitude, as precipitation will scavenge the aerosols and by moving up into the atmosphere the concentration of ^{7}Be ought to rise in magnitude.

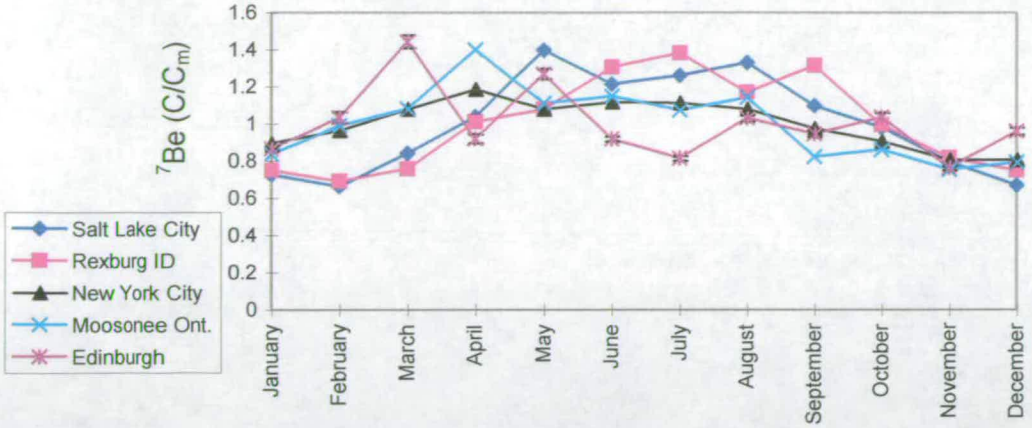

Figure 4.1. The average monthly concentrations of ^{7}Be (Bq m^{-3}) in four North American sites [cited in Feely et al., 1989], compared with this study (Edinburgh). C is the monthly concentrations and C_m is the mean concentration value.

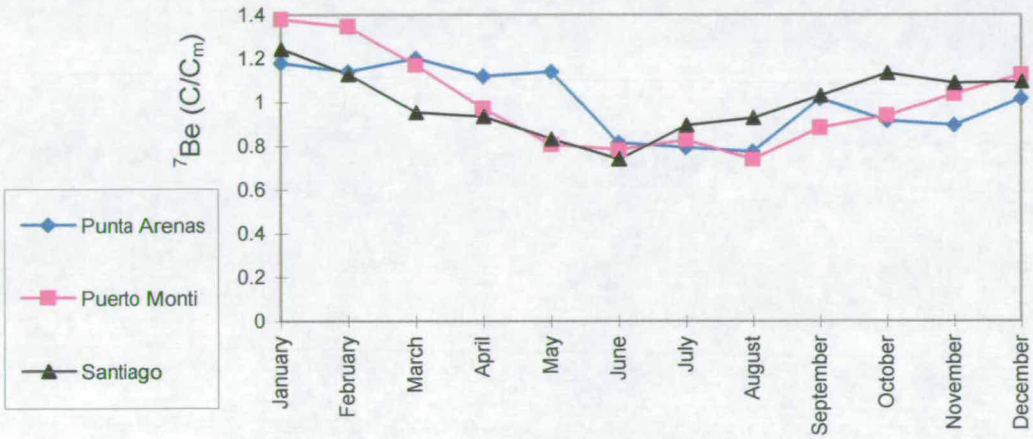

Figure 4.2. The average monthly concentrations of ^{7}Be (mBq m^{-3}) in surface air measured for three South American sites [Cited in Feely et al., 1989]. C is the monthly concentrations and C_m is the mean concentration value.

During the warmer months, the solar heating of the surface of the earth leads to the heating of the air in contact with the surface. Cooler air sinks, displacing the warm, less dense air and forcing it upward. This new air is heated in turn and is forced upward. A covective circulation is produced, carrying surface air upward and bringing downward air from higher levels. This vertical transport carries down to the surface layer the ^{7}Be that has been produced within the upper troposphere, as well as that which has entered the troposphere from the stratosphere [Feely et al., 1989]. The simplest interpretation of the seasonal ^{7}Be changes is therefore the vertical transport is mainly responsible for high concentration of ^{7}Be in the warmer period of the year.

4.1.4. Possible relationship between Ozone (O_3) and ^{7}Be concentrations.

Ozone in produced and destroyed throughout the atmosphere. The principal source of O_3 in the stratosphere is photolysis. Tropospheric O_3 is principally derived from two sources; episodic injection of air from the stratosphere where most of the earth's O_3 column inventory resides; and in situ photochemical production in the polluted continental boundary layer, where most of the nitrogen oxides (NO_x) and reactive volatile organic carbon compounds (VOC's) are emitted. Summer time O_3 is correlated with ^{7}Be, a product of cosmic ray interactions in the upper troposphere and stratosphere [Prospero et al., 1995; Graustein & Turekian, 1996]. Figure 4.3 has been plotted to investigate a possible relationship between the surface air concentration of ^{7}Be (mBq m^{-3}) and O_3 (ppb). The ozone concentration was increasing from January to its highest concentrations in April and then gradually decreasing thereafter to July, stayed almost constant during summer time (July, August and September) then once more decreasing to its lowest concentration value in November. The concentration of ^{7}Be was expected to be high for spring and in this case the highest concentration was during March; the behaviour in April was not expected.

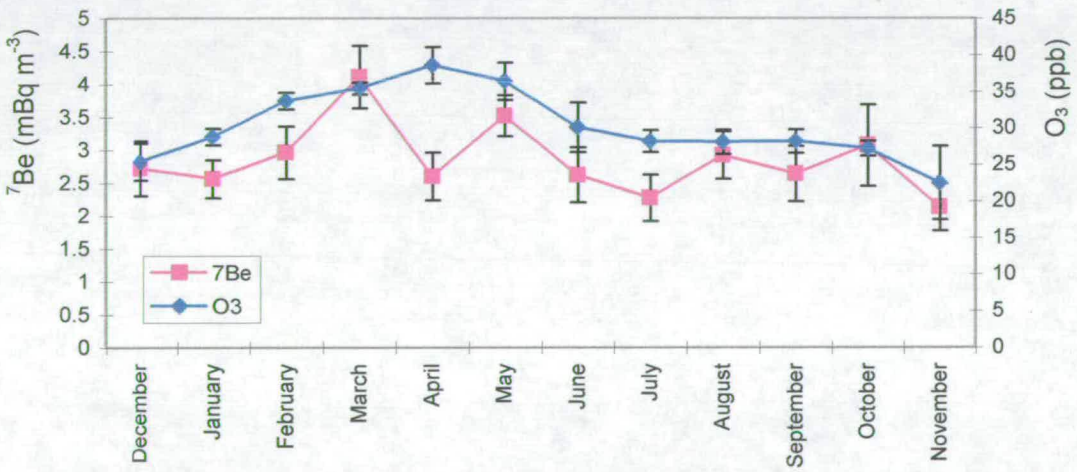

Figure 4.3. Concentration of ^{7}Be (mBq m^{-3}) in air samples compared with the concentrations of O_3 (ppb). The ozone data is from the Edinburgh Terrestrial Ecology, Edinburgh Research Station. The error bars shown on the diagram were the standard deviations of the concentrations.

This behaviour may be due to the washout effect in this period, since we have only one April measurement (April 1998) with a total monthly precipitation of 91.4 mm which was more than its average recorded value of 51 mm. Furthermore, from the surface pressure charts it is noticed that in April 1998 only 3 days of high pressure system were present over the sampling station.

Hence the low concentration of ^{7}Be could have been due to these effects or other meteorological activities. Therefore the summer time O_3 in this region is not closely correlated with ^{7}Be concentration and does not support the hyposesis of Prospero et al. (1995); and Graustein & Turekian (1996). There appears to be no single reason for this disagreement but the most probable cause is meteorological variability in a relatively short period of measurements. To reach a firm conclusion one needs several years of measurements at the similar meteorological regions to minimise the meteorological effects and establish a firm standard.

4.1.5. Averaged annual concentrations of ^{210}Pb in surface air.

The averaged annual concentration of ^{210}Pb was determined as 0.19 ± 0.06 mBq m^{-3}, which agrees with the reported values for the nearest locations to our sampling site. ^{210}Pb annual concentration values reported for the nearest locations to our site measured over many years are shown in table 4.1.

Name of the place	Lat.	Long.	Alt. (m)	Prec. (mm)	Sampling period (y)	Concentration (mBq m^{-3})
Riso (Denmark)	55.7	12.1	10	587	<3	0.21
Chilton (UK)	51.5	-1.5	350	741	5	0.23
Colones (Ireland)	54.2	-7.2		1020	1	0.14±0.03
Dundalk (Ireland)	54	-8.5		850	1	0.20±0.02
Mullingar (Ireland)	53.5	-7.3		970	1	0.15±0.02
Dublin (Ireland) site 1	53.4	-6.2		900	1	0.24±0.06
Dublin (Ireland) site 2	53.3	-6.2		900	1	0.22±0.02
Galway (Ireland)	53.3	-9		600	1	0.22±0.04
Rosslare (Ireland)	52.2	-6.3		980	1	0.36±0.05
Caherciveen (Ireland)	51.9	-10.2		1470	1	0.17±0.02
Midleto (Ireland)	51.9	-8.2		1040	1	0.31±0.04
This study	55.6	-3.9	85	820*	2	0.19±0.06

Table 4.1. Surface air concentrations of ^{210}Pb (mBq m^{-3}) from this study compared with the nearest locations to our sampling site [taken from ^{210}Pb world-wide data base, Preiss et al., 1998]. * This is the average value for the year 1997 (710 mm) and year 1998 (930 mm).

Although at, only about one fifth of the air masses were originally from continents (fig. 3.15), we clearly see the significant effect of continental air masses on concentration of ^{210}Pb in surface air. This is compared with the reported published results in the literature shown in table 4.1.

At northern mid-latitudes (10° N-30° N), surface air concentration values of ^{210}Pb in air are high over continental areas with an average of 0.53 mBq m^{-3} (Table 4.2). In the central United States, concentration in surface air reaches high values (close to 1 mBq m^{-3}) compare to the coastal sites resulting from the low influence of the oceanic air masses, depleted in ^{210}Pb [Preiss et al., 1996].

Latitude band	60°-80° N	30°-60° N	0°-30° N	0°-30° S	30°-60° S	60°-90° S
^{210}Pb concentration mBq m^{-3}	0.31	0.53	0.56	0.28 *	0.13	0.024

Table 4.2. Mean annual ^{210}Pb concentration in surface air over continents. The concentrations are extracted from Preiss et al., (1996). * Including coastal data only.

In Europe measurements are scarce and range from 0.2 to 0.5 mBq m^{-3}. Low values, 0.18 mBq m^{-3} at Lisbon [Carvalho, 1990] are associated with the western Oceanic coast under the influence of oceanic air masses. The relatively low concentration in the centre of the continent, around 0.3 mBq m^{-3} in Poland [Kownacka et al., 1990], is difficult to explain, but the absence of other measurement sites rules out any attempt to identify a trend. Figure 4.4 shows a Europe map with the ^{210}Pb air concentration at different locations. For more details of these measurements see Preiss et al. (1998).

4.1.6. Averaged annual concentrations of ^{7}Be in surface air.

Table 4.3 shows the estimated values of the equilibrium concentrations for ^{7}Be that would be expected at several locations within the ground level air if the only processes affecting the ^{7}Be were its production and its radioactive decay. The table also shows some typical concentrations actually found at these locations. We would not expect to find concentrations equalling or exceeding the equilibrium values within the troposphere because storms affecting the middle and lower troposphere will periodically washout the aerosols that carries the ^{7}Be and should prevent it from reaching equilibrium.

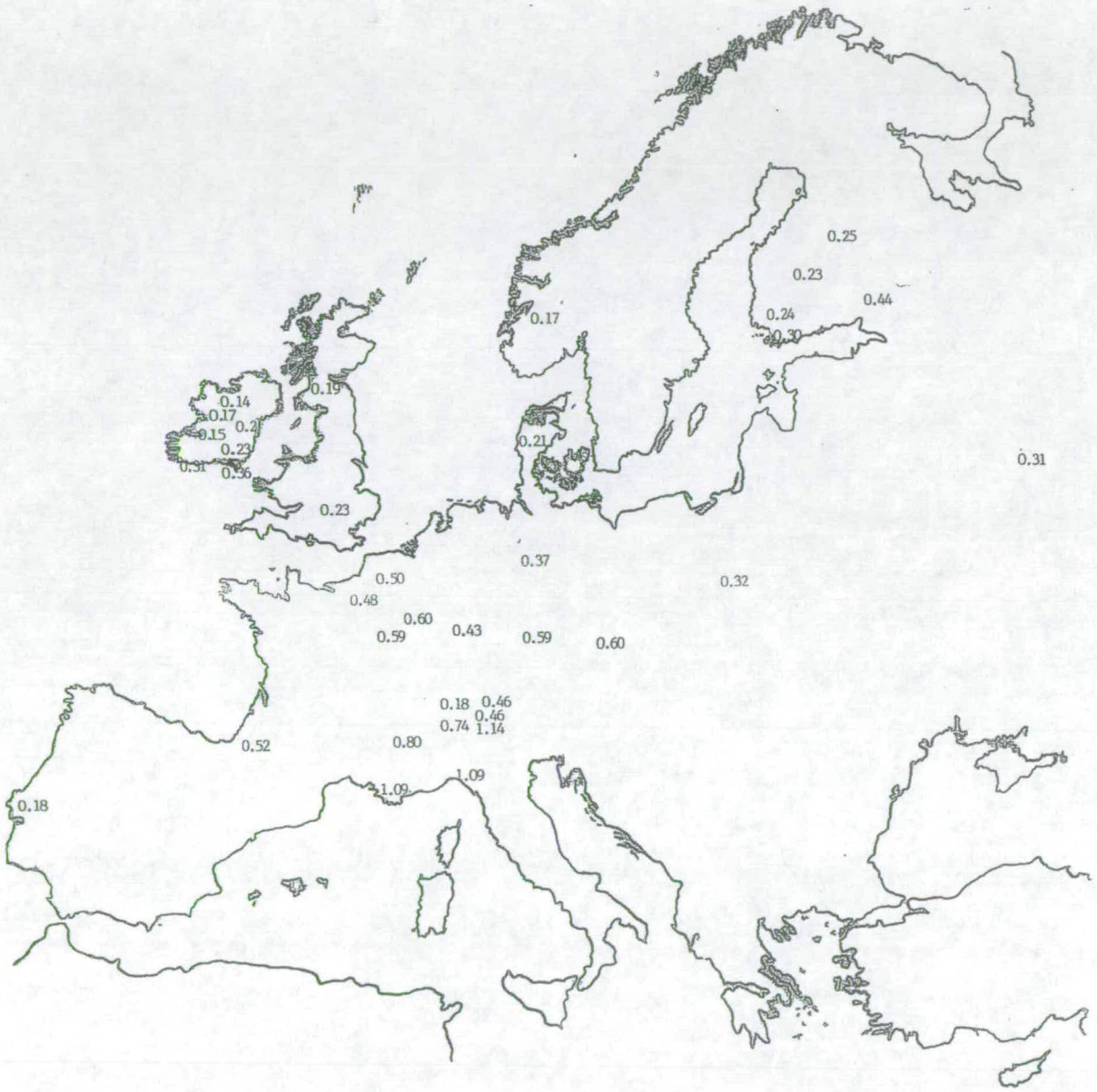

Figure 4.4. The measured and reported surface air concentration of ^{210}Pb (mBq m^{-3}) at different locations in Europe. The data reported on the map was taken from Preiss et al. (1998).

The annual average concentrations of ^{7}Be, in surface air was determined as 2.71 $\pm$0.66 mBq m^{-3} (i.e. 73 $\pm$ 18 fci m^{-3}). From table 4.4, our measured concentrations for ^{7}Be in surface air agree well with the other measured values reported in the literature for the nearest available reported locations. There were no reported ^{7}Be concentrations in the literature that could be compared with our determined concentration.

Latitude	Equilibrium concentrations mBq m^{-3} (fci m^{-3})	measured concentrations mBq m^{-3} (fci m^{-3})
60° - 70° N	<7.40 (200)	2.78 (75)
20° - 40° N	<5.55 (150)	5.18 (140)
0° - 20° N	<3.70 (100)	2.41 (65)
55.6° N♣		2.71 (73)

Table 4.3. Equilibrium ^{7}Be concentrations and some typical measured concentrations in ground level air, [taken from Feely et al., 1989]. ♣The data is from this study.

Location	Latitude	Longitude	Altitude (m)	month of sampling	Concentrations (mBq m^{-3})
Chilton (UK)*	51.0	-1.5		23	2.10
Riso (Denmark)+	55.5	12.10	10	266	2.55
Bronholm (Denmark)+	55.0	14.90	10	79	2.47
This study	55.6	-3.90	85	25	2.71 $\pm$ 0.66

Table 4.4. Surface air concentrations of ^{7}Be (mBq m^{-3}) measured for different locations. [+ cited in Brost et al., 1991. * Taken from Peirson, 1963].

The concentrations of ^{210}Pb and ^{7}Be have not previously been measured in air in this area, these concentrations give the first measurements for this region of the UK.

4.2. Rain measurements.

Since atmospheric ^{210}Pb and ^{7}Be are carried by aerosols they are subject to precipitation scavenging. The size distributions of the carrier aerosols for ^{210}Pb and ^{7}Be are similar [Bondietti et al., 1988], so they are removed with similar efficiencies by scavenging processes. The mean residence time of these aerosols in the troposphere is a few days to a few weeks [Graustein & Turekian, 1996], depending principally on altitude and regional climatology.

The use of artificial collectors appears to be the most reliable technique to measure the annual ^{210}Pb and ^{7}Be wet deposition flux directly. However, while wet deposition is easy to measure, dry deposition of aerosols to the landscape is much more difficult and Deposition to the natural landscape presents a problem. Moreover, the rain collector technique is able to measure seasonal variations which are very useful for understanding transfer and deposition mechanisms [Baskaran et al., 1993]. Direct atmospheric flux measurement methods consist of trapping ^{210}Pb and ^{7}Be fallout directly into artificial collectors placed a few metres above the ground.

In this study, a set of collection trays, total area of 0.55 m^2, were prepared and set out to investigate the concentrations of ^{210}Pb and ^{7}Be in rain. The method of collection and sample preparation are explained in chapter 2, section 2.2. The concentrations and fluxes of ^{210}Pb and ^{7}Be were determined, analysed and reported in chapter 3. The discussion of these results are presented here in the following sections.

4.2.1. Meteorological effects on ^{210}Pb and ^{7}Be concentrations in precipitation.

To determine the effects of continental and oceanic weather systems, the air mass trajectories were tracked back in time for 4 days to find out their origin using the surface pressure charts from the European Meteorological Bulletin. For each continental and oceanic air mass which passed through our sampling station +1 and -1 were adopted, respectively, the units for the x-axis of these graphs are explained in section 3.1.4. A zero was adopted for the air masses which were mixed, from which figures 3.25 and 3.26 were plotted for average monthly concentrations of the ^{210}Pb and ^{7}Be, respectively. As it is clearly seen from the trend line on figure 3.25 when the origin of air masses are more continental the concentrations of ^{210}Pb is higher and when the air masses are less continental the ^{210}Pb concentrations are lower. Although the origins of ^{210}Pb and ^{7}Be isotopes are different, figure 3.26 shows that a similar relationship for ^{7}Be concentration with respect to the air mass origin. The high-low

pressure index was plotted in figure 3.24 for ^{7}Be. This shows a relationship between the high concentrations of ^{7}Be with the high pressure of the air mass system. This bar diagram showed that in the presence of high pressure systems the contributions of ^{7}Be were higher, normally high pressure and continental air are associated with each other. This agrees with the hypothesis that when high pressure is present the air masses from the top of the atmosphere sink to the lower surfaces bringing more ^{7}Be enriched air. This shows the vertical transport of the air masses is very important for high concentrations of ^{7}Be in the atmosphere. There are other processes which could be important at the same time when the vertical transport is in progress, such as precipitation. The concentrations of ^{210}Pb and ^{7}Be in each rain sample were plotted in figures 3.19 and 3.20, respectively.

4.2.2. Seasonal effects on ^{210}Pb and ^{7}Be.

Investigation of the atmospheric ^{210}Pb and ^{7}Be in many places around the globe show that there are seasonal variations on the depositional fluxes of these nuclides, high in winter in a few places, while in most places the maximum occurs in spring. One-month collection periods are not adequate to study short temporal variations, especially where strong seasonal differences exist. Even annual deposition at most stations is not as highly correlated with annual precipitation as would be desired for a good representation of the flux.

Figures 3.27 and 3.28 show the seasonal fluxes of ^{210}Pb and ^{7}Be in precipitation. For the measured period of November 1997 to January 1999 the highest value of concentrations was in spring (May 1998) which agrees with the surface air sample results in this period. It has been shown that there are seasonal variations of the depositional fluxes of ^{210}Pb and ^{7}Be. For a constant annual flux of ^{210}Pb or ^{7}Be, any increase in the depositional fluxes of ^{210}Pb and ^{7}Be during one season in a year should theoretically lead to a minimum depositional flux during another season in the same year.

4.2.3. Estimate of dry deposition for ^{210}Pb and ^{7}Be.

Atmospheric aerosols may be removed either by precipitation-scavenging (wet deposition) or by settling under the influence of gravitational, turbulent deposition or electrostatic forces (dry deposition). In general, total deposition (wet + dry) data are of greater value in estimating atmospheric ^{210}Pb deposition at a given

locality than are data on individual precipitation events since dry deposition is included. Dry deposition of particles has received far less attention then the deposition of gases. This is partly because of results of wind tunnel studies suggesting that the deposition velocity may be very small for sub-micron particles where the majority of the aerosol phase pollutants is located. Also, with the complexity of deposition processes for particles it is difficult to perform field measurements. Even in the case of the dry deposition of particulate sulphur and nitrogen over Europe there are important uncertainties over the magnitude of the flux [Gallagher et al., 1997], (note: ^{210}Pb and ^{7}Be attach to the same size aerosols as $SO_4^{=}$ and NO_3^{-} would attach). However, it is necessary to quantify fluxes to evaluate critical loads of acidic deposition and abatement strategies of atmospheric pollution [Ruijgrok et al., 1995].

The watershed-ecosystem estimates of dry deposition, measured by Likens et al. (1990), using the Y-intercept and mass balance methods are similar in magnitude (430 and 410 eq $SO_4^{=}$/ha-year, respectively). Dry deposition contributed about 37% of total S deposition, varying from 12% in 1964-65 to 61% in 1983-84, (Figure 4.5). Other studies have suggested that dry deposition can contribute up to 60% of total inputs of sulphur to forest and lake ecosystems [Likens et al., 1990]. This fraction changes with the gas-particle fraction for atmospheric sulphur and hence distance from major emission source areas [Gibson, 1986] and with different time period studies [Likens et al., 1990].

Measurements of stemflow and throughfall fluxes also have been used to estimate dry deposition of S in some forest ecosystems. Using the radioactive isotope ^{35}S, Lindberg and Garten (1988) found that >85% of the $SO_4^{=}$ in net throughfall below three tree species in eastern Tennessee was due to dry deposition.

In the idealised linear model for ^{210}Pb deposition versus precipitation, the intercept at zero precipitation for a regression line has been used as an estimate of dry deposition. Since a large portion of the depositional fluxes of atmospherically derived nuclides are derived through wet precipitation, the amount of precipitation has a major influence on the depositional fluxes of ^{210}Pb and ^{7}Be. Even though the production rate and transport are important, they do not vary in time as precipitation does. The amount of precipitation primarily controls the depositional concentrations [Turekian et al., 1977]. However, Turekian et al. estimate of dry deposition is for a

tray filled with water, which is not appropriate to quantify aerosol inputs to the vegetated landscapes.

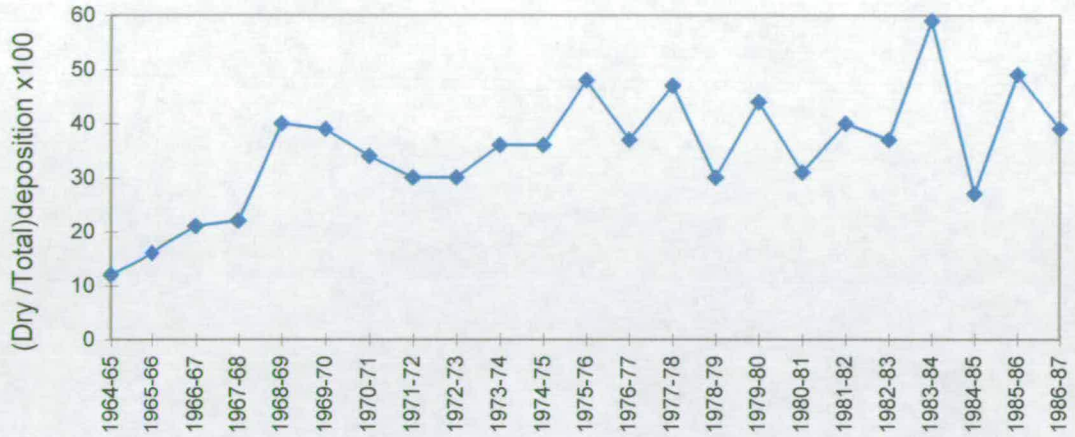

Figure 4.5. Annual dry deposition as a percent of annual total deposition of $SO_4^=$ for Watershed 6 of the Hubbard Brook Experimental Forest (HBEF) during 1964- 65 through 1986- 87, [Taken from Likens et al., 1990].

The contribution of dry deposition processes to the total ^{210}Pb and ^{7}Be flux is difficult to evaluate with direct measurements. An indirect evaluation (comparing ^{210}Pb and ^{7}Be deposition in the wet-only and bulk samples collected at a Norfolk site) indicates that dry deposition accounts for less than 10% of the total ^{210}Pb and ^{7}Be flux to bucket collectors [Todd et al., 1984]. The contribution of dry deposition measured this way is of marginal value to quantify the dry deposition to the countryside.

Another indirect evaluation of dry deposition can be obtained from the respective Y intercepts of the total (wet and dry) ^{210}Pb and ^{7}Be monthly fluxes versus precipitation. These Y-axis intercepts estimates of dry deposition are subject to two distinct types of errors. One is the statistical counting error and the other is the scattering of the points (figures 3.21 and 3.22). Since it appears that ^{210}Pb and ^{7}Be can be enriched in rain during the early stages of precipitation events, it seems reasonable to suppose that the concentration of ^{210}Pb and ^{7}Be in rain will be higher in drier months than in wetter months or periods characterised by prolonged rain. This bias will increase the value of the Y-axis intercept at zero precipitation and will yield a larger estimate of dry deposition than the contribution (about <10%) implied by the wet-only and bulk deposition samples at Norfolk [Todd et al., 1984].

In this study, the intercepts with the ^{210}Pb flux-axes, of figures 3.21 and 3.22, indicate that averages of (41 ± 13)% and (35 ± 9)% of the total deposition were contributed by dry deposition for ^{210}Pb and ^{7}Be, respectively. The dry deposition values from this study for ^{210}Pb and ^{7}Be were similar. In table 4.5, estimates of dry deposition of ^{210}Pb from the intercept of the least-squares line for other studies and this study are compared. For the nearest location to our measuring site, this was (33 ± 11)% which agrees with our determined value and it is on the lower side of the rest of the reported values.

A comparison of the ^{7}Be results with other data is not made since the dry deposition of ^{7}Be has not been reported in the literature.

	total	dry	dry/total
Kaitaia *	61.4 ± 16.6	33.2 ± 6.6	0.54 ± 0.18
Darwin*	89.6 ± 24.9	48.1 ± 6.6	0.54 ± 0.17
Milford Haven*	84.9 ± 13.3	28.2 ± 8.3	0.33 ± 0.11
New Haven*	152.7 ±14.9	93.0 ± 21.6	0.61 ± 0.15
This study	51.8 ± 7.7	21.2 ± 6.7	0.41 ± 0.13

Table 4.5. Estimate of Dry-Deposition from the intercept of the least-squares line. ^{210}Pb annual deposition (Bq m^{-2} y^{-1}).[* Taken from Turekian et al., 1977].

Although an attempt to measure the dry deposition is provided by the above procedures, this does not yield the true dry deposition to the landscape, as it is to the collector tray or bucket alone. From the soil inventory results of this study and calculations in the following section, the effect of vegetation and trees on the dry deposition have been quantified as described in 4.3.4.2.

4.2.4. Washout scavenging coefficient (W_S).

The washout scavenging coefficient (W_S), is defined as

$$W_S = C_R / C_A \quad .....(4.2),$$

where, C_R is the Concentration in Rain (Bq kg^{-1} of rain), and

C_A is the Concentration in Air (Bq kg^{-1} of air)

The magnitude of W_S calculated in this way is dependent upon the intensity and duration of the rain. The effect of rain intensity and duration is reduced by averaging the rain and air concentration for a year of measurements [Cambray et al., 1970]. Assuming the same relationship apply to ^{210}Pb and ^{7}Be aerosols, the washout scavenging coefficients for these isotopes were determined, using equation (4.2) and the results are given in table 4.6.

	concentrations of isotopes in rain (mBq l^{-1})	concentrations of isotopes in air (mBq m^{-3})	Washout Scavenging ratio (W_S)
^{210}Pb	62.6 ± 9.3	0.19 ± 0.06	402 ± 60
^{7}Be	732 ± 27	2.71 ± 0.66	330 ± 12

Table 4.6. The washout scavenging ratio for ^{210}Pb and ^{7}Be measured from the precipitation and surface air samples. Density of air was taken as 1.22 kg m^{-3}.

A washout scavenging ratio of 400 was found for ^{210}Pb by Knuth et al., (1983). Junge (1963a) predicted a washout scavenging ratio of 500 for ^{210}Pb. The W_S of 402 ±60 for ^{210}Pb from this study agrees well with the W_S found in the reported literature. The W_S for ^{7}Be is 330 ±12 from this study. No reported value was found for comparison.

4.2.5. Averaged annual concentrations of ^{210}Pb and ^{7}Be in precipitation.

The ^{210}Pb and ^{7}Be concentrations in a sample representing a single precipitation event will clearly depend on a complex array of variables, including the history of the air mass and the particular characteristics of the storm (intensity, duration, height of cloud, etc.). It is therefore not surprising that ^{210}Pb and ^{7}Be concentrations in precipitation vary considerably. In 31 rainfall samples determined these concentrations range from 17.4 ± 2.3 to 326.2 ± 20.6 (mBq l^{-1}) for ^{210}Pb and from 265 ± 4 to 3311 ± 69 (mBq l^{-1}) for ^{7}Be. Generally light rain (or early fraction of heavier ones) tend to have higher concentration of ^{210}Pb and ^{7}Be than heavy rain (or bulk samples). A volume weighted average of ^{210}Pb and ^{7}Be concentration is the correct method of computing the annual deposition of ^{210}Pb and ^{7}Be. That is:

$$^{210}Pb_{flux}\,(Bq\ cm^{-2}\ y^{-1}) = \lambda_{Pb}\ \Sigma(r_i\ [^{210}Pb]_i)/f \qquad .....(4.3)$$

$$^{7}Be_{flux}\,(Bq\ cm^{-2}\ y^{-1}) = \lambda_{Be}\ \Sigma(r_i\ [^{7}Be]_i)/f \qquad .....(4.4)$$

Where, for an individual precipitation event i, r_i is the volume of precipitation per cm^2 of earth surface, and $[^{210}Pb]$ and $[^{7}Be]$, are the concentration of ^{210}Pb and ^{7}Be,

respectively. λ_{Pb} and λ_{Be} the decay constant for ^{210}Pb and ^{7}Be, respectively. And f is the fraction of the annual precipitation represented by Σr_i.

The annual fluxes of ^{210}Pb and ^{7}Be in rain were determined to be 68 ± 10 (Bq m^{-2} y^{-1}) for ^{210}Pb and 787 ± 29 (Bq m^{-2} y^{-1}) for ^{7}Be. These are to be compared with the reported values ranging from 68 to 147 (Bq m^{-2} y^{-1}) for ^{210}Pb and 774 to 863 (Bq m^{-2} y^{-1}) for ^{7}Be. These concentrations were on the lower side of the range. The average deposition rate of ^{210}Pb and ^{7}Be on surface of the earth for different locations are shown in tables 4.7 and 4.8.

Location	Lat.	Long.	Prec. (mm)	Sampling period (y)	Conc. (mBq l^{-1})	Flux (Bq m^{-2} y^{-1})
Brotherswater ♠	54.5	-3	2108		70	147
Milford Haven ♠	51.7	-5	916	3	103	85 ± 13
Plymouth ♠	50.4	-4.2	1240	2	84	68
This study	55.6	-3.9	930♥	>1	63 ± 9	68 ± 10

Table 4.7. The concentrations of ^{210}Pb in rain compared with the other UK reported values, [♠Preiss et al., 1998].♥Rain in 1998 measured at the sampling site.

Location	Lat.	Long.	Prec. (mm)	Sampling period (months)	Conc. (mBq l^{-1})	Flux (Bq m^{-2} y^{-1})
Chilton ♥	51.0	-1.4	1576	23	1345	827
Milford Haven ♥	51.7	-5	2545	23	1378	863
Plymouth ♣	50.4	-4.2	1240	24	960±42	774 ± 34
This study	55.6	-3.9	930♠	15	732 ± 27	787± 29

Table 4.8. The concentrations of ^{7}Be in rain compared with the other UK reported values, [♥ Peirson , 1963; ♣ Clifton, 1991]. ♠Rainfall in 1998.

The deposition of ^{7}Be to the earth's surface varies with season, latitude and local meteorological conditions. Because of the short half-life of ^{7}Be and the large seasonal and meteorological effects on its deposition, ^{7}Be fluxes averaged over an entire year are not the most appropriate input function when using the distribution of

^{7}Be as a tracer in terrestrial and aquatic systems. An improved estimate may be obtained from average fluxes calculated from linear correlation with the amount of precipitation which can be used to provide a better estimate for the ^{7}Be input prior to precipitation and help correct for meteorological conditions. The average monthly fluxes required to support the ^{7}Be inventories plotted in figure 3.17 range from 1.62 mBq cm^{-2} ($\pm$ 0.03) to 14.02 mBq cm^{-2} ($\pm$ 0.13).

Although the production source function of these two nuclides are distinctly different, a relatively high correlation between the ^{210}Pb fluxes and the ^{7}Be fluxes has been observed in different places. This high correlation between fluxes of ^{210}Pb and ^{7}Be appears to suggest that the atmospheric removal behaviour of ^{210}Pb and ^{7}Be are similar, and that these two nuclides can not be used as two independent atmospheric tracers [Baskran, 1995]. Figure 3.18 shows a linear relationship between the concentrations of ^{210}Pb and ^{7}Be (mBq l^{-1}) in precipitation.

On the basis of comparison with the other reported measurements in the literature, it appears that our results, 68 Bq m^{-2} y^{-1} ($\pm$10) for ^{210}Pb and 787 Bq m^{-2} y^{-1} ($\pm$29) for ^{7}Be, are in the range of these reported values. The flux of 68 to 147 Bq m^{-2} y^{-1} for ^{210}Pb in UK (table 4.7) and 774 to 863 Bq m^{-2} y^{-1} for ^{7}Be in UK (table 4.8) are reported in the literature. The mean UK ^{210}Pb flux has been estimated at 77 ($\pm$14) Bq m^{-2} y^{-1} per metre of rainfall [Smith et al., 1997].

Reporting the flux per metre of rainfall is misleading as it leads to an under estimate for the wet regions and over estimate in the dry regions.

The washout ratios obtained from this study are 402 ($\pm$60) and 330 ($\pm$12) for ^{210}Pb and ^{7}Be, respectively. From these values it is clear that the scavenging ratio of both isotopes are in a similar range and that these isotopes are being scavenged at similar rates. It is reasonable to assume therefore that they must be subject to the same removal procedures from the atmosphere.

4.3. Soil inventory measurements of atmospherically derived ^{210}Pb and ^{137}Cs.

The use of soil samples as integrating collectors of atmospheric deposition has two principal advantages over direct precipitation collection. First, the time and expense required to obtain and analyse samples is greatly reduced. Second, the deposition rates obtained are free of artefacts introduced by the artificial collection apparatus. ^{210}Pb and ^{137}Cs are present in the atmosphere as single atoms residing in sub-micrometre aerosols. When the carrier aerosols are deposited to the landscape, the ^{210}Pb and ^{137}Cs are retained by soils [Graustein & Turekian, 1986]. Because organic matter in soils retains ^{210}Pb quantitatively, many soils act as efficient integrating collectors of the atmospheric deposition of ^{210}Pb [Turekian et al., 1977; Nozaki et al., 1978]. The measurement of ^{210}Pb in soils is a practical way to study the effects of local variables, such as elevation, clouds or vegetation, on the rate of delivery of sub-micrometre aerosols to the land surface [Graustein & Turekian 1983].

Measuring the activity of the atmospherically derived ^{210}Pb in a soil core is therefore equivalent to measuring the time-averaged aerosol deposition rate. For a soil to reach steady state with respect to a radionuclide it must remain undisturbed for about 5 half-lives, about 100 years in the case of ^{210}Pb. An additional requirement is that the ^{210}Pb derived from the atmosphere be correctable for the ^{210}Pb produced by the decay of ^{222}Rn in the soil itself [Graustein and Turekian 1983].

4.3.1. Distributions of ^{210}Pb and ^{137}Cs in top soils.

Both ^{210}Pb and ^{137}Cs are deposited from the atmosphere to earth's surface and most of each nuclide is confined to the upper 15 to 30 cm of soils [Graustein & Turekian, 1986]. If the soil is at steady state with respect to ^{210}Pb, the rate of loss of ^{210}Pb by radioactive decay is exactly equal to the rate of atmospheric input. Benninger et al. (1975) showed that undisturbed soil profiles can be treated as good repositories for atmospherically supplied ^{210}Pb. Most of the ^{210}Pb is trapped and preserved with a residence time of thousands of years in the organic-rich top soil. Very little percolates into the ground water regime or flows off into stream channels. On this basis it is evident that a soil profile measured for ^{210}Pb and ^{226}Ra should show excess ^{210}Pb inventory [Turekian et al., 1977]. Forest soils are generally well suited for ^{210}Pb deposition rate measurements [Graustein & Turekian, 1983].

The experimental results for this study, analysed and reported in chapter 3 section 3.3, indicate that the distribution of ^{210}Pb and ^{137}Cs in top soils is

approximately exponential for all of the core samples, shown in figures 3.29 to 3.48. Depths of penetration of deposited radionuclides are quite variable, and strongly dependent on the soil density.

The depth profile of ^{210}Pb in the soil samples, figures 3.29-3.38, generally show that ^{210}Pb is efficiently immobilised in the surface horizons of soil. On average 88% (ranging from 78% to 96%) of the atmospheric inventory concentrated is in the top 10 cm, reported in section 3.3.4. The depth profiles of ^{137}Cs in the soil samples, figures 3.39-3.48, generally show that ^{137}Cs is less efficiently immobilised in the surface horizons of soil compared to ^{210}Pb for the same soil with average value 78% (ranging from 55% to 96%) of the atmospheric inventory concentrated in the top 10 cm (reported in section 3.3.4).

While ^{210}Pb is absorbed strongly and retained efficiently by the organic matter present in the soils (Lewis, 1977), soil variables contribute to more variations in ^{137}Cs present in the soil. Depths of penetration of fall-out radionuclides are quite variable, and strongly dependent on the soil density and chemical properties of the element. In some cases there are indications of penetration of activity into deeper sections of the cores due to the mobility of ^{137}Cs radionuclide in these soils, see section 1.8.

4.3.2. ^{210}Pb inventories in Rothamsted soils.

Under the reasonable assumption of steady state between the atmospheric supply of ^{210}Pb and its radioactive decay in soil, the mean flux to the open grassland is 117±4.3 Bq m^{-2} y^{-1}. Considering the average annual rainfall of 700 mm for this site, (the rainfall data are taken from the reported values from Rothamsted 1969 to 1999), gave a mean concentration of ^{210}Pb in rainfall of 170±6 mBq l^{-1}. The mean concentration of ^{210}Pb in rainfall was determined using the following equation,

$$F_{Pb}\ (Bq\ m^{-2}\ y^{-1}) = C\ (mBq\ l^{-1}) \times R\ (m\ y^{-1}) \qquad ....(4.5),$$

where, F_{Pb} (Bq m^{-2} y^{-1}) is the atmospheric flux of ^{210}Pb in soil, C (mBq l^{-1}) concentration of ^{210}Pb in rain and R (m y^{-1}) the amount of rainfall per year.

Table 4.9 gives the mean ^{210}Pb flux for each site calculated using equation 3.24 compared with the reported results in the literature for the UK. From table 4.9 the fluxes of ^{210}Pb reported ranges from 67 Bq m^{-2} y^{-1} to 187 Bq m^{-2} y^{-1}. The results achieved from this study for open grassland are 117±4.3 Bq m^{-2} y^{-1}, for Geescroft canopy 144±4.2 Bq m^{-2} y^{-1} and for Broadbalk canopy 151±3.8Bq m^{-2} y^{-1}, which fit in

Location	Alt.	Long.	Prec. (mm)	Invent. (Bq m^{-2})	Flux (Bq m^{-2} y^{-1})	Reference
Fenwick (Scotland)						
Core 3	55.7	-4.4	1400	3432	106	Mac Kenzie et
Core 5	55.7	-4.4	1400	2165	67	al., (1995)
Mean (n=2)					86 ± 19	
Inverness (Scotland)						
Core A	55.4	-4.2	950	6000	187	Pulford et al.,
Core B	55.4	-4.2	950	2700	83	(1995)
Core C	55.4	-4.2	950	>2700	>83	
Core D	55.4	-4.2	950	>3600	>112	
Mean (n=4)					>116	
Brotherswater	54.5	-3.0	2535	5200	162	Eakins et al., (1984)
Brotherswater Mean (n=6)	54.5	-3.0	2400	4886	152	Smith et al., (1997)
Blelham Tarn Mean (n=6)	54.4	-3.0	1814	3689	115	Smith et al., (1997)
Devoke Water) Mean (n=8)	54.4	-3.0	1840	5755	179	Smith et al., (1997)
Jackmore Brook	50.7	-3.5	882	3050	95	He & Walling (1997)
River Start	50.7	-3.5	882	5200	162	He & Walling (1997)
Merrick (Galloway)						
Low ground	55.1	-4.2	1000	1000±400	31±13	Mourne,
High ground	55.1	-4.2	2400	4500±600	140±19	(1993)
Great Dun Fell (Cumbria)						
Low ground	55.5	-3.5	1040	1900±400	59±13	Mourne,
High ground	55.5	-3.5	1760	5800±500	181±16	(1993)
Ben Cruachan (Strathclyde)	56.3	-5.1	2170	3700±300	116±9	Mourne,
Low ground	56.3	-5.1	3600	10500±900	328±28	(1993)
High ground						
Beinn Dorain (Strathclyde)	56.3	-4.4	2400	4100±400	128±13	Mourne,
Low ground	56.3	-4.4	2800	7300±900	228±28	(1993)
High ground						
Ben Lawers (Tayside)						
Low ground	56.3	-4.2	1650	3100±300	97±9	Mourne,
High ground	56.3	-4.2	2500	5500±600	172±19	(1993)
Dunslair Heights (Scotland)						
Grass (mean)	55.4	-3.8	1200	2325±114	73±4	Moghadam,
Forest (mean)	55.4	-3.8	1200	3195±346	100±11	(1998)
Dun Coilich, Scotland						
Grass (mean)	56.4	-4.1	1300	3175±440	98±14	Moghadam,
Forest (mean)	56.4	-4.1	1300	4309±317	135±10	(1998)
Rothamsted, Harpenden						
Grass (mean)	51.6	-0.6	700	3753 ±139	117 ±4	
Canopy (mean)	51.6	-0.6	700	4726 ±130	148 ±4	This study

Table 4.9. The results from the earlier studies for ^{210}Pb inventories (Bq m^{-2} y^{-1}) in the UK soil, expressed as a ^{210}Pb concentrations in rainfall.

the range of the other reported values for the UK soil inventories.

Table 4.10 gives the mean ^{210}Pb flux for each site calculated using equation 4.5, the deposition per meter of rainfall (expressed as a ^{210}Pb concentrations in rainfall), also shown are the results from the earlier studies, some of which were based on direct rainfall measurements.

Smith et al. (1997) report the mean UK ^{210}Pb flux is 77 ±14 Bq m^{-2} y^{-1} per metre of rainfall. This procedure has been widely used by other researchers. It is useful to show from published data that expressing the ^{210}Pb deposition per metre on rainfall is misleading. From the data in table 4.10, the mean ^{210}Pb flux is calculated as 108 ±76 Bq m^{-2} y^{-1} per metre of rainfall (values from this study are not included in calculating the mean value). Also Rothamsted soil inventories beneath the canopies are larger than this mean value, determined as 211 ±6 Bq m^{-2} y^{-1} per metre of rainfall for average flux to the canopies (206 ±6 Bq m^{-2} y^{-1} per metre of rainfall for Geescroft canopy, and 216 ±6 Bq m^{-2} y^{-1} for Broadbalk canopy), and for open grassland 167 ±6 Bq m^{-2} y^{-1}.

Clearly, both wet deposition of ^{210}Pb and the concentration of ^{210}Pb in precipitation show marked variability across the UK. It is therefore not useful (or best) to present the ^{210}Pb deposition data per metre of rainfall.

4.3.3. ^{137}Cs inventories in Rothamsted soils.

The measured ^{137}Cs inventory results were presented and analysed in chapter 3, section 3.3.4. ^{137}Cs inventories follow a similar trend to that of atmospheric derived ^{210}Pb inventories. Although significant levels of fall-out ^{137}Cs were found at depths of up to 20 cm. In most cases, the bulk of the inventory remained in the top 10 cm soils, (in average 78% of the total measured inventories were detected in top 10 cm, discussed in section 4.3.1).

In two major studies of weapons ^{137}Cs fall-out in the UK (Cawse, 1983; Cawse et al., 1988), it was shown that there was a significant correlation between mean annual rainfall and ^{137}Cs inventories in soil cores. The reported fluxes of ^{137}Cs measured in soils for different parts of UK are presented in table 4.11. These values are decay corrected for 1998 to be compared with the obtained values for this study.

Location	Alt.	Long.	Flux ($Bq\ m^{-2}\ y^{-1}$) per metre of rainfall	Reference
Fenwick, Scotland	55.7	-4.4	62±14	Mac Kenzie et al., (1995)
Inverness, Scotland	55.4	-4.2	122	Pulford et al., (1995)
Brotherswater	54.5	-3.0	64	Eakins et al., (1984)
Brotherswater	54.5	-3.0	63	Smith et al., (1997)
Blelham Tarn	54.4	-3.0	63	Smith et al., (1997)
Devoke Water	54.4	-3.0	97	Smith et al., (1997)
Jackmore Brook	50.7	-3.5	108	He & Walling (1997)
River Start	50.7	-3.5	184	He & Walling (1997)
Merrick (Galloway) Low ground High ground	 55.1 55.1	 -4.2 -4.2	 31±13 59±8	Mourne, (1993)
Great Dun Fell (Cumbria) Low ground High ground	 55.5 55.5	 -3.5 -3.5	 57±12 103±9	Mourne, (1993)
Ben Cruachan (Strathclyde) Low ground High ground	 56.3 56.3	 -5.1 -5.1	 53±4 91±8	Mourne, (1993)
Beinn Dorain (Strathclyde) Low ground High ground	 56.3 56.3	 -4.4 -4.4	 53±5 81±10	Mourne, (1993)
Ben Lawers (Tayside) Low ground High ground	 56.3 56.3	 -4.2 -4.2	 59±6 69±8	Mourne, (1993)
Dunslair Heights, Scotland Open (mean) Forest (mean)	 55.4 55.4	 -3.8 -3.8	 61±3 83±9	Moghadam, (1998)
Dun Coilich, Scotland Open (mean) Forest (mean)	 56.4 56.4	 -4.1 -4.1	 75±11 104±8	Moghadam, (1998)
Rothamsted, Harpenden Open (mean) Forest (mean)	 51.6 51.6	 -0.6 -0.6	 167±6 211±6	This study
Brotherswater *	54.5	-3.0	147	Eakins et al., (1984)
Milford Haven *	51.7	-5.0	85	Peirson et al., (1966)
Plymouth *	50.4	-4.2	68	Thomson et al., (1993)
Plymouth *	50.4	-4.2	68	Clifton (1991)
Edinburgh *	55.6	-3.9	68±10	This study

Table 4.10. The results from the earlier studies for ^{210}Pb inventories in UK soils, expressed as ^{210}Pb concentrations in rainfall. * These results were based on direct measurements of rainfall.

Location	Lat.	Long.	Flux (Bq m^{-2})	Prec. (mm)	Flux (Bq m^{-2}) (decay corrected)*	Reference
Bleham	54.4	-3.0	4738	1814	4528	Smith et al., (1997)
Devoke Water	54.4	-3.0	5012	1840	4789	Smith et al., (1997)
Brotherswater	54.5	-3.0	7267	2535	5286	Eakins et al., (1984)
Merrick (Galloway) Mean value	55.1	-4.2	13500±400	1700	10756±318	Mourne, (1993)
Great Dun Fell (Cumbria) Mean value	55.5	-3.5	4040±400	1400	3292±326	Mourne, (1993)
Ben Cruachan (Strathclyde) Mean value	56.3	-5.1	4850±800	2885	4045±667	Mourne, (1993)
Beinn Dorain (Strathclyde) Mean value	56.3	-4.4	7600±500	2600	6338±417	Mourne, (1993)
Ben Lawers (Tayside) Mean value	56.3	-4.2	18200±1300	2075	15178±1081	Mourne, (1993)
Dunslair Heights, Scotland						Moghadam,
Open (mean)	55.4	-3.8	1830±320	1200	1662±291	(1998)
Forest (mean)	55.4	-3.8	2460±404	1200	2234±367	
Dun Coilich, Scotland						Moghadam,
Open (mean)	56.4	-4.1	8050±641	1300	7311±582	(1998)
Forest (mean)	56.4	-4.1	10971±1203	1300	9964±1093	
Rothamsted, Harpenden						
Open (mean)	51.6	-0.6	1246±115	700	1246±115	This study
Forest (mean)	51.6	-0.6	1888±142	700	1888±142	

Table 4.11. The results from the earlier studies for ^{137}Cs (Bq m^{-2}) inventories in the UK soils, compared with the results from this study.
* decay corrected to the date of measurements extracted from the references.

A clear pattern could not be seen for ^{137}Cs isotope since ^{137}Cs is a fission product and its retention by type of soil is also more complex. ^{137}Cs is only emitted to the atmosphere by nuclear bomb testing and nuclear reactor accidents and it is not easily compared between different locations.

4.3.4. Deposition velocity of ^{210}Pb carrier aerosols.

The total deposition velocity, V, of a nuclide is taken as the ratio;

$$V = F / C \qquad \text{....(4.6)}$$

Where, F is the total flux to the earth's surface, and

C is the concentration in air at some reference level.

The definition of the total deposition velocity in equation 4.6 includes both wet precipitation and dry deposition. Using equation 4.6 and the rain and soil data from this study and the earlier reported studies the total deposition velocity for ^{210}Pb is determined and reported in the following sections.

4.3.4.1. Deposition velocity calculated from rain data.

The total average deposition velocity (V) of ^{210}Pb for Australia, England and New-York Connecticut is about 8.5 mm s^{-1} ranging from 4.3 to 13.3 mm s^{-1}. The total average deposition velocity of ^{210}Pb for UK is reported to be 13.3 mm s^{-1} [Turekian et al., 1977]. The deposition velocity reported above is the washout amount of particles to a known area of collection tray or bucket. The true deposition velocity to land surface can vary greatly between adjacent locations, depending on the vegetation and canopy cover on the land, which is fully explained in the following section.

4.3.4.2. Dry deposition velocity calculated from soil data.

The mechanisms by which air pollutants are transferred to forests is by dry and wet deposition. Dry deposition is the processes whereby gases and aerosols are deposited directly from the atmosphere to terrestrial surfaces. Wet deposition is measured by collecting precipitation in samplers placed in the open field.

Dry deposition of particles has received less attention than the deposition of acidic gases. This is partly because the results of wind tunnel studies suggest that the deposition velocity may be very small for sub-micron particles. Also, the complexity of deposition processes of particles implies that it is difficult to perform field measurements appropriately.

In this study we have demonstrated that the dry deposition of aerosols to open grassland and trees is much larger than previously thought from the wind tunnel findings. The dry deposition velocity of ^{210}Pb aerosols to vegetation and trees was calculated using the flux and concentration of ^{210}Pb at the nearest and similar

meteorological location to Rothamsted. Harwell was chosen for rain flux and Chilton for air concentration of ^{210}Pb. The rain flux at Harwell is reported as 83 Bq m^{-2} y^{-1} (Burton and Stewart, 1960) and the Chilton air concentration reported as 0.23 mBq m^{-3} (Peirson et al., 1966). Because we are taking the average inventory over a 30 years period (mean life time of ^{210}Pb is 32.2 years) the values above are appropriate for these calculations. Subtracting the rain flux from the total flux to vegetation and trees we could measure the excess flux due to dry deposition input due to vegetation and trees. To make the calculation equations 4.6 was used together with the following equation.

$$U(z) = \{U_*/k\}\{\ln[(Z-d)/Z_0]\} \quad \ldots. (4.7)$$

where, U(z) is the wind velocity at height Z, m s^{-1}.

Z is the height above the surface, m.

U_* is friction velocity, m s^{-1}.

h is the height of roughness element, m.

k is the vonkarman constant, =0.41.

Z_0 is the roughness length, =0.1h, m.

d is zero plane displacement, =0.7h, m, [Monteith & Unsworth, 1990].

The results obtained using the above rain and air concentrations of which were reported in table 4.12.

The averaged wind velocity U(z) at Rothamsted at 2 metres above ground is reported as 1.4 m s^{-1}. Therefore, the wind velocity was assumed constant for 2 metre above the vegetation and trees.

Location	U(z) (m s^{-1})	U_* (m s^{-1})	V_{dd} (mm s^{-1})	h (m)	Z_0 (m)
Open grassland	1.4	0.14	4.6±0.6	0.3	0.03
Geescroft Woodland	1.4	0.36	8.3±0.6	10	1
Broadbalk Woodland	1.4	0.36	9.4±0.5	10	1

Table 4.12. The dry deposition velocity (V_{dd}) mm s^{-1} for Rothamsted Vegetation and trees calculated using equations 4.6 and 4.7.

The results of these calculations together with the results from different studies and the wind tunnel results are plotted in figure 4.6. For the size distribution of the ^{210}Pb aerosols table 4.13 was used. Table 4.13 shows the range of particle size for carrier

aerosols of ^{210}Pb measured at different locations. They all agree that the size distribution of ^{210}Pb aerosol carriers are less than 1 μm mainly in the range of 0.3-0.4 μm.

Location	% present	size (μm)	References
Continental USA (near Boulder)	83±13	< 0.6	Moore et al. (1980)
Mediterranean Sea (Aden Gulf & Indian Ocean)	70-90	< 1.2	Sanak et al. (1981)
New Jersey (Chester)	71	< 0.58 (75% is in the range of 0.3-0.4)	Knuth et al. (1983)
Washington DC	85	< 1	Lockhart et al. (1965)
Continental USA	100	< 1	Moore et al. (1973); Knuth et al. (1981, 1982)
Pacific Ocean	90	< 1 (mainly 0.3-0.4)	Turekian et al. (1989)

Table 4.13. The size distribution of ^{210}Pb aerosols carriers reported in the literature.

The deposition velocity determined for ^{210}Pb aerosols are an order of magnitude higher than what have been predicted by the wind tunnel results. This certainly means that in the field, the deposition velocity of submicron aerosols such as ^{210}Pb is larger than the values predicted by Slinn (1982), and depend on the roughness area of the land.

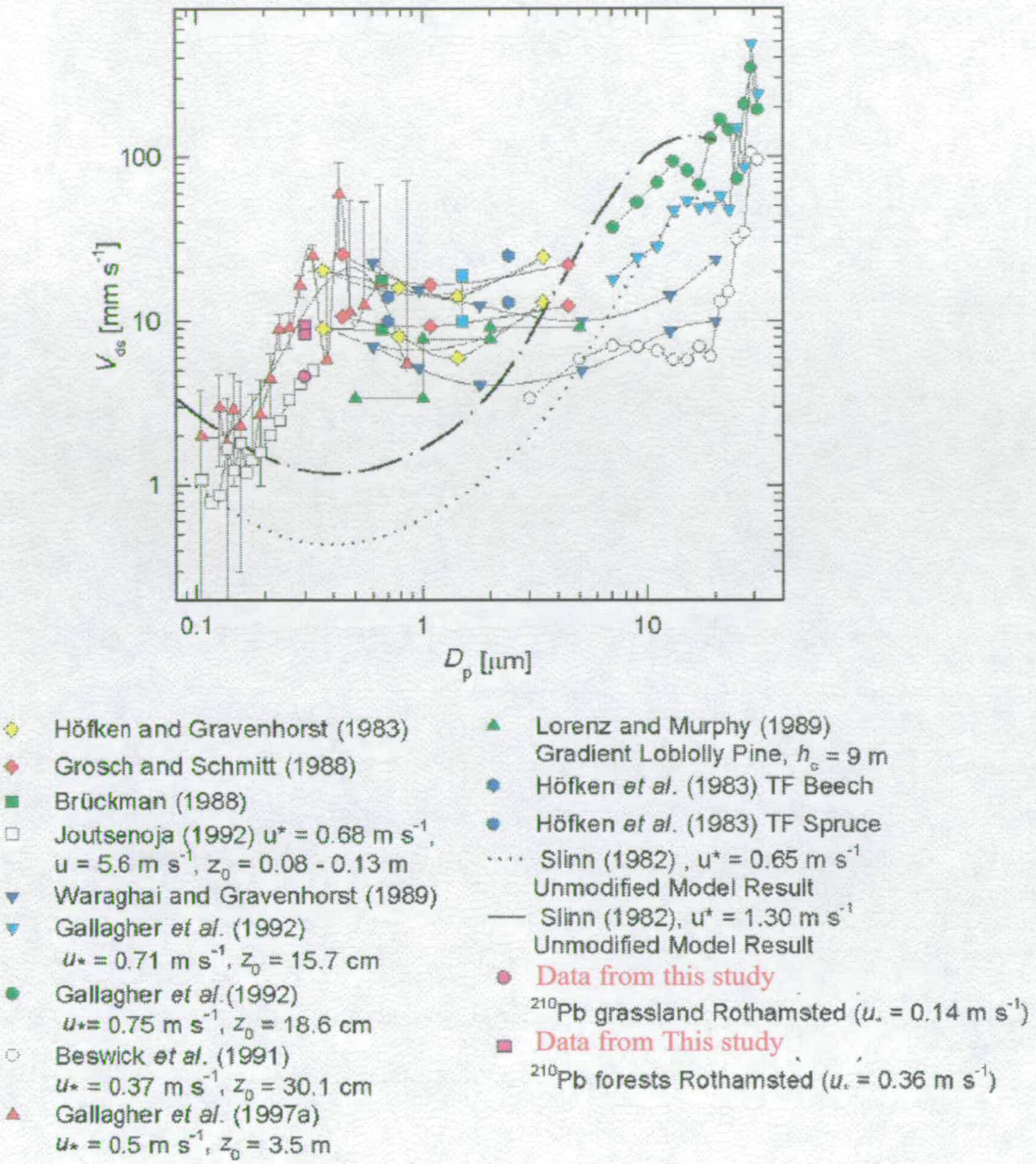

Figure 4.6. Deposition velocity of atmospherically derived ^{210}Pb into the Rothamsted soil compared with the wind tunnel measurements and other measured values [taken from Gallagher et al. (1997)]. Details of the references above could be found in Gallagher et al. (1997).

4.3.5. ^{210}Pb inventories into the canopies.

The atmospherically derived ^{210}Pb inventories into the canopies exceed those in adjacent open areas, indicating that forest sites receive more atmospheric inputs. The mean ^{210}Pb inventories are 3753 ±139 Bq m^{-2} for open grassland, 4607 ±135 Bq m^{-2} for Geescroft canopy and 4844 ±124 Bq m^{-2} for Broadbalk canopy. The excess inventories to the canopies compared to the grassland for ^{210}Pb were 23% and 29% for Geescroft and Broadbalk canopies, respectively, shown in figure 3.57. Assuming that the precipitation input is the same for all sites, the increase may therefore be assumed to result from aerosol capture by the trees in excess of that by the grassland. The ^{210}Pb inventories in different cores from the same catchment were relatively uniform; the standard deviation of measurements were around 20% for open grassland, 22% for Geescroft canopy, and 14%, for Broadbalk canopy.

4.3.6. ^{137}Cs inventories into the forests.

The atmospherically derived ^{137}Cs inventories into the forests exceed those in adjacent open areas, indicating that forest sites receive more atmospheric inputs. The increase in canopy inventories of 49% for Geescroft and 54% for Broadbalk relative to the open grassfield was measured. The average values of these inventories are 1246 ±115 Bq m^{-2} for open grassland, 1856 ±119 Bq m^{-2} for Geescroft forest and 1920 ±164 Bq m^{-2} for Broadbalk forest.

^{137}Cs compared to ^{210}Pb is more mobilised in soils and could migrate through the soil depth when it is exposed to acid rain and therefore it would penetrate deeper than ^{210}Pb. Hence its inventory in forest is larger than in the open grassland (see section 1.8). We assumed that the same amount of rain is deposited to the grassland area and the canopies. Because of the bigger surface area of the trees, some of the rain to the trees will evaporate and hence less rain will reach the soil under the trees. As less rain reaches the soils, then ^{137}Cs will migrate less in the canopies soils and therefore the excess inventories of ^{137}Cs into the canopy soils are larger than those of ^{210}Pb for the same area.

4.3.7. The edge of the forest effects on deposition.

The deposition of atmospherically derived ^{210}Pb and ^{137}Cs to the edge of forest has been investigated. Figures 4.7 and 4.8 show the excess inventories of ^{210}Pb to Geescroft and Broadbalk canopies, respectively. Figure 4.7 shows that more

deposition is at the edge of the Geescroft forest (site R3) and as we go inside the forest the deposition decreases. The input to the edge of the forest is larger than that to the rest of the forest and also larger than that to the adjacent open land. This could be due to the interception of the aerosols by the trees. The Broadbalk forest is a narrow forest (about 30 m wide) compared to Geescroft and could be considered as an edge at all together. Because of that the input to this forest between the 3 sites measured had less variations and therefore the deposition to this forest is more uniform, and larger than its adjacent open grassland.

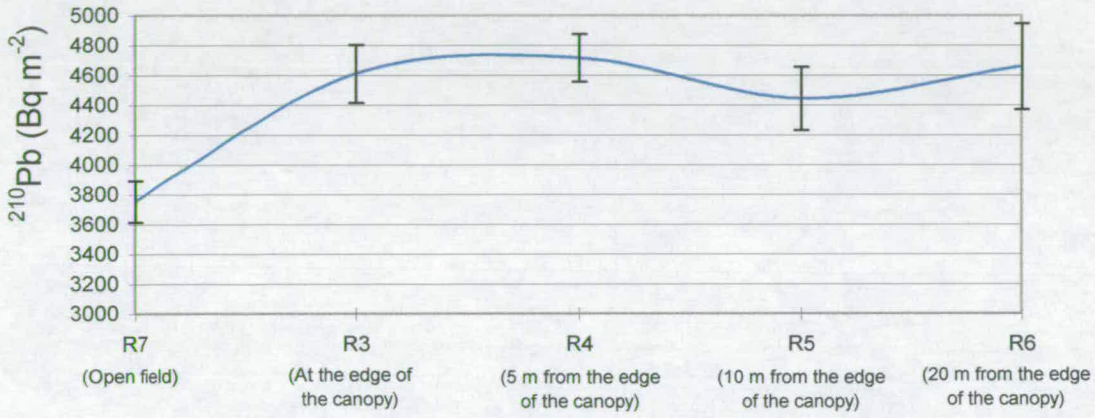

Figure 4.7. The mean inventories of ^{210}Pb (Bq m^{-2}) in open grassland (R7) compared with the Geescroft forest, at the edge of the forest (R3), 5 m from the edge (R4), 10 m from the edge (R5), and 20 m from the edge (R6). The error bars are the standard deviation in each site.

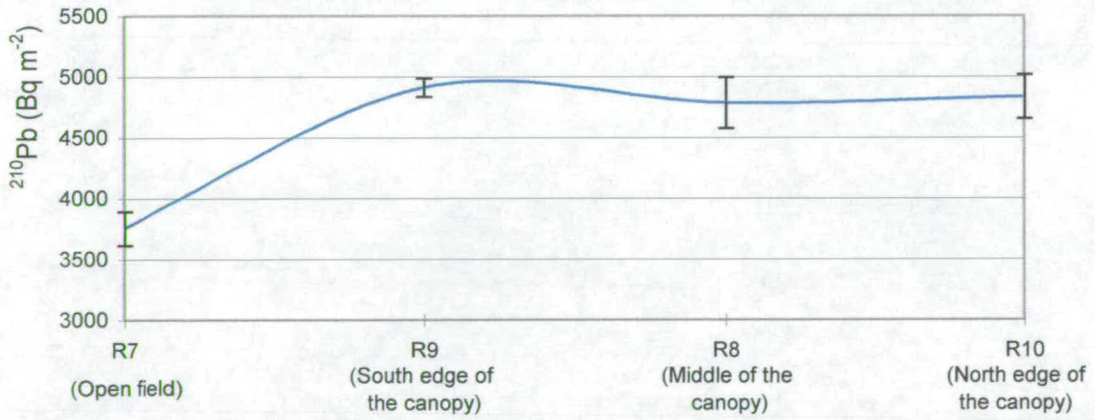

Figure 4.8. The atmospheric derived ^{210}Pb (Bq m^{-2}) inventories to the open grassland (R7) compared with the Broadbalk forest, at the south edge (R9), in the middle (R8) and at the north edge of the forest (R10). The errors are the standard deviations of each site.

Similar results are found for the deposition of ^{137}Cs into the forest which are shown in figures 4.9 and 4.10. The ^{137}Cs input to the forest is also larger than those to the adjacent open grassland.

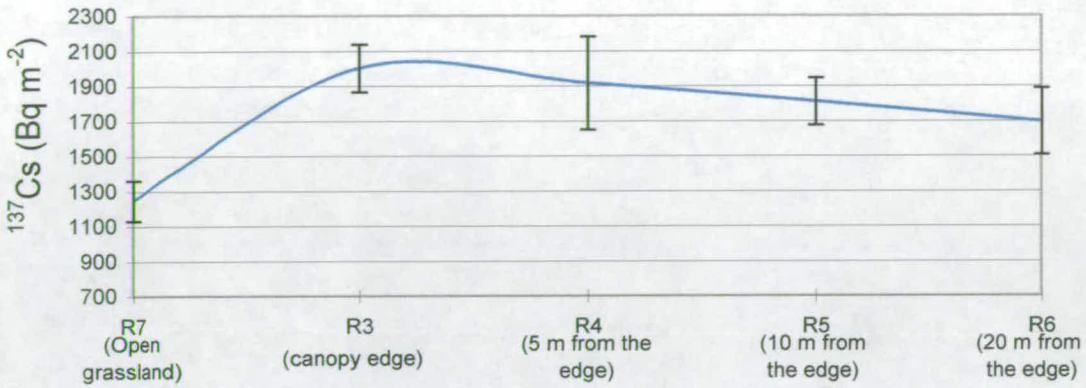

Figure 4.9. The mean inventories of ^{137}Cs (Bq m^{-2}) in open grassland (R7) compared with the Geescroft forest, at the edge of the forest (R3), 5 m from the edge (R4), 10 m from the edge (R5), and 20 m from the edge (R6). The error bars are the standard deviation in each site.

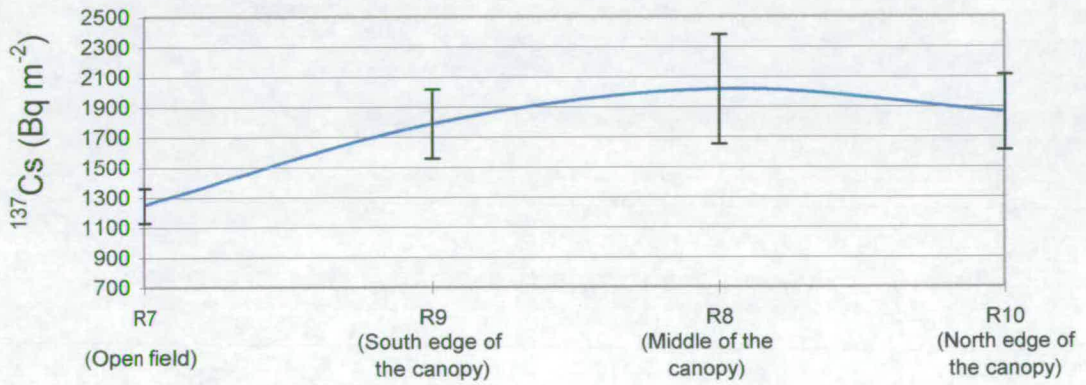

Figure 4.10. The atmospheric derived ^{137}Cs (Bq m^{-2}) inventories to the open grassland (R7) compared with the Broadbalk forest, at the south edge (R9), in the middle (R8) and at the north edge of the forest (R10). The errors are the standard deviations of each site.

Chapter 5

5. Conclusions.

The aim of this study was to use the soil inventory of atmospherically derived ^{210}Pb (radioactive half-life of 22.3 years) to quantify the enhancement in aerosol deposition by aerodynamically rough canopies in low level regions relative to short vegetation, in particular the increased capture of aerosols by trees.

For further understanding and interpreting of ^{210}Pb deposition to forest soils and support of this investigation the concentrations of ^{210}Pb in surface air and its flux in precipitation were measured. This information assisted in further understanding of the deposition mechanism of this radioisotope.

At the same time in air and rain samples the concentrations of cosmogenic radioisotope ^{7}Be (radioactive half-life of 53.4 days) were obtained. From the soil samples ^{137}Cs (product of nuclear fission, and nuclear weapons with radioactive half-life of 30.2 years) were measured and reported.

Non-destructive gamma-spectrometry was used for all three parts of this study using two high purity germanium (HPGe) detectors, one of which is fitted with a Compton suppression system (used for soil samples only). The direct gamma-spectrometry technique for determination of ^{210}Pb in soil allowed measurements on the same sample for other radionuclides such as ^{137}Cs and ^{214}Pb. The measured inventories of ^{214}Pb were used to correct the supported ^{210}Pb due to in situ decay of ^{222}Rn.

The location for surface air and rain sampling was the King's Buildings area in Edinburgh, Scotland, UK (55.6° N, 3.9° W). The soil samples were collected from Rothamsted experimental farms, Harpenden, England, UK (51.6° N, 0.6° W). The gamma spectroscopy measurements and preparation of the samples were done in the Nuclear Physics Group of the Physics and Astronomy Department in the University of Edinburgh.

The concentrations of ^{210}Pb, ^{137}Cs and ^{7}Be have not previously been measured in any of these areas.

In the following sections are a summary of conclusions drawn from this study. Presented in section 5.1, 5.2 and 5.3 are the conclusions of the surface air, rain and Rothamsted soil results, respectively.

5.1. Surface air samples.

• *Annual concentrations of ^{210}Pb and ^{7}Be:* Surface air was filtered during the period 4th of December 1996 to the 31st of January 1999 to measure the concentrations of radioisotopes ^{210}Pb and ^{7}Be in surface air for this region. In total, 100 air samples were collected and analysed. One-month collection periods are not adequate to study short term variability in concentrations of ^{210}Pb and ^{7}Be, because strong seasonal differences exist. ^{210}Pb concentration varied from 0.028 ±0.008 mBq m^{-3} to 0.619 ±0.016 mBq m^{-3} and this variations for ^{7}Be in surface air was from 0.782 ± 0.058 mBq m^{-3} to 6.81 ± 0.128 mBq m^{-3}. These variations were due to a number of effects, including the type of air mass, precipitation events, deposition mechanisms and transportation of air masses. Many literature values of ^{210}Pb report short periods measurements (as short as 1 month) to estimate annual deposition or concentrations. Such short periods do not sample the full range of variability in annual ^{210}Pb concentration and fail to clarify seasonal effects. It is therefore necessary to sample for the full year to obtain a satisfactory estimate of annual deposition or concentrations.

The annual average value for ^{210}Pb concentration obtained as 0.19 mBq m^{-3} (±0.06) and ^{7}Be concentration was measured to be 2.71 mBq m^{-3} (±0.66). The only measured concentrations for ^{210}Pb in UK was reported as 0.23 mBq m^{-3} (Peirson et al., 1966). ^{7}Be concentrations in surface air have not been reported for any part of the UK and therefore this study gives the only measured long term average value for ^{7}Be in UK.

• *Frequency distributions of ^{210}Pb and ^{7}Be concentrations:* The frequency distributions of ^{210}Pb and ^{7}Be were compared with widely known distributions. For ^{210}Pb the frequency distribution was a Lognormal Distribution fit with equation 3.1 and for ^{7}Be the distribution was a Normal (Gaussian) Distribution fit with equation 3.2, (section 3.1.1).

• *Meteorological effects on the concentrations of ^{210}Pb and ^{7}Be:* To determine the pressure, wind direction and the origin of air masses, meteorological surface pressure maps were used. The air mass back trajectories for 4 days were used to identify the source and air mass type. Precipitation events during this time or other meteorological changes to the air parcel were not considered. From the surface chart analyses the air masses were 22.2% from continental regions, 69.4% from oceanic regions and 8.4% from mixed continental and oceanic regions.

Larger concentrations of ^{210}Pb were associated with continental air masses and low concentrations of ^{210}Pb were associated with oceanic air masses (section 4.1.2).

The high pressure (anti-cyclonic) and low pressure (cyclonic) surface air pressure were extracted from pressure charts and plotted against ^{210}Pb concentration. When high pressure is over the sampling station ^{210}Pb concentration is larger and at low pressure the value of ^{210}Pb concentration is smaller (section 4.1.1).

There is a weak relationship between ^{7}Be concentrations and the type of air mass. The concentrations of ^{7}Be isotope was larger when high pressure was present. This is probably due to the fact that most of the time continental air masses are associated with high pressure, which is associated with sinking air that would bring more ^{7}Be isotopes to the surface.

In each measuring month the variations of ^{210}Pb and ^{7}Be could be considerable depending on the type of air mass and precipitation. There was a clear decline in concentrations of both ^{210}Pb and ^{7}Be in air as volume of precipitation during the sampling period increased.

• *Seasonal effects on the concentrations of ^{210}Pb and ^{7}Be:* The highest and lowest seasonal concentrations of ^{210}Pb are in September and January, respectively. Investigating the origin of the air masses at these two periods, we determined for the high concentration of ^{210}Pb (September), and the low concentrations of ^{210}Pb (January), the origin of the air masses from continents were 52 and 24% of the total, respectively. Therefore, air masses originated from continental regions are enriched with ^{210}Pb and have higher concentrations of ^{210}Pb isotopes compared with the oceanic originated air masses.

It is believed that at least four processes are important in causing the seasonal variations in ^{7}Be concentrations, (section 4.1.3). Each of the four processes has its own seasonal cycle, so that the seasonal cycle of surface concentration of ^{7}Be is some complicated product of the four processes. At different locations different processes may be dominant, and the seasonal cycle in ^{7}Be can have one or more maxima in any season or maxima in many combinations of seasons [Feely et al., 1988]. The seasonal high for ^{7}Be was determined in March for this study, which agrees with the prediction of other researchers [e.g. Feely et al., 1988; Brost et al., 1991; Tokieda et al., 1996], that the high concentrations of ^{7}Be occurs in early spring and some times late winter, depending on the meteorological conditions.

• *Comparing the atmospheric O_3 with ^{7}Be concentration:* The concentrations of atmospheric O_3 (ppb) was plotted against the concentrations ^{7}Be (mBq m^{-3}) in surface air (figure 4.1) and discussed in chapter 4, section 4.1.4. Summer time O_3 is said to be highly correlated with ^{7}Be in surface air [Prospero et al., 1995; Graustein and Turekian, 1996], as both of these isotopes are brought to the surface by troposphere-stratosphere exchange.

The high concentration of ^{7}Be for this study was measured in spring and the peak O_3 for this region is also in spring. There is a good correlation between these two isotopes in late spring and early summer (i.e. May, June and July). There was a low concentration of ^{7}Be in April. This was not expected at this time of the year. The main reason for this low concentration was due to meteorological effects, discussed in section 4.1.4.

5.2. Rainfall measurements.

• *Annual concentrations and fluxes of ^{210}Pb and ^{7}Be in rain:* The ^{210}Pb and ^{7}Be concentration in a sample representing a single precipitation event will clearly depend on a complex array of variables, including the history of the air mass and the particular characteristics of the storm (intensity, duration, height of cloud, etc.). It is therefore not surprising that ^{210}Pb and ^{7}Be concentrations in precipitation vary considerably. In 31 rainfall samples measured these concentrations range from 17.4 ± 2.3 to 326.2 ± 20.6 (mBq l^{-1}) for ^{210}Pb and from 265 ± 4 to 3311 ± 69 (mBq l^{-1}) for ^{7}Be. Generally light rain (or early fraction of heavier ones) tends to have higher concentration of ^{210}Pb and ^{7}Be than heavy rain (or bulk samples). A volume weighted average of ^{210}Pb and ^{7}Be concentration is the correct method of computing the annual deposition of ^{210}Pb and ^{7}Be (section 4.2.5).

The annual flux of ^{210}Pb for this study is 68 ±10 Bq m^{-2} y^{-1}, compared with the UK values reported in Table 4.7 ranging from 68 to 147 Bq m^{-2} y^{-1}. This is on the lower side of the range. Considering the meteorological effects on the concentrations of ^{210}Pb in rain for this region (discussed in sections 4.2.1), it was expected that the value for this region to be low.

The averaged annual flux of ^{7}Be for this study is 787 ±29 Bq m^{-2} y^{-1}, compared with the mean UK value of 818 ±44 Bq m^{-2} y^{-1} ranging from 774 to 863 Bq m^{-2} y^{-1} for ^{7}Be. This study's data are not included in calculating the mean UK value

which was calculated from table 4.8. Therefore our measured concentration for ^{7}Be is also in the lower side of this range.

• *Meteorological effects on the concentrations of ^{210}Pb and ^{7}Be:* Although the production source functions of these two nuclides are distinctly different, a relatively high correlation between the ^{210}Pb fluxes and the ^{7}Be fluxes has been observed in this study and different places (Baskaran, 1995). This high correlation appears to suggest that the atmospheric removal processes of ^{210}Pb and ^{7}Be are similar.

Considering the type of air masses passing our sampling station, when the origin of air masses are more continental the concentrations of ^{210}Pb is larger and when the air masses are less continental the ^{210}Pb concentrations are smaller (section 4.2.1). Although the origin of ^{210}Pb and ^{7}Be isotopes are different, figure 3.26 shows that a similar relationship for ^{7}Be concentration with respect to the air mass origin exist.

In presence of high pressure systems the concentrations of ^{7}Be were larger and normally high pressure and continental air are associated with each other. This agrees with the theory that when high pressure is present the air masses from the top of the atmosphere sink to the lower surfaces bringing more ^{7}Be enriched air. This shows the vertical transport of the air masses is very important for high concentrations of ^{7}Be in the atmosphere. There are other processes which could be important at the same time when the vertical transport is in progress, such as precipitation.

The concentrations of ^{210}Pb and ^{7}Be in each rain sample show the relationship of these isotopes with the amount of rainfall are exponential, as explained in section 4.2.1.

• *^{210}Pb and ^{7}Be seasonal variations:* Investigation of the atmospheric ^{210}Pb and ^{7}Be in many places around the globe indicate that there are seasonal variations of the deposition fluxes of these nuclides, in most places the high occurring in spring. For the measured period of November 1997 to January 1999 the highest values of concentrations for ^{210}Pb and ^{7}Be were in spring (May 1998) which agrees with the surface air sample results at this period. It has been shown that there are seasonal variations on the depositional fluxes of ^{210}Pb and ^{7}Be.

• *Estimate of dry deposition:* Turekian et al. (1977) have obtained the dry deposition contribution of ^{210}Pb to a known area of rain collectors from the respective Y-intercepts of the total (wet and dry) ^{210}Pb monthly flux versus

precipitation. As discussed in section 4.2.1 and 4.3.4.1 the measured dry deposition by researchers such as Turekian et al. (1977) and Todd et al. (1984) could not be considered as a useful measure of dry deposition as this value applies only to the collector used and is not the same as dry deposition to the landscape. The best estimate of the dry deposition is the method introduced in this study in section 4.3.2.1.

- *The washout scavenging ratio (W_s):* The washout scavenging ratios obtained from this study are 402 (±60) and 330 (±12) for ^{210}Pb and ^{7}Be, respectively (section 4.2.4). The washout scavenging ratio for ^{210}Pb has been reported as 400 (Knuth et al., 1983) and 500 (Junge, 1963a), which agrees well with our measured values. From the above values we could conclude that the removal processes of the ^{210}Pb and ^{7}Be aerosol carriers are similar.

5.3. Atmospherically derived inventories of ^{210}Pb and ^{137}Cs in soil.

- *^{210}Pb inventories in Rothamsted soils:* Under the reasonable assumption of steady state between the atmospheric supply of ^{210}Pb and its radioactive decay in soil, the mean flux to the open grassland is 117±4.3 Bq m^{-2} y^{-1}, 144±4.2 Bq m^{-2} y^{-1} for Geescroft canopy and 151±3.8 Bq m^{-2} y^{-1} Broadbalk canopy which fit in the upper side of the range of other reported values for UK soil inventories, ranging from 67 Bq m^{-2} y^{-1} to 187 Bq m^{-2} y^{-1}, (section 4.3.2). In the Rothamsted region more continental air masses may be present and the air masses may be enriched in ^{210}Pb, as discussed in section 4.1.2.

- *Distributions of ^{210}Pb and ^{137}Cs in top soils:* Both ^{210}Pb and ^{137}Cs are deposited from the atmosphere to the earth's surface and most of each nuclide is confined to the upper 10 cm of the Rothamsted soils. The experimental results for this study indicate that the distribution of ^{210}Pb and ^{137}Cs in top soils is approximately exponential for all of the core samples, (section 4.3.1). The depths of penetration of deposited radionuclides are quite variable, and strongly dependent on the soil density.

The depth profiles of ^{210}Pb in the soil samples generally show, that ^{210}Pb is efficiently immobilised in the surface horizons of soil; on average 88% (ranging from 78% to 96%) of the atmospheric inventory is concentrated in the top 10 cm.

^{137}Cs inventories follow a similar trend to that of atmospheric derived ^{210}Pb inventories, although significant levels of fall-out ^{137}Cs were found at depths of up to

20 cm. In most cases, the bulk of the inventory remained in the top 10 cm of soil. On average 78% (ranging from 55% to 96%) of the total measured inventories were detected in the top 10 cm. The depth profiles of ^{137}Cs in the soil samples for the same soil, generally show that ^{137}Cs is less efficiently immobilised in the surface horizons of soil compared to ^{210}Pb. In some cases there are indications of penetration of activity into deeper sections of the cores due to the mobility of ^{137}Cs radionuclide in these soils.

• *Dry deposition velocity (V_{dd}) for ^{210}Pb:* The results of calculations from this study (section 4.3.4.2) showed substantially larger dry deposition velocities (V_{dd}) in size range of ^{210}Pb carrier aerosols (sub-microns) than the wind tunnel prediction of dry deposition. The values of V_{dd} for this study were 4.6±0.6 mm s^{-1} for grassland, 8.3±0.6 mm s^{-1} for Geescroft woodland and 9.4±0.5 mm s^{-1} for Broadbalk woodland. These values are an order of magnitude larger than the wind tunnel results, which imply that the wind tunnel measurements do not assume the full range of processes occurring in the field. Furthermore, the measurements from this study show that V_{dd} can be measured directly by determinig the soil inventory, rain flux and air concentration of the isotope.

• *Atmospheric derived ^{210}Pb inventory to the canopies:* The atmospherically derived ^{210}Pb inventory into the canopies exceed those in adjacent open areas indicating that forest sites receive more atmospheric inputs. The mean ^{210}Pb inventories are 3753 ±139 Bq m^{-2} for open grassland, 4607 ±135 Bq m^{-2} for Geescroft canopy and 4844 ±124 Bq m^{-2} for Broadbalk canopy.

The average excess inventories to the canopies compared to the grassland for ^{210}Pb were about 23% and 29% for Geescroft and Broadbalk canopies, respectively, (section 4.3.6). Assuming that the precipitation input is the same for all the sites, the increase may therefore be assumed to result from aerosol capture by the trees in excess of that by the grassland. The ^{210}Pb inventories in different cores from the same catchment were relatively uniform; the standard deviations of measurements were around 20% for open grassland, 22% for Geescroft canopy, and 14%, for Broadbalk canopy.

• *Atmospheric derived ^{137}Cs inventories to the canopies:* The atmospherically derived ^{137}Cs inventories into the forests exceed those in adjacent open areas, indicating that forest sites receive more atmospheric inputs. The averaged increase in under canopy inventories was about 49% for Geescroft and 54% for Broadbalk

relative to the open grassfield. The average values of these inventories are 1246 ±115 Bq m^{-2} for open grassland, 1856 ±119 Bq m^{-2} for Geescroft forest and 1920 ±164 Bq m^{-2} for Broadbalk forest.

^{137}Cs compared to ^{210}Pb is more mobilised in soils and could migrate through the soil depth when it is exposed to acid rain. It would therefore penetrate deeper than ^{210}Pb. Hence, its inventory to forest gives a larger difference to the open grassland (see section 1.8). We assumed that the same amount of rain is deposited to the grassland area and the canopies, but because of the larger surface area of the trees and the fact that some of the rain to the trees will evaporate, less rain will reach the soil under the trees. Since less rain reaches the soils, ^{137}Cs migration is slower in the canopy soils compared to the grassland and therefore the excess inventories of ^{137}Cs into the canopy soils are larger than those of ^{210}Pb for the same core.

- *^{210}Pb and ^{137}Cs depositions to the edge of the forest:* The investigations from this study show at the edge of the forests the atmospheric derived inventories of ^{210}Pb and ^{137}Cs are larger than that to the rest of the forest. This could be due to the interception of the aerosols by the trees. Comparing the input of atmospherically derived aerosols to Geescroft and Broadbalk forests, we could conclude that although these two forests areas are not far from each other and have the same altitude, the inventories for Broadbalk forest are larger than those for Geescroft forest and this could be due the fact that Broadbalk forest is acting as an edge, because of its small width.

Appendix (A) :

The table of results for the surface air samples is presented in this section. Table 3.1 has 10 column which are as follow:

Column 1 is the file name identifying each filter.

Column 2 is the sampling date and shows the starting and finishing date of sampling.

Column 3 is the exact duration of sampling in hours recorded from the meter mounted on the sampler.

Column 4 is the flow rate of air sucked through each filter, (calculation procedures were described in section 2.1).

Column 5 is the total volume of the air through each filter for the duration shown in column 3.

Columns 6 and 7 are the concentrations of ^{210}Pb and one-sigma counting statistical error (mBq m^{-3}) in air, respectively.

Columns 8 and 9 are the concentrations of ^{7}Be and one-sigma counting statistical error (mBq m^{-3}) in air, respectively. The calculation methods used to calculate these concentrations were described in chapter 2 and 3.

Column 10 is the amount of rain (mm) for each of the sampling times reported by the Turnhouse weather station at the Edinburgh airport, which is the nearest meteorological whether centre to our sampling site.

Table 3.1. The complete data of the air samples collected from December 1996 to January 1999. The errors are the counting statistical errors (±σ). The rain data are from the meteorological weather centre , Turnhouse (Edinburgh Airport).

File name	Date of sampling	Sampling time (hours)	Flow rate (m^3 min^{-1})	Volume of air through the filters (m^3)	Concentrations of ^{210}Pb (mBq m^{-3})	Error in ^{210}Pb (mBq m^{-3})	Concentrations of ^{7}Be (mBq m^{-3})	Error in ^{7}Be (mBq m^{-3})	mm of rain
AIR001	4/12/ TO 5/12/96	24	2.53	3600	0.028	0.008	0.782	0.058	0.2
AIR002	9/12/ TO 11/12/96	48.09	2.53	7214	0.338	0.017	2.19	0.052	2.1
AIR003	11/12/ TO 13/12/96	48.23	2.53	7235	0.218	0.013	1.92	0.049	0.3
AIR004	13/12/ TO 14/12/96	24	2.53	3600	0.231	0.02	6.81	0.128	0
AIR005	16/12/ TO 17/12/96	24	2.53	3600	0.118	0.015	2	0.076	9.6
AIR006	17/12/ TO 19/12/96	48	2.53	7200	0.582	0.02	4.84	0.072	23.6
AIR007	10/1/ TO 16/1/97	145	2.53	21750	0.155	0.006	1.15	0.019	3.6
AIR008	20/2/ TO 26/2/97	124	2.53	11308	0.066	0.003	2.15	0.017	26.9
AIR009	19/3/ TO 28/3/97	212.7	2.53	31905	0.063	0.002	1.64	0.005	11.3
AIR010	28/3/ TO 7/4/97	239.66	2.53	36430	0.093	0.005	1.5	0.016	6.6
AIR011	7/4/ TO 17/4/97	240.68	2.53	36585	0.21	0.003	3.06	0.014	0
AIR012	17/4/ TO 28/4/97	270	2.53	41042	0.238	0.005	2.26	0.02	11.6
AIR013	9/5/ TO 16/5/97	163.27	2.53	24818	0.096	0.003	1.37	0.012	33.1
AIR014	16/5/ TO 23/5/97	169.69	2.53	25794	0.104	0.003	1.48	0.014	22
AIR015	31/5/ TO 7/6/97	175.52	2.53	26680	0.191	0.004	2.89	0.019	7.5
AIR016	7/6/ TO 14/6/97	178	2.53	27057	0.119	0.004	2.03	0.016	54
AIR017	16/6/ TO 23/6/97	166.23	1.65	16424	0.142	0.005	2.82	0.024	35
AIR018	23/6/ TO 30/6/97	169	1.65	16698	0.13	0.005	2.73	0.023	8.1
AIR019	30/6/ TO 7/7/97	167.17	1.65	16517	0.134	0.004	2.46	0.019	33.8
AIR020	7/7/ TO 11/7/97	95	1.65	10504	0.165	0.005	2.58	0.023	0
AIR021	11/7/ TO 17/7/97	141.16	2.79	23603	0.117	0.002	2.12	0.011	4.1
AIR022	17/7/ TO 28/7 97	258.26	1.14	17665	0.312	0.005	4.19	0.021	19.2

Table 3.1 continued from page 154:

AIR023	28/7/ TO 1/8/97	101.2	1.14	6922	0.127	0.006	2.97	0.027	6.7
AIR024	1/8/ TO 7/8/97	143.08	1.14	9787	0.206	0.006	2.99	0.023	0
AIR025	8/8/TO 15/8/97	171.45	1.14	11728	0.43	0.008	4.27	0.028	11.7
AIR026	15/8/ TO 20/8/97	117.91	1.14	8065	0.619	0.016	4.69	0.045	2.8
AIR027	20/8/ TO 26/8/97	142.99	0.89	7607	0.215	0.011	2.91	0.036	2.6
AIR028	26/8/ TO29/8/97	73.28	0.89	3899	0.101	0.01	2.76	0.068	7.1
AIR029	29/8/ TO 3/9/97	122.97	0.89	6542	0.077	0.006	1.83	0.032	10.3
AIR030	3/9/ TO 8/9/97	120.52	0.89	6412	0.133	0.009	2.96	0.042	1.3
AIR031	8/9/ TO 12/9/97	69.96	1.65	6912	0.25	0.012	4.54	0.046	1.2
AIR032	12/9/ TO 17/9/97	122.16	1.65	12069	0.082	0.005	1.73	0.022	21.6
AIR033	17/9/ TO 22/9/97	119.05	2.28	16286	0.16	0.009	2.26	0.024	0
AIR034	22/9/ TO 29/9/97	167.87	2.28	22965	0.52	0.006	3.88	0.023	0.2
AIR035	29/9/ TO 4/10/97	118.53	2.28	16215	0.284	0.006	4.39	0.029	0
AIR036	6/10/ TO 13/10/97	168.69	2.28	23077	0.086	0.003	1.86	0.016	27.9
AIR037	20/10/ TO 24/10/97	79.5	1.52	7250	0.136	0.009	3.36	0.047	0
AIR038	24/10/ TO 28/10/97	99.28	1.52	9054	0.218	0.009	2.66	0.036	0
AIR039	28/10/ TO 5/11/97	190.44	1.01	11579	0.124	0.008	1.65	0.03	1.9
AIR040	5/11/ TO 12/11/97	172.77	1.01	10504	0.136	0.008	1.24	0.028	25.4
AIR041	12/11/TO 21/11/97	213	0.76	9713	0.126	0.009	3	0.045	7.1
AIR042	21/11/ TO 28/11/97	166.87	0.76	7609	0.359	0.015	1.76	0.041	9.1
AIR043	28/11/ TO 5/12/97	169.36	1.52	15446	0.208	0.008	3.09	0.054	17.2
AIR044	5/12/ TO 12/12/97	166.44	1.52	15179	0.141	0.008	2.43	0.032	48.5
AIR045	12/12/ TO 18/12/97	144.54	1.52	13182	0.347	0.012	4.64	0.048	1.7
AIR046	18/12/ TO 23/12/97	116.27	1.52	10604	0.238	0.014	1.31	0.033	27.8
AIR047	23/12/ TO 31/12/97	190.64	1.52	17386	0.097	0.006	1.94	0.027	22.4
AIR048	31/12/ TO 7/1/98	166.83	1.52	15215	0.058	0.006	3.09	0.035	33.6
AIR049	7/1/ TO 14/1/98	168.45	1.52	15363	0.246	0.009	3.49	0.038	27.9

Table 3.1 continued from page 155:

AIR050	14/1/ TO 21/1/98	172.92	1.52	15770	0.11	0.007	2.46	0.029	23.4
AIR051	21/1/ TO 30/1/98	57.62	1.52	5255	0.197	0.013	3.63	0.054	13
AIR052	30/1/ TO 5/2/98	145.65	1.52	13283	0.153	0.008	2.27	0.031	1.5
AIR053	5/2/ TO 10/2/98	118.01	1.52	10763	0.11	0.006	2.82	0.028	17.8
AIR054	10/2/ TO 16/2/ 98	96.28	1.52	8781	0.522	0.021	3.72	0.061	8.5
AIR055	16/2/ TO 23/2/98	163.65	1.52	14925	0.138	0.006	2.21	0.027	3.2
AIR056	23/2/ TO 2/3/98	167.4	1.52	15267	0.108	0.005	3.8	0.029	21.2
AIR057	2/3/ TO 6/3/98	96.96	1.52	8843	0.079	0.006	3.41	0.031	10.4
AIR058	6/3/ TO 13/3/98	168.22	1.52	15342	0.131	0.007	3.03	0.03	10.9
AIR059	13/3/ TO 20/3/98	168.48	1.52	15365	0.229	0.011	4.25	0.044	0
AIR060	20/3/ TO 26/3/98	127.3	1.52	11610	0.259	0.014	5.48	0.055	7.5
AIR061	26/3/ TO 31/3/98	118.71	1.52	10826	0.347	0.016	4.38	0.053	9.7
AIR062	31/3 TO 6/4/98	145.2	1.52	13242	0.1	0.006	1.68	0.022	52.4
AIR063	6/4/ TO 12/4/98	137.16	1.52	12509	0.159	0.007	2.62	0.027	11.7
AIR064	12/4/ TO 18/4/98	143.93	1.52	13126	0.158	0.007	3.67	0.031	8.6
AIR065	18/4/ TO 24/4/98	145.64	1.52	13282	0.216	0.011	2.3	0.034	11.3
AIR066	25/4/ TO 1/5/98	140.2	1.52	12786	0.146	0.007	2.73	0.036	10.1
AIR067	1/5/ TO 8/5/98	171.11	1.52	15605	0.163	0.005	3.42	0.025	28.2
AIR068	8/5/ TO 15/5/98	165	1.52	15048	0.244	0.007	3.29	0.028	5.9
AIR069	15/5 TO 22/5/98	171.06	1.52	15601	0.34	0.011	4.62	0.037	2.9
AIR070	22/5 TO 27/5/98	117.89	1.52	10752	0.204	0.007	3.16	0.041	5.8
AIR071	27/5/ TO 31/5/98	102.11	1.52	9312	0.198	0.009	3.11	0.034	41.3
AIR072	31/5/ TO 6/6/98	137.31	1.52	12523	0.181	0.007	3.67	0.027	12.5
AIR073	6/6/ TO 12/6/98	145.67	1.52	13285	0.084	0.005	1.22	0.016	25.1
AIR074	12/6/ TO 19/6/98	161.91	1.52	14766	0.187	0.01	3.15	0.036	19.4
AIR075	19/6/ TO 25/6/98	139.68	1.52	12739	0.273	0.011	3.64	0.042	5.7
AIR076	25/6/ TO 1/7/98	142.7	1.52	13014	0.098	0.006	1.4	0.024	14.7

Table 3.1 continued from page 156:

AIR077	1/7/ TO 9/7/98	184.73	1.52	16847	0.141	0.006	1.8	0.025	3.4
AIR078	9/7/ TO 16/7/98	169.06	1.52	15418	0.153	0.008	2.33	0.036	40.5
AIR079	16/7/ TO 24/7/98	168.89	1.52	15403	0.079	0.005	1.46	0.024	35.8
AIR080	24/7/ TO 31/7/98	167.89	1.52	15312	0.092	0.005	1.08	0.02	20.5
AIR081	31/7/ TO 7/8/98	172.31	1.52	15715	0.14	0.005	1.9	0.021	23.8
AIR082	7/8/ TO 14/8/98	165.86	1.52	15126	0.183	0.01	2.67	0.041	1.2
AIR083	14/8/ TO 28/8/98	338.86	1.52	20586	0.115	0.006	2.39	0.029	24.4
AIR084	28/8/ TO 4/9/98	166.86	1.52	15217	0.221	0.01	2.17	0.033	16.5
AIR085	4/9/ TO 11/9/98	166.73	1.52	15206	0.182	0.006	1.62	0.021	10.8
AIR086	11/9/ TO 17/9/98	143.81	1.52	13115	0.089	0.006	2.2	0.025	8.2
AIR087	17/9/ TO 24/9/98	168	1.52	15321	0.275	0.009	2.67	0.034	0
AIR088	24/9/ TO 1/10/98	170.66	1.52	15564	0.591	0.014	3.38	0.043	17.7
AIR089	5/11/ TO 12/11/98	162.42	1.52	14812	0.124	0.006	3.01	0.026	4.9
AIR090	12/11/ TO 19/11/98	165.46	1.52	15090	0.121	0.007	1.86	0.027	14.9
AIR091	19/11/ TO 25/11/98	146.91	1.52	13398	0.184	0.007	2.23	0.026	13.2
AIR092	25/11/ TO 30/11/98	121.78	1.52	11106	0.174	0.007	2.3	0.023	7.7
AIR093	30/11/ TO 4/12/98	94.07	1.52	8579	0.124	0.007	2.87	0.031	0.6
AIR094	4/12/ TO 11/12/98	115.23	1.52	10509	0.128	0.007	3.09	0.032	2.5
AIR095	11/12/ TO 18/12/98	171.47	1.52	15638	0.151	0.008	3.14	0.04	12
AIR096	18/12/ TO 25/12/98	164.18	1.52	14973	0.081	0.004	2.31	0.02	6.6
AIR097	25/12/ TO 1/1/99	170.54	1.52	15553	0.112	0.005	2.37	0.023	27.2
AIR098	1/1/ TO 7/1/99	139.72	1.52	12742	0.055	0.004	2.28	0.021	33
AIR099	7/1/ TO 25/1/99	438.1	1.52	39955	0.089	0.003	2.05	0.013	59.6
AIR100	25/1/ TO 1/2/99	169.87	1.52	15494	0.094	0.005	1.53	0.016	2

Appendix B:

The complete data set for rain samples is reported in table 3.2 and presented in this section. Table 3.2 consists of 12 column which are explained as follows:

Column 1 is the file name identifying each period of sampling.

Column 2 is the duration of each sampling period and shows the starting and finishing date of sampling. Sampling was started and terminated at about noon of each date.

Columns 3 and 4 are the amount of precipitation (mainly rainfall) in, mm and litres of rain, respectively, measured at the sampling site using a standard rain gauge.

Columns 5 and 6 are the calculated concentrations of ^{7}Be in rain and the counting statistical one-sigma ($\pm\sigma$) error (mBq l^{-1}), respectively.

Columns 7 and 8 are the calculated concentrations of ^{210}Pb in rain and the counting statistical one-sigma ($\pm\sigma$) error (mBq l^{-1}), respectively.

Columns 9 and 10 are the calculated flux (mBq cm^{-2}) of ^{7}Be in collected rain and the counting statistical one-sigma ($\pm\sigma$) error, respectively.

Columns 11 and 12 are the calculated flux (mBq cm^{-2}) of ^{210}Pb in rain and the counting statistical one-sigma ($\pm\sigma$) error, respectively.

Table 3.2. The complete data of the rain samples collected from 24th of October 1997 to 31st of January 1999. The error for ^{210}Pb and ^{7}Be are the measured counting statistical one-sigma error (±σ). The rain data were measured at the sampling site using a standard funnel of 15 cm in diameters.

Sample	Duration of sampling	Rain	Rain	^{7}Be	Error	^{210}Pb	Error	^{210}Pb	Error in ^{210}Pb	^{7}Be	Error in ^{7}Be
		(mm)	(litre)	(mBq l^{-1})	(mBq l^{-1})	(mBq l^{-1})	(mBq l^{-1})	(mBq cm^{-2})	(mBq cm^{-2})	(mBq cm^{-2})	(mBq cm^{-2})
Rain01	24/10 to 05/11/97	11.9	6.5	1407	60	62.3	6.2	0.074	0.007	1.68	0.071
Rain02	05/11 to 09/11/97	18.4	10	947	29	73.5	7.6	0.135	0.014	1.73	0.053
Rain03	17/11 to 01/12/97	20.6	11.5	787	25	43.3	4.8	0.091	0.01	1.66	0.052
Rain04	01/12 to 12/12/97	45.1	24.6	158	8	17.4	2.3	0.078	0.01	0.71	0.036
Rain05	12/12 to 22/12/97	27.6	15.65	674	19	130.8	6.6	0.361	0.019	1.86	0.053
Rain06	22/12 to 27/12/97	25.7	13.2	988	23	26.9	4.2	0.069	0.011	2.54	0.06
Rain07	27/12 to 05/01/98	36	18.65	1253	21	219.4	29	0.079	0.01	4.51	0.074
Rain08	05/01 to 14/01/98	24.5	11.3	918	16	73.1	4.5	0.179	0.011	2.25	0.04
Rain09	14/01 to 20/01/98	23.7	12.1	409	13	55.3	4.3	0.131	0.008	0.97	0.03
Rain10	20/01 to 26/01/98	23.1	11.85	649	14	61.5	3.6	0.142	0.008	1.5	0.033
Rain11	06/02 to 12/02/98	7	3.4	843	36	187.2	23.8	0.131	0.017	0.59	0.025
Rain12	26/02 to 02/03/98	13.4	5.85	121	2	129.1	7.4	0.173	0.01	3.9	0.05
Rain13	02/03 to 09/03/98	10.6	4.4	1208	33	104.7	9.7	0.111	0.01	1.28	0.035
Rain14	09/03 to 11/03/98	11.4	5.63	798	22	103.5	8	0.118	0.009	0.91	0.026
Rain15	25/03 to 27/03/98	4.9	2.1	2816	59	159.2	12.4	0.078	0.006	1.38	0.029
Rain16	27/03 to 31/3/98	5.3	1.97	3311	69	326.2	20.6	0.173	0.011	1.76	0.037
Rain17	31/03 to 08/04/98	52	26.2	613	9	44.1	2.6	0.229	0.013	3.19	0.049
Rain18	08/04 to 19/04/98	11.3	4.1	1998	33	108.1	6.7	0.122	0.008	2.26	0.038
Rain19	19/04 to 26/04/98	17.82	6.9	935	16	76.6	4.8	0.136	0.009	1.67	0.028
Rain20	26/04 to 30/04/98	10.3	3.75	1570	32	109.7	7.7	0.113	0.008	1.62	0.033

Table 3.2 continued from page 159:

Rain21	01/05 to 31/05/98	72.5	27.15	1934	18	140.7	3.9	1.02	0.028	14.02	0.128
Rain22	31/05 to 07/06/98	18.7	7.37	1713	23	111.8	5.9	0.209	0.011	3.2	0.043
Rain23	07/06 to 12/06/98	29.7	14.05	376	9	32.5	2.3	0.096	0.007	1.12	0.026
Rain24	12/06 to 30/06/98	43.4	9.25	1159	18	72.6	3.6	0.315	0.016	5.03	0.077
Rain25	30/06 to 03/08/98	108.3	37.5	576	7	36.2	1.6	0.392	0.017	6.24	0.079
Rain26	03/08 to 02/09/98	59	15.2	651	9	38.5	2.1	0.227	0.012	3.84	0.053
Rain27	02/09 to 01/10/98	45.5	14.6	688	10	58.6	2.9	0.267	0.013	3.13	0.046
Rain28	01/10 to 31/10/98	95.9	41.25	458	6	33.2	1.5	0.318	0.015	4.3	0.062
Rain29	31/10 to 30/11/98	71.5	32.25	336	6	23.6	1.6	0.169	0.012	2.4	0.045
Rain30	30/11 to 31/12/98	46.6	19.25	347	7	18.9	1.6	0.088	0.007	1.62	0.033
Rain31	31/12 to 01/02/99	93.6	37.25	265	4	18	0.8	0.169	0.007	2.48	0.04

Appendix C:

The complete table of data and the results of the soil samples are reported in this section in tables 3.3_a, 3.3_b and 3.4. Table 3.3a consists of 11 column which are described as follows:

Column 1 is the file name to identify each of the sub-divisions of the soil. These start with "R" followed by a number, which is the site number, then two alphabetical symbols. The capital character identifies the core and the small one shows the sub-division in each core.

Columns 2 and 3 are the corrected gamma counts per second for ^{210}Pb and the percentages of one-sigma counting statistical measuring error, respectively.

Columns 4 and 5 are the corrected gamma counts per second for ^{214}Pb and the percentages of one-sigma counting statistical measuring error, respectively.

Columns 6 and 7 are the corrected gamma counts per second for ^{137}Cs and the percentages of one-sigma counting statistical measuring error, respectively. The details of correction method has been fully described in chapter 2.

Columns 8, 9, 10 and 11 are the calculated activity (Bq) for total ^{210}Pb (atmospheric and in-situ), ^{214}Pb, atmospheric ^{210}Pb and ^{137}Cs, respectively, in each sample holder.

Table 3.3_b consists of 8 columns which show the complete calculation, made from the results of table 3.3_a and is described as follow:

Column 1 has the same definition as the column 1 in table 3.3_a.

Columns 2 and 3 are the weight corrected activity (Bq) of atmospherically derived ^{210}Pb and ^{137}Cs, respectively, as explained in the chapter 2.

Columns 4 and 5 are the specific activity (Bq kg^{-1}) of ^{210}Pb and ^{137}Cs, respectively, achieved by dividing the total activity by the total dry weight in each sub-division.

Columns 6 and 7 are the total inventory (Bq m^{-2}) of each sub-division for ^{210}Pb and ^{137}Cs, respectively, calculated using the total activities for each sub-sample divided by the surface area of 10.2 cm corer.

Column 8 is the corrected time decay to the 2nd of February 1998 of the total inventory of ^{210}Pb (listed in column 7) for each sub-division.

Table 3.4 is the complete ^{210}Pb specific activity (Bq kg^{-1}) and inventories (Bq m^{-2}) together with the errors for each sub-sample and the density of each sub-sample consisting of 7 columns which are described as follow:

Column 1 is the same as described in table 3.3a and also includes the depth of each soil in cm.

Column 2 is the density (g cm^{-3}) of the dry soil for each sub-sample which varies from 402 to 1303 g cm^{-3}.

Columns 3 and 4 are the final value for the inventory of atmospherically derived ^{210}Pb (Bq m^{-2}) and its one-sigma counting errors, respectively, detected in each sub-division of the soil.

Columns 5 and 6 are the final values for the flux of atmospherically derived ^{210}Pb (Bq kg^{-1}) and its one-sigma counting statistical measuring errors, respectively, detected in each sub-division of the soil.

Column 7 is the one-sigma counting statistical measuring percentage errors for ^{210}Pb and it varies with the activity of each sample.

Table 3.3_a. The complete data of the soil samples collected on 2nd of February 1998 from the Rothamsted experimental farms to measure the atmospheric inventories of ^{210}Pb and ^{137}Cs. The errors are the statistical counting errors ($\pm\sigma$).

File name (core section)	Gamma counts per sec. x 10^{-3} (corrected for attenuation, capture and background) ^{210}Pb	% Error for ^{210}Pb ($\pm\sigma$)	Gamma counts per sec. x 10^{-3} (corrected for attenuation, capture and background) ^{214}Pb	% Error for ^{214}Pb ($\pm\sigma$)	Gamma counts per sec. x 10^{-3} (corrected for attenuation and capture) ^{137}Cs	% Error for ^{137}Cs ($\pm\sigma$)	Total activity of ^{210}Pb for holder (Bq)	Total activity of ^{214}Pb for holder (Bq)	Total atmospheric deposition for ^{210}Pb in holder (Bq)	Total atmospheric deposition for ^{137}Cs for holder (Bq)
R1Aa	15.66	5.47	13.72	3.66	10.16	4.27	6.48	1.83	4.65	1.2
R1Ab	17.5	6.07	24.06	2.81	14.66	3.52	7.24	3.21	4.03	1.73
R1Ac	17.11	4.07	46.33	1.47	3.86	5.3	7.08	6.18	1.25	0.46
R1Ba	22.57	3.67	16.13	2.24	12.47	2.55	9.33	2.15	7.18	1.47
R1Bb	18.18	5.32	29.36	1.73	17.69	2.2	7.52	3.92	3.6	2.09
R1Bc	16.22	7.68	37.7	2.39	5.24	6.82	6.71	5.03	1.68	0.62
R1Ca	21.87	5.24	15.04	3.4	11.4	3.96	9.05	2.01	7.04	1.4
R1Cb	20.22	4.96	29.17	2.51	17.11	3.12	8.36	3.89	4.47	2.02
R1Cc	16.94	4.77	43.45	1.76	11.34	2.93	7.01	5.8	1.21	1.34
R1Da	25.99	4.77	22.45	2.67	12.69	3.56	10.75	3	7.75	1.5
R1Db	19.12	6.81	33	2.4	15.02	3.39	7.91	4.4	3.51	1.77
R1Dc	15.15	8.75	42.39	2.35	6.1	5.97	6.27	5.66	0.61	0.72
R1Ea	21.44	4.3	16.08	2.95	10	3.86	8.87	2.15	6.72	1.18
R1Eb	19.35	5.89	27.68	2.72	13.74	3.84	8	3.69	4.31	1.62
R1Ec	12.86	11.74	37.04	2.42	6.88	5.98	5.32	4.94	0.38	0.81
R2Aa	16.67	6	11.92	4.01	8.89	4.8	6.89	1.59	5.3	1.05
R2Ab	16.62	6.19	23.4	2.69	13.54	3.48	6.87	3.12	3.75	1.6
R2Ac	15.61	6.57	37.21	2.3	9.94	4.03	6.45	4.97	1.48	1.17
R2Ba	17.73	5.48	12.26	3.56	10.35	3.97	7.33	1.64	5.69	1.22
R2Bb	17.01	6.49	24.25	2.66	13.56	3.59	7.04	3.24	3.8	1.6
R2Bc	13.4	8.06	32.77	2.51	9.32	4.3	5.54	4.37	1.17	1.1
R2Ca	16.67	5.76	11.28	3.89	10.69	4.05	6.89	1.51	5.38	1.26
R2Cb	18.41	7.23	25.31	2.6	14.36	3.51	7.61	3.38	4.23	1.7

Table 3.3_a continued from page 163 :

R2Cc	16.76	6.95	34.43	2.49	12.87	4.05	6.93	4.59	2.34	1.52
R2Da	18.47	4.68	13.58	3.58	10.05	4.14	7.64	1.81	5.83	1.19
R2Db	16.01	6.19	24.66	2.57	16.31	3.15	6.62	3.29	3.33	1.93
R2Dc	13.83	4.48	31.96	1.58	7.76	3.16	5.72	4.26	1.46	0.92
R2Ea	19.27	5.29	11.28	3.79	10.69	4.5	7.97	1.83	6.14	1.1
R2Eb	15.41	6.62	25.31	2.53	14.36	3.71	6.37	3.49	2.88	1.51
R2Ec	12.9	5.77	37.03	1.84	12.87	3.39	5.34	4.09	1.25	1.12
R3Aa	23.13	4.47	11.88	3.44	18.91	2.57	9.57	1.59	7.98	2.23
R3Ab	24.39	6.48	27.13	2.53	27.69	2.32	10.09	3.62	6.47	3.27
R3Ac	13	8.77	33.75	2.41	14.56	3.49	5.38	4.5	0.88	1.72
R3Ba	24.73	5.15	17.75	3.08	23.72	2.55	10.23	2.34	7.89	2.8
R3Bb	19.46	5.89	27.68	2.57	22.46	2.68	8.05	3.69	4.36	2.65
R3Bc	15.4	4.34	36.45	1.44	9.14	2.92	6.37	4.89	1.51	1.08
R3Ca	26.73	5.22	17.43	3.28	23.07	2.71	11.06	2.33	8.73	2.72
R3Cb	19.96	6.41	28.25	2.72	25.02	2.62	8.26	3.77	4.49	2.95
R3Cc	16.1	6.82	37.88	2.18	8.3	4.74	6.66	5.05	1.61	0.98
R3Da	25.67	6.42	23	2.68	29.81	2.59	10.62	2.94	7.68	3.52
R3Db	17.54	7.54	30.8	2.51	12.09	4.06	7.32	4.69	2.63	1.43
R3Dc	15.05	7.9	40.79	2.15	4.2	7.87	6.23	5.44	0.79	0.5
R3Ea	29.67	5.36	19.82	3.43	27.59	2.45	12.27	2.64	9.63	3.26
R3Eb	19.77	6.83	33.32	2.32	14.77	3.54	8.18	4.37	3.81	1.74
R3Ec	15.89	7.72	43.84	2.16	3.01	9.42	6.57	5.85	0.72	0.36
R4Aa	21.4	4.4	11.05	3.88	25.69	2.38	8.85	1.47	7.38	3.03
R4Ab	20.84	5.95	25.68	2.38	17.8	2.82	8.62	3.43	5.19	2.1
R4Ac	15.83	7.42	36.14	1.82	5.89	4.75	6.55	4.82	1.73	0.7
R4Ba	24.53	3.75	10.88	3.89	24.12	2.43	10.15	1.45	8.7	2.85
R4Bb	24.47	6.05	25.86	2.7	26.97	2.46	10.12	3.45	6.67	3.19
R4Bc	15.18	7.86	35.06	2.56	11.65	4.38	6.28	4.68	1.6	1.38
R4Ca	27.63	4.7	17.51	2.96	38.97	1.88	11.43	2.34	9.09	4.6
R4Cb	22.46	6.82	28.19	2.42	15.74	3.09	9.29	3.8	5.49	1.86
R4Cc	18.47	6.05	35.1	1.75	7.76	3.76	7.64	4.72	2.92	0.92
R4Da	22.17	4.82	15.8	2.94	24.46	1.9	9.17	2.11	7.06	2.89

Table 3.3_a continued from page 164 :

R4Db	16.79	6.19	31.15	2.32	16.49	2.78	6.94	4.16	2.78	1.94
R4Dc	16.89	5.19	44.68	1.68	4.17	4.04	6.99	5.96	1.03	0.49
R4Ea	26.69	3.96	12.04	3.72	20.75	2.71	11.04	1.61	9.43	2.45
R4Eb	23.45	5.42	31.56	2.38	18.39	3.48	9.7	4.21	5.49	2.17
R4Ec	15.54	6.5	35.2	2.27	7	5.32	6.43	4.7	1.73	0.83
R5Aa	22.81	4.66	12.86	3.62	19.99	2.71	9.43	1.72	7.71	2.36
R5Ab	17.67	4.26	26.14	1.82	25.42	1.74	7.31	3.49	3.82	3
R5Ac	17.81	6.73	41.31	2.15	6.83	5.6	7.36	5.49	1.87	0.81
R5Ba	20.36	5.25	14.92	3.59	22.66	2.56	8.42	1.99	6.43	2.68
R5Bb	21.38	6.93	32.7	2.25	11.56	3.82	8.84	4.36	4.48	1.37
R5Bc	16.88	4.95	40.69	1.53	1.78	10.08	6.98	5.43	1.55	0.21
R5Ca	20.19	4.2	10.29	4.7	17.33	3.33	8.35	1.37	6.98	3.1
R5Cb	20.72	5.16	27.87	2.54	27.72	2.4	7.95	3.72	4.33	3.27
R5Cc	15.23	7.45	42.97	2.21	2.34	12.1	6.3	5.73	0.57	0.28
R5Da	21.98	4.54	9.42	4.33	26.57	2.38	9.09	1.26	7.83	3.14
R5Db	18.86	5.59	29.39	2.49	15.89	3.29	7.8	3.96	3.88	1.88
R5Dc	14.99	6.96	41.57	2.77	3.24	9.48	6.2	5.55	0.65	0.38
R5Ea	20.61	3.57	3.94	7.1	21.96	2.87	8.52	0.53	7.99	2.59
R5Eb	19.94	4.22	16.69	3.54	25.91	1.53	8.25	2.66	5.59	3.06
R5Ec	13.3	6.47	34.62	2.3	5.39	2.1	5.5	4.62	0.88	0.64
R6Aa	22.78	3.6	14.15	3.6	28.82	1.57	9.42	1.89	7.53	3.4
R6Ab	25.83	5.92	28.88	2.47	9.72	4.4	10.68	3.85	6.83	1.15
R6Ac	17.21	6.52	42.87	2.18	3.52	8.77	7.12	5.72	1.4	0.42
R6Ba	25.83	4.48	14.49	3.33	34.5	2.07	10.68	1.93	8.75	4.07
R6Bb	19.6	8.29	29.24	2.5	15.38	3.4	8.11	3.9	4.2	1.82
R6Bc	15.31	8.05	41	2.41	2.02	12.83	6.33	5.47	0.86	0.24
R6Ca	22.5	4.39	15.14	3.18	22.69	2.53	9.31	2.02	7.29	2.68
R6Cb	19.9	6.22	30.44	2.48	17.92	3.12	8.23	4.06	4.17	2.12
R6Cc	17.71	9.56	40.57	2.08	2.75	10.02	7.32	5.41	1.91	0.32
R6Da	24.66	4.76	16.4	3.04	31.42	2.11	10.2	2.19	8.01	3.71
R6Db	20.93	5.84	27.41	2.44	12.51	3.67	8.66	3.66	5	1.48
R6Dc	16.71	6.41	37.58	2.13	3.19	8.65	6.91	5.01	1.9	0.38

Table 3.3_a continued from page 165 :

R6Ea	26.87	4.17	15.29	3.55	26.09	2.63	11.12	2.04	9.08	3.08
R6Eb	19.75	6.2	29.52	2.49	14.28	3.59	8.17	3.94	4.23	1.69
R6Ec	17.58	4.45	46.19	1.58	3.4	6.7	7.27	6.16	1.11	0.4
R7Aa	23.87	6.1	13.11	3.66	11.1	3.72	10.71	1.75	8.96	1.31
R7Ab	23.42	6.75	23.59	2.83	12.01	3.74	9.69	3.15	6.54	1.42
R7Ac	13.99	6.81	31.32	2.46	11.84	3.78	5.78	4.18	1.60	1.4
R7Ba	23.9	5.62	16.82	3.27	12.24	3.79	9.88	2.24	7.64	1.45
R7Bb	18.41	7.75	22.6	2.92	15.2	3.31	7.62	3.26	4.36	1.8
R7Bc	13.34	8.19	34.7	2.5	10.18	4.32	5.52	4.63	0.89	1.25
R7Ca	25.79	5.92	16.68	2.95	12.57	3.68	10.67	2.23	8.44	1.48
R7Cb	20.72	5.93	23.5	2.02	14.06	3.51	8.57	3.14	5.43	1.66
R7Cc	14.19	7.85	33.85	2.69	8.3	4.97	5.87	4.52	1.35	0.98
R7Da	25.53	4.99	18.76	3.04	10.68	4.32	10.56	2.5	8.06	1.26
R7Db	18.93	6.2	27.18	2.62	15.16	3.52	7.83	3.63	4.2	1.79
R7Dc	13.02	7.61	32.57	2.55	6.18	6.23	5.38	4.35	1.03	0.73
R7Ea	21.76	5.11	19.15	2.86	12.85	3.61	9	2.56	6.44	1.52
R7Eb	19.61	5.77	25.32	2.74	15.3	3.43	8.11	3.38	4.73	1.81
R7Ec	14.97	6.81	30.42	2.67	13.66	3.62	6.19	4.06	2.13	1.61
R8Aa	29.78	4.94	19.86	2.91	18.55	3.04	12.32	2.65	9.67	2.19
R8Ab	24.82	6.28	25.82	2.61	19.98	2.84	10.26	3.45	6.81	2.36
R8Ac	13.31	7.46	32.77	2.46	13.84	3.51	5.5	4.37	1.13	1.63
R8Ba	25.11	5.99	19.29	2.93	18.13	2.99	10.39	2.57	7.82	2.14
R8Bb	19.78	5.89	24.43	2.69	19.17	2.96	8.18	3.26	4.92	2.26
R8Bc	13.41	8.04	32.1	2.67	13.07	3.85	5.55	4.28	1.27	1.54
R8Ca	26.16	6.17	18.83	2.96	24.63	2.52	10.82	2.51	8.31	2.91
R8Cb	21.87	5.88	24.64	2.78	29.74	2.31	9.05	3.29	5.76	3.51
R8Cc	14.38	6.57	32.66	2.46	14.86	2.51	5.95	4.35	1.59	1.76
R8Da	22.99	5.16	18	2.76	18.14	2.74	10.25	2.4	7.95	2.14
R8Db	22.47	4.93	20.78	2.01	21.55	2.02	9.29	2.77	6.52	2.55
R8Dc	20.47	5.97	41.88	2.72	18.2	3.09	8.47	5.59	2.88	2.15
R8Ea	27.40	6.28	17.17	2.91	19.34	2.85	11.34	2.29	9.05	2.28
R8Eb	16.51	7.08	25.43	2.59	17.46	3.04	6.83	3.39	3.44	2.06

Table 3.3_a continued from page 166 :

R8Ec	16.94	6.63	32.81	2.55	12.62	3.84	7.01	4.38	2.63	1.49
R9Aa	21.72	6.18	15.67	3.23	27.42	2.31	8.98	2.09	6.89	3.24
R9Ab	20.05	6.17	26.87	2.64	6.13	6.35	8.29	3.59	4.7	0.72
R9Ac	11.93	7.12	33.87	2.23	2.48	9.9	4.93	4.52	0.41	0.29
R9Ba	22.48	5.28	13.94	3.79	24.89	2.2	9.3	1.86	7.44	2.94
R9Bb	21.97	5.86	21.84	2.96	28.46	2.37	9.09	2.91	6.18	3.36
R9Bc	13.92	5.69	33.54	1.67	4.6	5.2	5.76	4.48	1.28	0.54
R9Ca	27.63	4.75	20.42	2.82	16.98	3.06	11.43	2.72	8.71	2.01
R9Cb	20.32	5.54	28.18	2.37	19.11	3.81	8.4	3.76	4.64	2.25
R9Cc	12.87	7.46	25.53	2.3	2.14	12.05	5.32	3.41	1.91	0.25
R9Da	24.14	5.22	18.42	3.05	22.1	2.61	9.98	2.46	7.52	2.61
R9Db	21.71	5.07	26.2	2.59	14.9	3.28	8.98	3.5	5.48	1.76
R9Dc	14.4	7.48	34.46	2.5	6.88	5.95	5.96	4.6	1.36	0.81
R9Ea	25.49	4.75	17.61	2.89	18.39	2.8	10.54	2.35	8.19	2.17
R9Eb	19.18	6.31	25.81	2.49	15.24	3.26	7.93	3.44	4.09	1.8
R9Ec	13.21	7.2	33.12	2.57	11.15	4.1	5.46	4.42	1.04	1.32
R10Aa	20.03	7.11	12.56	3.3	14.36	3.44	8.28	1.68	6.6	1.7
R10Ab	18.49	7.16	23.88	2.78	19.79	3.21	7.64	3.19	4.45	2.33
R10Ac	18.28	5.61	31.05	1.84	11.18	3.04	7.56	4.14	3.15	1.32
R10Ba	25.78	5.45	17.11	3.11	15.21	3.31	10.66	2.28	8.38	1.8
R10Bb	18.46	6.44	23.45	2.74	18.66	2.9	7.63	3.13	4.5	2.2
R10Bc	14.44	8.7	35.07	2.56	10.94	3.87	5.97	4.68	1.29	1.29
R10Ca	27.93	5.38	18.21	3.17	18.49	2.98	11.55	2.43	9.12	2.18
R10Cb	23.17	5.78	27.42	2.54	19.58	2.85	9.58	3.66	5.92	2.31
R10Cc	15.04	6.65	30.14	2.58	15.26	3.29	6.22	4.02	2.2	1.8
R10Da	26.47	3.7	18.54	1.8	16.08	1.93	10.95	2.47	8.48	1.9
R10Db	17.38	6.29	24.48	2.72	19.86	2.92	7.19	3.27	3.92	2.35
R10Dc	12.45	7.64	25.83	2.71	17.11	3.1	5.15	3.81	1.33	2.02
R10Ea	25.4	5.97	18.53	2.9	19.78	2.78	10.51	2.47	8.04	2.34
R10Eb	21.43	6.25	24.45	2.82	20.47	3.01	8.86	3.26	5.6	2.42
R10Ec	14.97	10.22	30.54	2.51	9.95	4.3	6.19	4.08	2.11	1.18

Table 3.3$_b$. The atmospheric inventories of ^{210}Pb and ^{137}Cs to the Rothamsted soil, samples taken at 2nd of Feburary 1998. ^{210}Pb activities were corrected for the time decay to the data of sample collection.

File name (core section)	Total atmospheric deposition of ^{210}Pb corrected for the weight of the sample (Bq)	Total atmospheric deposition of ^{137}Cs corrected for the weight of the sample (Bq)	Total inventory of ^{210}Pb for each sample (Bq kg^{-1})	Total inventory of ^{137}Cs for each sample (Bq kg^{-1})	Total inventories of ^{210}Pb (Bq m^{-2})	Total inventories of ^{137}Cs (Bq m^{-2})	Total inventories of ^{210}Pb corrected for time decay (Bq m^{-2})
R1Aa	12.2	3.15	74	18.65	1493	385	1535
R1Ab	14.06	6.03	44	18.23	1721	738	1769
R1Ac	6.48	3.31	8	3.91	793	405	815
R1Ba	14.98	3.07	94	18.74	1833	376	1886
R1Bb	11.22	5.88	33	16.6	1373	720	1413
R1Bc	6.99	2.58	14	4.92	855	316	880
R1Ca	11.12	2.21	92	17.82	1361	270	1390
R1Cb	14.8	6.69	11.5	18.6	1811	819	1850
R1Cc	6.7	7.41	11	10.75	820	907	838
R1Da	18.96	3.67	79	14.97	2320	449	2370
R1Db	10.81	5.45	31	15.22	1323	667	1351
R1Dc	2.27	2.68	5	6.26	278	328	284
R1Ea	14.01	2.46	89	15.46	1715	301	1730
R1Eb	14.59	5.48	40	14.84	1786	671	1802
R1Ec	1.41	3.01	3	6.87	173	368	175
R2Aa	12.65	2.51	79	15.19	1548	307	1590
R2Ab	15.26	5.66	37	13.48	1868	693	1919
R2Ac	5.52	3.25	13	7.39	676	398	695
R2Ba	15.24	3.26	87	18.14	1865	399	1916
R2Bb	13.45	5.66	37	15.11	1646	693	1692
R2Bc	3.45	3.25	10.5	9.65	422	398	434
R2Ca	13.58	3.18	76	17.51	1662	389	1699
R2Cb	12.48	5.02	38	15	1527	614	1561
R2Cc	10.85	7.05	19	12	1328	862	1358
R2Da	12.08	2.47	74	14.9	1478	302	1507
R2Db	11.61	6.73	32	18.33	1421	824	1449

Table 3.3_b continued from page 168 :

R2Dc	5.73	3.61	13	7.93	701	442	714
R2Ea	13.78	2.47	76	13.42	1686	302	1721
R2Eb	10.48	5.5	29	14.98	1283	673	1310
R2Ec	3.68	3.29	12	10.31	450	403	459
R3Aa	21.44	5.99	112.5	30.62	2624	733	2693
R3Ab	15.23	7.7	58	28.57	1864	942	1914
R3Ac	1.43	2.79	8	15.71	175	341	180
R3Ba	20.87	7.41	81	27.95	2554	907	2619
R3Bb	10.34	6.28	36	21.31	1265	769	1298
R3Bc	3.71	2.65	13	8.99	454	324	467
R3Ca	25.67	8	94	28.43	3141	979	3222
R3Cb	7.7	7.08	27	24.37	942	866	966
R3Cc	2.76	1.68	13	7.52	338	206	347
R3Da	28.11	12.89	67	30.5	3440	1577	3471
R3Db	6.38	3.47	15	11.77	781	425	788
R3Dc	2	1.27	6	3.59	245	155	247
R3Ea	28.84	9.76	92	30.7	3529	1194	3561
R3Eb	6.83	3.12	30	13.51	836	382	844
R3Ec	3.5	1.71	5	2.54	428	209	432
R4Aa	21.53	8.84	106	42.5	2635	1082	2706
R4Ab	12.17	4.93	44	17.49	1489	603	1529
R4Ac	2.56	1.04	16	6.18	313	127	321
R4Ba	21.46	7.03	129	41.23	2626	860	2697
R4Bb	14.56	6.96	59	27.44	1782	852	1830
R4Bc	2.13	1.84	13	11.32	261	225	268
R4Ca	22.74	11.51	98	48.28	2783	1409	2845
R4Cb	10.26	3.48	46	15.38	1256	426	1284
R4Cc	4.27	1.35	23	7.25	523	165	535
R4Da	25.04	10.24	90	36.14	3064	1253	3125
R4Db	7.45	6.27	24	16.30	912	636	930
R4Dc	4.45	2.12	8	3.82	545	259	556
R4Ea	24.37	6.33	130	33.19	2982	775	3044

Table 3.3_b continued from page 169 :

R4Eb	11.45	4.53	44	19.26	1401	554	1430
R4Ec	3.82	1.83	15	6.93	468	224	478
R5Aa	21.1	6.46	112	33.33	2582	791	2648
R5Ab	8.46	6.65	38	29.14	1035	814	1062
R5Ac	5.14	2.23	15	6.25	629	273	645
R5Ba	23.51	9.8	89	36.22	2877	1199	2955
R5Bb	8.65	2.64	37	10.88	1059	323	1088
R5Bc	3.97	0.54	12	1.58	486	66	499
R5Ca	18.4	8.18	108	47.74	3139	1001	3169
R5Cb	9.01	6.98	39	30.1	1103	854	1113
R5Cc	1.39	0.68	43	2.1	455	83	459
R5Da	22.65	9.08	119	47.19	2772	1111	2798
R5Db	9.95	4.82	34	16.35	1218	590	1229
R5Dc	1.22	0.71	5	2.93	149	87	150
R5Ea	20.88	6.77	196	63.02	2555	825	2573
R5Eb	12.83	7.02	75	40.94	1570	859	1581
R5Ec	1.98	1.44	8	5.54	242	177	244
R6Aa	17.19	7.76	94	41.5	2104	950	2157
R6Ab	17.94	3.02	59	9.75	2196	370	2252
R6Ac	2.38	0.68	11.5	3.22	291	83	298
R6Ba	20.67	9.62	116	52.54	2530	1177	2593
R6Bb	11.3	4.9	35	14.75	1383	600	1418
R6Bc	2.45	0.69	7	1.91	300	84	307
R6Ca	18.2	6.69	87	32.09	2227	819	2261
R6Cb	11	5.59	35	17.25	1346	684	1367
R6Cc	6.33	1.06	15	2.49	775	130	788
R6Da	23.28	10.78	97	43.89	2849	1319	2906
R6Db	11.75	3.48	47	13.71	1438	426	1467
R6Dc	5.01	1	16	3.16	613	122	625
R6Ea	23.22	7.88	110	24.91	2841	964	2899
R6Eb	12.11	4.84	37	14.45	1482	592	1512
R6Ec	3.56	1.29	9	3.18	436	158	445

Table 3.3_b continued from page 170 :

R7Aa	12.57	1.84	71	12.82	1539	225	1943
R7Ab	13.62	2.96	56	11.83	1667	362	1707
R7Ac	2.62	2.29	3	11.48	321	280	328
R7Ba	15.86	3.01	74	13.88	1941	368	1988
R7Bb	11.51	4.75	37	14.85	1409	581	1443
R7Bc	2.83	3.99	7	9.66	346	458	354
R7Ca	15.39	2.7	75	13.2	1883	330	1902
R7Cb	10.23	3.09	45	13.69	1252	378	1265
R7Cc	3.69	2.68	10	7.36	451	328	456
R7Da	14.26	2.23	82	12.69	1745	273	1764
R7Db	12.3	5.24	39	16.39	1505	641	1521
R7Dc	3.42	2.43	8	5.66	419	297	424
R7Ea	12.97	3.06	63	14.67	1587	374	1604
R7Eb	13.28	5.08	40	15.1	1625	622	1643
R7Ec	3.42	2.59	18	13.34	419	317	424
R8Aa	18.93	4.29	89	19.74	2317	525	2372
R8Ab	15.05	5.21	59	19.8	1842	638	1885
R8Ac	4.57	6.59	9	12.85	559	807	572
R8Ba	21.13	5.78	77	20.54	2586	707	2647
R8Bb	14.66	6.73	42	18.87	1794	824	1836
R8Bc	4.11	4.99	11	12.56	503	611	515
R8Ca	21.12	7.4	75	25.95	2585	906	2616
R8Cb	13.3	8.11	51	30.93	1627	993	1647
R8Cc	4.79	5.29	13	14.42	586	647	593
R8Da	19.04	5.12	77.5	20.46	2330	628	2373
R8Db	12.64	4.94	58	22.14	1547	605	1575
R8Dc	6.98	5.22	24	17.73	854	639	869
R8Ea	24.37	6.14	81.5	20.16	2982	751	3037
R8Eb	7.22	4.32	28	16.65	884	529	900
R8Ec	3.96	2.24	21	11.58	485	274	494
R9Aa	22.82	10.73	76	34.95	2793	1313	2857
R9Ab	16.85	2.58	35	6.46	2062	316	1722

Table 3.3_b continued from page 171 :

R9Ac	2.14	1.51	3.5	2.39	262	185	268
R9Ba	18.4	7.27	93	35.81	2252	890	2304
R9Bb	13.72	7.46	58	30.64	1679	913	1718
R9Bc	6.43	2.71	11	4.49	787	332	805
R9Ca	21.54	4.97	87	19.82	2636	608	2664
R9Cb	13.41	6.51	40	19.04	1641	796	1658
R9Cc	5.56	0.73	16	2.09	680	89	687
R9Da	24.19	8.39	78	26.87	2960	1027	2995
R9Db	12.13	3.9	48	15.28	1484	477	1501
R9Dc	3.37	2.01	12	6.95	412	245	417
R9Ea	26	6.89	89.5	23.41	3182	843	3222
R9Eb	9.94	4.36	45.5	16.9	1216	534	1438
R9Ec	2.4	3.05	9	11.47	294	373	298
R10Aa	14.46	3.72	67	16.92	1770	455	1810
R10Ab	11.52	6.05	56	20.78	1559	740	2003
R10Ac	7.06	2.96	26	10.66	864	362	884
R10Ba	22.24	4.78	82	17.17	2722	585	2780
R10Bb	11.78	5.76	38.5	18.41	1442	705	1473
R10Bc	5.8	5.8	11	10.52	710	710	725
R10Ca	21.69	5.19	82	19.34	2655	635	2687
R10Cb	14.81	5.78	39	18.96	1813	707	1455
R10Cc	4.99	4.08	19	15.53	611	499	618
R10Da	21.79	4.88	82	18.03	2667	597	2717
R10Db	12.52	7.51	36	21.04	1532	919	1561
R10Dc	3.13	4.71	12	17.69	383	576	390
R10Ea	18.3	5.33	75	21.41	2240	652	2283
R10Eb	15.99	6.91	48	20.37	1957	846	1994
R10Ec	6.4	3.58	21	11.65	783	438	798

Table 3.4. The complete data set of soil densities and inventories of ^{210}Pb in the Rothamsted soil. The depth of each core is reported in column one. The errors were the counting statistical errors (±σ).

Core (depth cm)	Density (dried soil) kg m^{-3}	Total inventory corrected for time decay from measuring date 02/02/1998 ^{210}Pb (Bq m^{-2})	Error ^{210}Pb Bq m^{-2}	Flux of ^{210}Pb Bq kg^{-1}	Error for ^{210}Pb Bq kg^{-1}	One-sigma % error for ^{210}Pb
R1Aa (0-5 cm)	630	1535	84	74	4.05	5.47
R1Ab (5-10 cm)	928	1769	107	44	2.67	6.07
R1Ac (10-20 cm)	1151	815	33	8	0.33	4.07
R1Ba (0-5 cm)	768	1886	69	94	3.45	3.67
R1Bb (5-10 cm)	1112	1413	75	33	1.76	5.32
R1Bc (10-15 cm)	1233	880	68	14	1.08	7.68
R1Ca (0-5 cm)	768	1390	73	92	4.82	5.24
R1Cb (5-10 cm)	1063	1850	92	11	0.55	4.96
R1Cc (10-20 cm)	1221	838	40	11	0.53	4.77
R1Da (0-5 cm)	981	2370	113	79	3.77	4.77
R1Db (5-10 cm)	1138	1351	92	31	2.11	6.81
R1Dc (10-16 cm)	1125	284	25	5	0.44	8.75
R1Ea (0-5 cm)	747	1730	74	89	3.83	4.3
R1Eb (5-10 cm)	1068	1802	106	40	2.36	5.89
R1Ec (10-15 cm)	1154	175	21	3	0.35	11.74
R2Aa (0-5 cm)	677	1590	95	79	4.74	6
R2Ab (5-10 cm)	1011	1919	119	37	2.29	6.19
R2Ac (10-16 cm)	1157	695	46	13	0.85	6.57
R2Ba (0-5 cm)	657	1916	105	87	4.77	5.48
R2Bb (5-10 cm)	1036	1692	110	37	2.40	6.49
R2Bc (10-16 cm)	1117	434	35	11	0.89	8.06
R2Ca (0-5 cm)	704	1699	98	76	4.38	5.76
R2Cb (5-10 cm)	1105	1561	113	38	2.75	7.23
R2Cc (10-20 cm)	1250	1358	94	19	1.32	6.95
R2Da (0-5 cm)	783	1507	71	74	3.46	4.68
R2Db (5-10 cm)	1031	1449	90	32	1.98	6.19
R2Dc (10-16 cm)	1134	714	32	13	0.58	4.48
R2Ea (0-5 cm)	803	1721	91	76	4.02	5.29
R2Eb (5-10 cm)	988	1310	87	29	1.92	6.62
R2Ec (10-14 cm)	1062	459	27	12	0.69	5.77
R3Aa (0-5 cm)	713	2693	120	112	5.01	4.47
R3Ab (5-10 cm)	1121	1914	124	58	3.76	6.48
R3Ac (10-15 cm)	1070	180	16	8	0.70	8.77
R3Ba (0-5 cm)	981	2619	135	81	4.17	5.15
R3Bb (5-10 cm)	1217	1298	76	36	2.12	5.89
R3Bc (10-15 cm)	1212	467	20	13	0.56	4.34
R3Ca (0-5 cm)	937	3222	168	94	4.91	5.22
R3Cb (5-10 cm)	1184	966	62	27	1.73	6.41
R3Cc (10-17 cm)	1275	347	24	13	0.89	6.82
R3Da (0-5 cm)	1130	3471	223	67	4.30	6.42
R3Db (5-10 cm)	1224	788	42	15	1.13	7.54
R3Dc (10-15 cm)	1367	247	20	5.7	0.45	7.90
R3Ea (0-5 cm)	1039	3561	191	92	4.93	5.36
R3Eb (5-10 cm)	1262	844	58	30	2.05	6.83
R3Ec (10-20 cm)	1382	432	33	5	0.39	7.72
R4Aa (0-5 cm)	698	2706	119	106	4.66	4.40
R4Ab (5-10 cm)	1000	1529	91	55	2.62	5.95

Table 3.4 continued from page 173 :

R4Ac (10-15 cm)	1113	321	24	16	1.19	7.42
R4Ba (0-5 cm)	677	2697	101	129	4.84	3.75
R4Bb (5-10 cm)	1137	1830	111	59	3.57	6.05
R4Bc (10-14 cm)	1193	268	21	13	1.02	7.86
R4Ca (0-5 cm)	933	2845	134	98	4.61	4.7
R4Cb (5-10 cm)	1185	1284	88	46	3.14	6.82
R4Cc (10-15 cm)	1241	535	32	23	1.39	6.05
R4Da (0-5 cm)	782	3125	151	90	4.34	4.82
R4Db (5-10 cm)	1166	930	58	24	1.49	6.19
R4Dc (10-20 cm)	1256	556	29	8	0.42	5.19
R4Ea (0-5 cm)	722	3044	121	130	5.15	3.96
R4Eb (5-10 cm)	1102	1430	78	55	2.98	5.42
R4Ec (10-18 cm)	1173	478	31	15	0.98	6.5
R5Aa (0-5 cm)	693	2648	123	112	5.22	4.66
R5Ab (5-10 cm)	1269	1062	45	38	1.62	4.26
R5Ac (10-20 cm)	1008	645	43	15	1.01	6.73
R5Ba (0-5 cm)	724	2955	155	89	4.67	5.25
R5Bb (5-10 cm)	1230	1088	75	37	2.56	6.93
R5Bc (10-15 cm)	1303	499	25	12	0.59	4.95
R5Ca (0-5 cm)	635	3169	133	108	4.54	4.2
R5Cb (5-10 cm)	1063	1113	57	56	2.89	5.16
R5Cc (10-19 cm)	1303	459	34	43	3.20	7.45
R5Da (0-5 cm)	651	2798	127	118	5.36	4.54
R5Db (5-10 cm)	1125	1229	69	34	1.91	5.59
R5Dc (10-16 cm)	1271	150	10	5	0.35	6.96
R5Ea (0-5 cm)	402	2573	92	196	7	3.57
R5Eb (5-10 cm)	731	1581	67	75	3.17	4.22
R5Ec (10-17 cm)	1133	244	16	8	0.52	6.47
R6Aa (0-5 cm)	802	2157	78	94	3.38	3.6
R6Ab (5-10 cm)	1155	2252	133	59	3.49	5.92
R6Ac (10-16 cm)	1217	298	19	12	0.78	6.52
R6Ba (0-5 cm)	759	2593	116	116	5.2	4.48
R6Bb (5-10 cm)	1209	1418	118	35	2.90	8.29
R6Bc (10-17 cm)	1223	307	25	7	0.56	8.05
R6Ca (0-5 cm)	817	2261	99	89	3.91	4.39
R6Cb (5-10 cm)	1203	1367	85	34	2.11	6.22
R6Cc (10-17 cm)	1255	788	75	15	1.43	9.56
R6Da (0-5 cm)	827	2906	138	97	4.62	4.76
R6Db (5-10 cm)	1057	1467	86	47	2.74	5.84
R6Dc (10-20 cm)	1167	625	40	16	1.03	6.41
R6Ea (0-5 cm)	824	2899	121	119	4.96	4.17
R6Eb (5-10 cm)	1145	1512	94	37	2.29	6.2
R6Ec (10-18 cm)	1235	445	20	9	0.40	4.45
R7Aa (0-5 cm)	1001	1943	119	90	4.45	6.1
R7Ab (5-10 cm)	1177	1707	115	56	3.78	6.75
R7Ac (10-15 cm)	1195	328	22	3	2.32	6.81
R7Ba (0-5 cm)	1023	1988	112	75	4.22	5.62
R7Bb (5-10 cm)	1185	1443	112	37	2.87	7.75
R7Bc (10-20 cm)	1268	354	29	7	0.57	8.19
R7Ca (0-5 cm)	1097	1902	113	72	4.26	5.92
R7Cb (5-10 cm)	1187	1265	75	44	2.61	5.93
R7Cc (10-16 cm)	1303	456	36	10	0.79	7.85
R7Da (0-5 cm)	972	1764	88	82	4.1	4.99

Table 3.4 continued from page 174 :

R7Db (5-10 cm)	1069	1521	94	39	2.42	6.2
R7Dc (10-17 cm)	1265	424	32	8	0.61	7.61
R7Ea (0-5 cm)	1014	1604	82	63	3.22	5.11
R7Eb (5-10 cm)	1173	1643	95	40	2.31	5.77
R7Ec (10-18 cm)	1182	424	29	18	1.23	6.81
R8Aa (0-5 cm)	1086	2372	117	89	4.4	4.94
R8Ab (5-10 cm)	1166	1885	118	59	3.71	6.28
R8Ac (10-20 cm)	1242	572	43	9	0.67	7.46
R8Ba (0-5 cm)	1019	2647	159	77	4.61	5.99
R8Bb (5-10 cm)	10173	1836	108	42	2.47	5.89
R8Bc (10-17 cm)	1200	515	41	11	0.88	8.04
R8Ca (0-5 cm)	1098	2616	161	75	4.63	6.17
R8Cb (5-10 cm)	1111	1647	97	51	3	5.88
R8Cc (10-17 cm)	1193	593	39	13	0.85	6.57
R8Da (0-5 cm)	1025	2373	122	65	3.35	5.16
R8Db (5-10 cm)	1127	1575	78	58	2.86	4.93
R8Dc (10-16 cm)	1187	869	52	24	1.43	5.97
R8Ea (0-5 cm)	1106	3037	191	71	4.46	6.28
R8Eb (5-10 cm)	1211	900	64	28	1.98	7.08
R8Ec (10-15 cm)	1258	494	33	21	1.39	6.63
R9Aa (0-5 cm)	907	2857	177	76	4.7	6.18
R9Ab (5-10 cm)	1090	1722	106	35	2.16	6.17
R9Ac (10-20 cm)	1187	268	19	3	0.21	7.12
R9Ba (0-5 cm)	803	2304	122	93	4.91	5.28
R9Bb (5-10 cm)	1073	1718	101	58	3.4	5.86
R9Bc (10-19 cm)	1175	805	46	11	0.63	5.69
R9Ca (0-5 cm)	992	2664	127	87	4.13	4.75
R9Cb (5-10 cm)	1157	1658	92	40	2.22	5.54
R9Cc (10-17 cm)	1177	687	51	16	1.19	7.46
R9Da (0-5 cm)	950	2995	156	78	4.07	5.22
R9Db (5-10 cm)	1129	1501	76	48	2.43	5.07
R9Dc (10-15 cm)	1141	417	31	12	0.9	7.48
R9Ea (0-5 cm)	907	3222	153	89	4.23	4.75
R9Eb (5-10 cm)	1041	1438	91	46	2.89	6.31
R9Ec (10-15 cm)	1129	298	21	9	0.65	7.2
R10Aa (0-5 cm)	983	1810	129	67	4.76	7.11
R10Ab (5-10 cm)	1100	2003	143	56	4.01	7.16
R10Ac (10-19cm)	1210	884	50	26	1.46	5.61
R10Ba (0-5 cm)	1027	2780	152	82	4.47	5.45
R10Bb (5-10 cm)	1170	1473	95	38	2.45	6.44
R10Bc (10-20 cm)	1199	725	63	10	0.87	8.7
R10Ca (0-5 cm)	1104	2687	145	82	4.41	5.38
R10Cb (5-10 cm)	1192	1455	84	39	2.25	5.78
R10Cc (10-15 cm)	1133	618	41	19	1.26	6.65
R10Da (0-5 cm)	1032	2717	101	82	3.04	3.7
R10Db (5-10 cm)	1093	1561	101	36	2.26	6.29
R10Dc (10-16 cm)	1117	390	30	12	0.92	7.64
R10Ea (0-5 cm)	1071	2283	136	75	4.48	5.97
R10Eb (5-10 cm)	1163	1994	125	48	3	6.25
R10Ec (10-17 cm)	1194	798	82	21	2.15	10.22

Appendix D

The conversion factors listed here have been used to compare our results to the reported measurements found in the literature.

dpm = disintegration per minute

1 Bq = 1 disintegration per second

curie = Ci

becquerel = Bq

1 Ci = 37 GBq

$G = 10^{9}$

$p = 10^{-12}$

$f = 10^{-15}$

1 dpm = 0.45 pCi

1 dpm = 0.0166 Bq

1 pCi = 0.037 Bq

1 fCi = 3.7×10^{-5} Bq

1 fCi = 145.9 atoms of ^{7}Be

1 fCi = 37569 atoms of ^{210}Pb

1 fCi m^{-3} = 27 mBq m^{-3} (STP)

1 fCi = 1.4×10^{-4} mol of ^{210}Pb per mol of air

1 dpm ^{210}Pb cm^{-2} y^{-1} = 0.54 atom ^{222}Rn cm^{-2} s^{-1}

1 atom ^{222}Rn cm^{-2} s^{-1} = 1.865 dpm ^{210}Pb cm^{-2} y^{-1}

Bibliography

Aalst R. M. van and J. W. Erisman (1991). Atmospheric input. In: Acidification research in the Netherlands (eds. Heij G. J. and T. Schneider) Studies in Environmental Science 46, Elsevier, Amsterdam, 239-288.

Adams J. A. S. et al. (1959). The geochemistry of thorium and uranium. In: Physics and Chemistry of the Earth 3, New York, Pergamon Press, 298-348.

Adames P. J., J. H. Seinfeld and D. K. Kock (1999). J. Geophs. Res. 104 (D11): 13795.

ANSI (1991). American National Standard Calibration and use of Germanium Spectrometer for the Measurement of Gamma-Ray Emission Rates of Radionuclides. IEEE, New York.

Balkanski Y.J., D.J. Jacob and G.M. Gardner (1993). Transport and residence times of tropospheric aerosols inferred from a global three dimensional simulation of ^{210}Pb: J. Geophys. Res. 98 D11: 20573-20586.

Barretto R. M. C., R. B. Clark and J. A. S. Adams (1972). Physical characteristics of ^{222}Rn emanation from rocks, soils and minerals: its relation to temperature and alpha dose. USERDA report conf. 720805- p2: the natural radiation environment 2, 731-740.

Baskaran M., C. H. Coleman and P. H. Santschi (1993). Atmospheric depositional fluxes of ^{7}Be and ^{210}Pb at Galveston and college station, Texas: J. Geophys. Res., 98 D11: 20555-20571.

Baskaran M. (1995). A search for seasonal variability on the depositional fluxes of ^{7}Be and ^{210}Pb: J. Geophys. Res., 100 D2: 2833-2840.

Beck J.N. and P.K. Kuroda (1966). Radio-Strontium fallout from the nuclear explosion of Oct. 16, 1964: J. Geophys. Res., 71, 2451-2456 .

Benninger L. K., D. M. Lewis and K. K. Turekian (1975). The use of natural ^{210}Pb as a heavy tracer in the river- estuarine system, in Marine Chem. in the Coastal Environ. Symp. Ser., 18: edited by T.M. Church, American Chemical Society, Washington DC. pp. 201-210.

Bondietti, E. A. et al., (1984). Air- to- vegetation transfer rates of natural submicron aerosols, J. Environ. Radioact., 1: 5-28.

Bondietti E.A. , J.N. Brantley and C. Rangarajan (1988). Size distributions & growth of natural & Chernobyl-derived submicron aerosols in Tennessee: J. Environ. Radioactivity, 6: 99-120.

Brachet (1987). Acidic deposition and its gaseous precursors. In: National Acidic Precipitation Assessment Program. vol.III: Washington DC. Chapter 5: 5-2 to 5-116.

Branford D., R. D. Mourne and D. Fowler (1998). Spatial variation of wet deposition rates in an extended region of complex topography deduced from measurements of ^{210}Pb soil inventories. J. Environ. Radioactivity, 41, No. 2: 111-125.

Brimblecombe Peter (1996). Air composition and chemistry, Camb. Univ. press, 2nd Edd., ISBN 0521 453666, PP55, 173-176.

Brost R. A., J. Feichter and M. Heimann (1991). Three- dimensional simulation of ^{7}Be in a global climate model: J. Geophys. Res. 96 D12: 22423-22445.

Burton W. M. and N. G. Stewart (1960). Use of long-lived natural radioactivity as an atmospheric tracer: J. Nature, 186: 584-589.

Cambray R. S., Miss E. M. R. Fisher, W. L. Brooks and D. H. Peirson (1970). Radioactive fallout in air and rain. U K Atomic Energy Authority. AERE-R 6556.

Carvalho F. P.(1990).Contribution a l'etude du cycle du polonium-210 et du Plomp-210 dans l'environnement. These de l' Univ. Sophia-Antipolis, Nice, France.

Cawse P.A. (1983). The accumulation of Cs and $^{239+240}$Po in soils of UK, and transfer to vegetation. In: P.J. Coughtrey et al. (eds.), Ecological Aspects of Radionuclide Release. Blackwell Scientific, Oxford, England.

Cawse P. A., Cambray R. S., Baker S. J. and Barton P. J. (1988). A survey of background levels of environmental radioactivity in Wales, 1984 - 1986 (pre-Chernobyl). AERE, R-12535, HMSO: London.

Chamberlain A.C. (1991). Radioactive aerosols. Cambridge Uni. Press. Chapter one: ISBN 052 1401216.

Clifton R. J. (1991). The use of radio-nuclides (unsupported ^{210}Pb, ^{7}Be and ^{137}Cs) in describing the mixing characteristics of Estuarine sediments:in Radionuclides in the study of marine processes (eds. P. J. Kershaw and D. S. Woodhead): Elsevier: 255-264.

Crick M. J. and G. S. Linsley (1983). An assessment of the radiological impact of the Windscale reactor fire of October 1957. National Radiological Protection Board, Chilton. Report R-135, Addendum.

Cutshall N. H., I. L. Larsen and C. R. Olsen (1983). Direct analysis of ^{210}Pb in sediments samples; self absorption corrections: J. Nucl. instr. and meth., 206: 309-312.

Danielson E. F. (1968). Stratospheric-Tropospheric exchange based on radioactivity, ozone and potential vorticity. J. Atmos. Sci., 25: 502-518.

Dibb J. E. (1989). Atmospheric deposition of ^{7}Be in the Chesapeake Bay Region: J. Geophys. Res., 94 D2: 2261-2265.

Dorr H. (1984). Investigation of the gas and water budgets in unsaturated soils layer using carbon dioxide and ^{222}Rn, in Germany: PhD thesis, univ. of Heidelberg, Germany.

Dorr H., L. Katruff and I. Levin (1993). Soil texture parameterisation of the methane uptake in aerosol soils: Chemosphere, 26:, 697-713.

Draaijers G.P.J. and J.W. Erisman (1993).Atmospheric sulphur deposition onto forest stands: throughfall estimates compared to estimates from inference. Atmosph. Environ., 27A: 43-55.

Dutkiewicz V.A. and L. Husain (1985).Stratospheric and tropospheric components of ^{7}Be in surface air: J. Geophys. Res., 90 D3: 5783-5788.

Eakians J. D., Cambrary R. S., Chambers K. C. and Lally A. E. (1984). The transfer of natural and artificial radionuclides to Brotherswater from its catchment. In: Lake sediments and environmental history. Hawort E. Y. and J. W. G. Lund (eds), Leister University press, 125-144.

Eaton J.S., G.E. Likens and F.H. Borman (1978). The input of gaseous and particulate sulphur to a forest ecosystem. Tellus 30: 546-551.

Eaton J.S., G.E. Likens and F.H. Bormann (1980).Wet and dry deposition of sulphur at Hubbard Brook. In: Effect of acid precipitation on terrestrial ecosystems.

NATO Conf. Series 1: Ecology 4 (eds. T. Hutchinson and M. Havas). Plenum publishing Corp., 69-75.

Erisman J. W. and D. D. Baldocch (1994). Dry deposition of SO_2. Tellus, 46B: 159-171.

Evans M., N. Hastings and B. Peacock (1993). Statistical Distributions. 2nd ed., John Wiley & Sons, inc., ISBN-0-471-55951-2.

Feely H. W. et al. (1966). Transport and fallout of stratospheric radioactive debris. Tellus, 18, 31328.

Feely H.W., L. Toonkel and R. J. Larsen (1981). ^{7}Be in surface air, in Environmental measurements Laboratory Annual Report- calendar year 1980, DOE / EML-392, ed. by H. L. Volchoh 7-8, Envi. Meas. Lab. New York.

Feely H.W., R.J. Larsen and C.G. Sanderson (1988). Annual report of the surface air sampling program: USDOE Environ. Meas. Lab. New York.

Feely H.W., R.J. Larsen and C.G. Sanderson (1989). Factors that cause seasonal variation in ^{7}Be concentrations in surface air: J. Envir. rad. 9: 223-249.

Feichter J., R.A. Brost and M. Heimann (1991). Three- dimensional modelling of the concentration and deposition of ^{210}Pb aerosols: J. Geophys. Res. 96: 22447-22460.

Fisenne I. M. (1968). Distributions of ^{210}Pb and ^{226}Ra in soils. Report UCRL-18140, U. S. dep. of Energy, Washington, 145-158.

Fowler D. and J.N. Cape (1984).The contamination of rain samples by dry deposition on rain collectors. Atmospheric Environment, 18: 183-189.

Fowler D. (1986). The transfer of air pollutants to the ground by wet and dry deposition, regional and long range transport of air pollution: Elsevier science publis: s. Sandroni (ed), 95-126.

Fowler D., J.N. Cape and M.H. Unsworth (1989). Deposition of atmospheric pollutants on forests: Phil. Trans. R. Soc. London: B324: 247-265.

Fowler D., J. H. Duyzer and D. D. Baldocchi (1991). Inputs of trace gases, particles and cloud droplets to terrestrial surfaces: Proceedings of the Royal society of Edinburgh: 97B: 35-59.

Fowler D., R. Mourne and D. Branford (1995). The application of ^{210}Pb inventories in soil to measure long-term average wet deposition of pollutants in complex terrain: Water, air and soil pollution: 85: 2113-2118.

Gaggeler H., H. R. Van Gunten and U. Nyffeler (1976). Determination of ^{210}Pb in lake sediments and in air samples by direct gamma ray measurements:J. Earth and planetary sci. lett. 33: pp119-121.

Gallagher M.W. et al. (1997). Measurements of Aerosol Fluxes to Speulder Forest Using a Micrometeorological Technique. Atmospheric Environment, Vol. 31, No. 3: pp 359-373.

Gavini M. B., J. N. Beck and P. K. Kuroda (1974). Mean residence times of the long-lived Radon daughters in the atmosphere: J. Geophys. Res. 79, (30): 4447-4452.

Gibson J.H. (1986).Acid deposition: Long term trends. Environmental Studies Board, National Academy Press, Washington, DC, pp506.

Graf Hans- F., J. Feichter and B. Langmann (1997). Volcanic sulphur emissions: Estimates of source strength and its contribution to the global sulphate distribution. J. Geophs. Res. 102 (D9): 10727-10738.

Graustein W.C. and K.K. Turekian (1983). ^{210}Pb as a tracer of the deposition of submicrometre aerosols. In: Precipitation scavenging, dry deposition, and resuspensions. 1315-1324.

Graustein W. C. and K. K. Turekian (1986). ^{210}Pb and ^{137}Cs in air and soils measure the rate and vertical profile of aerosol scavenging: J. Geophys. Res., 91, D13: 14355-14366.

Graustein, W.C. and Turekian, K.K. (1996). ^{7}Be and ^{210}Pb indicate on upper troposphere source for elevated ozone in the summertime subtropical free troposphere of the eastern North Atlantic. J. Geophys. Res., 23, No. 5: 539-542.

Grennfelt P., S. Larsson, P. Leyton and B. Olsson (1985). Atmospheric deposition in the lake Gardsjon area, SW Sweden. Ecol. Bull. (Stockholm) 37: 101-108.

Hicks B. B. et al., (1987). A preliminary multiple resistance routine for deriving dry deposition velocities from measured quantities. Water, Air and Soil pollution, 36: 311-330.

Hicks B. B. et al., (1989). Atmospheric processes research and processes model development. State of Science/Technology report no.2. National Acid Precipitation Assessment Program.

He Q. and D. E. Walling (1997). The distribution of fallout ^{137}Cs and ^{210}Pb in undisturbed and cultivated soils. Appl. Radiat. Isot., 48: 677-690.

Hotzl H., G. Rosner and R. Winkler (1991). Correlation of ^{7}Be concentrations in surface air and precipitation with the solar cycles: Neturwissenschaften: 78: 215-217.

Hultberg H. (1985). Budgets of base cations, chloride, nitrogen and sulphur in the acid Lake Gardsjon catchment, SW Sweden. Ecoll. Bull.(Stockholm) 37: 133-157.

Jacob D. J. and M. J. Prather (1990). ^{222}Rn as a test of convective transport in a general circulation model: J. Tellus: 42B: 118-134.

Joshi S. R. (1987). Non- destructive determination of ^{210}Pb and ^{226}Ra sediments by direct photon analysis. J. Radioana. and nucl chem., 116,(1): 169-182.

Junge C. E. (1963a). Air Chemistry and Radioactivity. Academic, San Diago, California.

Junge C. E. (1963b). Radioisotopes produced by cosmic radiation. Chapter 3, Atmos. radioactivity, 230-238.

Keller G. et al. (1982). Methods for the determination of ^{222}Rn (radon) and ^{220}Rn (thoron) exhalation rates using alpha spectroscopy. Radiation Protection Doseimetry. 3: 83-89.

Kiang L. L. et al. (1993). A study on T- shape Compton suppression spectrrometers by Monte Carlo simulations. Nucl. Instr. Methods Phys. Res., A327: 427-432.

Knoll G. F. (1989). Radiation detection and measurements: 2nd edd. Lithium-drifted Germanium detectors. John Wiley, New York. Chapt.12: 414-470.

Knuth R. H. and E. Knutson (1981). U. S. Department of Energy, EML-399, 31-37.

Knuth R.H. et al.(1982). In: Precipitation scavenging, dry deposition, and resuspensions. 1325-1335.

Knuth R.H., E.O. Knutson, H.W. Feely and H.L.Volchok (1983). Size distribution of atmospheric Pb and ^{210}Pb in rural New Jersey. In:H.R. Pruppacher et al.(eds.), Precipitation Scavenging, Dry Deposition and Resuspension. Elsevier, New York: 1325-1335.

Koch D.M. and M.E. Mann (1996). Spatial and temporal variability of ^{7}Be surface concentration. Tellus, 48B: 387-396.

Koch D.M., D.J. Jacob and W.C. Graustein (1996). Vertical transport of tropospheric aerosols as indicated by ^{7}Be,and ^{210}Pb in a chemical tracer model: J. Geophys. Res. 101 D13: 18651-18666.

Kocher, D. C. (1981). Radioactive decay data tables. DOE/TIC-11026.

Kownacka L. et al. (1990). Vertical distributions and flows of lead and natural radionuclides in the atmosphere. The Sci. Tot. Env. 91: 199-221.

Lal D. (1963). On the investigations of geophysical processes using cosmic ray produced radioactivity : In earth science and Meteoritic, copied by J. Geiss and E. D. Goldberg: North Holland, New York: pp312.

Lal D. and B. Peters (1967). Cosmic ray produced radioactivity on the earth: Handbook of Physics: 46: 551-612.

Lambert G. et al. (1982). Cycle du Radon et de ses descendants: Application a' l' etude Des exchanges troposphere-stratosphere: Ann. geophys. 48: 497-531.

Lambert G., J. Sanak & G. Polian (1983). Mean residence time of the submicrometre aerosols in the Global troposphere. 1353-1359.

Larsen R.J. (1993).Global decrease of ^{7}Be in surface air:J. Environ. Radio. 18: 85-87.

Lewis D. M. (1977). The use of ^{210}Pb as a heavy metal tracer in the Susquehanna River system: J. Geochimica et cosmochimica Acta: 41: 1557-1564.

Likens G.E., F.H. Bormann, R.S. Pierce, J.S. Eaton and N.M. Johnson (1977). Biogeochemistry of a forested ecosystem. Springer-Verlag New York Inc., pp146.

Likens G. E., F. H. Bormann and L. O. Hedin (1990). Dry deposition of sulphur: 23 years record for the Hubbard Brook Forest ecosystem. Tellus, 42B: 319-329.

Lindgerg S. E., G. M. Lovett, D. D. Richter and D. W. Johnson (1986). Atmospheric deposition and canopy interactions of major ions in a forest. Science 231:141-145.

Lindgerg S.E. and C.T.Jr. Garten (1988). Sources of sulphur in forest canopy throughfall. Nature 336: 148-151.

Lindstrom R. M. et al. (1990). A low background gamma-ray assay laboratory for activation analysis. Nucl. Instr. Methods Phys. Res., A299: 425-429.

Liu S. C., J. R. Mc Afee and R. J. Cicerone (1984). ^{222}Rn and tropospheric vertical transport : J. Geophys. Res. 89 D5: 7291-7297.

Lockhart Jr. L. B. et al. (1965). Distribution of air- borne activity with particle size. In:A.W. Klement (ed.), Radioactive fallout from nuclear weapons tests. Conf. 765, NTIS, Springfield, Va. (20150 010043908).

Lovett G. M. (1988). A comparison of methods for estimating cloud water deposition to a New Hampshire USA. Subalpine forests. In: Acid deposition at high elevation sites (eds. Unsworth M. H. and D. Fowler). 309 - 320. Kluwer, Dordrecht, the Netherlands.

Mac Kenzie A. B., E. Logan, G. T. Cook, and I. D. Pulford (1995). Radionuclide and metal distributions in peat deposition in Scotland. In: Heavy Metals in the Environment; Int. Conf. held in Humburg, Sep. 1995. edited by R. D. Wilken, U. Forstner, A. Knockel. ISBN 0 90594156X. vol.1: 113-116.

Martell E.A. (1985). Enhanced ion production in convective storms by transpired Rn isotopes and their decay products: J. Geophys. Res. 90 D4: 5909-5916.

Mattsson R. (1970). Seasonal variation of short-lived Rn progeny, ^{210}Pb and ^{210}Po in ground level air in Finland: J. Geophys. Res. 75: 1741-1744.

Milford J. B. and C.I. Davidson (1987). The size of particulate sulphate and nitrate in the atmosphere, JAPCA 37: 125-134.

Monaghan M.C. (1989). ^{210}Pb in surface air and soils from California:Implication for the behaviour of trace elements in the planetary boundary layer: J. Geophys. Res., 94 D5: 6449-6456.

Moghaddam M.V. (1998). Study of surface roughness effects on deposition of atmospheric aerosols using ^{210}Pb soil inventories. PhD thesis, Univ. of Edinburgh.

Monteith J.L. & M.H. Unsworth (1990). Principles of Environmental Physics. (2nd edd.), chapter 7, ISBN 0-7131-2931-X.

Moore H.E., S.E. Poet and E.A. Martell (1973). ^{222}Rn, ^{210}Pb, ^{210}Bi and ^{210}Po profiles and aerosol residence times versus altitude: J. Geophys. Res. 78 No.30: 7065-7074.

Moore H. E. and S. E. Poet (1976). ^{210}Pb fluxes determined from ^{210}Pb and ^{226}Ra soil profiles: J. Geophys. Res. 81 No.6: 1056-1058.

Moore H.E., S.E. Poet and E.A. Martell (1980). Size distribution and origin of ^{210}Pb, ^{210}Bi and ^{210}Po on airborne particles in the troposphere. 415-429.

Mourne R. (1993). ^{210}Pb as a tracer for acidic deposition in areas of complex topogr-aghy. PhD thesis, University of Edinburgh.

Myrick T. E. et al. (1983). Determination of concentrations of selected radionuclides in surface soils in the US Health Physics. 45: 631.

Nevissi A.E. (1985).Measurement of ^{210}Pb fluxes determined from ^{210}Pb atmospheric flux in the pacific Northwest, Health Phys., 48: 169-175.

Norton S. A. et al. (1988). Regional patterns and local variability of dry and occult deposition strongly influence sulphate concentrations in Maine lakes. The Science of the total Environment 72: 183-196.

Nozaki Y., D.J. DeMaster, D.M. Lewis and K.K. Turekian (1978).Atmospheric ^{210}Pb fluxes determined from soil profiles: J. Geophys. Res. 83, C8: 4047-4051.

O'Brien K., A. De La Z. Lerner, M. A. Shea and D. F. Smart (1991). The production of cosmogenic isotopes in the earth's atmosphere and their inventories. In: The sun in time. edited by C. P. Sonett, M. S. Giampapa and M. S. Matthaws. 317-342.

Olsen C. R. et al. (1985_a). Atmospheric flux and marsh- soil inventories of ^{7}Be and ^{210}Pb. J. Geophys. Res. 90 D6: 10487-10495.

Olsen C. R. et al. (1985_b). Atmospheric flux and marsh- soil inventories of ^{7}Be and ^{210}Pb. J. Geophys. Res. 90 D13: 14355-14366.

Patterson R.L. and Lockhart Jr. L. B.(1964). Part I, Radioactivity in the atmosphere, 383,the Natural Radiation Environment (edited by Adams and Lowder), Univ. of Cambridge Press.

Peirson D. H. (1963). ^{7}Be in air and rain. J. Geophs. Res. 68(13): 3831-3832.

Peirson D. H., R. S. Cambray and G. S. Spicer (1966). ^{210}Pb and ^{210}Po in the atmosphere: J. Tellus: 18 (2): 427-433.

Peng T.H., W.S. Broecker, G.G. Mathieu, Y.H. Li and A.E. Bainbridge (1979). Rn evasion rates in the Atlantic and Pacific Oceans as determined during the gausses program. J. Geophys. Res., 84 (C5): 271-2486.

Preiss N. et al. (1996).A compilation of data on ^{210}Pb concentration in surface air and fluxes at the air-surface and water- sediment interfaces. J. Geophys. Res., 101 (D22): 28847-28862.

Preiss N. et al. (1998). Database on ^{210}Pb concentration in surface air, ^{210}Pb atmospheric deposition and water- sediments fluxes: http://glaciog.ujf-grenoble.fr/equipes/glaciers.

Prospero J. M. et al. (1995). Temporal variability of summer-time ozone and aerosols in the free troposphere over the eastern North Atlantic. J. Geophs. Res. Lett, 22 (21): 2925-2928.

Pul W. A. J. van et al. (1992). Deposition of air pollution at a forest edge: a simple approach. In:The EUROTRAC Annual Report 1991; BIATEX (ed. J.Slanina). EROTR-AC,Garmisch Parten-kirchen, Germany.

Pulford I. D., C. S. Maguire, G. T. Cook and A. B. MacKenzei (1995). Heavy metals in the environment, Humburg, Sept. 1995. edited by R. D. Wilken, U. Foster, A. Knockel, ISBN 090594156 X. 137-140.

Reiter et al. (1975). Measurements of stratospheric residence times, Ser. A.: Arch. Meteor. Geophys. Bioklimatol. 24: 41-51.

Rehfeld S. and M. Heimann. (1995). Three dimensional atmospheric transport simulation of the radioactive tracers ^{210}Pb, ^{7}Be and ^{90}Sr: J. Geophys. Res.100 D12: 26141-26161.

Romer F.G. et al. (1990). The chemical composition of dew and the deposition flux of water vapour: field measurements and modelling. Final report no. 50583-MOC90-3411, KEMA, Arnhem, the Netherlands.

Ruijgrok W., C.I. Davidson and K.W. Nicholson (1995).Dry deposition of particles: Implications and recommendations for mapping over Europe, Tellus, 47B: 587-601.

Sanak, J.A., A.Gaudry and G.Lambert (1981). Size distribution of ^{210}Pb aerosols over oceans, Geophys. Res. Lett., 8: 1067-1070.

Schuler C. et al. (1991). A multitracer study of radionuclides in lake Zurich, Switzerland, 1, Comparison of atmospheric and sedimentary fluxes of ^{7}Be, ^{10}Be, ^{210}Pb, ^{210}Po and ^{137}Cs, J. Geophys. Res., 96: 17051-17065.

Seinfeld J. H., and S.N. Pandis (1998). Atmospheric Chemistry and Physics: From air pollution to climate change, pp 1002. "A Wiley- Interscience publication" (ISBN 0-471-17815-2).

Shepard J.P., M.J. Mitchell, T.J. Scott, Y.M. zhang and D.J. Raynal (1990). Measurements of wet and dry deposition in a northern Hardwood forest. Water, Air, and Soil Pollution. (cited in G. E. Likins et al. 1990).

Slinn W.G.N. (1982). Predictions for particle deposition to vegetative canopies. Atmospheric Environment, 16: 1785-1794.

Smith J.T., P.G. Appelby, J. Hilton and N. Richardson (1997).Inventories and fluxes of ^{210}Pb, ^{137}Cs and ^{241}Am Determined from the soils of 3 Small Catchments in Cumbria, UK. J. Environ. Radioactivity, 37 (2): 127-142.

Tannor A.B. (1964). Rn migration in the ground: a review. In: The Natural Radiation Environment. ed. J. A. S. Adams and W. M. Lowder, University of Chicago Press, 161-190.

Thomson J., S. Colley, R. Anderson, G.T. Cook and A.B. MacKenzie (1993).^{210}Pb in the sediments and water column of the Northeast Atlantic from 47 to 59° N

along 20° W: Earth and planetary science letters: Elsevier science publishers B. V. Amsterdam. 115: 57-87.

Todd J.F., G.T.F. Wong, C.R. Olsen and I.L. Larsen (1984). Atmospheric deposition fluxes of ^{7}Be and ^{210}Pb to lower Chesapeake Bay (abstract), Eos Trans. AGU, 65: 227.

Todd J. F. et al. (1989). Atmospheric depositional characteristics of ^{7}Be and ^{210}Pb along the South Eastern Virginia Coast: J. Geophys. Res. 94 D8: 111106-111116.

Tokieda T. et al. (1996). Seasonal variations of residence time and upper atmospheric contribution of aerosols studied with ^{210}Pb, ^{210}Bi, ^{210}Po and ^{7}Be. Tellus,48(B): 690-702.

Tsoulfanidis N. (1989). Measurements and Detection of Radiation. Mc Graw- Hill series in Nuclear Engineering. Hemisphere, Washington.

Turekian K. K., Y. Nozaki and L. K. Benninger (1977). Geochemistry of atmospheric Radon and Rn products: J. Ann. Rev. Earth Planet Sci., 5: 227-255.

Turekian K. K., W. C. Graustein and J. K. Cochran (1989). ^{210}Pb in the SEAREX program: An aerosol tracer across the pacific: J. Chem. Oceanography. 10: pp 51-81.

Twomey S. (1979). Atmospheric aerosols : Elsevier scientific publishing company.

Unsworth M.H. and Wilshaw J.C. (1989). Wet, Occult and dry deposition of pollutants on forests : J. Agricultural and forest material : 47: 221-238.

Volchok H. L. (1980). Atmospheric deposition of man- made radioactivity. In: T. Y. Torbara et al. (eds.), Polluted Rain. Plenum, New York, 435-448.

Whitby K. T. (1978). Physical characteristics of sulphur aerosols, Atmos. Environ. 12: 135-160.

Wilkening M. H. et al. (1972). ^{222}Rn flux measurements in widely separated regions. In: Natural Radiation Environment II, ed. J.A.S. Adams W.M. Lowder and T.F. Gasell, 717-730, Springfield, Va., NTIS.

Wilkening M. H. and Clements W. E. (1975). Radon-222 from the ocean surface. J. Geophys. Res. 80: 3828-3830.

Wiman B.L.B. (1988). Aerosol capture by complex forest architecture. In: Vegetation structure in relation to carbon and nutrient economy (eds.) Verhoeven J. T. A., G. W. Heil and M. J. A. Werger), 157-183.

Young J. A. and W. B. Silker (1974). The determination of air- sea exchange and oceanic mixing rates using ^{7}Be during the Bomex experiment. J. Geophys. Res. 79 (30): 4481-4489.